LA-8944-C

Conference

Proceedings of the Reversed-Field Pinch Theory Workshop

Held at Los Alamos National Laboratory
April 29—May 2, 1980

Los Alamos

Los Alamos National Laboratory
Los Alamos, New Mexico 87545

DISCLAIMER

Proceedings of the Reversed-Field

Pinch Theory Workshop

Held at Los Alamos National Laboratory

April 29—May 2, 1980

Compiled by

H. Ralph Lewis

Los Alamos

Los Alamos National Laboratory
Los Alamos,New Mexico 87545

ATTENDEES

NAME	INSTITUTION
Thomas Armstrong	Los Alamos National Laboratory
Stefano Atzeni	University of Rome
Don Baker	Los Alamos National Laboratory
Daniel Barnes	Los Alamos National Laboratory
Herb Berk	Lawrence Livermore National Laboratory
M. K. Bevir	Culham Laboratory
Amitava Bhattacharjee	Princeton University
A. Bondeson	University of Maryland
Allan Boozer	Princeton Plasma Physics Laboratory
Lou Burkhardt	Los Alamos National Laboratory
Nelson Byrne	Science Applications Inc.
Edward Caramana	Los Alamos National Laboratory
P. G. Carolan	Culham Laboratory
Morrell Chance	Princeton University
Chia Lui Chang	University of Maryland
Richard Christian	Purdue University
Chang Chu	General Atomic Company
John Chu	Columbia University
Ming S. Chu	General Atomic Company
J. P. Christiansen	Culham Laboratory
William Condit	Lawrence Livermore National Laboratory
J. W. Connor	Princeton University

Rostom Dagazian	Los Alamos National Laboratory
Joseph DiMarco	Los Alamos National Laboratory
Jacques Denavit	Northwestern University
Harry Dreicer	Los Alamos National Laboratory
Richard Gerwin	Los Alamos National Laboratory
C. G. Gimblett	Culham Laboratory
Nevel T. Gladd	University of Maryland
George C. Goldenbaum	University of Maryland
Harold Grad	New York University
Ray Grimm	Princeton University
Albert Haberstich	Los Alamos National Laboratory
Randy L. Hagenson	Los Alamos National Laboratory
Seishi Hamasaki	Jaycor
Dennis Hewett	Los Alamos National Laboratory
R. B. Howell	Los Alamos National Laboratory
Abram R. Jacobson	Los Alamos National Laboratory
Tom Jarboe	Los Alamos National Laboratory
John L. Johnson	Princeton University
Abe Kadish	Science Applications, Inc.
Ichiro Kawakami	Nihon University
Robert A. Krakowski	Los Alamos National Laboratory
H. Ralph Lewis	Los Alamos National Laboratory
Carl Lilliequist	Los Alamos National Laboratory
Ralph Linsker	Princeton Plasma Physics Laboratory
H. C. Lui	Columbia University
Wallace M. Manheimer	Naval Research Laboratory
George J. Marklin	University of Maryland

William Matthaeus   College of William and Mary

George H. Miley   University of Illinois

Guthrie Miller   Los Alamos National Laboratory

J. P. Mondt   Los Alamos National Laboratory

David C. Montgomery   College of William and Mary

Ronald Moses   Los Alamos National Laboratory

Don Monticello   Princeton University

Gianfranco Nalesso   University of Padua

Richard Nebel   Los Alamos National Laboratory

A. A. Newton   Culham Laboratory

Michio Okabayshi   Princeton Plasma Physics Laboratory

Thomas Oliphant   Los Alamos National Laboratory

Sergio Ortolani   University of Padua

Ken D. Partain   General Atomic Company

Francis W. Perkins   Princeton Plasma Physics Laboratory

James A. Phillips   Los Alamos National Laboratory

Warren Quinn   Los Alamos National Laboratory

S. Neil Rasband   Brigham Young University

Allan H. Reiman   Cornell University

Keith Roberts   Culham Laboratory

Harvey Rose   Los Alamos National Laboratory

Michael G. Rusbridge   UMIST (Manchester, UK)

Michael J. Schaffer   General Atomic Company

Theo J. Schep   FOM - Jutphaas

Dalton Schnack   Lawrence Livermore National Laboratory

Kurt F. Schoenberg   Los Alamos National Laboratory

Anthony Sgro   Los Alamos National Laboratory

W. R. Spears   Culham Laboratory

Ross L. Spencer   Los Alamos National Laboratory

J. Bryan Taylor   Culham Laboratory

Keith S. Thomas   Los Alamos National Laboratory

Alan M. Todd   Grumman Aerospace Corporation

Leaf Turner   Los Alamos National Laboratory

William C. Turner   Lawrence Livermore National Laboratory

Robert G. Watt   Los Alamos National Laboratory

Michael R. C. Watts   Culham Laboratory

Paul Webber   Los Alamos National Laboratory

Tomejiro Yamagishi   General Atomic Company

CONTENTS

SESSION 2B - RELATED CONCEPTS

Chairman: G. C. Goldenbaum
           University of Maryland

SESSION 3A - RFP STARTUP

Chairman: R. W. Moses, Jr.
           Los Alamos National Laboratory

SESSION 4A - HEATING AND TRANSPORT OF REVERSED-FIELD PINCH DISCHARGES

Chairman: Richard S. Christian
           Purdue University

SESSION 5A - RELAXATION AND TURBULENCE OF REVERSED-FIELD PINCH DISCHARGE

Chairman: D. Montgomery
           College of William and Mary

SESSION 5B – POSSIBILITIES FOR INTERNATIONAL COORDINATION OF THE REVERSED-
         FIELD PINCH EFFORT

Chairman: K. V. Roberts
            Culham Laboratory

This session consisted of a discussion; no written papers were submitted.

SESSION 5C – SUMMARY AND DISCUSSION

PROCEEDINGS OF THE REVERSED-FIELD PINCH THEORY WORKSHOP

April 29 - May 2, 1980

Held at

Los Alamos National Laboratory
Los Alamos, New Mexico 87545

Compiled by

H. Ralph Lewis

ABSTRACT

The Reversed-Field Pinch Theory Workshop was held in

Los Alamos during April 29 - May 2, 1980. The

Proceedings contain a table of contents, which lists the

papers and authors in each session, a list of attendees,

and copies of the contributed papers.

PHYSICS CONSIDERATIONS OF THE REVERSED-FIELD PINCH FUSION REACTOR[*]

R. L. Hagenson
Science Applications, Inc.
Ames, Iowa 50010
and
R. A. Krakowski
University of California
Los Alamos Scientific Laboratory
Los Alamos, New Mexico 87545

ABSTRACT

A conceptual engineering design of a fusion reactor based on plasma confinement in a toroidal Reversed-Field Pinch (RFP) configuration is described. The plasma is ohmically ignited by toroidal plasma currents which also inherently provide the confining magnetic fields in a toroidal chamber having major and minor radii of 12.7 and 1.5 m, respectively. The DT plasma ignites in 2-3 s and undergoes a transient, unrefueled burn at 10-20 keV for ~ 20 s to give a DT burnup of ~ 50%. Accounting for all major energy sinks yields a cost-optimized system with a recirculating power fraction of 0.17; the power output is 750 MWe(net).

I. INTRODUCTION

The conceptual Reversed-Field Pinch Reactor (RFPR) study[1] has emphasized the development and evaluation of a realistic reactor-plasma model; an extensive parameter study based on this model has focused on a system with minimum power cost. Two major priorities and/or constraints are imposed. First, the engineering system uses only conventional technology when possible, and, secondly, the ease of plant maintenance is stressed. The first-wall/blanket consists of a water-cooled copper and stainless-steel structure, with tritium breeding occurring in a granular-Li_2O packed bed. A direct-cycle, low-superheat steam system is proposed, thereby eliminating an expensive secondary coolant loop. Ohmic heating of the DT plasma to ignition is inherently made possible by the RFP confinement scheme. A batch-burn (unrefueled) operation is also chosen to eliminate advanced ash/impurity-control (divertors) and fueling systems, although steady-state operation is not necessarily precluded by the RFP approach. Confinement scaling for the RFP is independent of toroidal aspect ratio, allowing a mechanically open structure and a more easily maintained system.

II. PHYSICAL PRINCIPLES

Like the tokamak, the RFP is a toroidal, axisymmetric confinement device. Both systems use a combination of poloidal, B_θ, and toroidal, B_ϕ, magnetic fields to confine a plasma in a minimum energy state. The poloidal field for both systems is created by inducing through transformed action a toroidal

---

current, I_ϕ, within the plasma column; the toroidal field is created by external coils. Figure 1 compares the radial field and pressure profiles for both the RFP and tokamak systems. Toroidal equilibrium can be provided by either a conducting shell located near the plasma, an external vertical field or a combination of both schemes. The RFP requires a conducting shell for plasma stabilization against unstable magnetohydrodynamic (MHD) modes with wavelengths in excess of the shell radius, r_w, whereas the tokamak may not necessarily be subjected to this requirement. Localized MHD modes in the RFP are suppressed by the strongly sheared magnetic fields caused by a slight reversal of the toroidal field at the plasma edge. Although the tokamak may not require a conducting shell near the plasma column, avoidance of the kink instability establishes specific requirements on the relative magnitude of B_θ, B_ϕ, the plasma radius, r_p, and the major radius of the torus, R. Specifically, for the tokamak the parameter $q = (r_p/R)(B_\phi/B_\theta)$ must be greater than unity. The criterion $q > 1$ assures that MHD kink modes with wavelengths in excess of the major circumference will be stable. Experimental values of $q \sim 2$-3 at the plasma edge are required for stable tokamak operation. On the other hand, the RFP operates with q less than unity, q actually falling through zero and becoming negative outside the plasma region. The RFP approach essentially "differentiates away" the $q > 1$ constraint imposed on tokamaks and in its place requires $dq/dr \neq 0$. The positive implications of the RFP stability criterion are:

- The aspect ratio R/r_p can be chosen solely on the basis of engineering considerations and convenience (i.e., desired power output and related economic considerations).

- The β limits predicted for the RFP are at least 10 to 50 times greater than $q > 1$ systems if ideal MHD theories are used. The predictions of resistive MHD theories reduce this factor to the range 3-10.

- The plasma may be ignited by ohmic heating alone.

- The confinement of high-to-moderate β plasma is achieved primarily by poloidal fields, which characteristically decrease with increased distance from the plasma, thereby reducing fields and stresses at the magnets.

- The use of highly sheared fields near the plasma edge for the RFP configuration makes possible a "vacuum" (low current) region between the plasma and first wall.

Although implications of these RFP characteristics are significant from a technological viewpoint, these benefits are accompanied by the need for a passively conducting first wall. Additionally, the energy that must be expended in establishing and maintaining the near minimum-energy RFP plasma is not known, but if this setup/sustenance energy is significant, operation as an ohmically-heated ignition device is made more difficult. Lastly, little or no consideration has been given by this study to the physics implications of fueling and ash-removal systems required for a steady-state operation; the RFPR design presented here is based on a long-pulsed (25-30 s) batch-burn operation. The favorable energy balance (recirculating power fraction is 0.17) computed for the batch-burn mode of operation reflects an efficient use of magnetic field energy that is characteristic of the RFP; technological issues associated with pulsed superconducting magnets and energy transfer/ storage systems, however, require further development and study.

III. PLASMA BURN AND REACTOR DESIGN POINTS

This section summarizes the physics models and computational results used to describe reactor startup, thermonuclear burn and postburn plasma quench. The design presented herein is based on a profile-averaged, zero-dimensional (point) plasma model. The poloidal and toroidal magnetic-field profiles within the plasma are described by the Bessel functions $A_\theta J_1(\alpha r)$ and $A_\phi J_0(\alpha r)$, respectively, which show good agreement with calculated MHD-stable profiles. The constants A_θ and A_ϕ are determined by the conservation of total current and flux within the plasma column. Enforcing pressure balance and integrating over the isothermal plasma cross-section results in the spatially-averaged parameters used for the calculation of burn dynamics. A numerical calculation of the multi-species plasma (ions, electrons, and alpha particles) follows the plasma radius (i.e., field reversal point) with time in conjunction with the voltages and currents in both the plasma and associated electrical circuitry. Alpha-particle thermalization using a Fokker-Planck formalism, ohmic heating using classical resistivity, radiation (Bremsstrahlung, cyclotron, and line) losses, and anomalous (radial) thermal conduction and particle diffusion are included in this time-dependent model. As part of a continuing parametric analysis and refinement of the RFPR concept, a more realistic one-dimensional (radial) plasma model has been developed and applied[2] to the point design reported herein. The total power output computed by the one-dimensional simulation is within 5% of that determined by the zero-dimensional model.

The startup time is taken as 10% of the energy containment time, which is estimated to be ~ 1 s for a reactor plasma. A conducting copper first wall, with an electrical skin depth equal to the startup time, stabilizes the plasma and promotes field reversal during the 0.1-s startup phase. An initially, uniform toroidal field, $B_{\phi 0}$, is superposed onto an increasing toroidal plasma current and results in a field configuration that is similar to a tokamak. This initially q-stabilized system (i.e., q > 1) must be transformed into a high-β RFP configuration by proper field programming, self-reversal of the magnetic fields or a combination thereof (i.e., assisted self-reversal). Stability and quiescence during this setup phase seems unlikely, and turbulence similar to or greater than that exhibited in tokamaks may result. Energy losses incurred during this startup are not known and have not been explicitly included.

Burn cycles were adopted that operate near the minimum-energy plasma state, as defined by Taylor[3], and beta limits established by resistive MHD calculations[1] were enforced. Operating near the RFP minimum-energy state requires[4] $\Theta = 1.5-2.0$ and $F = 1.0$. Maximum poloidal betas of 0.25-0.40 are inferred from resistive-MHD stability calculations. Transport scaling for RFP plasmas is unknown, although use of accepted tokamak scaling gives an anomalous electron thermal conduction with an energy confinement time $\tau_E \sim 200\ \tau_{Bohm}$[5]. Anomalous transport would be caused by local instabilities and may be the result of pressure-driven modes, such as the resistive g-mode. As β_θ is increased transport would be enhanced, and a poloidal-beta limit at which the burn temperature would saturate results, yielding thermal stability. The use of an enhanced loss given by $\tau_E = 200\ \tau_{Bohm}$ or a loss mechanism that is driven explicitly by a limiting beta[6] give similar results for reactor sizes of economic interest ($r_w = 1-2$ m).

The burn trajectory shown in Fig. 2 is used as the reference case for evaluation of reactor performance. This thermally stable burn achieves ignition in ~ 3 s. The ~ 15-s batch burn is followed by a 2-3 s quench period during which time the trapped magnetic field and post-burn plasma would be thermally dissipated at the first wall. Flushing the system with neutral gas, while continuously evacuating the alpha-particle ash, readies the chamber for the

4

subsequent burn cycle. The burn cycle is sustained for 21.6 s, and 5 s is allowed for evacuation and refueling; the total cycle would be 26.6 s.

IV. REACTOR ENGINEERING AND TECHNOLOGY

The physics principles described in Sec. II and the burn simulations described in Sec. III have been combined in a parametric study to give a cost-optimized design point by which key engineering and technological issues could be examined. Table I gives a summary description of key reactor parameters that have emerged from this study. A parallel but independent, reactor study[7-8] yields plasma characteristics and reactor performance close to those reported here.

The RFPR design presented here would operate as an unrefueled (batch-burn) system in which preionization, field reversal and ignition by ohmic heating would occur in a run-up period $\tau_R \simeq 0.1$ s. The transient burn would occur for $\tau_B = 21.6$ s in a 12.7-m major radius torus with a first-wall radius equal to 1.5 m. Approximately 50% of the DT fuel would be consumed, yielding a total thermal energy each pulse of 79.8 GJ (3000 MWt average thermal power) and an average fusion neutron wall current of 2.7 MW/m^2. The recirculating power fraction for the 750-MWe(net) plant would be $\varepsilon = 1/Q_E = 0.17$.

The power-plant embodiment that has been developed on the basis of this reactor operation is depicted in Fig. 3. The 1.5-m-radius plasma chamber is formed by 40, 2-m-long first-wall/blanket/shield modules, four of which are depicted in Fig. 3. The 12.7-m major-radius torus is constructed within a vacuum tunnel and is completely detached from the PFC system. A separate water-cooled copper first wall (20-mm thick) provides an electrically conducting shell and operates near the blanket temperature (530 K).

An important objective of the preliminary plant layout depicted in Fig. 3 is to quantify the reactor maintenance procedure. The two major coil systems that drive the RFPR would be permanently fixed. The PFC system would consist of large, superconductors (NbTi/Cu/stainless-steel) that encircle the inner and outer major radii of the reactor. The PFC system would be permanently fixed to structure associated with the walls of the toroidal vacuum tunnel and would not interfere with procedures needed to remove any of the 40, 2-m-long modules. The TFC structure would be fixed and would be sufficiently open to permit removal of blanket/shield modules by simple translational and vertical motions. The TFC system consists of twenty low-field (2.0-T) circular coils that are positioned over alternate reactor modules; each NbTi/Cu/stainless-steel TFC would have a 3.6-m radius, a 1.2-m length and 0.5-m thickness. The current distribution in the PFC system would assure that the vertical field component is sufficient to maintain the plasma in toroidal equilibrium. Small, normal-conducting feedback-stabilization coils would be placed between the blanket and shield these slow-pulsed coils (< 10-Hz) are considered part of the reactor module assembly.

V. CONCLUSIONS

As for most conceptual fusion reactor studies, the credibility and feasibility of most engineering systems is determined in large part by the physics assumed to generate the reactor plasma model and related energy balances. Energy loss from the plasma incurred during initiation and sustenance of the field-reversed configuration represents the major uncertainty. The plasma/field/first-wall response during the rundown phase of the long-pulse power cycle presents a second important uncertainty. Within the constraints of the assumptions made for both energy confinement and rundown processes, feasible technical designs for all engineering systems have been identified. Furthermore, sensitivity studies of the influence of key physics (i.e., beta) and engineering parameters (i.e., energy transfer/storage efficiency) indicate

that a relatively safe margin for error exists before a serious degradation in RFPR system performance and cost is incurred.

In many ways the RFPR presents desirable system on which to examine the technical and economic feasibility of magnetic fusion power, given a favorable resolution of the abovementioned physics issues. The results of this study indicate that an efficient power plant may emerge from the relatively low technology requirements embodied in ohmic heating and batch-burn operation. Specifically, the postponement of advanced heating, fueling and ash-removal systems from the first-generation power plant, while simultaneously operating with a strong promise of high efficiency and low cost, could lead to a lower-risk approach to fusion power. Once uncertainties are resolved and experience is gained through batch-burn operation, improvement of system performance can be achieved by incorporating fueling and ash-removal systems, leading ultimately to a steady-state power plant. These improvements would be achieved from the stronger technology base and operating experience that could be built from economic, batch-burn operation.

REFERENCES

1. R. L. Hagenson, R. A. Krakowski, and G E. Cort, "The Reversed-Field Pinch Reactor (RFPR) Concept," Los Alamos Scientific Laboratory report LA-7973-MS (1979).

2. R. A. Nebel, R. L. Hagenson, R. W. Moses, and R. A. Krakowski, "Comparison of Zero-Dimensional and One-Dimensional Thermonuclear Burn Computations for the Reversed-Field Pinch Reactor (RFPR)," Los Alamos Scientific Laboratory report LA-8185-MS (1980).

3. J. B. Taylor, "Relaxation of Toroidal Discharges," Proc. 3rd Topical Conference on Pulsed High Beta Plasmas," Culham, United Kingdom, 59 (1975).

4. A. A. Newton, Li Yin-An, J. W. Long, and B. C. Yeung, "Numerical Investigation of Reversed Field Pinches," Proc. 3rd Topical Conference on Pulsed High Beta Plasmas," Culham, United Kingdom, 323 (1975).

5. R. L. Hagenson and R. A. Krakowski, "A Cost-Constrained Design Point for the Reversed-Field Pinch Reactor," Am. Nucl. Soc. Third Topical Mtg. on the Technology of Cont. Nucl. Fus., Santa Fe, New Mexico, 1, 90-100 (1978).

6. B. C. Yeung, J. W. Long, and A. A. Newton, "Reactor Burning Calculations for a Model Reversed Field Pinch," Proc. 3rd Topical Conference on Pulsed High Beta Plasmas," Culham, United Kingdom, 575-579 (1975).

7. R. Hancox, M. Bagatin, L. J. Baker, S. Bobbio, H. J. Crawley, and P. A. Davenport, "A 600 MW(e) Reversed Field Pinch Reactor Study," in Fusion Reactor Design Concepts (IAEA Workshop on Fusion Reactor Design, Madison Wisconsin, 1977), IAEA, Vienna 319 (1978) (Also Culham Laboratory report CLM-P 501).

8. R. Hancox and C. R. Walters, "A Reversed Field Pinch with Superconducting Windings," Proc. 7th International Conference on Plasma Physics and Controlled Nuclear Fusion Research, Innsbruck, Austria (1978).
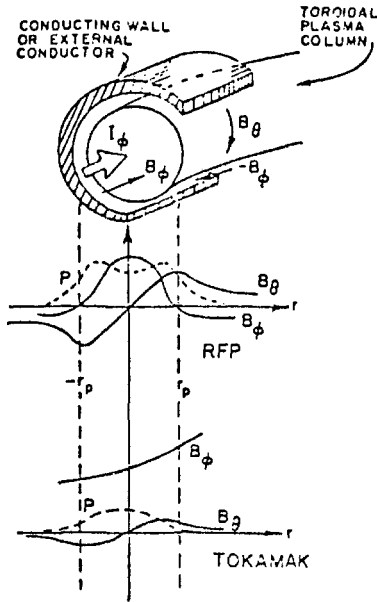
Fig. 1. Comparison of magnetic and pressure profiles for a dq/dr ≠ 0 stabilized RFP and a q > 1 stabilized tokamak.

Fig. 2. RFPR (superconducting coils, air-core system burn parameters using confinement time $\tau_E = 200 \, \tau_{Bohm}$. The burn trajectory is in good agreement with that required by the high-B model for a minimum-energy configuration.

Table I
Summary Description of RFPR Design Parameters

Parameter	Value
First-wall radius, r_w(m)	1.5
Major radius, R(m)	12.7
Toroidal plasma current, I_ϕ(MA)	20.0
Toroidal field at the coil, $B_{\phi c}$(T)	2.0
Poloidal field at the coil, $B_{\theta c}$(T)	2.0
Toroidal coil energy, $W_{B\phi}$(GJ)	3.7
Poloidal coil energy, $W_{B\theta}$(GJ)	11.0
Field rise time, τ_R(s)	0.1
Burn time, τ_B(s)	21.6
Cycle time, τ_C(s)	26.6
Average fuel burnup, f_B	0.5
Average plasma density, $n(10^{20}/m^3)$	2.0
Average plasma temperature, $T_{i,e}$(keV)	15
14.1-MeV neutron current at first wall, I_w(MW/m²)	2.7
Engineering Q-value, Q_E	5.8
Recirculating power fraction, $\epsilon = 1/Q_E$	0.17
Average blanket power density, P_{BLK} (MW/m³)	4.7
Average system power density, P_{SYS} (MW/m³)	0.9
Total thermal power, P_{TH}(MWt)	3000
Net electrical power, P_E(MWe)	750
Net plant efficiency, $\eta_p = \eta_{TH}(1-\epsilon)$	0.25

Fig. 3. Isometric view of RFPR power plant.

RECENT CULHAM REACTOR STUDIES WITH RFP RELEVANCE

W.R. Spears
Culham Laboratory, Abingdon, Oxon. OX14 3DB, U.K.
(Euratom/UKAEA Fusion Association).

1. INTRODUCTION

The Culham based design of a Reversed Field Pinch Reactor (RFPR) with super-conducting magnetic field windings was undertaken in 1977/78 (1). During 1979, in order to put this RFPR design in perspective the design of a Tokamak has been developed operating with a pulsed burn under the same engineering constraints as the Culham RFPR. More recently, the Culham and LASL (2) concepts of the RFPR have been compared. This note summarises briefly these reactor comparisons, drawing particular attention to the key areas of plasma behaviour in which un-certainties and a lack of understanding are hindering further progress in the engineering design of the RFPR.

2. THE CULHAM RFPR DESIGN

Between 1975 and 1978 detailed conceptual studies were carried out to define the physical conditions, technological requirements and optimum parameters for econ-omic operation of a reactor exploiting where possible the special features of the RFP. The first design (3-7) employed a magnetic field system with normal wind-ings and consequently incurred considerable cost and energy penalties. The pres-ent design with superconducting windings was therefore developed. Reactor para-meters are shown in Table I.

Simulations of the plasma burn (using an ideal MHD stable field profile due to Robinson (8) in which $\theta = 2(F=-0.75)$ and $\beta_\theta=0.35$) showed that for a significant value of energy multiplication factor Q (thermal energy output/circulating energy to sustain plasma cycle) a plasma temperature control mechanism is required. Since, at present, no divertor or refuelling concept has been suggested for the RFP the burn must be pulsed, and this mechanism must produce an energy contain-ment time during the plasma burn, τ_E much shorter than the burn time, τ_b, which itself must be shorter than the particle containment time τ_p. Typically τ_p/τ_E must be greater than 10, and calculations show that Q is maximised at a burn temperature of 10 keV with fractional burnup of 30%. No such mechanism has yet been observed, but it is thought that, controlled plasma expansion and compression or instabilities dependent on beta limits may produce sufficiently rapid energy expulsion from the plasma.

During the establishment of the RFP configuration by the process of self-reversal, plasma current must be raised to its operating value in a time which is a com-promise between the high capital costs and energy losses associated with rapid energy transfer and switching systems and the increasingly significant plasma magnetic energy dissipation incurred by slower creation. A time of 0.5 seconds was chosen for these studies.

An intrinsic advantage of the RFP configuration is the possibility of sufficient-ly rapid ohmic heating to ignition provided certain restrictions are observed. These restrictions, first formulated by Lawson (4), require that the product of neutron wall loading and the cube of the plasma radius be less than some number dependent on plasma field profiles and operating temperature. The total particle, conduction, impurity radiation and charge exchange energy losses must also be much less than bremsstrahlung. For a heating time much less than the burn time these relationships lead to the choice of a wall radius of 1.5m in the reactor design.

The magnetic and kinetic energy recoverable from the RFP configuration during controlled rundown at the end of the burn is an important factor in the circulating energy of the reactor and needs further study. Culham studies have assumed that 40% of the energy inside the first wall may be recovered by plasma expansion against the magnetic field, the remainder being dissipated as heat on the first wall.

Ideally, the production of the RFP configuration takes place within a perfectly conducting shell which conserves toroidal flux, maintains equilibrium and supresses kink instabilities. In a practical system flux and equilibrium can be controlled by currents in external conductors, provided gaps exist in the shell to permit field penetration. In the Culham design, a passive 2.5 cm thick copper shell was proposed for controlling short (0.5 sec.) timescale instabilities with longer timescale control afforded by actively driven windings behind the blanket. For the shell to be effective its assembled length must be much greater than its radius, and in this design the length has been assumed to be four times the plasma radius.

Engineering requirements, in addition to those implied by the plasma physics constraints described above were placed on the reactor design. An electrical power output of 600 MW was chosen to reflect the desirability of constructing small units. To produce a tolerable coolant temperature rise in the first wall, which receives greater than 25% of the pulsed plasma heat output, requires the choice of a low mean neutron wall loading (1.5 MW/m^2). For thermal energy conversion efficiency to be as high as possible the Culham solution was to insert a high temperature radiation shield between the plasma and the passive shell which is thermally insulated and operated at lower temperature to preserve its conductivity. This, with the assumption that the blanket and inner shield would be maintainable in a series of simple, remotely controlled operations has led to a design in which for an acceptably low(4% peak to peak) field ripple, toroidal field coils and poloidal field coils must be movable to withdraw a blanket segment. Since both poloidal and toroidal field systems are pulsed, they are as close to the plasma as possible to minimise energy storage and transfer requirements but poloidal field windings do not link the toroidal field coils.

Sensitivity analyses performed on the Culham design show that to maximise energy multiplication and minimise cost the energy per reaction, plasma pressure ratio β_θ and mean neutron wall loading must be maximised.

3. COMPARISON WITH LASL DESIGN

The reactor parameters shown in Table I were derived by independent optimisation studies performed by the two groups based at Culham and LASL. Despite the uncertainties of the plasma physics models used and differences in the assumed engineering constraints these designs have many similarities. The major difference between the designs occurs in the way in which the passive shell is incorporated.

In the Culham design, with separate helium cooled radiation shield and passive shell, thermal conversion efficiencies of 40% may be possible. However, thermal insulation is required between the shell and the adjacent radiation shield and blanket, and because of the difficulty of welding shell segments together behind a radiation shield, segment length is determined by shell effectiveness leading to a horizontal maintenance procedure between movable toroidal and poloidal field coils.

9

In the LASL design a water cooled combined radiation shield and shell is used. Although the shell aids neutron multiplication it cannot be too thick without impairing tritium production and a thickness of 2 cm has been assumed. With this shell 38% of the reactor thermal output is dissipated in the first wall/ shell resulting in higher temperature operation, lower thermal conversion efficiency, and control over instabilities on only a 0.1 second timescale. The power consumed in active feedback in this design is therefore likely to be higher than the 14 MW estimated for the Culham design. Note, however, that the shells of both designs are capable of controlling instabilities on the timescale of their respective current risetimes. The shorter shell segments ($\sim$ 2m) of the LASL concept, which may be welded together to form an adequately effective shell if required,allow a vertical maintenance procedure between fixed toroidal and poloidal field coils, but the extent to which the number of toroidal field coils and the distance of poloidal field coils from the plasma can be reduced depends to a large extent on the tolerable levels of toroidal field ripple at the outer plasma edge.

The cost and energy analysis of the designs are in quite good agreement. Recirculating power requirements are $\sim$ 20%, and are dominated by plasma energy losses during startup and rundown. Before these designs develop further it is essential that these losses be quantified and minimised.

4. COMPARISON WITH TOKAMAK

Any RFP/Tokamak comparison can only be tentative at this stage, since experimental confirmation of Tokamak physics is further advanced than that of the RFP. While significant effort is now being made to extend the Tokamak plasma burn to quasi-steady state no studies have been carried out on the application of divertors and refuelling to the RFP. For these reasons a Tokamak design (9) has been made at Culham, using the same ground rules as were used for the Culham RFPR study, and in particular operating at the same neutron wall loading and net power output. The main parameters of this device are also shown in Table I.

In the RFP, there is little restriction on plasma aspect ratio and a small minor radius and high toroidal current density should permit rapid ohmic heating to ignition. In the Tokamak, a tight aspect ratio is needed for stability, and this is achieved using a larger minor radius and vertical plasma elongation (b/a = 1.68) to give the same wall area as the RFP. For an adequate safety factor at the plasma edge, plasma current cannot be too large and ohmic heating is insufficient to reach ignition. Additional heating (neutral injection assumed) must therefore be provided.

The tighter aspect ratio of the Tokamak reduces the mutual inductance of plasma and primary leading to higher primary current in the Tokamak despite the lower plasma current. The equilibrium field of the non-circular Tokamak plasma is also larger than for the circular RFP. Although both devices have similar toroidal field values on the plasma centreline, in the RFP only the small reversed field at the plasma edge needs to be supplied by the external coils, whereas in the Tokamak the similarity of vacuum and plasma toroidal fields results in high field at the coil. However, the steady state toroidal field systems of the Tokamak can be of simpler construction as pulsed fields are greatly reduced. Despite this, the magnetic confinement system as a whole is cheaper in the RFP than in the Tokamak as would be expected from the difference in total beta values.

10

The energy multiplication factors computed for the Tokamak and the RFPR are very similar. Losses of magnetic and kinetic energy during plasma current startup and rundown are more than ten times larger for the RFP than for the Tokamak if scaling laws based on ZETA results can be extrapolated to reactor dimensions. This is an important area of understanding where the possible benefits of the RFP are being held back by the lack of knowledge of the physical processes involved. The cost analyses of the two devices, though tentative, seem to indicate that not only can the magnetic confinement of the RFP be cheaper than that of the Tokamak, but also the lack of additional heating produces a further cost saving. Energy storage and transfer requirements of the two devices are also similar with the pulsed poloidal and toroidal field supplies of the RFP balancing those for the poloidal field and neutral injection in the Tokamak.

5. UNRESOLVED PHYSICS QUESTIONS WITH MAJOR REACTOR DESIGN IMPLICATIONS

Listed below are some of the major questions which need to be answered before RFP reactor design can proceed further.

a) Is a passive shell necessary? If yes, how long and thick must it be to be effective? What are the requirements of active feedback and the effect of gaps?

IMPLICATIONS: Blanket segmentation; Maintenance method and frequency; Thermal efficiency; Vacuum pumping; Energy of active control; First wall design; Blanket multiplication.

b) How can exhaust and refuelling be carried out on the RFP configuration?

IMPLICATIONS: Wall loading; Burn time; Blanket, shell and magnet design.

c) How do plasma losses during startup and rundown scale, and can they be controlled in magnitude? What is the cost (energetically and financially) of such control? How much plasma energy is recoverable at the end of the burn?

IMPLICATIONS: Energy transfer and storage; Energy multiplication factor; Wall loading.

d) What is the maximum toroidal field ripple at the outer plasma edge?

IMPLICATIONS: Maintenance method and availability; Magnetic energy requirements.

e) Is ohmic heating to ignition possible and sufficiently rapid?

IMPLICATIONS: Wall radius; Wall loading; Energy multiplication factor.

f) Can a mechanism providing $\tau_E < \tau_b < \tau_p$ be demonstrated?

IMPLICATIONS: Energy multiplication factor.

---

6. ACKNOWLEDGEMENTS

7. REFERENCES

1. HANCOX, R., WALTERS; C.R. Proc. 7th Int. Conf. on Plasma Physics and Controlled Nuclear Fusion Research, Innsbruck (1978).

2. HAGENSON, R.L., KRAKOWSKI, R.A., CORT, G.E. Los Alamos Scientific Laboratory Report LA-7973 MS (1979).

3. HANCOX, R. et al. Proc. IAEA Workshop on Fusion Reactor Design, Madison (1977).

4. LAWSON, J.D., Culham Laboratory Report CLM-R171.

5. HANCOX, R., SPEARS, W.R., Culham Laboratory Report CLM-172 (1977).

6. HOLLIS, A.A., MITCHELL, J.T.D., Culham Laboratory Report CLM R173 (1977).

7. BOBBIO, S. et al, Padua University Report UPee 77/05 (1977).

8. ROBINSON, D.C., Plasma Physics 13 (1971) 439.

9. SPEARS, W.R., HANCOX, R., Culham Laboratory Report CLM-R197 (1979).

TABLE I

COMPARISON OF CULHAM RFPR, LASL RFPR AND CULHAM PULSED TOKAMAK DESIGNS

Parameter	Culham RFPR	LASL RFPR	Culham Tokamak
Net output power (MWe)	600	750	600
Gross thermal power (MW$_t$)	1900	3000	1825
Thermal conversion efficiency	0.4	0.3	0.4
Major radius (m)	14.5	12.7	7.8
Minor radius (m)	1.5	1.5	2.0
Mean neutron wall loading (MW/m^2)	1.5	2.7	1.5
Toroidal plasma current (MA)	17	20	11
Average poloidal beta	0.35	0.3	2.5
Average total beta	0.19	0.20	0.08
Duration of current rise (s)	0.5	0.1	1.0
Duration of heating phase (s)	4	5	6
Duration of burn excluding heating (s)	25	19	27
Duration of full cycle (s)	37	27	41
Toroidal flux density on axis (T)	3.8	3.8	3.9
Toroidal flux density at coil (T)	-1.0	-2.0	8.3
Number of toroidal field coils	28	20	20
Primary current (MA)	28	32	68
Startup and rundown energy losses (GJ)	2.92	1.77	0.27
Energy storage requirement (GJ)	8.5	14.7	8.2
Recirculating power fraction	0.21	0.17	0.19
Direct specific cost ($/kWe)	1500	1100	1900

OHMIC HEATING AND IGNITION STUDIES

R. Gerwin, R. W. Moses, Jr., R. Spencer
Los Alamos Scientific Laboratory
Los Alamos, New Mexico 87545

R. A. Nebel
University of Illinois
Urbana, Illinois 61801

I. OHMIC HEATING MODEL

We perform an ohmic heating calculation for a fixed profile of minor radius, a, with $\beta \ll 1$. This procedure is meaningful because of the time scales involved. The characteristic heating time is $\tau_H \sim \beta a^2/D_\parallel$, where $D_\parallel \equiv (c^2/4\pi)\eta_\parallel$ with $\eta_\parallel$ being the parallel resistivity. The fields undergo resistive evolution over a much longer time of order $a^2/D_\parallel$, denoted by τ_η. (This occurs because there is no cylindrically symmetric resistive steady state with a reversal in $B_z(r)$.) The cross field particle diffusion takes place on a still longer time scale of order $\beta^{-1}a^2/D_\parallel$. (These estimates are valid provided $\beta\eta_\perp \ll \eta_\parallel$.)

The classical equipartition time, is approximately $\tau_{eq.} \sim \tau_H \beta^{-1}(c^2/\omega_{pi}^2 a^2)$. For $n > 10^{14}$ cm^{-3}, and $a > 20$ cm, one finds $\tau_{eq.} < \tau_{OH}$ provided $\beta > 2\%$. Equality of species temperatures then becomes a fair approximation which improves rapidly with increasing minor radius.

If the cross-field thermal conduction time, τ_E, were classical, it would be much longer than τ_H. Here, however, we assume this process to be anomalous, with $\tau_E \sim \tau_H$. Then, the simplification of a uniform temperature becomes relevant.

These considerations suggest that a low beta RFP retains its initial field profiles during the heating, which occurs with roughly equal and uniform species temperatures.

II. PRESSURE BALANCE

Suppose that the density profile $n(r) = n_o(1 - r^2/a^2)$ is a good representation for $r < a$, and that the toroidal field exhibits a small reversal near the edge of the plasma, so that $B_z(r) = B_o(1 - r^2/a^2)$ is also a good representation for $r < a$. Then one finds $B_\theta(r)$ from pressure balance, $\underline{J}(\underline{r})$ from $\nabla \times \underline{B}$, and the total heating rate from $\int_o^a \eta_\parallel J_z^2 2\pi r dr$.

Some useful relations with the poloidal beta are $\beta_p I^2 = $ const. $\times$ NT where N is the line density, T is the temperature, and I is the toroidal current; and $B_o = B_\theta(a)(2\beta_p/\beta_o)^{1/2}$, where β_o is the local beta at $r = 0$.

Pressure balance at $r = a$ can be written as $\beta_p^{-1} = 1 + (1.5\beta_o)^{-1}$, and also as $I(1-\beta_p)^{1/2} = $ const. $\times \phi_z/a$, where ϕ_z is the toroidal flux trapped within the plasma during the time τ_H. The latter form suggests that heating at constant current is untenable because the radius "a" increases, and heating at constant β_p is untenable because "a" decreases, losing wall stabilization. The best scheme would be to slightly increase I as β_p increases, thus holding the radius "a" constant.

III. POWER BALANCE

Evaluation of the heating rate as outlined above yields $D_\parallel B_o^2$ to a good approximation, for $\beta_o < 30\%$. (Here, we have suppressed a complicated function of β_o, $g(\beta_o)$, as a multiplicative factor that is close to unity. For more general profiles, there will occur yet another multiplicative shape factor of order unity in this expression.) Because of the short heating time at low beta compared to the resistive evolution time, power balance will be achieved while

13

the profiles retain their initial shapes. Ignoring impurity radiation, this (global) power balance condition is,

1) Ohmic heating + Alpha heating = Bremsstrahlung losses + $3NT/\tau_E$

where the final term represents anomalous thermal conduction losses. Here, substitute the above expression of the heating rate, and well-known expressions for radiation losses and heating by alpha particles. Take $\eta_\parallel$ (but not $\eta_\perp$) to be strictly classical (with $\ln(\Lambda) = 16$) and employ pressure balance and the relation between B_0 and $B_\theta(a)$. Then Eq. (1) can be put in the Pease form,

2) $\beta_p I(\text{amps}) = 2 \times 10^6/[1+(\tau_b/\tau_E) - (\tau_b/\tau_\alpha)]^{1/2}$

where $\tau_b = \text{const.} \times T^{1/2}/n_0$ is a characteristic cooling time due to radiation, and τ_α is a characteristic heating time due to alpha particle deposition. (One has $\tau_b/\tau_\alpha = \text{const.} \times \langle\sigma v\rangle_{DT} T^{-1/2}$). (Again a complicated function of β_0 has been suppressed as a multiplicative factor that is very close to unity for $\beta_0 < 30\%$, and Eq. (2) is more accurate at lower beta values.) This Pease relation requires neither a steady state, nor classical cross field resistivity.

Thus, if radiation were the only loss ($\tau_E \gg \tau_b$) and if there were no alpha deposition ($\tau_\alpha \gg \tau_b$), one would require a toroidal current of at least 4 MA to observe a power balance with $\beta_p < 50\%$ (for ideal MHD stability). For $\beta_p < 20\%$, one has $I > 10$ MA. The necessity for such high currents is softened by the presence of additional losses (τ_E).

IV. ALTERNATIVE REPRESENTATIONS OF POWER BALANCE
   Combining Eq. (2) with $\beta_p I^2 = \text{const.} \times NT$, one finds

3) $\beta_p N(\text{m}^{-1}) \, T(\text{keV}) = 6.3 \times 10^{20}/[1 + (\tau_b/\tau_E) - (\tau_b/\tau_\alpha)]$.

(The full expression with the complicated β_0-dependence is about 30% smaller at $\beta_0 \sim 30\%$, and Eq. (3) is more accurate at lower beta values.) Division of Eq. (2) by Eq. (3) yields

4) $\left(\dfrac{10^{15}}{3.1}\right) \, IN^{-1} \, (\text{amp-meter}) = T_{keV} \left(1 + (\tau_b/\tau_E) - (\tau_b/\tau_\alpha)\right)^{1/2}$

(The full expression with the β_0-dependence is about 15% larger at $\beta_0 \sim 30\%$, and Eq. (4) is more accurate at lower beta values.) This form is convenient for the display of power-balance and ignition conditions, as noted by the Padua group (S. Ortolani, private communication).
   Writing Eq. (3) more completely (in cgs units) as

$$\beta_p \, NT = \frac{9}{2} \frac{g(\beta_0)}{1+1.5\beta_0} \frac{c^2}{S_\perp b} \frac{1}{1 + (\tau_b/\tau_E) - (\tau_b/\tau_\alpha)}$$

where $\eta_\parallel^{-1} = 2S_\parallel T^{3/2}$, and where the radiation power density is $P_{brem} = bn^2 T^{1/2}$, with $S_\parallel$ and b constants, pressure balance is used to express β_p in terms of β_0, and β_0 can then be solved for. One finds

$$5) \quad \beta_0 = \frac{32}{3} g(\beta_0) \frac{\tau_b/\tau_\eta}{1 + (\tau_b/\tau_E) - (\tau_b/\tau_\alpha)}$$

14

(Note that $g(\beta_o)$ is close to unity.) Equation (5) displays the intimate connection between the beta value achieved in a state of power balance and the ratios of the fundamental time scales of the problem. Equation (5) also implies that the average ohmic heating rate per particle at power balance is given by $((3/32)\beta_o\tau_\eta)^{-1}$, which is consistent with a time-dependent analysis of the heating of the RFP. Thus, Eqs. (3, 4, 5) are all equivalent to the Pease relation, Eq. (2).

V. THE APPROACH TO POWER BALANCE

If Eq. (1) is replaced by a time-dependent equation, with the difference between the instantaneous heating and loss rates set to $3NdT/dt$, then one has a description of the temperature rise. Use of the power balance condition (denoted by "f" for final value) in yet another form,

$$g(\beta_{of}) = \frac{8}{3} S_\perp b \frac{n_o^2 \pi^2 a^2 T_f^2}{B_o^2 c^2} \left(1 + \frac{\tau_{bf}}{\tau_{Ef}} - \frac{\tau_{bf}}{\tau_{\alpha f}}\right) ,$$

and normalization of the temperature to T_f (normalized temperature called $\tilde{T}$), and normalization of the time to $(3/32)\beta_{of}\tau_{nf}$ (normalized time called τ), allows the resulting ordinary differential equation to be written as

$$6) \quad \frac{d\tilde{T}}{d\tau} = g(\beta_o)\tilde{T}^{-3/2} - g(\beta_{of}) \frac{1 - (\tau_b/\tau_\alpha)}{1 + (\tau_{bf}/\tau_{Ef}) - (\tau_{bf}/\tau_{\alpha f})} \tilde{T}^{1/2}$$

$$- g(\beta_{of}) \frac{(\tau_{bf}/\tau_{Ef})}{1 + (\tau_{bf}/\tau_{Ef}) - (\tau_{bf}/\tau_{\alpha f})} \frac{\tau_{Ef}}{\tau_E} \tilde{T} .$$

Here, $g(\beta_o)$ is practically unity for cases of interest. Also $\tau_E(T)$ is an arbitrary function of temperature and (τ_b/τ_α) is a known function of temperature. Field depletion has been neglected. Taking it into account changes the asymptotic approach to power balance to one where the balance is achieved at a finite time.

Eq. (6) is a convenient O.D.E. for describing temperature versus time during RFP heating. It depends on only three parameters, the final loss time ratio (τ_{bf}/τ_{Ef}), and the initial and final temperatures. It predicts that subignition states of power balance are approached in a manner that is insensitive to these three parameters. In particular, the time $(3/32)\beta_{of}\tau_{nf}$ is always a good measure of the time needed to approach power balance, as verified by our 1-D transport codes.

VI. NUMERICAL RESULTS: IGNITION, WETWOOD BURNERS, AND TEMPERATURE RISE

A. Ignition Conditions

The general structure of the ignition criterion is obtained by treating (τ_{bf}/τ_{Ef}) simply as a parameter. Then, the right side of the power balance condition, Eq. (4), looks like the hill plotted in Fig. 1a. The intersection points of the hill and the horizontal line representing a given value of the toroidal current-line density ratio, I/N, then determine the states of power balance. From Fig. 1a, we see two such states for one value of I/N. Their significance is seen in Fig. 1b where the rate of temperature rise, Eq. (6), is schmatically plotted. The S power balance point is stable and the U point is

15

unstable. These correspond to the two points in Fig. 1a. To achieve ignition (thermal run-away), make S coincide with U. From Fig. 1a, this is done by raising the value of (I/N) until the horizontal line just grazes the top of the hill. At that special value, ignition just becomes possible for the given loss parameter (τ_b/τ_E).

This view of ignition has been nicely checked by our self-consistent 1-D transport-burn code, RFPBRN (described elsewhere in these proceedings), as shown in Fig. 2, in which (I/N) and $\langle T \rangle$ were followed in time by the code, with (τ_b/τ_E) a given constant. Similarly, good agreement was obtained when both approaches incorporated a more sophistocated loss mechanism of the Bohm type. In the code, the electrical boundary conditions were continuously adjusted so as to keep the pinch radius fixed, as envisioned also in the analytic model.

We see that, for $\tau_E \sim \tau_b$, ignition generally requires (I/N) values on the order of 10^{-14} Ampere-meters, as pointed out by the Padua group (S. Ortolani, private communication). However, for very lossy systems ($\tau_b/\tau_E \gg 1$), it may be difficult to raise (I/N) enough to achieve ignition. We examine this possibility next.

B. Wetwood Burners

A wetwood burner state is an unignited condition of power balance that operates at the thermally stable point S. If such a state is formed at many kilovolts, the thermonuclear output may make the device sufficiently useful to be extensively studied experimentally. Here, we indicate the possibility of forming such states in modest devices.

As suggested by Eqs. (2) and (4), for fixed β_p, n, and T, small currents and small dimensions should be associated with lossy systems (large τ_b/τ_E). For example, we choose $\tau_b/\tau_E = 100$, T = 8 keV, and plot in Fig. (3) the allowed locus of power balance points from the analytic model equations. We see that very low beta ($\sim 1\%$) operation requires uncomfortably large dimensions and high currents at the lower densities, and requires rather large magnetic fields at the higher densities. However, at somewhat larger beta ($\sim 10\%$), we do indeed find power balance states of modest size (a ~ 0.25 m), modest current (I ~ 2 MA), and modest field strength ($B_0 \sim 30$ kgauss) for n $\approx 10^{14}$ cm^{-3}. So a very lossy system (by reactor standards) exhibits a power balance at 8 keV, with modest size, current, field strength, and reasonable beta value. In Fig. 4 we show verification by the code RFPBRN, running with the indicated losses by Bohm-type thermal conduction.

In Fig. 5, we see that a toroidal current of 2MA is sufficient to ensure that most of the alpha particles remain within the RFP configuration. This result was obtained by calculating their orbits in Bessel function fields. It depends only on the toroidal current, not on machine size.

C. Temperature Rise

It is of interest to follow the temperature rise during ohmic heating. In Fig. 6 we have plotted the solutions of Eq. (6), $\tilde{T}(\tau)$, with no alpha particle deposition and τ_E independent of T, for simplicity. The solutions are practically independent of the two available parameters (τ_{bf}/τ_{Ef}) and (T_i/T_f). The time $(3/32)\beta_{of}\tau_{nf}$ provides a good practical estimate of the time to reach a subignition state of power balance. Thus, a power balance at $\beta = 10\%$, T = 2 keV, in a machine with a = 50 cm would be reached in about 0.5 seconds.

The above situation does not change appreciably when τ_E depends on temperature, for example $\tau_E \propto T^{-1}$ or T^{-2}, and when alpha particle deposition is included. Thus, if one has some estimate of a representative loss ratio (τ_b/τ_E) then the above formulation even provides a quick estimate of the time needed to reach ignition.

VII. SUMMARY

A Pease-current relation characterizes a condition of global power balance in the RFP, even though the perpendicular resistivity may not be classical, and the RFP profile is not a true steady state. The (I/N) ignition criterion has been clarified and used to check our 1-D transport-heating code, RFPBRN. An unignited power balance state of over 5 keV has been shown to exist in a lossy RFP ($\tau_b/\tau_E = 100$) of modest size, current, and field strength with acceptable values of beta and density. Finally, a quasi-universal description of the temperature rise has been exhibited.
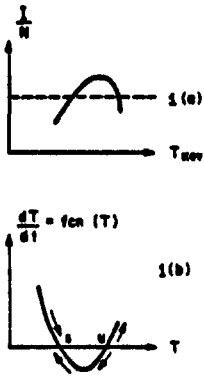
Fig. 1
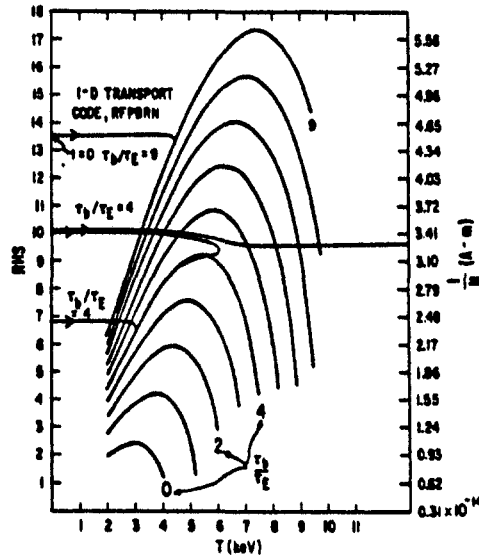
Fig. 2
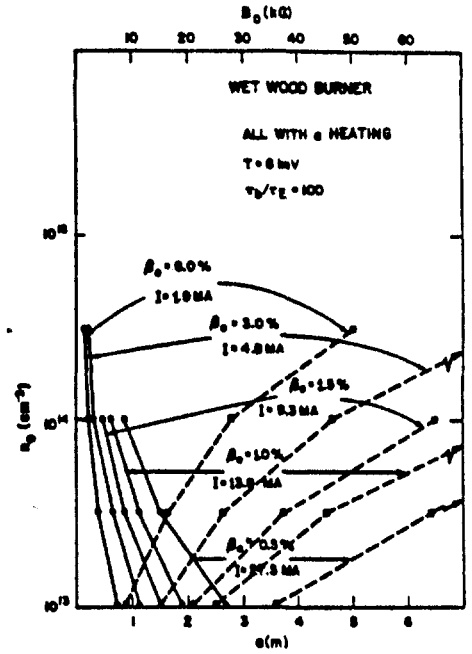
Fig. 3
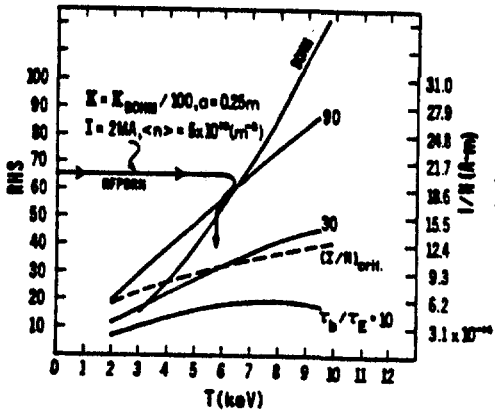
Fig. 4
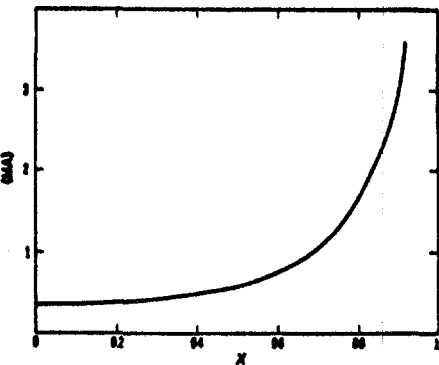
Fig. 5
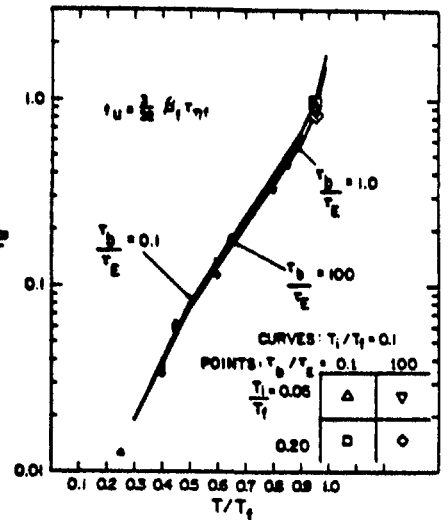
Fig. 6

FIGURE CAPTIONS

1-a. Schematic plot of Eq. (4). Solid curve is right side, dashed curve is left side, intersections represent solutions of Eq. (4).

1-b. Schematic plot of Eq. (6).

2. Solid hill curves represent actual right side of Eq. (4). Right vertical axis represents left side of Eq. (4), rescaled to show I/N directly. Horizontal curves show progression of I/N values during various code runs.

3. Analytic representations of possible power balance points for given T and τ_b/τ_E. Solid curves show minor radius vs. central density. Dashed curves show central field vs. central density.

4. Same format as Fig. 2. Dashed curve is (I/N) as a function of T such that toroidal current drift velocity equals ion thermal velocity. curve labelled "Bohm" represents right side of Eq. (4) when τ_E is related to Bohm-like thermal conduction as given by RFPBRN parameter I<.

5. Toroidal current (MA) necessary to trap a fraction (χ) of alpha particles born in a Bessel function RFP configuration.

6. Solutions, $\tilde{T}(\tau)$, of Eq. (6) neglecting alpha deposition, with τ_E = const., for several values of the final loss-time ratio, τ_b/τ_E, and the initial-to-final temperature ratio, T_i/T_f.

18

One Dimensional Burn Computations for RFPR*

by

R. A. Nebel and G. H. Miley
Fusion Studies Laboratory
University of Illinois

R. W. Moses and R. L. Hagenson
Los Alamos Scientific Laboratory

I. Introduction

Previous studies[1] of the Reversed Field Pinch Reactor (RFPR) have been done with a zero-dimensional or "point-properties" formulation which averages all plasma profiles over the radius. In order to allow a closer examination of the RFPR performance and explore other phenomena, a more realistic one-dimensional (radial) plasma model (RFPBRN) has been developed[2] and applied to RFPR.

The earlier global model assumes flat temperature profiles, classical particle confinement, and magnetic field profiles determined through a pressure balance model alone. In contrast, the one-dimensional model determines the temperature and field profiles self-consistently and allows for instability induced transport as well. It also checks the plasma profiles' local and global stability characteristics. A major objective of this study was to determine how these additional physical effects would influence the RFPR design. Also, this new code allowed a more detailed optimization of the RFPR. Both aspects of the study are discussed here.

II. The Model

RFPBRN is a three fluid (ions, electrons, and alphas) one-dimensional, Lagrangian mesh transport and stability code. A quasi-static assumption is used so the plasma evolution can be followed on a resistive time scale. Linear ideal MHD stability is then periodically monitored as the profiles evolve in time.

The solution is found by integrating the temperature, density, and field profiles forward in time and then adiabatically readjusting the mesh to satisfy pressure balance. A variable time step predictor-corrector numeric technique is used to solve the diffusion section. The degree of implicitness for the numerics is controlled externally.

Transport coefficients are assumed to scale classically[3] except for thermal conduction which, based on a review of data from Zeta experiments, is taken to be ~ 1/200th Bohm. The perpendicular resistivity also assumes Bohm-like scaling in regions where Suydam's stability criterion[4] is violated. The modeling in these regions is that of Christiansen and Roberts[5].

MHD stability is monitored for both global and local modes. Local stability is monitored using Suydam's criterion while gross modes are checked using Newcomb's form of the ideal MHD energy principle[5]. The energy principle is minimized directly by using a Rayleigh-Ritz trial function expansion with arbitrary coefficients. The technique has the advantage that is shows whether the plasma is unstable to modes with wide (non-localized) eigenfunctions as well as determining the plasma's absolute stability characteristics.

III. Results

A. Zero-Dimensional and One-Dimensional Comparison

In order to match the global model as close as possible, the plasma edge was required to be the reversal point and the radius varied as:

$$r_p (t) = r_p (t=o)/\sqrt{1-\beta_\theta (t)} \tag{1}$$

Initial conditions for temperature, density and field profiles were also taken consistent with the global model's pressure balance assumptions[6].

Results generally showed similar trends, the principle difference being that the 1-D code ignited faster, burned out quicker, and had lower

fractional burnup (see Fig. 1). All of these features can be attributed to profile effects. The lower burnup resulted in an overall reduction in the energy gain factor Q_p to about 3/5's of that predicted by the 0-D code. While this is a significant difference, the agreement is still considered "good" in view of the many differences between the two codes (See Table I).

Inclusion of Suydam induced turbulent transport flattened the density profiles but had little effect on plasma performance. The reason this effect was small is that the stable outer region provided confinement while the Suydam induced energy transport was already dominated by the assumed Bohm-like thermal conductivity (See Table II).

B. Optimized Burn

In view of the reduced energy gain predicted by the 1-D model, a decision was made to use it to optimize Q_p. The density was raised to increase the power level near the global simulation parameters. The toroidal and poloidal fields were then reduced to the marginal amount required to ignite the plasma. Poloidal β and global stability were checked to see if the plasma maintained stability (which it did).

The results of the optimization are shown in Table I where it is seen that Q_p was increased by a factor of two. The principle reason that Q_p was doubled is that the radially varying temperature profile allows ignition on the magnetic axis which then propagates radially through the plasma. This allows the current (magnetic field energy) required for ignition to be lower which in turn raises Q_p.

Summary

Studies of the RFPR have been done using a one-dimensional three fluid transport and stability code. Results have verified trends predicted by

previous global studies. However, inclusion of profile effects, princi-pally centerline ignition,has enabled the RFPR design to be optimized to obtain Q_p's as high as 20. Assuming classical parallel resistivity, global MHD stability can be maintained throughout the entire burn.

References

1. R. L. Hagenson, R. A. Krakowski, and G. E. Cort, "The Reversed-Field Pinch Reactor," Los Alamos report LA-7973-MS (1979).

2. R. A. Nebel, et al., "Comparison of Zero-Dimensional and One Dimensional Thermonuclear Burn Calculations for the Reversed Field Pinch Reactor (RFPR)," Los Alamos report LA-8185-MS (1980).

3. S. I. Braginskii, Reviews of Plasma Physics, (Edited by M. A. Leontovich, Consultants Bureau, New York (1965)), 1, 205-311.

4. B. R. Suydam, "Stability of a Linear Pinch," P 1354, USA (1958).

5. J. P. Christiansen and K. V. Roberts, Nuclear Fusion, 18, 181-197, 2 (1978).

6. R. L. Hagenson, "Preliminary Physics and Engineering Considerations for a Fusion Power Plant Based on Reversed-Field Z-Pinch (RFZP) Confinement," Los Alamos Report LA-UR-76-2190 (1976).
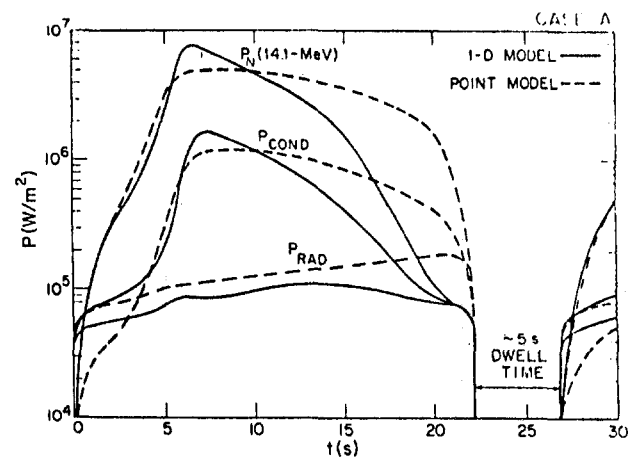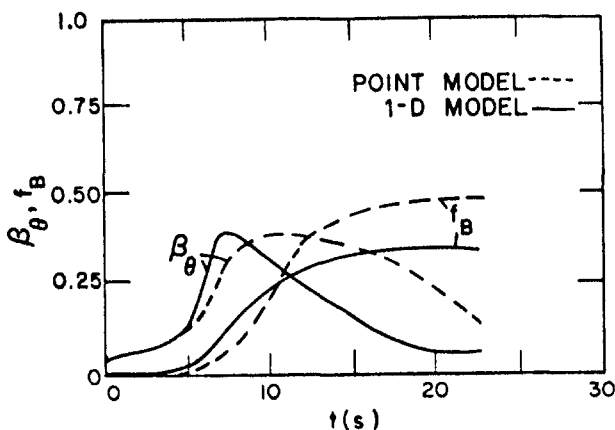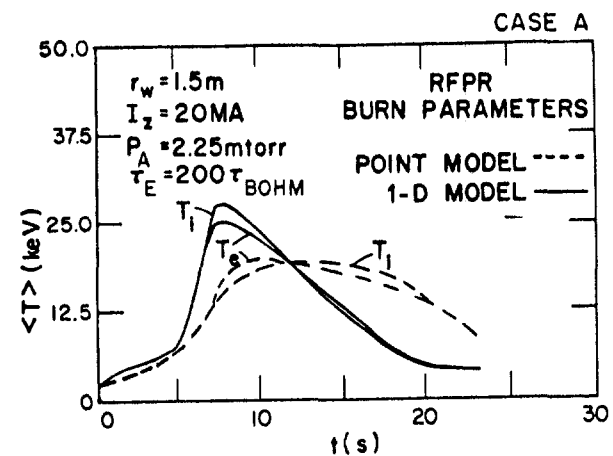
Figure 1. Global Parameters and wall load for 1-D and point model comparison.

Table I. Comparison of Energy Balance for Zero- and One-Dimensional Burn Models

PARAMETER (MJ/m)	ZERO-D	ONE-D[a] CASE A	ONE-D[b] CASE D (OPTIMIZED)
Burn time τ_B(s)	21.6	21.6	22.0
Initial plasma energy, W_{pi}	0.05	0.7	.99
Final plasma energy, W_{pf}	2.5	1.9	3.68
Radiation energy, W_{RAD}	28.1	14.3	19.3
Ohmic heating energy, W_{OHM}	7.1	8.9	8.93
Plasma energy loss (conduction), W_{COND}	147.5	93.0	146.7
Plasma expansion energy, W_{PV}	0.7	1.1	0.0
Magnetic-field energy inside first wall at end of burn cycle, W_{Bf}	51.6	45.0	30.6
Fusion Neutron Energy, W_N(14.1 MeV)	676.5	410.0	646.2
Q_p (fusion energy)/(ohmic + field energy)	14.4	9.5	20.4

[a] radius forced to follow zero-dimensional case

[b] fixed plasma radius, Bohm conduction

Table II. Comparison of Energy Balance for Nonturbulent and Turbulent Transport

PARAMETER (MJ/m)	ONE-D[a] CASE B	ONE-D[b] CASE C
Burn time τ_B(s)	24.6	25.0
Initial plasma energy, W_{pi}	0.3	0.3
Final plasma energy, W_{pf}	3.0	3.1
Radiation energy, W_{RAD}	14.3	13.9
Ohmic heating energy, W_{OHM}	10.4	12.4
Plasma energy loss (conduction), W_{COND}	115.2	114.5
Plasma expansion energy, W_{PV}	0.0	0.0
Magnetic-field energy inside first wall at end of burn cycle, W_{Bf}	45.1	45.5
Fusion Neutron Energy, W_N(14.1 MeV)	493.5	469.7
Q_p = (fusion energy)/(ohmic + field energy)	11.1	10.1

[a] fixed plasma radius, no Suydam turbulence

[b] fixed plasma radius, Suydam turbulence

The Compact Reversed Field Pinch (CRFP) Reactor Concept

by

George H. Miley and Richard A. Nebel
Fusion Studies Laboratory
University of Illinois

Introduction

A criticism of fusion reactor concepts studied to date has been that they are typically large and complex, making maintenance difficult, integration into smaller electrical networks impractical, and posing financial problems due to the large capital costs involved. In response to this criticism, a new class of concepts, termed, compact tori, evolved[1]. These concepts are currently viewed as including Field Reversed Mirrors, Field Reversed Theta Pinches, and Spheromaks. They all share, to a varying extent, the common features of high-β created by confinement fields that are mostly created by internal plasma currents. These characteristics lead to smaller, more compact reactor concepts that answer the criticisms noted above. Since the Reversed Field Pinch (RFP) has a magnetic configuration that is similar in many respects to the CT, it is a natural candidate for a "compact" system.

Prior RFP Conceptual Reactor Characteristics

RFP conceptual reactor studies have been carried out at both Culham Laboratory ahd the Los Alamos Scientific Laboratory[2-5]. These reactor devices have typically had a major radius of ~ 12-15 m and a minor radius of ~ 1.5-1.75m. Thermal power levels are of the order of 2000-3000 MW. As such, these reactors are neither compact or small. This does not infer that they may not ultimately be attractive, however. Indeed, the RFP has a series

24

of notable features that have been cited as important advantages. Thus, the ability to heat to ignition with ohmic heating alone provides both a cost savings and simplicity compared to approaches requiring auxiliary heating via neutral beams or RF. The relatively high β provides a good power density and the possibility of eventually extending the concept to advanced fuels like catalyzed-deuterium. The lack of an aspect ratio constraint allows the large aspect ratio design which, by virtue of the open central region, lends itself to ease of maintenance and modular construction.

In summary, while the "conventional" RFP reactor has many attractive features, prior studies resulted in large plants in terms of power level. The question prompting the present study then was: can a "small" reactor in the 100 MWe range be designed using the RFP concept? Such a reactor, labeled a Compact RFP (CRFP), would provide a flexibility in reactor size that may be essential for exploration of fusion power, and provide a route to a lower capital cost reactor suitable for a near term demonstration plant.

CRFP Studies

Scaling down the dimensions of the large RFP designs by roughly a factor of two provides a plasma volume compatible with the goal of a 100 MWe output. In order to examine the transport and stability properties of an RFP burn in a plasma of this size, we employed the 1-D dynamic burn code developed earlier for RFP studies and described elsewhere[6]. This code includes both global and local stability checks. Violation of the former results in burn termination while local violations are assumed to result in a turbulent transport. Continuity balances and alpha heating are treated in a conventional manner. Results from these calculations are presented in Table 1 along with comparison parameters for the LASL RFPR reference design. It is

observed that, while the volume of the CRFP is decreased by a factor of 8 compared to the RFPR, its net electrical output is only reduced by a factor of 7.5. Consequently, the CRFP enjoys a slight advantage in power density although its Q_p-value has dropped from 14.4 to below 10, indicating an undesirable increase in recirculating energy. The output power of 100 MWe is near the goal, but a further decrease in size causes a further rapid decrease in Q_p due to radial energy losses via thermal conduction. (As in the LASL design, an energy transport $\tau_E \sim 200$ τ_{Bohm} was employed in this study.) Indeed, to avoid excessive losses in the CRFP shown, it was necessary to increase magnetic field strength by a factor of 1.9 in order to increase the density as shown in Table 1. This was thought to be at the limit of potentially available magnetic technology so further improvements were not attempted.

Table I. Summary Description of Design Parameters

PARAMETER	RFPR	CRFP
First-Wall Radius, r_w(m)	1.5	.75
Major Radius, R(m)	12.7	6.35
Burn Time, τ_B(s.)	21.6	10.3
Cycle Time, τ_c(s)	26.6	15.3
Average Fuel Burnup, f_B	0.5	.23
Average Plasma Density, n(1/m^3)	$2.0(10)^{20}$	$3.8(10)^{20}$
14.1-MeV Neutron Current at First Wall, (MW/m^2)	2.7	2.4
Total Thermal Power, P_{TH}(MWt)	3000	628
Net Electrical Power, P_E(MWe)	750	100
Q_p = (fusion energy)/(ohmic & field energy)	14.4	9.7

The CRFP burn was shorter as indicated by the reduced burn up fraction

compared to the RFPR. Gross MHD stability was maintained throughout the

burn, but Suydam's criterion was violated on centerline leading to a

turbulent core region that resulted in enhanced transport. However, as found

in the RFPR[6], the turbulence did not result in a major deterioration in the

energy balance since the outer radius zone remained quiescent.

A feeling for the relative size of the CRFP can be gained from Fig. 1.

Its relative location between the RFPR and Zeta reinforces the earlier

suggestion that a smaller device of this type would be potentially attractive

as an early demonstration device.
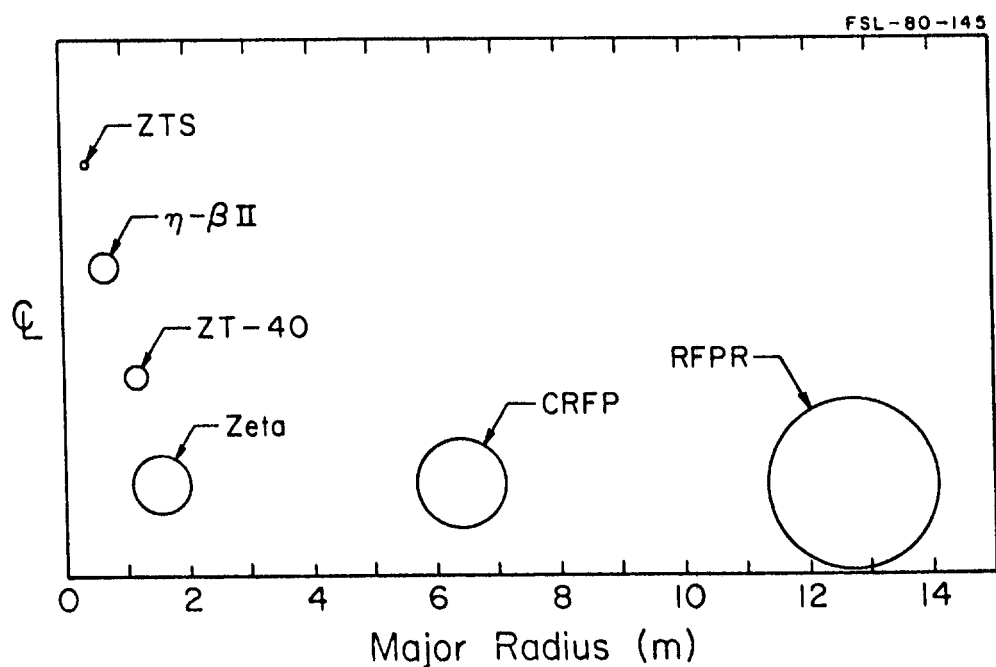
Figure 1. Relative Sizes of RFP Experiments and Reactors.

Problems and Possible Improvements

Due to its capital intensive character to be competitive economically,

any fusion reactor in the 100 MWe range must, of necessity, offer high

performance and modular construction (providing ease of maintenance and mass production of key components). It appears that the same design considerations employed in the RFPR can lead to satisfaction of the latter requirements. On the other hand, the low Q_p and associated recirculation power requirement suggests an undesirable expense.

Previous work[7] has indicated that significant improvements in plasma performance can be obtained by refueling the plasma. This approach is currently being pursued for the compact RFP to try to improve Q_p. Pellets and gas puffing are both being considered.

References

1. G. H. Miley, "Theoretical Considerations and Applications of Compact Torus Concepts," Japanese-US Exchange Workshop on Compact Tori, Princeton University, Dec. 1979.

2. J. D. Lawson, "Reversed Field Pinch Reactor Study, I. Physical Principles," CLM-R 171 (1977).

3. R. Hancox and W. R. Spears, "Reversed Field Pinch Reactor Study, II. Choice of Parameters," CLM-R 172 (1977).

4. A. A. Hollis and J. T. D. Mitchell, "Reversed Field Pinch Reactor Study, III. Preliminary Engineering Design," CLM-R 173 (1977).

5. R. L. Hagenson, R. A. Krakowski, and G. E. Cort, "The Reversed-Field Pinch Reactor," Los Alamos report LA-7973-MS (1979).

6. R. A. Nebel, et al., "Comparison of Zero-Dimensional and One-Dimensional Thermonuclear Burn Computations for the Reversed-Field Pinch Reactor (RFPR)," Los Alamos report LA-8185-MS (1980).

7. R. Nebel and G. H. Miley, "Refueling and Control of RFP Burns," Third ANS Topical Meeting on the Technology of Controlled Nuclear Fusion, Santa Fe, NM (1978).

IGNITION AND BURN IN RFP REACTORS

P G Carolan

UKAEA, Culham Laboratory, Abingdon, Oxon OX14 3DB, UK
(Euratom/UKAEA Fusion Association)

INTRODUCTION

The purpose of this note is to highlight some of the problems associated with achieving ignition and burn in an RFP reactor. A particular RFP reactor scenario, which has been considered in depth elsewhere,[1] was used to exemplify practical consequences arising from steady state and time dependent (zero dimensional) studies. Various energy losses and confinement time scaling are considered and the advantage of using additional heating in reducing the period from ignition to burn is outlined.

PLASMA MODEL

In the time dependent calculations the circuit effects are ignored, e.g. the temporal behaviour of the plasma current is predetermined to follow a simple sine function until the peak is reached and thereafter it is maintained constant. The $\tau/4$ time is typically $\frac{1}{2}$ second.

Although spatially averaged quantities are used throughout, some account is taken of distributions of density, temperature and current during the ohmic heating phase by utilising correction factors derived from experimental results (principally ZETA) and from RFP plasma models. The equipartition time between the plasma species (ions, electrons, alpha particles) is considered to be much shorter than heating and loss times such that $T_i = T_e = T_\alpha$. The net heating rate, $d/dt(3NkT)$, is obtained by subtracting the loss terms from the joule + alpha + additional heating terms.

The plasma resistance, R, is obtained from $R = F(\theta)2R_{maj}\eta_{||} a^{-2}$ where the form factor, $F(\theta)$ takes account of the plasma compression and the plasma poloidal current. If we restrict the $\theta_{wall} \lesssim 1.5$ we can use the Bessel function model to give $F(\theta) = \theta/J_1(2\theta)$.

It is assumed that there is always an equal mixture of deuterium and tritium and no account is taken of fuel burn-up or 'ash'. The assumption is also made that the alpha particles are immediately thermalised.[2] We use[3]

29

$<\sigma v> = 3.68 \times 10^{-16} T^{-2/3} \exp(-199.4 T^{-1/3})$ for the D-T cross section. While peaked temperature and density profiles may facilitate a rapid transition from ignition to burn, this is clearly outside the scope of a global model code; therefore, in the present analysis, a uniform alpha particle heating is assumed.

Since an RFP reactor will probably rely totally on ohmic heating to reach ignition it is important to allow for rapid heating to reduce the volt seconds and the poloidal field coil current requirements. Impurity radiation and turbulent convection and conduction require that high temperatures are reached rapidly. These benefit by operating at the lowest density possible. It is conjectured that streaming related micro-instabilities will fix the lower limit of density. We define the electron drift parameter, ξ, given by (on axis):

$$\xi = \frac{j_{\phi 0}}{n_{eo} e} \left(\frac{m_e}{2eT_{eo}}\right)^{\frac{1}{2}} \propto \frac{\bar{j}_\phi}{n_e T_e^{\frac{1}{2}}} \frac{F(\theta)}{C_n C_T}$$

where $C_n = n_{no}/n_e$ and $C_T = T_{eo}^{\frac{1}{2}}/T_e^{\frac{1}{2}}$.

The ratios C_n and C_T will change as the plasma evolves but due to the lack of data, and to simplify the analysis, the product $C_n C_T$ was fixed at 4/3, which is consistent with ZETA scattering results.

Impurities, especially medium (e.g. iron) to high Z (e.g. molybdenum) can present radiation barriers which will prevent ignition. The impurities are considered to be in coronal equilibrium to give a radiation loss (per unit length) of:

$$P_I = \frac{N_e^2}{\pi a^2} f_I P_I(T_e)$$

where f_I is the fractional abundance of impurity. When this loss is balanced against ohmic heating we obtain a steady state temperature, $T = T(f_I, I'_\phi/N_e)$, where $I'_\phi = [F(\theta) \ln \Lambda/10]^{\frac{1}{2}} I_\phi$, in the plots shown in Fig 1 for various concentrations of iron and molybdenum. For $I_\phi = 20MA$ and $N_e = 2 \times 10^{21} m^{-1}$ concentrations of Fe and Mo in excess of 0.01% and 0.001% respectively, will prevent ignition.

RESULTS

In line with the Hancox et al RFP reactor study we have considered bremsstrahlung (z = 1) only (cyclotron emission accounts for at most a few percent of bremsstrahlung) in the time dependent calculations. If we take a fixed density of $2 \times 10^{20} m^{-3}$ and neglect all other losses we can easily calculate the temperature evolution and examine the level of ohmic heating required to minimise the

time between ignition and burn. In Fig 2 a range of heating levels up to four times ohmic (at $F(\theta) = 4$) is shown. (Increasing θ and allowing peaking of density, which enhances alpha particle heating, will reduce the energy replacement time and, consequently, burn conditions may be reached in less than 5s.)

When an energy confinement time that is derived empirically from tokamaks of the form, $\tau_E = \alpha_E na^2$ (Alcator scaling) is used we obtain the requirement for ignition, $an\epsilon^{\frac{1}{2}} \gtrsim 1.56 \times 10^{15} T^{5/6} \exp (9.77T^{-1/3})$, where $\epsilon = \alpha_E/3.8 \times 10^{-21} \equiv$ factor by which tokamak scaling is exceeded. The critical value of $an\epsilon^{\frac{1}{2}}$ as a function of temperature is shown in Fig 3. So, for example, to obtain ignition at 4keV with $a = 1.75m$ and $n = 2 \times 10^{20}m^{-3}$ and where the ohmic heating equals the radiation losses, a value of ϵ in excess of 5.7 is required, or, $n\tau_E \gtrsim 2.7 \times 10^{21}m^{-3}s$.

Even if ignition is achieved by ohmic heating alone, the time taken to reach burn conditions must be considered in the reactor economics. We have calculated the length of time involved in going from an initial temperature, T_i, to the burn temperature, here considered to be 15keV for single loss scalings. In Fig 4 the normalised ignition to burn time, nt, is plotted against T_i for various bremsstrahlung levels (i.e. $Z = 1 - 3$). For example, at $T_i = 5keV$, $Z = 1$, we require $nt = 12.5 \times 10^{20}m^{-3}s$ before burn occurs (alpha particle heating only). This time would be almost halved by increasing T_i to 6keV by additional heating.

Similar plots are shown in Fig 5 for various values of the parameter, $\gamma = an\epsilon^{\frac{1}{2}}$. Ignition will occur at 4.5keV if $\gamma \gtrsim 7.3 \times 10^{20}$, but even for $\gamma = 8 \times 10^{20}$ a nt $\approx 22 \times 10^{20}m^{-3}s$, time will elapse before burn conditions prevail.

Examples of temperature evolution of the Culham/Padua RFP reactor are shown in Fig 6 for various additional power levels in excess of that obtained by using $F(\theta) = 4$ and assuming a flat density and temperature profile. Bremsstrahlung losses ($Z = 1$) and an energy confinement time of 10 times Alcator scaling is used. It was necessary to increase T to 15keV and reduce n to $1.4 \times 10^{20}m^{-3}$ (from 10keV and $2 \times 10^{20}m^{-3}$) to obtain identical wall loading and β_θ values as in the Culham/Padua reactor. Additional power of about 2MW/m lasting 2 seconds is required to permit burning in less than 5 seconds.

Alternatively, it may be possible to burn more easily in smaller minor radius devices. For example, an RFP reactor with $a = 0.6m$, $I_\phi = 20MA$, $n = 7.5 \times 10^{20}m^{-3}$, burn obtains in less than 5 seconds without appealing to additional power and using Alcator scaling, as shown in Fig 7. The maximum β_θ value and

wall loading during burn were 27% and 38MW/m^2 respectively at a burn temper-
ature of 20keV. Because of the higher I/N ratio, more than double the
impurity levels of the Culham/Padua reactor are acceptable.
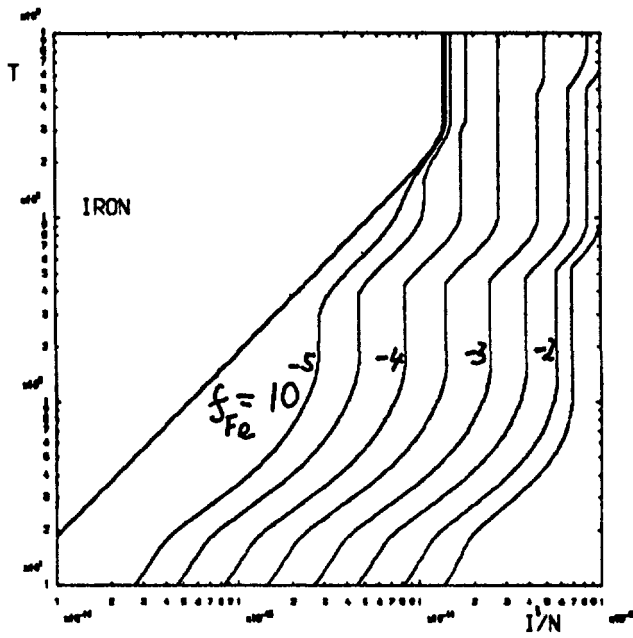
Fig 1(a)
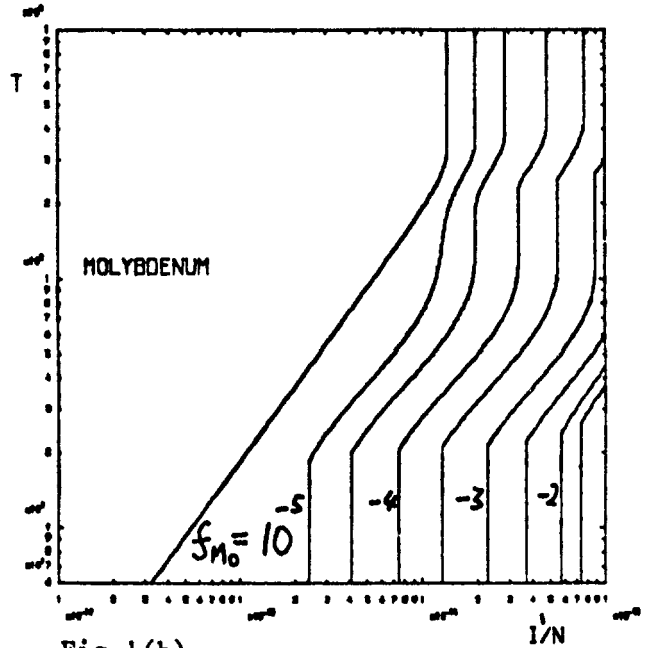
Fig 1(b)
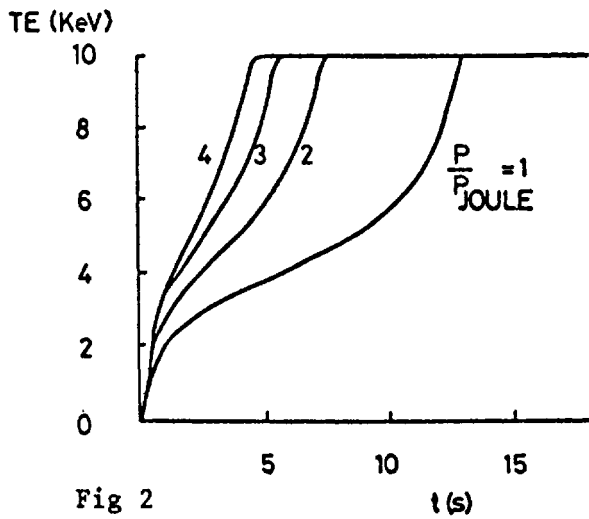
Fig 2
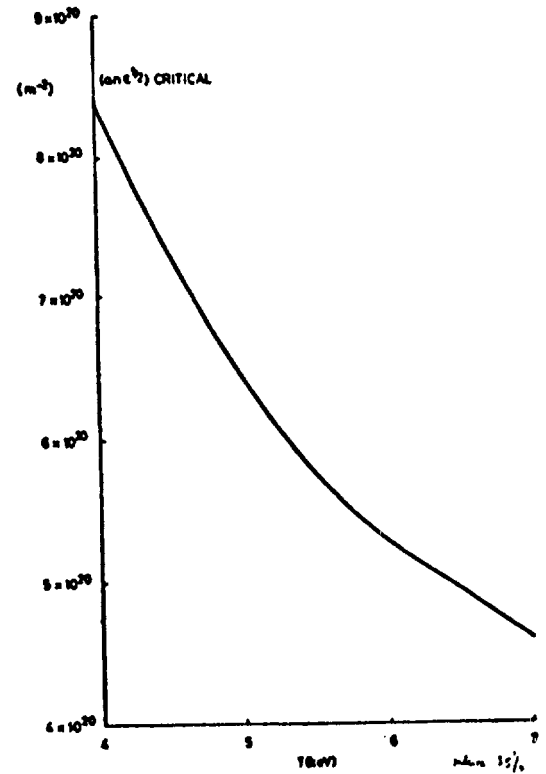
Fig 3
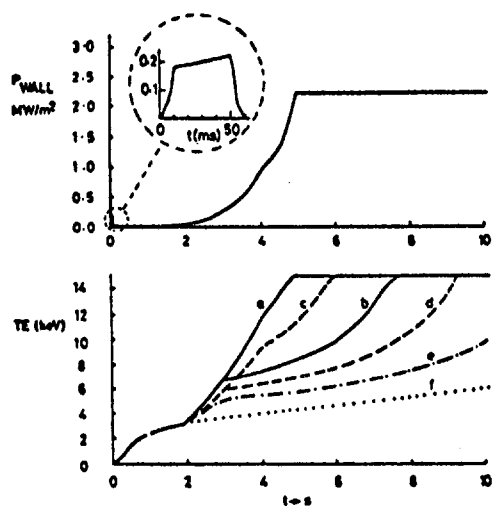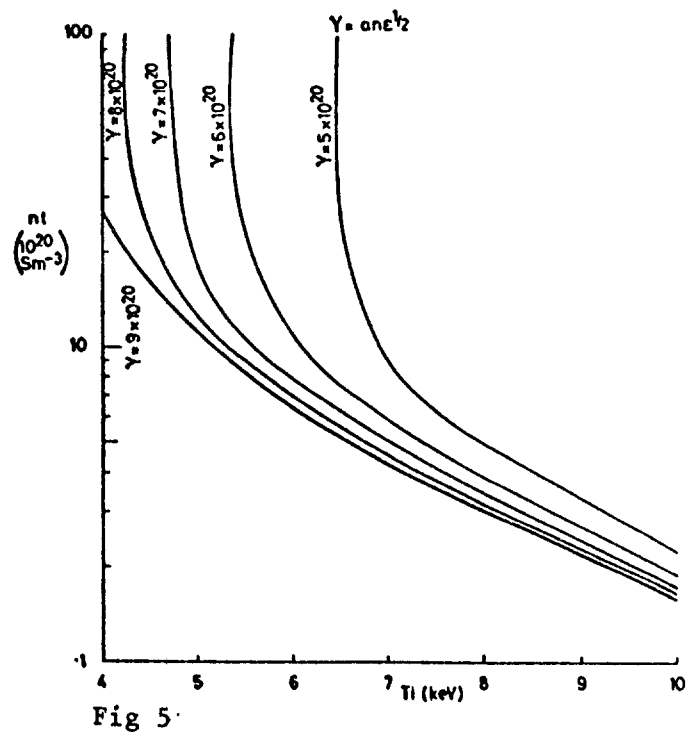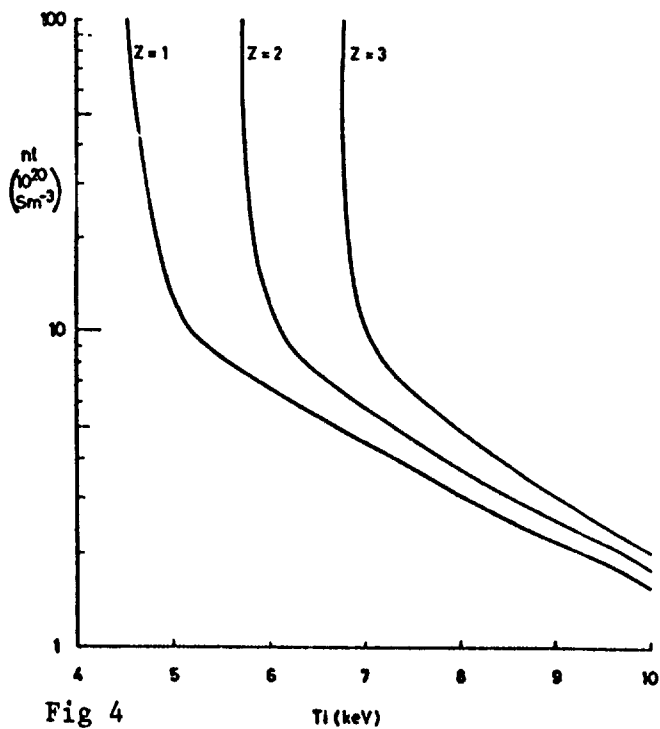
Fig 4

Fig 5

Fig 6

Fig 7
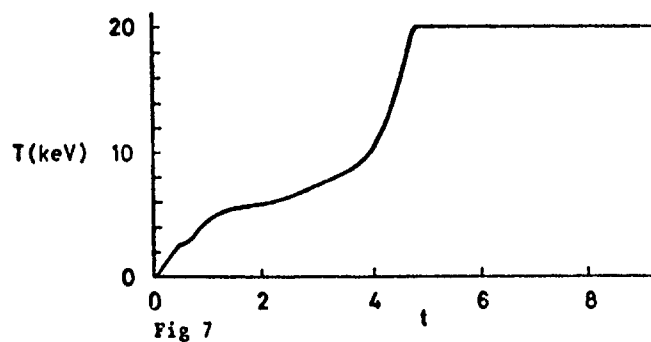
REFERENCES

[1]   R HANCOX et al: Culham Laboratory Preprint, CLM-P501

[2]   B C YEUNG: PhD Thesis, Culham Laboratory

[3]   S GLASTON AND R H LOVBERG: Controlled Thermonuclear Reactions, Kreiger, New York (1975)

33

Plasma Power Balance of a Pulsed RFP Reactor

J.P.Christiansen and K.V.Roberts

1.   Introduction

This paper describes a preliminary study of the power balance of a reactor plasma with variable plasma parameters. Some of the conditions for ignition by Ohmic heating and plasma stability are examined. The reactor configuration corresponds to the design by Lawson [1] of an RFP reactor which will be referred to as the PRFPR (pulsed RFP reactor).

We have found it instructive to study a simplified power balance model. An essential practical step is to treat the energy containment τ_E as an unknown quantity since it will depend on the reactor impurity level as well as on anomolous losses which cannot be predicted from present RFP experiments. In section 2 we define the energy replacement time τ_R per particle and determine analytically the surface $\tau_R(n,T)$ where n is density and T is temperature. This surface is exhibited by contours in Figure 1 and by an isometric projection in Figure 2. The surface $\tau_R(n,T)$ always has a saddle point (n_s,T_s) at which T_s has the fixed value 7.4Kev. The position (n_s,T_s) establishes a strategy for the approach to thermonuclear burn conditions irrespective of any scaling law that might apply for τ_E. The strategy dictates a 5 phase cycle of operation of the PRFPR comprising setting up, heating, gas-puffing, burn and pump-out. The time-scales for these phases are calculated analytically in section 3 and determine the minimum values of τ_E and the generating density required to achieve the design power level averaged over one cycle. Section 4 describes briefly the results from numerical computations on the transport,heating,equilibrium,gas-puffing and thermonuclear burn of the PRFPR cycle.

2.   Energy replacement time

The plasma power balance is

$$\frac{\partial w}{\partial t} = Y + 0 - U - R \qquad (1)$$

where w is the total plasma energy density, Y the heating rate by α-particles 0 the ohmic heating rate, U the thermal loss rate and R the radiation loss rate. Standard expressions are used, i.e.

$$w = 3nkT, \quad Y = \tfrac{1}{4}n^2 <\sigma v> E_{DT}, \quad 0 = \eta J^2$$

$$U = W/\tau_E \quad \text{and} \quad R = c_R n^2 T^{\frac{1}{2}}$$

where the symbols have their usual meaning. Line radiation and synchrotron radiation are assumed negligible. The resistivity has the form

$$n = c_a T^{-3/2} \qquad (2)$$

The energy replacement time per particle is defined as

$$\Gamma = \frac{1}{\tau_R} = \frac{1}{W}\frac{\partial W}{\partial t} = \frac{Y}{W} + \frac{O}{W} - \frac{1}{\tau_E} - \frac{R}{W} \qquad (3)$$

The equilibrium value τ_R corresponding to zero net power (i.e. steady state) is given by

$$\frac{1}{\tau_R} = \frac{1}{W}(Y + O - R) = \frac{1}{\tau_E}$$

It is instructive to study the behaviour of $\tau_R(n,T)$ since it does not contain the unknown parameter τ_E. Setting

$$A(T) = (Y-R)/3kn^2, \quad B(T) = T/\tau_R, \quad C(T) = O/3k$$

we get

$$\tau_R = \frac{nT}{An^2+C} \quad \text{or} \quad An^2 - Bn + C = 0 \qquad (4)$$

Contours in the (n,T) plane of constant τ_R for fixed J can easily be calculated from the solutions to (4)

$$n_{+,-} = \frac{1}{2A}(B \pm D^{\frac{1}{2}}), \quad D = B^2 - 4AC.$$

For $T<T_x = 4.18$ keV there is only one solution n_-; for $T = T_x$ we have $n_- = C/B$, and for $T>T_x$ there are 2, 1 or 0 solutions for $D>0$, $D=0$, $D<0$ respectively. Equation (4) always has a saddle-point (n_s, T_s) at which

$$\frac{\partial \tau_R}{\partial n} = 0, \quad \frac{\partial \tau_R}{\partial T} = 0 \quad \text{or} \quad T\frac{\partial}{\partial T} \ln AC = 2$$

The saddle-point value T_s is independent of any anomaly factor c_a in (2); indeed it is independent of J and varies only weakly with the atomic charge Z and the exponent of T in (2). For simplicity let n_s^*, J^* denote n_s, J in units $10^{20} m^{-3}$, MA m^{-2} respectively; the saddle-point values are then

$$T_s = 7.4 \text{ keV}, \quad N_s^* = 0.1622 \, J^*, \quad \tau_{Rs} = 19.65/J^*$$

The drift parameter and axial beta values are

$$\xi(n_s,T_s) = 0.017, \quad \beta_0(n_s,T_s) \simeq \frac{20}{\pi} \frac{g^2}{a^2 J^*}$$

The importance of the saddle-point is evident from Figure 2 showing contours $\tau_R(n,T)$ in the (n,T) plane and Figure 1 showing an isometric projection of the surface $\tau_R(n,T)$. To reach the reactor burn regime by Ohmic heating above we require

$$\tau_E > \tau_{Rs}$$

irrespective of any scaling law of τ_E. The extremum-points on the surface $\tau_R(n,T)$ define two curves at which the plasma is stable against density and temperature fluctuations. The curve (' denotes $\frac{\partial}{\partial T}$)

$$\frac{\partial \tau_R}{\partial T} = 0 \quad \text{or} \quad n_T^2(T) = \frac{TC' - C}{A - TA'}$$

is a marginal self-sustainment curve because

$$\tau_E > \tau_{RT} = \frac{n_T \, T}{A n_T^2 + C}$$

is required to make the plasma self-sustaining at the density n_T. Similarly the curve

$$\frac{\partial \tau_R}{\partial n} = 0 \quad \text{or} \quad n_n^2 = \frac{C}{A}, \quad \tau_{Rn} = (4AC)^{-\frac{1}{2}}$$

indicates those points in the (n,T) plane which are stable against density fluctuation Figure 3 shows a plot of (4) for 3 values of J together with 3 dashed lines representing the Hugill-Sheffield scaling law for τ_E [2] and a dotted-dashed line showing the Alcator scaling law [3], all for lines corresponding to $J = 7 \text{ MA m}^{-2}$.

In order to climb over the "ridge" at its lowest point (see Figure 2) we propose the 5-phase operating cycle mentioned earlier. Next we look at the heating, puffing and burn phases characterised by:

heating $n = n_o$ $0 < T < T_o$

gas puffing $n_o < n < n_1$ $T \approx T_o$

burn $n = n_1$ $T_o < T < T_1$

The setting-up and pump-out phases of duration τ_s and τ_{out} respectively are not considered; neither do we look at temperature stabilization during burn once the "ridge" has been overcome.

3. Heating, puffing and burn

There are in general two types of solutions during heating :

$$T_-(t) \qquad \tau_E \leq \tau_{RT}$$

$$T_+(t) \qquad \tau_E > \tau_{RT}$$

Empirical scaling laws suggest the first type and numerical integration of (1) leads to the set of solutions

$$T_-(t = \tau_H, \ \tau_E, \ J) = T_o$$

τ_H being the duration of the heating phase.

The gas-puffing phase has duration τ_p where

$$\tau_p(T_o, n_1, \tau_E, J) = \int_{n_o}^{n_1} \frac{1}{\Gamma n_o} \, dn, \tag{5}$$

Γ being given by (3). Three solutions $\tau_{p-}, \ \tau_{po}, \ \tau_{p+}$ arise corresponding to $\tau_E < \tau_{Rn}$, $\tau_E = \tau_{Rn}$, $\tau_E > \tau_{Rn}$. The solution τ_{po} is the limit $B \to 0$ of the other two solutions.

$$\tau_p = \frac{1}{D^{\frac{1}{2}}} \ \ell n \ \frac{(n_- - n_o) \ (n_+ - n_1)}{(n_+ - n_o) \ (n_- - n_1)} \tag{6a}$$

36

$$\tau_{p+} = \frac{2}{D^2} \cdot A \tan \frac{2(n_+ - n_-)(n_1 - n_0)}{(n_+ - n_-)^2 + (2n_1 - n_+ - n_-)(2n_0 - n_+ - n_-)} \qquad (6b)$$

which both require $\tau_E > \tau_R$. The derivation of (6) assumes a uniform transport across the discharge of the injected cold gas which maintains approximately constant temperature.

The burn phase has to produce sufficient power for the reactor output averaged over one cycle to meet the design value 2 GW thermal. The average power density is

$$\bar{P} = \frac{5 \, Y \, \tau_B}{\tau_s + \tau_N + \tau_p + \tau_B + \tau_{out}} = 5Y \frac{\tau_B}{\tau_0} = 5 Y \zeta \quad , \qquad (7)$$

the τ's denoting the time intervals of each phase in one cycle. We require $\bar{P} = 6$ MW m^{-3} in the centre of the PRFPR allowing for profile features. Assuming $\tau_s = 0.5$ sec, $\tau_{out} = 1$ sec and taking the highest value of τ_H we find

$$\tau_B \geq \frac{2 + \tau_p (n_1^*)}{\frac{5Y}{\bar{P}} n_1^* 2 - 1} \qquad (8)$$

where n_1^* is the operating density n, in units 10^{20} m^{-3}. Defining

$$\frac{1}{\tau_E^*} = \frac{1}{\tau_1} \int_0^{\tau_1} \frac{1}{\tau_E} \, dt \qquad (9)$$

as the mean energy containment time during the time interval $\tau_1 = \tau_s + \tau_H + \tau_p$ in which we "traverse the pass" we see that the minimum containment time required to complete one cycle is

$$\tau_{Emin}^* (T_1, n_0, n_1) = \tau_0 \qquad (10)$$

Eqns (8-10) can now be studied for various values of n_0, n_1, T_0, T_1. Figure 4 shows τ_{Emin}^*, ζ and Δf_{DT} which is the fractional burn-up of DT against n_1 for $T_1 = 20$ keV.

4. Conclusions

In order that the PRFPR can produce the necessary power (design value) we require $\tau_E^* \geq \tau_{Emin}^*$. For $\tau_{Emin}^* = 10$ sec (lowest value) the reactor power output profile (ζ) is undesirably peaked. As τ_{Emin}^* approaches 100 sec. ζ approaches unity. These results are also found in the numerical calculations which follow the heating, puffing and burn phases and in which τ_E follows the empirical scaling laws of [2].

[1] J.D.Lawson, Culham Report CLM-R177 (1977)

[2] J.Hugill, J.Sheffield, Nucl. Fusion 18 (1978) 15

[3] M.Murakami, H.P.Eubank, Physics Today May 1979.
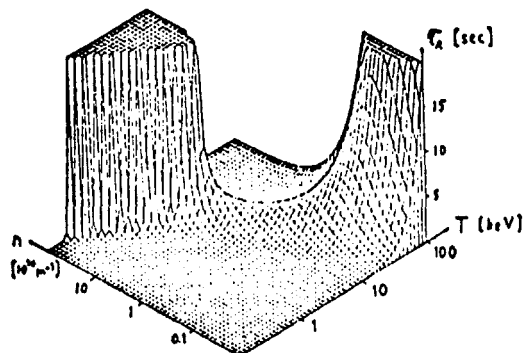
Figure 1. The $\tau_R(n,T)$ surface.
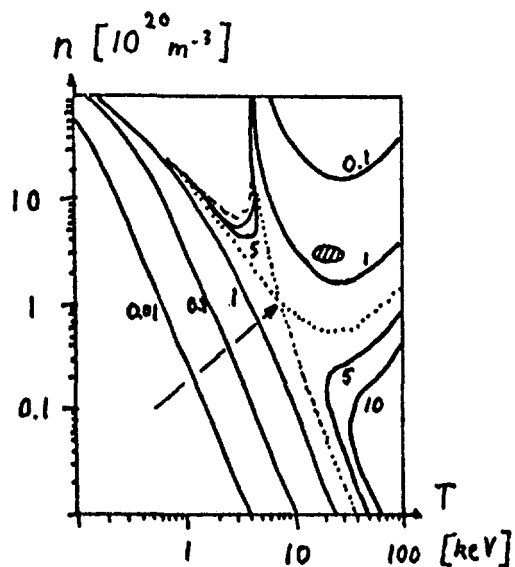
Figure 2. Contours of $\tau_R(n,T)$ in the (n,T) plane.
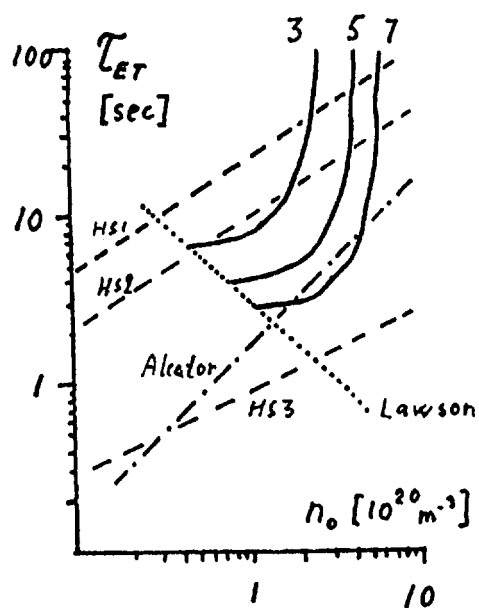
Figure 3. Confinement time τ_{ET} required for self-sustainment. Hugill-Sheffield and Alcator scaling laws for τ_E are also shown.
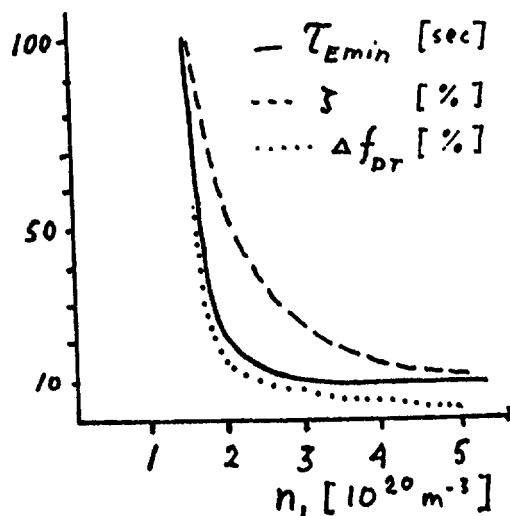
Figure 4. Minimum τ_E, power profile factor ζ, fractional burn up Δf_{DT} as functions of burn density.

38

ALPHA-PARTICLE CONSIDERATIONS RELEVANT TO THE REVERSED-FIELD PINCH REACTOR (RFPR)*

Ronald L. Miller
University of California
Los Alamos Scientific Laboratory
Los Alamos, NM 87545 USA

ABSTRACT

A primer on alpha-particle fundamentals as they relate to the conceptual design of the Reversed-Field Pinch Reactor (RFPR) is presented. A call for more research in this area is made.

I. INTRODUCTION

While not an issue for near-term physics experiments on the Reversed-Field Pinch (RFP) magnetic fusion concept, the behavior of D-T fusion-product alpha particles in anticipated fusion-test-reactor experiments or in eventual commercial power reactors will become increasingly important. Conceptual reactor design studies done to date[1,2] have incorporated simple models of relevant alpha-particle physics and project favorable reactor performance. The development of more detailed (less naive) reactor studies will require the timely incorporation of more sophisticated models of alpha-particle behavior in order to substantiate these projections. It is the purpose of this paper to stimulate interest in the study of alpha-particle issues so that, paced by continued favorable experimental results, an aggressive RFP research and development program through D-T buring experiments to a demonstration reactor is possible. This area of investigation for the RFP is a fertile one, although largely unexplored. A substantial body of research on alpha-particle issues in tokamaks[3,4] could and should be adapted to the RFP.

The balance of this paper will provide a primer on the fundamentals of alpha-particle behavior in reactor-class RFP systems. To assert that this treatment is comprehensive will serve to highlight the claim made above that precious little work has been done in this area to date. Unless otherwise indicated, SI units (except plasma temperature T expressed in keV) will be used.

II. CONFINEMENT AND IGNITION

The available kinetic energy, $U_{\alpha o} = 3.52$ MeV/alpha ($v_{\alpha o} = 1.3(10)^7$ m/s), ideally provides an ample heating source to offset radiation and transport losses in the background D-T plasma and yield an ignited thermonuclear burn once an initial Ohmic heating transient phase is completed in a plasma of appropriate size and current density. Utilization of this heating source presumes that the alpha particles remain in the plasma to deposit a substantial fraction, f_α, of their birth energy. That is to say, the alpha-particle confinement time, $\tau_{\alpha c}$, must exceed the thermalization time, $\tau_{\alpha t}$.

A D-T plasma confined in a RFP produces alpha particles at a spatially local rate, R_α (reactions/m^3/s), given by

$$R_\alpha = \frac{1}{4} n_i^2 <\sigma v> \quad , \tag{1}$$

where $n_i (m^{-3})$ is the ion particle density ($n_D = n_T = \frac{1}{2} n_i$) and $<\sigma v>$ (m^3/s) is the temperature-dependent, Maxwell-averaged D-T fusion reactivity, which for ion temperatures, T_i, in the range 8<T<20 keV can be approximated to within 10% of nominal values[5] by

$$<\sigma v> \simeq 1.1(10)^{-24} T_i^2 \quad . \tag{2}$$

For RFP density and temperature profiles which are peaked on-axis, the bulk of the alpha particles produced will be born correspondingly near the axis.

The gyroradius ρ_α(m) of a 3.52-MeV alpha particle in a magnetic field B(T) is bounded by

$$\rho_\alpha \lesssim 0.27/B \tag{3}$$

corresponding to a pitch angle of $\pi/2$ (i.e., no motion parallel to the magnetic-field lines). For a value[2] of $B = 3.8$ T one obtains $\rho_\alpha \sim 0.07$ m. Thus, finite orbit effects will tend to localize the alpha particles near the radius of birth, provided drifts are neglected. Pending detailed orbit computations, already available for tokamaks[6], studies to date have invoked idealized point-plasma models[1,2] or in situ energy deposition.[7]

The thermalization distance, λ_α(m), required to deposit all ($f_\alpha = 1$) of the available alpha-particle energy to a background D-T plasma ($T_i = T_e = T$, $n_i = n_e = n$) is approximately given by[8]

$$\lambda_\alpha = \frac{5.2(10)^{26} T^{3/2}}{n \ln(1/\delta^2)} \quad . \tag{4}$$

For $T = 5$ keV, $n = 3(10)^{20}$ m^{-3}, and $\ln(1/\delta^2) \sim 17$; corresponding to the early stages of a reactor burn; one obtains $\lambda_\alpha \sim 1.1(10)^6$ m! For a system[2] of major radius $R = 12.7$ m this staggering distance corresponds to $\lambda_\alpha/2\pi R = 14,000$ circuits around the torus, neglecting the important convolutions of the orbit itself. It seems there is ample opportunity for drift losses to cause the alpha particle to escape from the plasma before depositing its energy.

For nonideal ($f_\alpha < 1$) alpha-particle heating the "ideal ignition temperature"; T^* ($T_o^* \sim 4.2$ keV for $f_\alpha = 1$), obtained by balancing locally the alpha-particle heating power density, $f_\alpha P_\alpha \equiv f_\alpha R_\alpha U_{\alpha o}$, against the Bremsstrahlung loss power density P_{BR}(W/m^3) given by

$$P_{BR} = 5.35(10)^{-37} n_e^2 T_e^{1/2} \quad ; \tag{5}$$

scales (assuming $T_i = T_e = T$ and $n_i = n_e = n$) approximately as

$$T^*/T_o^* \sim f_\alpha^{-2/5} \quad . \tag{6}$$

Thus, if alpha-particle confinement is poor, the ideal ignition temperature is raised and Ohmic heating must be greater to achieve ignition (e.g., $T^* \sim 8$ keV for $f_\alpha = 0.2$).

III. TIME HISTORY OF ALPHA PARTICLES

The RFPR design points[1,2] to date have assumed ideal ($f_\alpha = 1$) energy utilization. The thermalization model used at LASL incorporates a classical, lossless Fokker-Planck treatment.[9] The alpha-particle energy spectrum is resolved (see Fig. 1) to compute the partition of alpha-particle kinetic energy among the background ion and electron populations. The alpha-particle energy spectrum is also used to compute an effective alpha particle temperature, $T_\alpha \equiv \frac{2}{3}$ $\langle U_\alpha \rangle$. The time dependence of T_α is plotted in Fig. 2 along with the background temperatures, T_i and T_e. In the batch-burn operating mode, the alpha-particle density, n_α builds up until the burn is terminated at $T \sim 20$ s. Losses[10-11] and

non-classical effects[12] have yet to be considered.   Other processes including field-ripple trapping and ash buildup/removal also remain as unresolved issues.

REFERENCES

1. R. Hancox and W. R. Spears, "Reversed Field Pinch Reactor Study II. Choice of Parameters," UKAEA Culham Laboratory report CLM-R 172, (1977).

2. R. L. Hagenson, R. A. Krakowski, and G. E. Cort, "The Reversed-Field Pinch Reactor (RFPR) Concept," Los Alamos Scientific Laboratory report LA-7973-MS, (August, 1979).

3. D. Pfirsch, "Alpha-Particles in Tokamaks," Physics of Plasmas Close to Ignition, Proc. of the Course held in Varenna, Italy I, 237-263, (EUR FU BRU/XII/476/80, August 27 - September 8, 1979).

4. Ya. I. Kolesnichenko, "The Role of Alpha Particles in Tokamak Reactors," Nuclear Fusion, 20, 727-780, (1980).

5. S. L. Greene, "Maxwell Averaged Cross Sections for Some Thermonuclear Reactions on Light Isotopes," Lawrence Livermore Laboratory report UCRL-70522, (May, 1967).

6. T. W. Petrie and G. H. Miley, "New Techniques for Studying Some Effects of Suprathermal Alpha Particles," Nuclear Science and Engineering, 64 151-162, (1977).

7. R. A. Nebel, R. L. Hagenson, R. W. Moses, and R. A. Krakowski, "Comparison of Zero-Dimensional and One-Dimensional Thermonuclear Burn Computations for the Reversed-Field Pinch Reactor (RFPR)," Los Alamos Scientific Laboratory report LA-8185-MS, (January, 1980).

8. T. Kammash, Fusion Reactor Physics, (Ann Arbor Science Publishers, Inc.) 1975.

9. T. A. Oliphant, "Fuel Burn-up and Direct Conversion of Energy in a D-T Plasma," Proc. B.N.E.S. Conf. on Nuclear Fusion Reactors, Culham UK, 306-321, (September, 1969).

10. H. Saito, M. Katsurai, H. Tsuji, and T. Sekiguchi, "Dynamic Characteristics of Alpha-Particle Heating Based upon the Fokker-Planck Equation in D-T Fusion Reactor Core Plasma," Proc. Sixth Int. Conf. on Plasma Physics and Controlled Nuclear Fusion Research, Berchtesgaden FRG, IAEA-CN-35, III, 337-346, (October, 1976).

11. H. Saito, T. Sekiguchi, M. Katsurai, and S. Mackawa, "An Approximate Theory of Steady-State and Dynamic Characteristics of Alpha-Particle-Heated D-T Fusion Reactors," Nuclear Fusion, 17, 919-928, (1977).

12. D. J. Sigmar and H. C. Chan, "Anomalous Alpha-Particle Transport in Thermonuclear Tokamak Plasma," Nuclear Fusion, 18, 1569-1581, (1978).
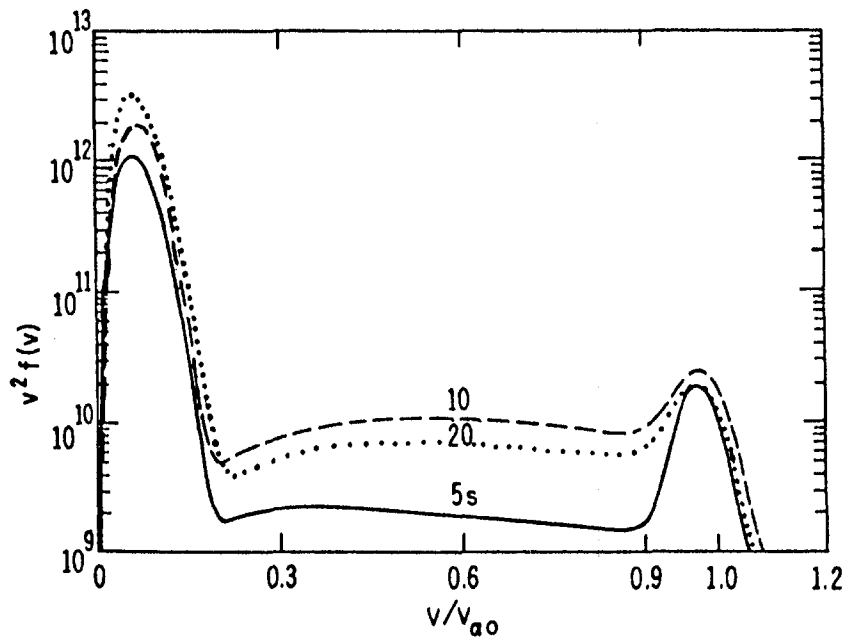
Fig. 1. Evolution of the energy spectrum of alpha particles in an ideal (f_α = 1) RFPR burn at several times (t = 5,10,20 s) into the burn pulse.
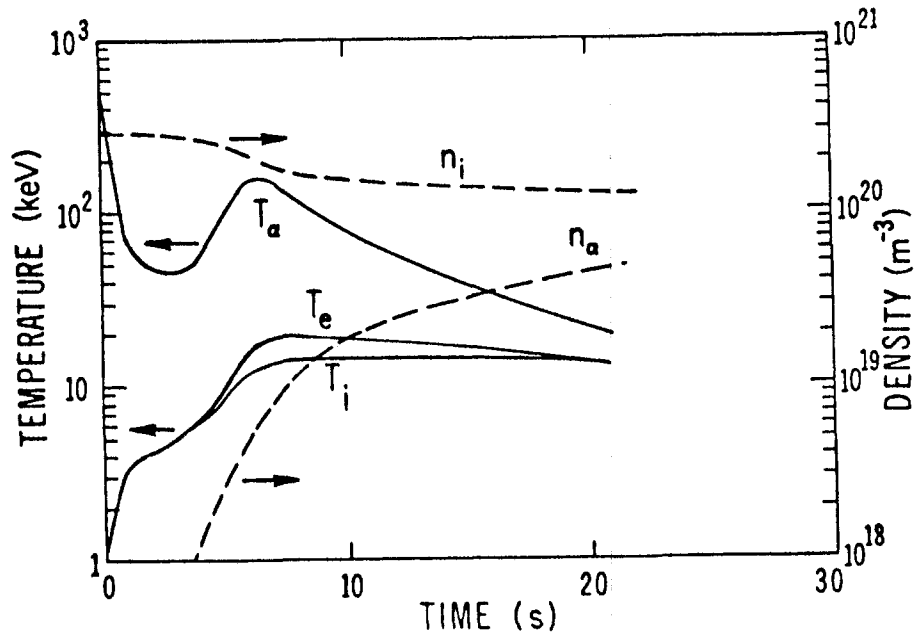
Fig. 2. Time histories of alpha-particle temperature, T_α, and density, n_α; as well as ion (electron) temperature, T_i, (T_e) and ion density, n_i; for the RFPR 20-s batch-burn pulse. By charge neutrality, $n_e = n_i + 2n_\alpha$.

43

MEASUREMENTS OF VOLT-SECONDS IN ZETA
AND THE SETTING UP PHASE

. A A Newton and E P Butt
UKAEA, Culham Laboratory and Halarose Limited, Oxford
(Euratom/UKAEA Fusion Association)

INTRODUCTION

The phenomenon of quiescence on ZETA, which is the natural occurrence of a near stable RFP, has been extensively discussed.[1][2] In this note we give a brief account of the current rise, or setting up phase, in which self reversal occurs when the toroidal flux is conserved in a closed shell. In particular we summarise new data on the azimuthal flux entering the liner, $\Delta\phi = \int V_\phi dt$, at conditions where the peak current, $\hat{I}$, pinch parameter, θ, (measured at the liner) and the rise time, τ_r, were varied. Good quiescence was obtained in all cases. Energy measurements, $\Delta W = \int IV_\phi dt$, were reported previously[3] for these conditions. We also discuss the main energy balance terms for the setting up phase and the scaling of these results to other devices.

RESULTS

(1) Flux Consumption and Energy

The voltage at the ZETA liner was obtained from measurements at the primary windings after applying analogue corrections for leakage inductance, primary winding resistance and turns ratio. These waveforms have been integrated up to the first voltage zero (which occurs just after peak current). Results at varying risetimes are plotted in Fig 1 at conditions where $\hat{I} = 0.40 \pm 0.002$MA, $\theta = 1.50 \pm 0.05$ and $\hat{p}_o = 1.75$mtorr D_2 were kept constant. These fit the relationship, $\Delta\phi = 2.49 \hat{I}(1 + \tau_r/\tau_V)$Vs, with good correlation (C > 0.96) where the time constant, $\tau_V = 5.85$ms (where $\hat{I}$ is in MA). The energy consumption has a similar characteristic, i.e. $\Delta W = 1.49 \hat{I}^2(1 + \tau_r/\tau_W)$MJ, where $\tau_W = 6.6$ms. Figure 3 shows that the scaling with $\hat{I}^2$ is valid over at least a factor of 5. Flux and energy (see Fig 4) increase roughly linearly with θ between $1.2 < \theta < 1.8$, which is the range of principal interest for quiescence. Above $\theta = 1.8$ measurements from coils within the liner show large fluctuations in the plasma displacement with a frequency of about 2kHz.

(2) Fluctuations and Plasma Resistance

Quiescence was defined as a reduction of the r.m.s. fluctuations of the dI/dt signal (measured inside the liner), $\langle \dot{I} \rangle$, by a factor of 3 or more from the value at $\hat{I}$.[4] Reductions of 10 or more were noted at some conditions. It was previously reported[3] that $\langle \dot{I} \rangle / \hat{I}$ was independent of current (in discharges which became quiescent) but in the discharges measured here, $\langle \dot{I} \rangle$ at $\hat{I}$ was observed to be dependent on rise time and hence on $\bar{V}_\phi$. An increase in τ_r also produces a decrease in plasma resistance at peak current as measured by $V(\hat{I})/\hat{I}$. Both these measurements are hard to quantify accurately owing to the large shot to shot variation, and in the case of resistance, to the difficulty of determining $V(\hat{I})$ with sufficient accuracy. Table 1 summarises typical data and clearly shows the trends noted above.

Table 1

Fluctuations and Resistance as a Function of τ_r

τ_r (ms)	R at $\hat{I}$ (mΩ)	$\langle \dot{I} \rangle$ r.m.s. A/s x 10^8
0.8	1.2 ± 0.2	1.0 ± 0.25
1.0	0.75 ± 0.15	0.9 ± 0.3
1.35	0.38 ± 0.2	0.56 ± 0.2
1.9	0.3 ± 0.15	0.54 ± 0.2
2.6	0.2 ± 0.1	0.42 ± 0.1

The reduction of $\langle \dot{I} \rangle$ as τ_r increases indicates that the ZETA definition of 'quiescence' is specialised and a more precise definition will be required for the next generation of experiments with long rise times.

(3) Energy Balance

The energy balance for setting up a particular discharge (τ_r = 1.4ms, which is a frequently studied condition at 0.4MA, θ = 1.5) is shown in Table 2. The increase in magnetic energy, $\Delta W_M = 1/8\pi \int (B_\theta^2 + B_\phi^2 - B_{\phi o}^2)dV$, where $B_{\phi o}$ is the initial toroidal field, is estimated from waveforms and probe plots taken at lower energies which give a value of $L_f = 2\Delta W_M / \hat{I}^2$ in good agreement with that obtained from $\Delta\phi$ extrapolated to τ_r = 0.

An integrating carbon pile bolometer was used to measure the total radiated energy (this is also sensitive to excaping neutral particles) giving an upper

limit to this loss. From time resolved measurements we expect only $\lesssim$ 50% of this energy to be radiated during the setting up phase. From Fig 2 it will be seen that this loss is relatively small. Table 2 shows a residual loss, W_x, of 0.06 < W_x < 0.09MJ in the setting up phase. This can only be due to thermal and particle losses, due to recycling processes and a net loss of the filling gas by the time of peak current.

Table 2

Energy Account for Setting up an RFP at τ_r = 1.4ms

Term	Energy (MJ)	Source
I_ϕ circuit input, ΔW_L	0.3	measured
Increase in magnetic energy, ΔW_M	0.2	measured
	0.1	
Ionisation/disassociation	0.002	estimated
Radiation - upper limit	$\leqslant$ 0.03	measured
Plasma thermal energy at $\hat{I}$	0.007	measured
	$\leqslant$ 0.039	
Other losses, W_x	0.06 to 0.09	difference

Applying these results to varying rise time experiments it is found that $W_x \sim 0.07$MJ at τ_r = 0.8ms and 0.095MJ at τ_r = 2.6ms. Taking the average power loss as W_x/τ_r we find that this quantity decreases by a factor of about 2.5 between the shortest and the longest rise times and the fluctuation level, $\langle \tilde{i} \rangle$, falls by a similar amount. This suggests a close relationship between the power loss and the fluctuation level.

(4) Magnetic Field Evolution

At $\theta \gtrsim 1.3$ the toroidal field is reversed so that a clearly non-paramagnetic, non-classical process has occurred. This is accompanied by an anomalously rapid penetration of the azimuthal field.[5] For the example given in Table 2 this energy, $W_{B\theta} = \frac{1}{2}L_g\hat{I}^2$, is about 0.17MJ. Full penetration of this field into a rigid conductor would be accompanied by the dissipation of $\sim 2W_{B\theta}$[6] i.e. 0.34MJ, which is much greater than the observed value of $W_x \sim 0.1$MJ.

(5) Scaling

Since for a given θ the field configurations are observed to be similar, the flux and energy changes due to the magnetic fields scale only with the plasma

length and current, i.e. $\Delta\phi/\hat{I}R$ = constant and $W_M/\hat{I}^2R$ = constant, where R is the major radius (note that ZETA was a racetrack with an effective major radius of 1.88m). There is insufficient experimental data to determine the rise time dependent contributions but since these appear to be of resistive origin one may assume that, τ_V, τ_W $\propto$ $a^2\bar{R}_p$. Non-classical models suggest that the mean plasma resistance, $\bar{R}_p$ $\propto$ I^n, where $n = -\frac{1}{2}$ to -1. Although the measured plasma resistance shows a classical scaling with current during quiescence[3] the value at peak current scales less favourably so that classical scaling ($n = -3$) is clearly not applicable to the setting up phase of ZETA.

CONCLUSIONS

It has long been known that in ZETA B_ϕ reversed at the liner, B_θ penetrated the plasma rapidly and the plasma energy at $\hat{I}$ was a small fraction of both the total magnetic energy and the energy dissipated. Here we have shown that during the setting up phase:

- the change in both the input energy and the input poloidal flux increased with rise time;
- both the plasma resistance and the fluctuations $\dot{I}$ at peak current decreased with rise time.

These observations indicate that non-laminar and non-classical processes occur in the setting up stage.

These results also indicate the need to identify more efficient ways of setting up the RFP.

REFERENCES

[1] Proc RFP Workshop, Padova (1978) UPee 78/08.

[2] H A B Bodin and A A Newton: to be published in Nuclear Fusion.

[3] E P Butt and A A Newton: in "Pulsed High Beta Plasmas", ed D E Evans, Pergamon (1976) p425.

[4] E P Butt et al: Proc IAEA Conf, Culham, vol 2 (1965) 751.

[5] D J Lees et al: Plasma Physics 7 (1965) 141.

[6] J D Lawson: Culham Laboratory Report (1977) CLM-R171.
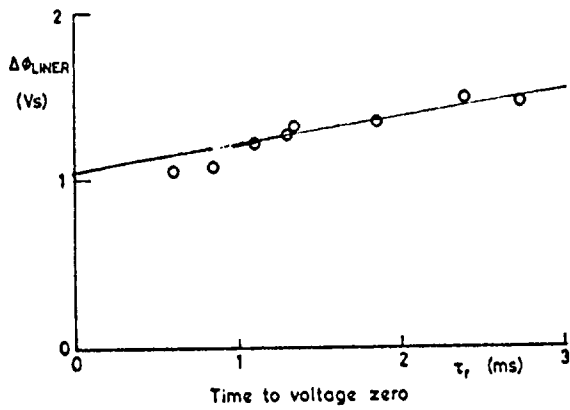
Fig 1 Azimuthal flux input to plasma
volume vs risetime (conditions
in text).
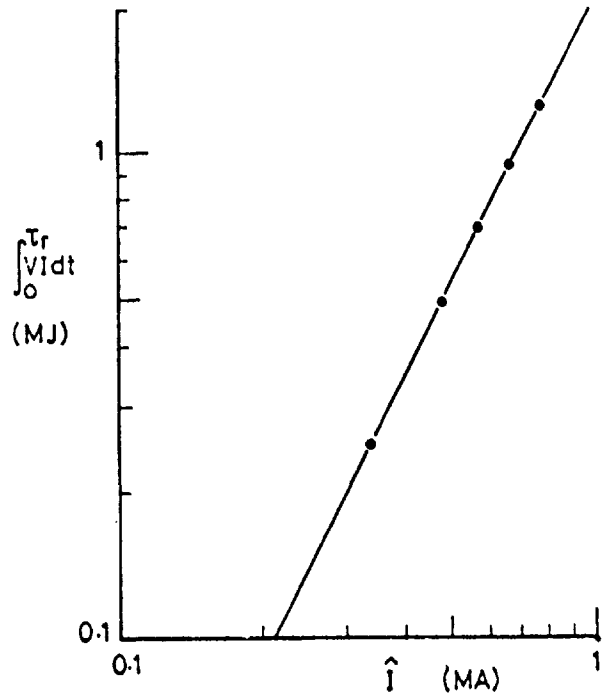
Fig 3 Energy input vs peak current
for $\theta = 1.6$, p_o = 2mtorr D_2.

Fig 2 Energy input and integrated
radiation loss vs risetime.
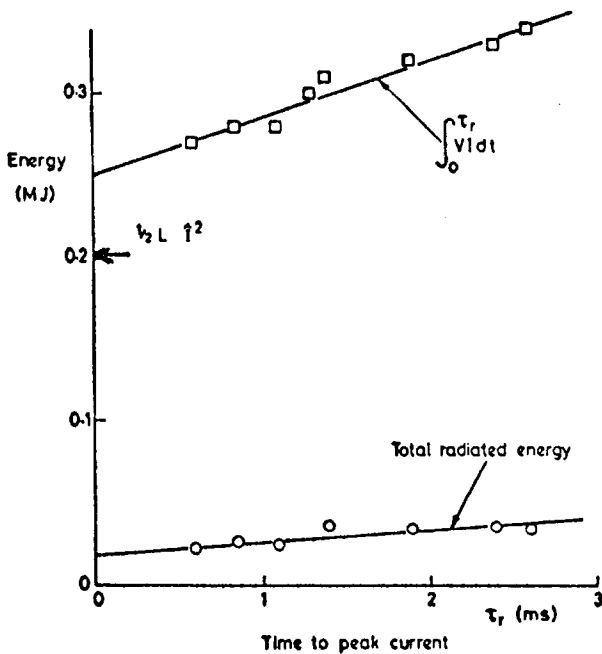
Fig 4 Normalised flux and energy
inputs vs pinch parameter, θ.

48
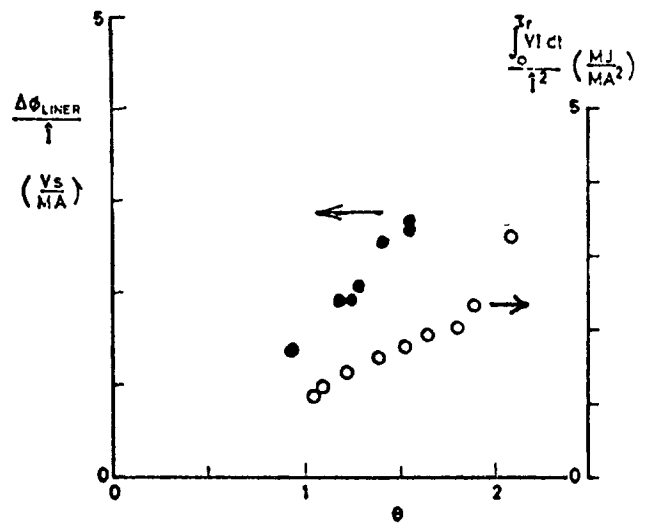
PROGRAMMING AND SELF-REVERSED PINCHES IN THE ETA-BETA II EXPERIMENT

Buffa A., Costa S., De Angelis R., Giudicotti L. Gowers C.W.[+], Nalesso G.F., Ortolani S., Puiatti M.[*], Scarin P., Watts M.R.C.[+]

Centro di Studio sui Gas Ionizzati
Consiglio Nazionale delle Ricerche – Università di Padova
Associazione Euratom – CNR, Padova, Italy

ABSTRACT

The effect of varying the field programming to produce a range of θ , is studied, one case being spheromak-like with toroidal field at the wall zero. New results for self-reversed pinches are also presented.

EFFECT OF VARYING THE PROGRAMMING 'SPHEROMAK'

This section describes the programming and refers to discharges controlled to have a range of different θ values at the end of the programming phase.

Figure 1(a) gives a 'standard' shot. The current is induced by V_ϕ applied from a capacitor bank; V_ϕ is switched on at 0.25 ms in the figure then, in ~90 μs falls to zero and is clamped. A peak current of ~250 kA is reached with θ ~1.5. The toroidal field circuit is used to establish a B_ϕ bias field before the plasma is created, then during the current rise the circuit is used to aid the reversal – $V_{\theta liner}$ is negative. This negative V_θ is also maintained after the current peak, producing additional reversal and lowering the plasma current. The circuit interaction is best understood with a model linking the two circuits [1]. It has not yet been found possible to create a quiescent RFP without using aided reversal and the initial high current peak and low θ have also so far been necessary. The evaluation of the discharge on the F–θ curve is seen to be similar to that of previous experiments [2,3]. Some excursion takes place at the end of the programming as B_ϕ equilibrates across the liner. Also shown in the figure is the signal of a flux loop wound around the liner. The scale is given in terms of the average magnetic field. The F and θ values discussed in this paper are defined as $F = B_{\phi wi}/<B_\phi>$ and $\theta = B_{\theta wi}/<B_\phi>$ where $B_{\phi wi}$ and $B_{\theta wi}$ are the values of the fields just inside the liner. $<B_\phi>$ is the average field measured by the flux loop.

In Fig. 1(b) the programming differs only in that the V_θ crowbar is applied 60 μs earlier; the discharge starts the qp with a higher current, lower θ and less reversal. In Fig. 1(c) the V_θ crowbar is a further 20 μs ealier. In all the three cases I_ϕ decays with a similar gradient and during the decay the discharges move up the F–θ curve at a similar rate. When F approaches zero (i.e.

---

the B_ϕ reversal is lost) and the discharge approaches a Spheromak state, the current decay rate increases sharply. If the discharge is programmed to decay from $\theta < 1.5$ (stabilised pinch) no quiescence is observed and approximately exponential current decay occurs [4].

SELF REVERSED PINCHES

The relaxation mechanism appears to be operating in the pinches described above, as indicated by the form of the F–θ curve. It is possible to demonstrate the process more clearly by forming entirely self reversed pinches (SRP). Figure 2(a) gives an example of an SRP. B_ϕ bias field is set up, the V_θ crowbar is applied and B_ϕ is allowed to equilibrate across the liner, then from ~.5 ms in the figure the I_ϕ current is induced. The discharge evolves along the usual curve in F–θ to become an RFP. For SRP's, however, no quiescence is observed, but the fluctuation level is seen to be substantially lower in the SRP even if the current decays rapidly. This could be due; to the fact that the SRP does not reach as high a peak current as the aided RFP; to the details of the profile established by programming; or to high wall interaction as the SRP must do work to reverse the field outside the liner (The area between B_ϕ flux conserver and the liner is high; $\lambda = \phi_{ext}/\phi_{int.} \simeq 1$). However the total radiation signal does not show a significant increase as compared to the aided RFP [5].

Figure 2(b) shows an example with a higher initial B_ϕ which therefore does not reverse. Comparison of (a) and (b) shows that, in the absence of quiescence, the field reversal does not improve the gross behaviour markedly.

The discharge traces the normal locus in F–θ where F–θ are defined just inside the liner. By contrast for F–θ defined just outside the liner or at the flux conserver, the F–θ curves are not unique, varying strongly with program – ming.

CONCLUSIONS

In the optimum I/N range [5], by varying the field programming configura – tions with different θ values are produced. Provided the toroidal field is re-versed at the wall, in all the cases the current decays with a similar gradient and during the decay the discharges move up to the F–θ curve at a similar rate. When F approaches zero (i.e. the B_ϕ reversal is lost) the current decay rate increases sharply and the discharge terminates. Self-reversed pinches have been formed in ETA–BETA II; the magnetic field fluctuations measured by internal probes are much lower than in stabilised pinches, however the long quiet decay observed for aided reversal RFP [5] is not observed.

ACKNOWLEDGEMENTS

50

REFERENCES

[1] Johnston J.W. et al., contributed paper to this Workshop.
[2] Bagatin M. et al., 7th Int. Conf. on Plasma Phys. and Contr. Nucl. Fus.,
    Innsbruck (1978), IAEA-CN-37-E-1-3.
[3] Carolan P.G. et al., 7th Int. Conf. on Plasma Phys. and Contr. Nucl. Fus.,
    IAEA-CN-37-E-1-2.
[4] Buffa A. et al., 9th European Conference on Controlled Fusion and Plasma
    Physics - Oxford, 1979, vol. II, 544.
[5] Buffa A. et al., contributed paper to this Workshop.
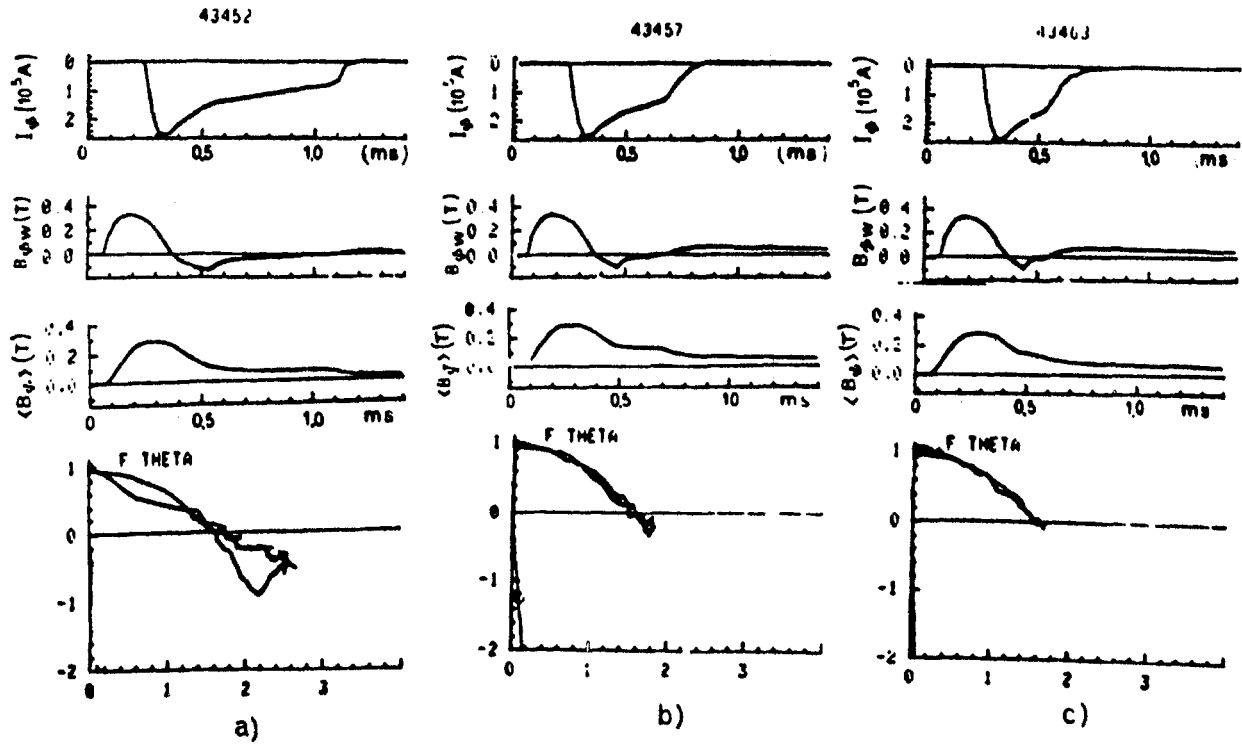
fig.1
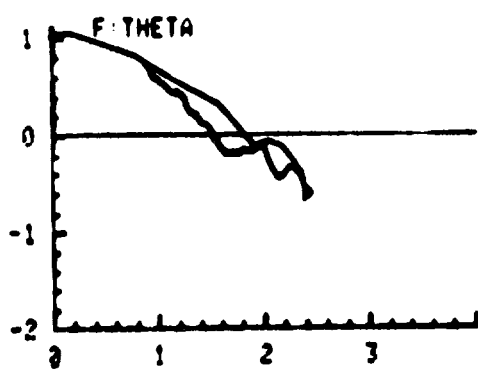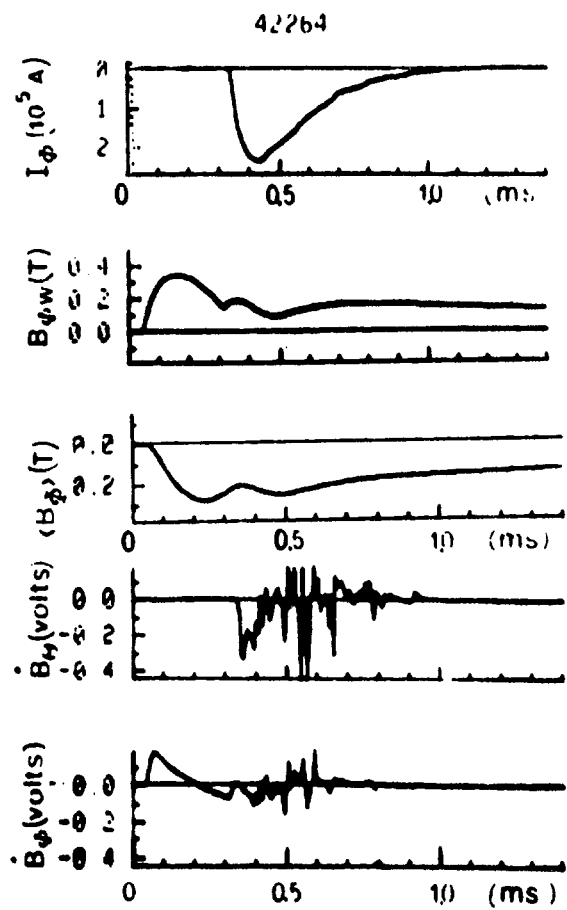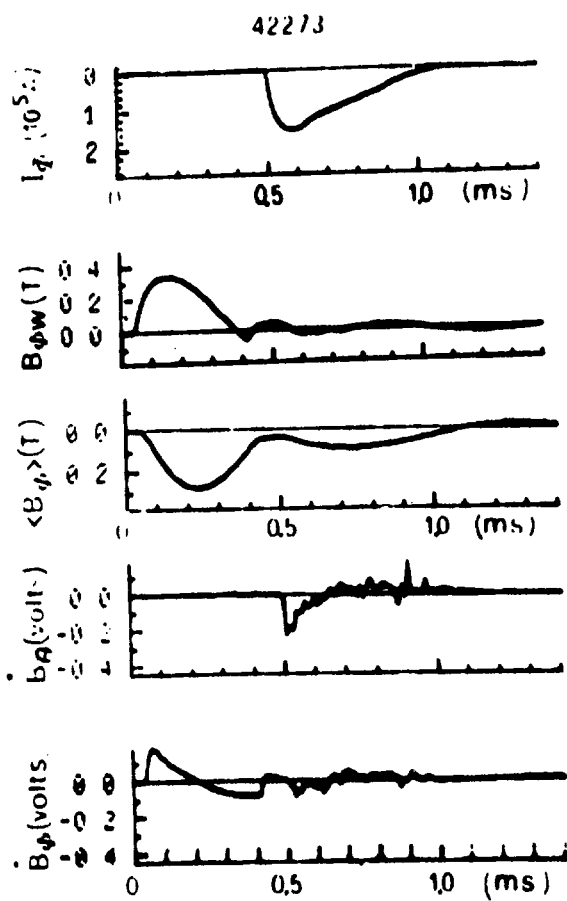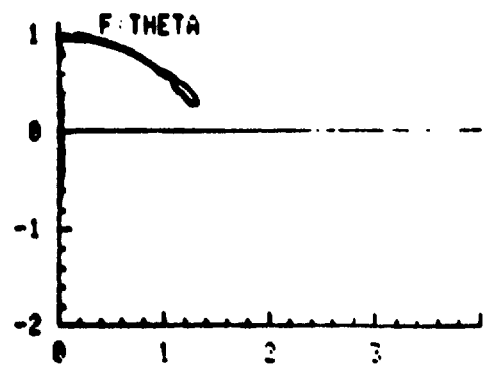
fig.2

OPTIMIZATION AND PROPERTIES OF REVERSED FIELD PINCHES
IN THE ETA-BETA II EXPERIMENT

Buffa A., Costa S., De Angelis R., Giudicotti L., Gowers C.W.[+], Nalesso G.F.,
Ortolani S., Puiatti M.[*], Scarin P., Watts M.R.C.[+]

Centro di Studio sui Gas Ionizzati
Consiglio Nazionale delle Ricerche – Università di Padova
Associazione Euratom – CNR, Padova, Italy

ABSTRACT

The range of parameters in which optimum heating and confinement of RFP's
is obtained is studied by varying the filling pressure and the toroidal current
amplitude. Impurity radiation losses are found to dominate at relatively high
densities ($p_0 \geq 10$ mtorr). Large magnetic field fluctuations are found at low
densities but an optimum range exists (at $I/N \approx 10^{-14} A \cdot m$) with small radiation
losses and reduced fluctuations characterized by long current duration (~ 1 ms)
and higher temperatures (~ 80 eV).

INTRODUCTION

The ETA-BETA II experiment has been operating since March 1979. RFP plasmas
have been studied produced by relatively slow setting-up, i.e. whose current
rise time ($\sim 100 \mu s$) is long compared with the relaxation time ($\tau_{MHD} \simeq 1 \mu s$).
ETA - BETA II has a stainless steel vacuum vessel ($r = .125$ m, $R = .65$ m) of
thickness .25 mm. Deuterium is used as filling gas.

Studies of RFP's at various filling pressures and the comparison between
RFP's produced by aided reversal and simple stabilized pinches have been
reported previously [1]. This paper describes further results which extend those
of [1] to lower densities and to different current levels. Results are reported
from additional diagnostics including interferometry and total radiation
measurements. New results for self-reversed pinches are described in another
paper [2] along with the effect of varying the field programming to produce a
range of θ, one case being Spheromak - like with toroidal field at the wall, B_{ϕ_w},
zero.

With the exception of the studies on self-reversed pinches all the cases
described have the same basic programming - aided reversal. In this mode $V_{\theta liner}$
is programmed to be small and tend to increase, or "aid", the reversal of B_{ϕ_w}
during the current rise time.

+ on leave from Culham Laboratory, U.K.
* graduating student

VARIATION OF BEHAVIOUR WITH FILLING PRESSURE AND CURRENT

The range of usable filling pressures, p_0, has been extended to a lower value, 3mtorr, by employing a heated filament which removes the erratic breakdown previously found below ~5 mtorr. Fig. 1 shows results from 3 RFP's where the filling pressure only has been varied. The top two waveforms, the total toroidal current, I_ϕ, and B_{ϕ_w} illustrate that while a similar peak current and reversed B_{ϕ_w} are attained at various p_0, the later evolution of the pinch depends strongly on p_0. The 6.6 mtorr example falls in an optimum pressure range in which the decay of I_ϕ and B_{ϕ_w} become much slower than in the high and low p_0 cases while the final termination is abrupt. The next three waveforms show $\dot{I}_\phi$, $\dot{B}_\theta$ and B_ϕ. The latter two are measured with an insertable probe in a porthole at minor radii 0·157 m (B_ϕ) and 0·145 m (B_θ). The level of fluctuation of these quantities is seen to fall as p_0 is increased. (For overall clarity the graphs show points every 10 μs only and thus any frequency above ~ 50 kHz is aliased). The signal P_{RAD} gives the total radiated power loss measured with a Sodium salicylate scintillator [3] and integrated along a minor diameter. The peak value of P_{RAD} increases with p_0 and the time behaviour changes from being approximately constant in time at high p_0 to falling sharply at ≤ 6 mtorr. The bottom traces show the line of sight density measured on a minor diameter with a laser interferometer [4]. The scale in the figure is in terms of average electron density corresponding to a uniform radial profile. The initial peak density is approximately proportional to p_0 and would correspond to an electron density, n_e, equivalent to twice p_0 distributed uniformly or a mildly peaked profile with total n_e equivalent to p_0. Thereafter the density is maintained in the high p_0 case whereas at $p_0 \leq 6$ mtorr the density falls markedly. (The base-line of the interferometer measurement is affected by vibration from ~ 0.7 ms).

The scan of filling pressure from which figure 1 shows examples has been repeated for 3 peak toroidal current levels; $I_\phi = 180$, 250 and 280 kA. Figure 2(a) summarises the results of the p_0 scans at 180 and 280 kA. In the figure τ_I re-presents the time for the current to decay to 1/e of its peak value. In both cases the radiated power (the maximum of the measured signal is reported) increases with p_0, first proportionally to p_0 then tending to saturate for $p_0 \geq 14$ mtorr as the temperature decreases. The results of temperature measurements on axis at various filling pressures (only in the range 6–15 mtorr) at the time of current peak are reported in figure 2(b) for the scan of p_0 with $I_\phi \simeq 250$ kA. The level of magnetic fluctuations, $\delta B/B$, is indicated also in figure 2(b) where the peak to peak of the high frequency (~ 100 kHz) fluctuation normalised to B_θ is reported. Also shown in figure 2(a) are, for the higher current case, the results from a zero-dimensional model in which the ETA-BETA II circuit drives a plasma with classical resistivity and in which the significant energy losses considered are impurity radiation from oxygen [5] and turbulent energy transport proportional to $\delta B/B$ [6]. When the measured values of $\delta B/B$ are used together with an oxygen impurity content of 4 10^{18}m-3 the code predictions for τ_I and P_{RAD} are similar to the observed values. The code indicates that at high pres-sure impurity radiation loss dominates whereas below the optimum pressure range

54

turbulent transport limits the electron temperature. In figure 2(b) the computed temperature is also compared with that measured in the range of pressures in which radiation losses dominate and measurements have been done so far.

Absolute measurements of the total radiation are not possible at moment; however the average energy of the measured photons has been evaluated by using various filters, including gas filters, |3| and the average energy does not vary significantly ($<\lambda>\sim 500$ Å) with filling pressure thus the relative comparison of the radiation at the various filling pressures is reasonable. The integrated power radiated can be compared with the energy input; the results are reported in figure 4 where it is assumed that the radiated energy represents the total energy loss at the highest pressure considered. At the lower filling pressures the radiated energy would correspondingly represent only $\lesssim 10\%$ of the total losses.

In figure 2(a) the optimum p_0 range is seen to be from about 6 to 8 mtorr for the higher current case and from ~ 4 to ~ 6 mtorr for the lower. At larger current the increased ohmic heating power allows burning through of the impurities at correspondingly higher densities. However the larger the current, the higher is the critical filling pressure below which large fluctuations appear and poor confinement is obtained. The relevant parameter seems to be I/N as discussed in |7,8|. In figure 3 the results of the pressure scans at the various current levels are plotted as a function of I/N. The optimum range is similar in the various cases and centered at about $1-1.5 \cdot 10^{-14}$ A·m. The value of N, the line density, used is that corresponding to p_0. The actual line density is known to vary in time from interferometry measurements, but is proportional to the filling density near the current peak. Subsequently, of course, both the current and density vary. As a scaling parameter the peak toroidal current divided by the number of electrons corresponding to the filling pressure is considered in the figure.

PROPERTIES OF THE 'QUIESCENT PHASE'

In Fig. 1, 6.6 mtorr case, the phase from 0.6 to 1.4 ms is noticeably different from that of the low and high pressure cases and is loosely termed the quiescent phase, (qp). During this phase the current decay is approximately linear and would fall to 1/e of its initial qp value in more than 1 ms, extrapolating. The qp is only seen for a certain filling pressure range, described above as the optimum p_0 range. The length of this phase, the current level and decay time are all reproducible from shot-to-shot and month-to-month. The qp is not seen if the internal probe is inserted more than ~ 4 cm or for the first few shots after air has entered the vacuum system. In these cases the current decay is more rapid and the abrupt termination is not seen. The qp has only been produced in aided reversal RFP's.

Figure 5 shows the evolution of the temperature and density of an RFP with quiescence. The electron temperature, T_e, on axis measured by Thomson scattering rises from ~ 40 eV at peak current to ~ 80 eV and T_e remains approximately 80 eV during the qp. The corresponding density on axis drops by a factor of about 2 at the start of quiescence, while the line of sight density (interferometer mea-

surement) drops by about 4 for a similar shot indicating that the electron density profile may vary as well. In more recent shots, an even more pronounced drop in the density measured by the interferometer was observed (see figure 1), to a level similar to the error of the measurement. Derivations of the energy confinement time, τ_E, based on some internal probe measurements and on the density and temperature measurements indicate that τ_E is $\sim 100\,\mu s$ during the slow current decay. An analysis of the current decay phase with a circuit model [9] indicate that the electrical resistance decreases rapidly during the initial current decay and that subsequently (during the linear decay phase) it stays constant or increases. This analysis is not in contrast with the electron temperature results shown in figure 5. Data has been collected on the fluctuating magnetic fields using an inserted probe just outside the plasma (Fig. 1) and inserted in the liner up to 3.75 cm. Preliminary analysis of the fluctuations show that the rms level of $\delta B/B$ is typically 0.5% during quiescence; ~ 5 times lower than during the programming. Frequencies from a few tens to a few hundreds of kHz are observed and it is found that δB_z and δB_θ are similar in amplitude.

As illustrated above, the qp is always found to end when B_w approaches zero. This is true for the range of programming and p_0 explored so far [2]. The termination is generally preceeded by increased activity on the probe signals for 10-50 μs (see for example figure 1(b)) then I_ϕ drops to zero over about 20 μs and B_{ϕ_w} becomes positive with a rapid change on the same timescale. The mechanism of the termination is not yet clear. As the current decays the discharge retraces the usual F-θ curve [2]. When F=0 is approached, the current terminates abruptly.

CONCLUSIONS

A period of "quiescence" (improved confinement) is observed in ETA-BETA II for a range of I/N centered at $1-1.5 \cdot 10^{-14}$ A·m. Impurity radiation is the dominant loss at relatively high densities (lower I/N) and turbulent transport associated with large magnetic field fluctuations dominates at lower densities (higher I/N) but an optimum exists, which shows "quiescence" with small radiation losses and reduced fluctuations. At the beginning of quiescence the density drops by a factor of 2-4 and the electron temperature doubles. During quiescence T_e is typically 80 eV, and τ_E is estimated to be $\sim 100\,\mu s$.

ACKNOWLEDGEMENTS

REFERENCES

[1] Buffa A. et al. 9th European Conference on Controlled Fusion and Plasma Physics - Oxford, 1979, vol. II, 544.
[2] Buffa A. et al. contributed paper to this Workshop.
[3] De Angelis R. et al. UPee report to be published.
[4] Jacobson A.R. Rev. Scient. Instr. 49(5), 1978, 673.

[5] Costa S., Ortolani S. UPee 75/06, 1975.

[6] Robinson D.C., Proc. Conf. on Pulsed high beta plasmas, Culham, 1975, p. 273.

[7] Ortolani S., Rostagni G., Padova internal note, GIP 79-20, 1979.

[8] Ortolani S., Proc. of Symp. on Compact Toruses and Energetic Particle Injection, Princeton, 1979, p. 89.

[9] Nalesso G.F., contribution to this Workshop.

fig. 1

fig. 2 a

fig. 2 b

58

fig. 3

fig. 4

fig. 5

59
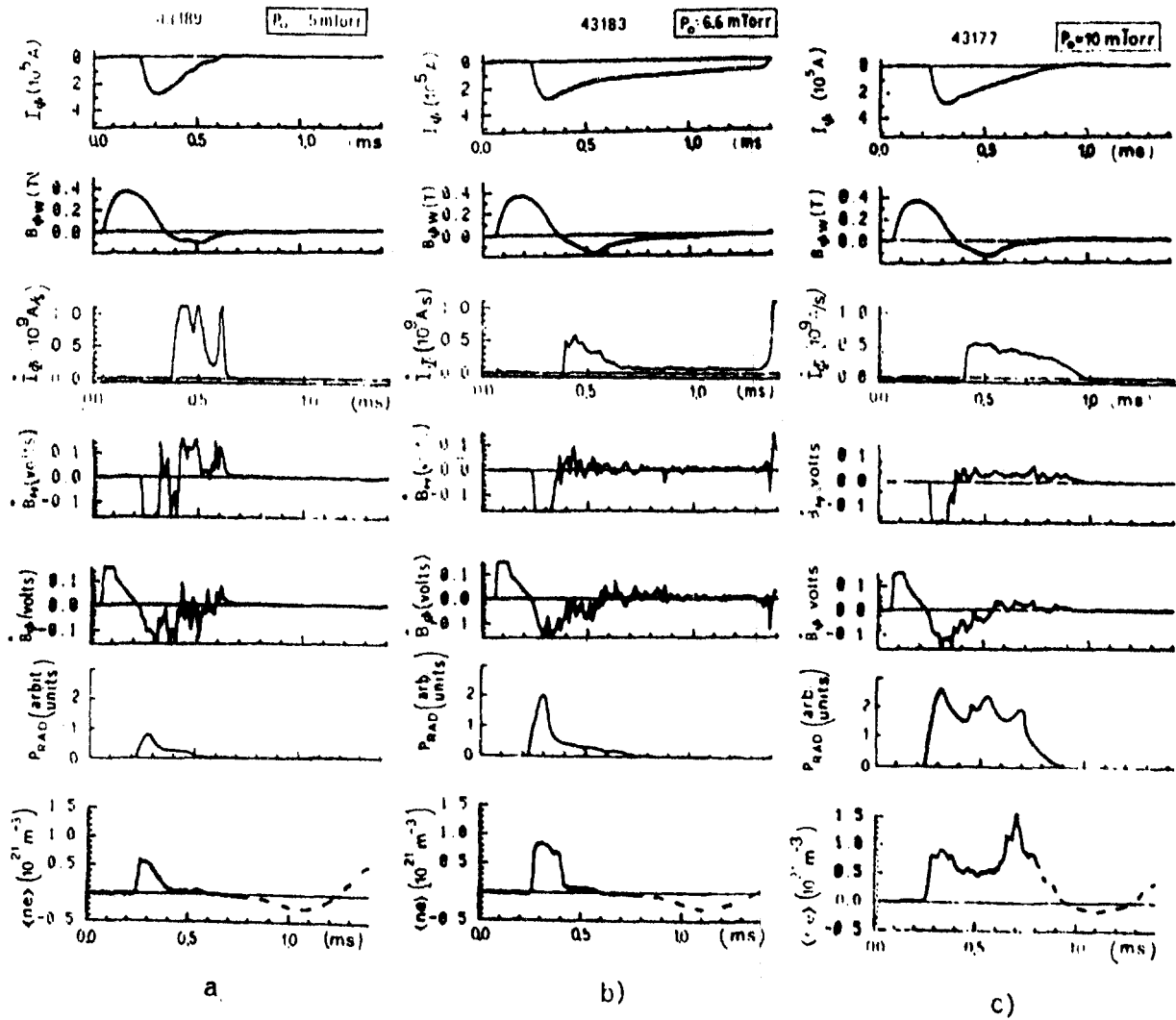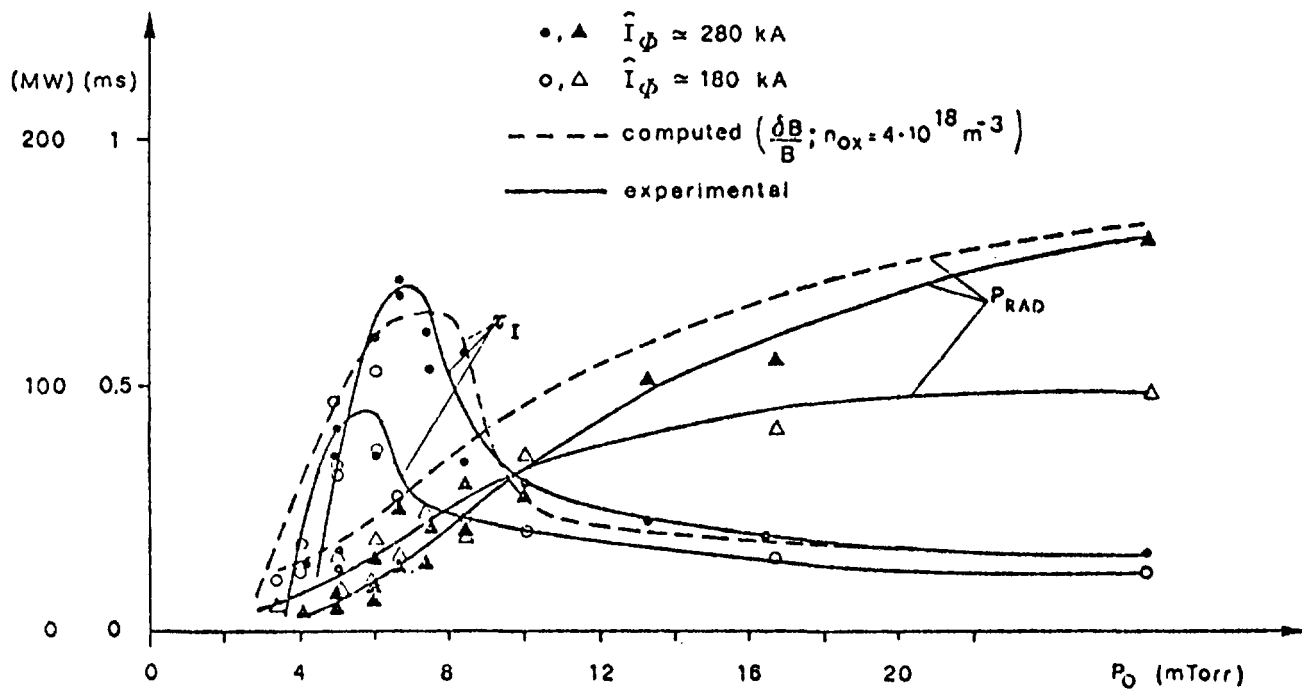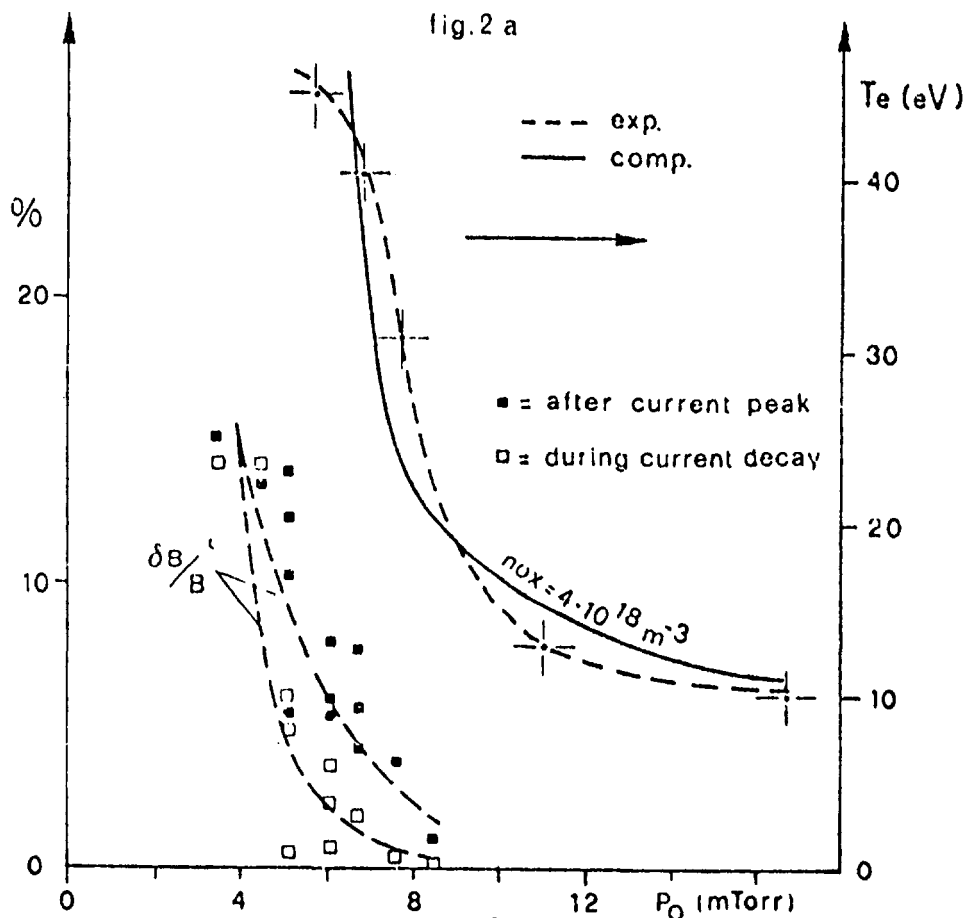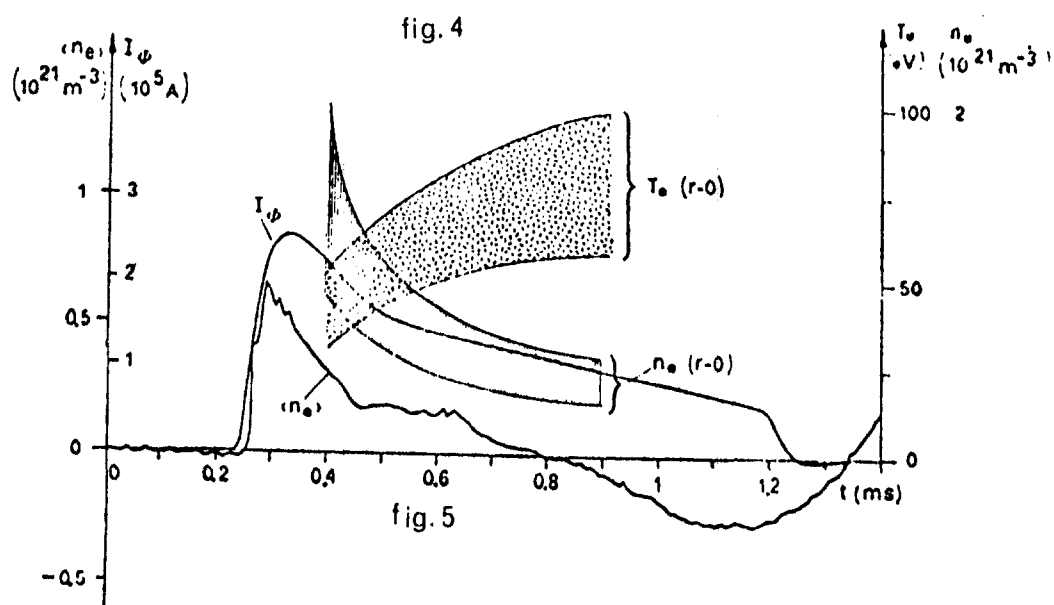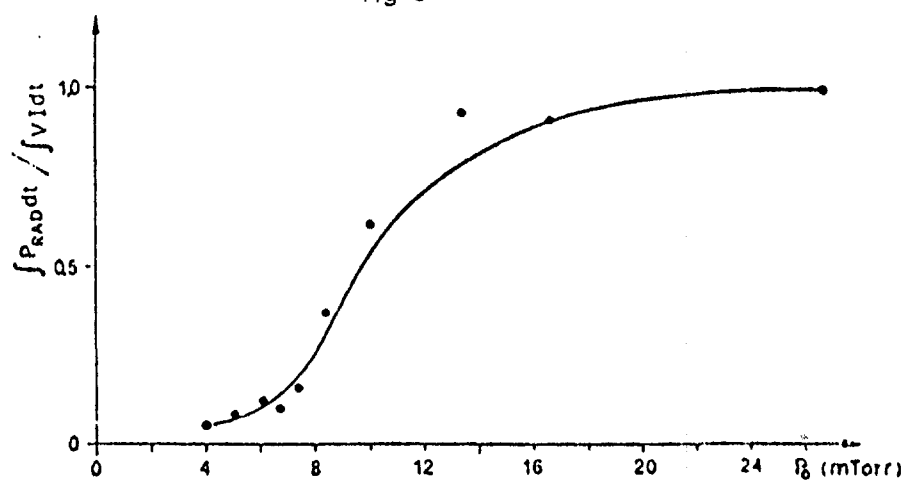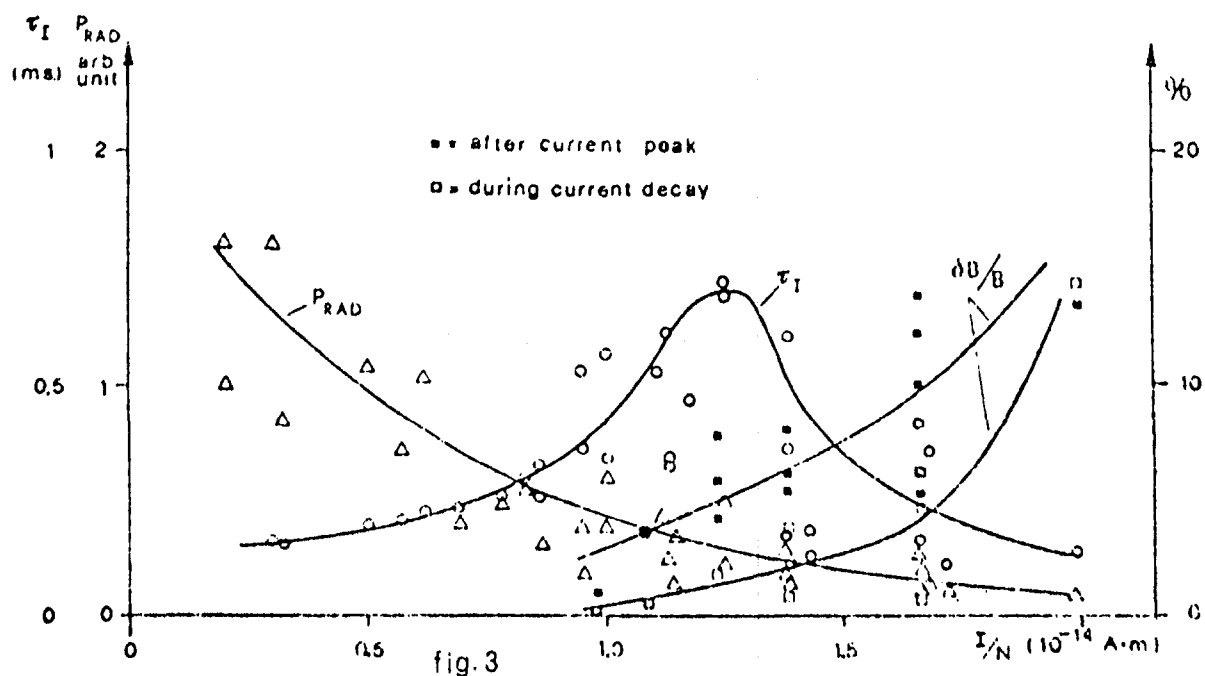
Plasma Resistance Behavior during the Linear
Decay Phase of RFPs in ETA BETA II

G. F. Nalesso

Centro di Studio sui Gas Ionizzati
del Consiglio Nazionale delle Ricerche e dell'Università di Padova
(Associazione Euratom-CNR)-Padova (Italy)

Introduction

In the "aided-reversal" mode RFP discharges produced in ETA BETA II,[1] the plasma current is characterized by a linear decay phase, which follows an approximately exponential phase. During the same period the measured toroidal voltage is negative and initially increasing in absolute value (exponential phase) and then decreasing to almost zero during the linear phase before the current termination (see Fig. 1). The same behavior of the current has been observed in the "quiescent phase" in Zeta[2] (see Fig. 2) where a negative toroidal electric field was also observed. In this note we present a model that can explain the linear decay phase and fits with the experimental parameters and allows us to estimate the plasma resistance behavior during the linear phase of slow reversed field pinch discharges.

Plasma Model

The electrical behavior of the discharge can be explained with a simple model where the plasma is considered as an impedance with a resistive part in series with an inductive part, both variable in time. We can then write the linear differential equation

$$V_\phi(t) = R_p(t)I_p(t) + \frac{d}{dt}\left[L_p(t)I_p(t)\right] \quad , \tag{1}$$

where V_ϕ is the voltage drop at the impedance (which is measured) and I_p the (plasma) current. To find a solution of the previous equation we assume a Taylor's series expansion for the functions L_p, R_p and V_ϕ, namely

$$L_p(t) = L_0\left[1 + \sum_1^\infty \frac{L^{(n)}}{L_0}\frac{t^n}{n!}\right]$$

$$R_p(t) = R_0\left[1 + \sum_1^\infty \frac{R^{(n)}}{R_0}\frac{t^n}{n!}\right]$$

$$v_\phi(t) = V_0 \left[1 + \sum_{1}^{\infty}{}_n \frac{v^{(n)}}{V_0} \frac{t^n}{n!}\right] \quad . \tag{2}$$

Let us first consider the simplified case where the time variation of the plasma inductance is negligible compared with the changes in the other quantities ($L = \text{cost} = L_0$). To the first order and with initial condition $I(o) = I_0$ we get

$$I(t) \simeq I_0 - \left(\frac{R_0}{L_0} I_0 + \frac{V_0}{L_0}\right) t \quad ,$$

$$\frac{dI}{dt} \simeq -\left(\frac{R_0}{L_0} I_0 + \frac{V_0}{L_0}\right) + \left[\frac{V_0}{L_0}\left(\frac{1}{\tau_V} + \frac{R_0}{L_0}\right) + \frac{R_0 I_0}{L_0}\left(\frac{R_0}{L_0} - \frac{1}{\tau_R}\right)\right] t \quad , \tag{3}$$

with $\dfrac{1}{\tau_R} = \dfrac{R^{(1)}}{R_0}$

$$V_\phi \simeq -V_0\left(1 - \frac{t}{\tau_V}\right) \qquad (\tau_V > 0) \quad . \tag{4}$$

It turns out then that only a resistance increasing with time ($\tau_R > 0$) can give a constant time derivative to the first order and, in this approximation this happens when

$$\frac{V_0}{L_0}\left(\frac{1}{\tau_V} + \frac{R_0}{L_0}\right) + \frac{R_0 I_0}{L_0}\left(\frac{R_0}{L_0} - \frac{1}{\tau_R}\right) = 0 \quad . \tag{5}$$

In the general case, assuming a time-dependent plasma inductance, it is easy to show that we can get, to the first order, the same solution as before, provided that the expression for R_0, L_0, τ_R and τ_V are substituted with

$$R_o' = R_o + L^{(1)}$$

$$L_o' = L_o$$

$$\frac{1}{\tau_R'} = \left(\frac{R_o}{R_o'}\right)\frac{1}{\tau_R} - \left[\frac{L^{(1)}}{L_o}\right]$$

$$\frac{1}{\tau_V'} = \left[\frac{1}{\tau_V} + \frac{L^{(1)}}{L_o}\right] \quad . \tag{6}$$

Now, if the plasma inductance is increasing in time ($L^{(1)} > 0$), to get a constant dI/dt to the first order it is necessary to have a bigger increase in the plasma resistance than in the previous case. However, if we assume a decreasing plasma inductance ($L^{(1)} < 0$), the linear behavior can be explained also with a constant or even decreasing plasma resistance. The condition for a linear behavior will read in this case

$$-\frac{L^{(1)}}{L_o} = \frac{V_o\left(\frac{1}{\tau_V} + \frac{R_o'}{L_o}\right) + \frac{R_o' I_o}{L_o}\left(R_o' - \frac{L_o}{\tau_R}\right)}{V_o + R_o' I_o + \frac{L_o I_o}{\tau_R}} \quad . \tag{7}$$

Numerical Results for ETA BETA II

If we now consider the following experimental parameters (in some typical conditions) for ETA BETA II (see Fig. 1),

$$V_o \simeq 25 \text{ V}$$

$$\tau_V \simeq 0.4 \text{ ms}$$

$$I_o \simeq 160 \text{ kA (at the beginning of the linear phase)}$$

$$\frac{dI}{dt} \simeq -10^8 \text{ A/s}$$

62

and an estimated initial plasma inductance

$$L_o \simeq 0.6 \ \mu H$$

we can deduce, for the constant inductance case,

$$R_o \simeq 2 \times 10^{-4} \ \Omega$$

$$\frac{L_o}{R_o} \simeq 3 \ ms$$

so that the current time derivative is constant if

$$\tau_R \simeq \tau_V \simeq 0.4 \ ms \quad .$$

For the general case of varying both the plasma resistance and inductance, let us consider the limiting case of constant resistance. We see, with the same parameters of the previous example, that Eq. (7) can be satisfied if

$$-\frac{L^{(1)}}{L_o} \simeq \frac{1}{2\tau_V} \simeq \frac{10^4}{8} \quad ,$$

and it follows that $R_o \simeq 1 \ m\Omega$. This simply means that we can get a constant plasma resistance of 1 mΩ if the initial plasma inductance of 0.6 μH is linearly going to zero in 0.8 ms.

To conclude this consideration on the ETA BETA II case it is easy to show that for a decreasing resistance we can get a maximum of $|\tau_R| \sim 1.6$ ms in the limiting case where $L^{(1)} \to \infty$.

Conclusions

The observed linear decay phase of the plasma current in the RFPs in ETA BETA II can be explained on the basis of a simple model assuming a plasma resistance increasing linearly with a characteristic time approximately equal to the time of the linear phase ($\tau_R \simeq 0.4$ ms for the considered case), if the plasma inductance varies in times much longer than this characteristic time.

However, if the plasma inductance decreases with a characteristic time of the same order, a constant or even slightly decreasing plasma resistance is compatible with the observed behavior. However, even if it is reasonable to assume a decreasing inductance, taking into account, e.g., the electron

density and the θ time behavior, the characteristic time would be of the order of some milliseconds, i.e., much longer than the lifetime of the linear phase, so that an increasing resistance is more likely to occur. The initial plasma resistance, on the basis of this model, can be estimated to lay between 0.2 mΩ and 1 mΩ.

To conclude we point out that the measured electron temperature on axis[3] shows a slight increase during the linear phase. Because the average resistance must be, at the most, constant in time, this would suggest, within the limitations of the model, the existence of an external region where the plasma is cooled down, but up to now no experimental results for the external region are available.

REFERENCES

1. A. Buffa, et al., Proc. IX EPS Conf., Oxford (1979) paper DP29.

2. Proc. Workshop on the RFP, Sept. 78, Padova VPee 78/08.

3. A. Buffa, et al., contribution to this workshop.

FIG. 1

FIG. 2

64
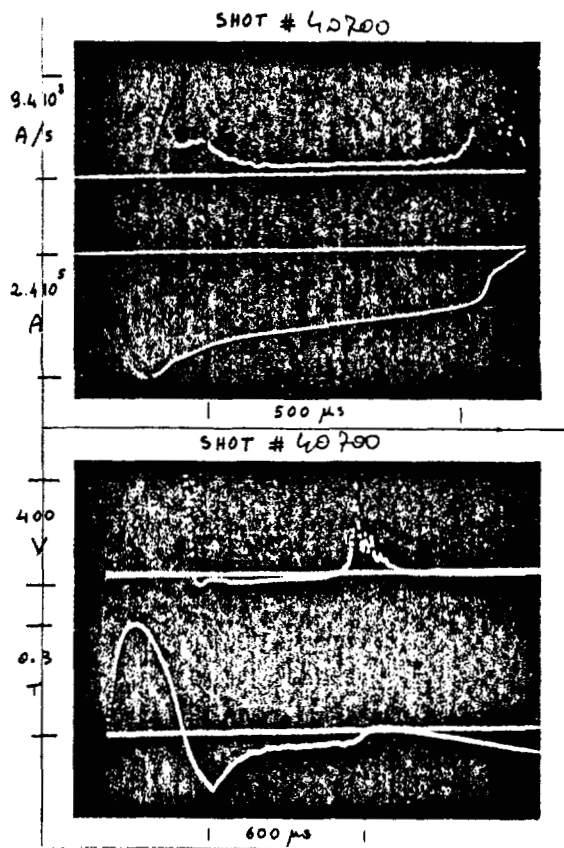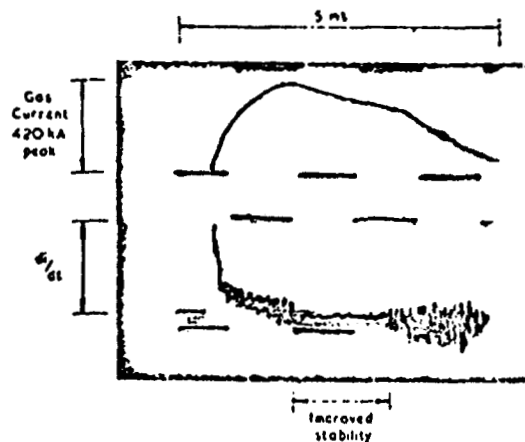
EXPERIMENTAL STATUS OF ZT-40*

A. Haberstich, D. A. Baker, M. D. Bausman, C. J. Buchenauer, L. C. Burkhardt, G. I. Chandler,
J. N. DiMarco, J. N. Downing, C. A. Ekdahl, P. R. Forman, K. B. Freese, R. F. Gribble,
R. B. Howell, A. R. Jacobson, F. C. Jahoda, K. A. Klare, E. M. Little, G. Miller, S. Ortolani**,
J.·A. Phillips, A. E. Schofield, K. S. Thomas, R. G. Watt, P. G. Weber, R. W. Wilkins, and
Y. Yoshida***

Los Alamos Scientific Laboratory, Los Alamos, N.M. 87545

INTRODUCTION

ZT-40 is a toroidal reversed-field pinch with major and minor diameters of 2.28 and 0.4 m. The discharge chamber is made of 99.5% pure alumina, and the experiment is designed for, and has been checked out at toroidal currents of up to 600 kA. In the present configuration, the rise time of the toroidal current can be varied from 250 to 100 μs by changing the number of toroidal feed points from 1 to 4. The rise time of the toroidal field is 50 μs. Preionization is accomplished by means of an RF discharge followed by a weak toroidal precursive current. The base pressure in the discharge chamber is 8×10^{-8} torr, and the main impurities have molecular weight 20 and 28.

ZT-40 has been in operation since October 5, 1979. There have been approximately 1800 shots, 80% of which were fired with 4 feeds and the remainder with 1 feed. The filling gas has been deuterium. A variety of programming modes has been explored. Here we present results for the stabilized (non-reversed) pinch, the self-reversed and the aided reversal modes.

The toroidal current is started in all 3 cases at the peak of the toroidal field. In the stabilized pinch mode, the toroidal field is crowbarred at the same time. The self-reversed pinch is simply a stabilized pinch with lower toroidal field, that is, a higher initial theta. Reversal is produced in the aided reversal mode by delaying the application of the toroidal field crowbar.

We begin the discussion with the formation phase of 4-feed stabilized pinches. We then describe observations made during the sustainment phase of 4-feed stabilized, self-reversed and aided reversal pinches. Finally we present preliminary results on the formation and sustainment of single feed stabilized pinches.

FORMATION PHASE

Figure 1 shows the toroidal current, toroidal flux and toroidal field at the wall of a typical 4-feed stabilized pinch at 20 mtorr filling pressure. The toroidal current starts at 50 μs. The behavior of the line integral of the electron density, as measured by IR interferometry (3.39 μm) along seven chords of the discharge tube, is shown in Fig. 2 for another 20 mtorr pinch. The chords are perpendicular to the midplane of the

experiment, and their positions relative to the major radius are -55, 5, 50, 79, 107, 126, and 164 mm.

The formation phase of the discharge lasts, in this case, from time 50 to 120 μs. It can be divided into an ionization phase (from time 50 to 75 μs), a quasi steady state phase (from time 75 to 87 μs), and a turbulent period followed at 120 μs by a substantial drop in density. This drop, which is more or less noticeable, depending on the
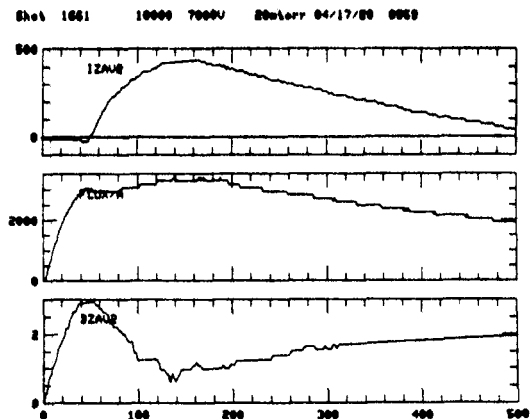
Fig. 1. Stabilized pinch. Toroidal current (kA), average toroidal field (G), and toroidal field at the wall (kG) vs time (μs).
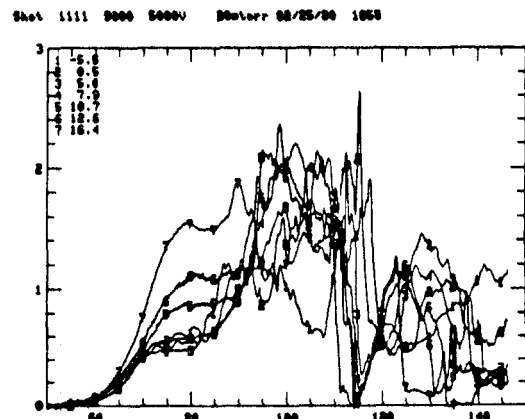
Fig. 2. Chord-averaged electron densities (fringes) vs time (μs).

65

discharge conditions, marks the beginning of the containment phase. The containment phase remains turbulent except for the quiet periods discussed below.

The ionization and quasi-steady state line densities are well behaved at this pressure. The outer chords show the highest readings, indicating a hollow ionization profile. As the fill pressure is lowered, the steady state period becomes shorter and the turbulence eventually reaches into the ionization phase.

The ionization phase is also characterized by a linear increase of the toroidal current and a nearly constant toroidal voltage, suggesting a constant initial discharge inductance. The value of this inductance is found to decrease from 0.16 μH per quadrant at 40 mtorr filling pressure to 0.08 μH at 10 mtorr, and then to increase sharply below that pressure.

CONTAINMENT PHASE

A. Stabilized Pinch

Typical current and field waveforms for this mode have been shown in Fig. 1. An important feature of the toroidal current trace is its decay time. This time is usually considered to be a measure of the resistivity of the plasma column. Note, however, that it is also a function of the circuit parameters, which are fairly well known, and of the inductance and rate of change of inductance of the plasma, about which we have little information.

The current decay rate for a series of 350 kA stabilized pinches is plotted in Fig. 3 as function of fill pressure. One sees that the decay rate increases rapidly at the lower pressures. This effect differs from the results of zero-dimensional calculations which predict longer decay times at lower pressure with constant impurity content.[1]
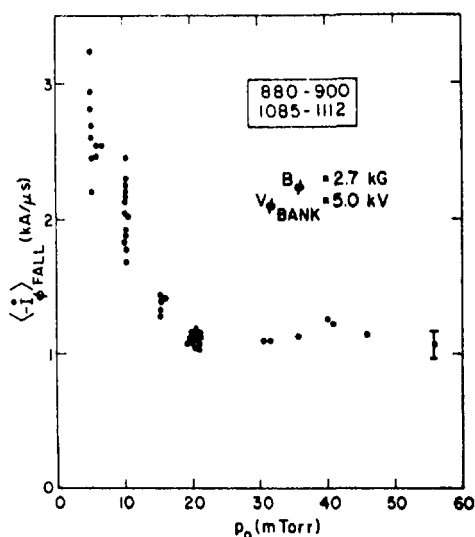
The 1/e of peak decay times at > 20 mtorr, at peak currents of 350 and 500 kA are, approximately, 200 and 250 μs. A model calculation assuming a perfectly conducting plasma, a uniform current density, and no compression gives comparable results. The decay times observed at high fill pressure appear, therefore, to be strongly affected by circuit parameters.

Abel inversion of line density measurements is made difficult by the density fluctuations and by uncertainties about the assumption of azimuthal symmetry. The general impression is that the density profiles during containment are either flat or hollow. This conclusion appears to apply to self-reversed and aided reversal pinches as well.

Figure 4 shows Thomson scattering measurements of the electron temperature on axis at peak toroidal current, as function of fill pressure. As in ETA-BETA II, there is an increase in temperature at lower pressure, but the temperature drops again below 5 mtorr. The fact that the temperature remains high at ~20 mtorr suggests a low impurity level.
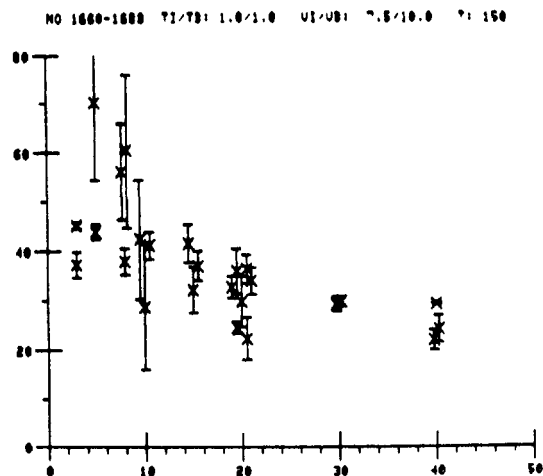
Fig. 4. Electron temperature (eV) on axis vs fill pressure (mtorr). Peak current 450 kA.

Both toroidal dI/dt and chord-integrated density traces show substantial levels of fluctuations. Details about these transient phenomena are given elsewhere in these proceedings. There are no quiet current or density periods under these non-reversed field conditions.

B. Self Reversal

Waveforms for this mode are shown in Fig. 5. The decay rates of the self-reversed discharges show a marked improvement over stabilized pinches in the sense that they remain approximately constant as the fill pressure is decreased. This is shown in Fig. 6. Thomson scattering temperatures under these conditions vary between 35 eV at 20 mtorr, and 50 eV at 5 mtorr.

Another interesting feature of self-reversed discharges at low fill pressure is the occurence of quiet periods. The symptoms differ from the

Fig. 3. Toroidal current decay rate vs fill pressure. Peak current 350 kA.
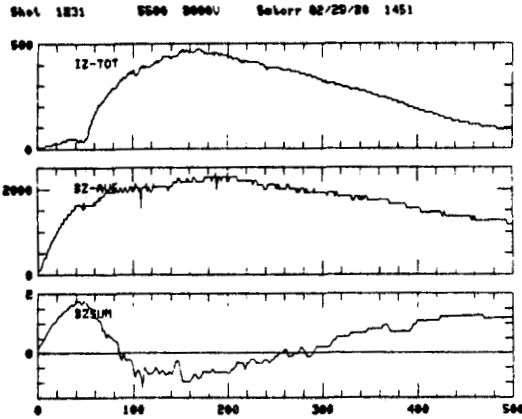
Fig. 5. Self-reversed pinch. Same measurements as in Fig. 1.
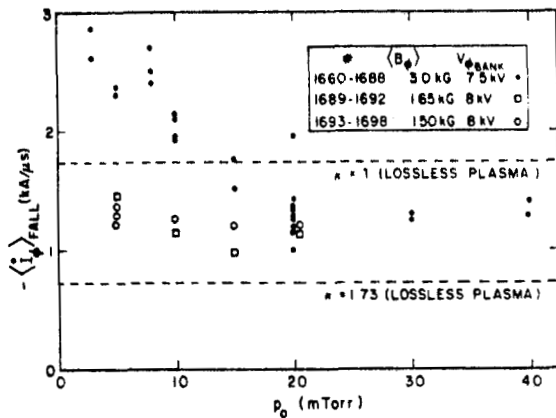
Fig. 6. Toroidal current decay rate vs fill pressure for self-reversed (open data points), and stabilized pinch (solid points). Peak current 450 kA.

Fig. 7. Self-reversed pinch. Toroidal current, time derivative of toroidal current, toroidal field at the wall, and time derivative of chord-integrated densities vs time. 5 mtorr fill.

quiescence observed on ETA-BETA II and on ZETA since quietness appears mostly on the density traces rather than on the toroidal dI/dt. This is shown in Fig. 7 for a fill pressure of 5 mtorr. A comparison of the frequency responses of the diagnostics used on the various RFP experiments is needed.

Figure 8 gives the time and duration of the quiet density periods observed during a series of self-reversed pinches. Approximately one out of three discharges is represented on the graph. The necessary conditions for extended quiet periods are: low density, reversed toroidal magnetic field and toroidal electric field at the wall. The dashed vertical lines indicate the average time during which these criteria are satisfied. The instantaneous value of theta at the beginning of this period is approximately 2.5.

Fig. 8. Toroidal current and field at the wall vs time. Horizontal bars represent the duration of quiet density periods for several discharges.

C. Aided Reversal

Typical waveforms for this mode are shown in Fig. 9. Since aided reversal is accomplished by delaying the toroidal field crowbar, it is possible to study the continuous transition between stabilized and aided reversal pinches. One then observes that aided reversal improves the toroidal current decay time at low fill pressure, and makes it comparable to the high pressure value. The abscissa in Fig. 10 represents the crowbar time of the toroidal field. The peaks of the toroidal and poloidal fields occur at 50 and 150 µs, respectively. The decay time increases from 140 µs without aided reversal to 260 µs or so at both 5 and 10 mtorr fills. The crowbar times above 110 µs in the diagram correspond to excessive negative values of the toroidal field, resulting in large toroidal field fluctuations.
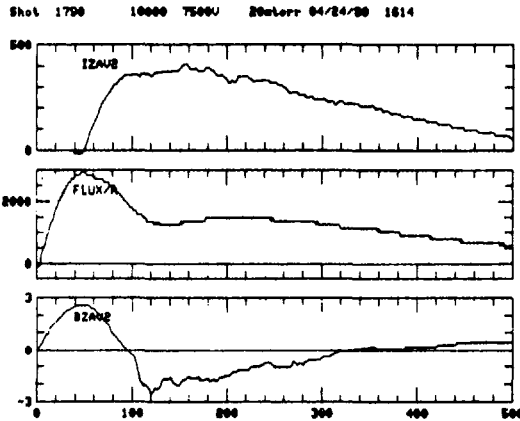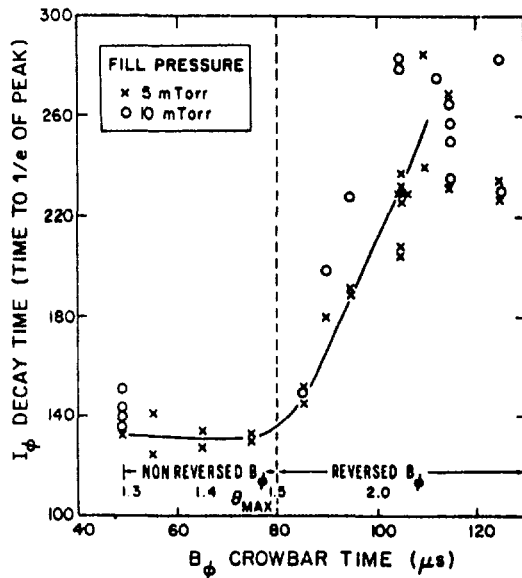
The decay times on ZT-40 still differ from ETA-BETA II results in the sense that they do not show a marked improvement at low fill pressure.[2] This may be due to the limiting effect of the ZT-40 external circuit parameters mentioned earlier.

Thomson scattering measurements during the aided reversal scan suggest an axial temperature rise with theta from 40 eV to 65 eV. An estimate of the electron temperature has also been obtained from UV spectroscopic measurements of OV(62.9 nm), OVI(103.2 nm), and CV(227.1 nm) impurity radiation. The OVI and CV waveforms are similar to what one would expect in a burn-through situation. Both the depth and duration of the burnthrough are found to improve with increasing theta over the range of 1.5 to 2.5.

Figure 11 shows simultaneous measurements of OVI and CV radiations. Since the excitation potential of the 227.1 nm carbon line is 305 eV, the appearance of this radiation during the early phase of the discharge indicates a relatively high electron temperature.

A model calculation using the zero-dimensional code mentioned earlier has been carried out in an attempt to relate the duration of the OVI radiation, that is the time taken to burn through this ionization stage, to an electron temperature. The method is to specify the time dependence of the electron temperature, and to calculate the population of OVI as function of time for various densities. The duration of this population is then compared with the duration of the observed OVI peak. The method relies on a number of assumptions. Preliminary results suggest electron temperatures of 50 to 100 eV for filling pressures of 20 to 2 mtorr, respectively, at a peak current of 500 kA.

Fig. 9. Aided reversal. Same measurements as in Fig. 1.

Fig. 10. Toroidal current decay time (µs) vs toroidal current crowbar time at 5 and 10 mtorr fill. Peak current 400-450 kA.
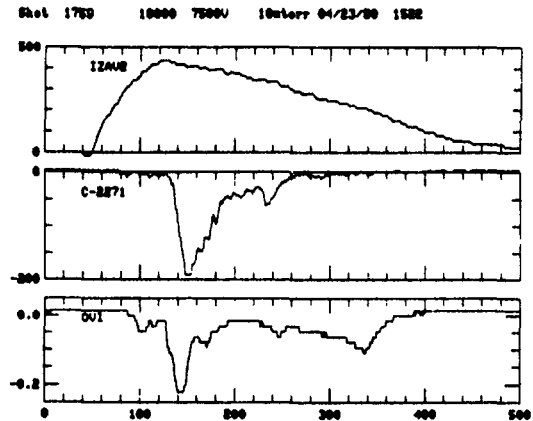
Fig. 11. Toroidal current (kA), CV (227.1 nm), and OVI (103.2 nm) line radiation vs time (µs).

Quiet toroidal current periods have been observed at 20 mtorr fill and peak discharge currents of 400 kA. These short periods are accompanied by quietness in the time derivative of the electron density and, sometimes, by a temporary improvement in the decay rate of the toroidal current.

SINGLE-FEED OPERATION

The slow rise time single-feed results presented here are for the stabilized pinch mode. As for the stabilized 4-feed configuration, there is a marked deterioration of the current decay time at lower fill pressures. Also, there is a considerable drop in peak toroidal current, typically from 400 kA at 20 mtorr, to 150 kA at 5 mtorr fill pressure. This effect, shown in Fig. 12 for 20 and 10 mtorr discharges, is believed to be due to excessive plasma losses.

An internal magnetic probe has been used to determine the poloidal field distribution in the outer half of the discharge radius. The probe was contained in a sapphire jacket and was made of bare aluminum wire to minimize contamination in case of breakage. Results, obtained during a series of 360 kA, 20 mtorr discharges, indicate that the toroidal current does not fully detach from the wall in this mode.
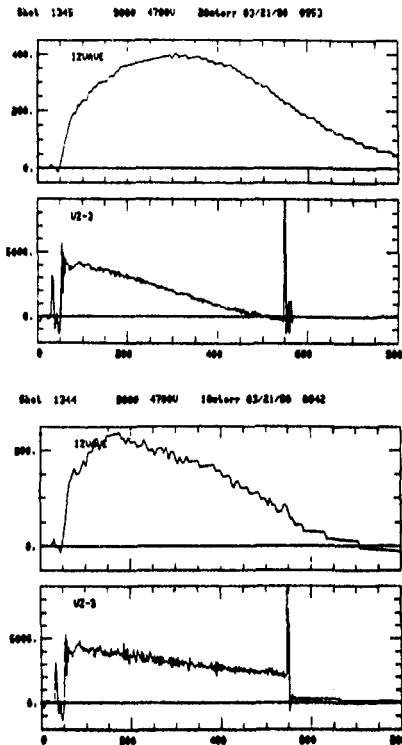
Fig. 13. Toroidal Volt-seconds vs time. Peak current 360 kA, 20 mtorr fill.

From the poloidal field measurement, one can calculate the poloidal magnetic flux content of the device and compare it with the Volt-seconds supplied to the experiment. This is shown, as function of time, in Fig. 13. The uppermost region of the graph represents the Volt-seconds dissipated in the plasma and aluminum primary.

The classical plasma resistance necessary to account for this loss leads to an electron temperature of the order of 15 eV. Thomson scattering measurements of the central electron temperature at 400 kA, 20 mtorr fill indicate a temperature of 20 to 25 eV at 300 μs, dropping to 10 eV at 700 μs in the discharge.

CONCLUSIONS

ZT-40 has been operated in the stabilized, self-reversed, and aided reversal modes with typical currents up to 500 kA. RFP operation has been obtained with electron temperature values of 40 to 70 eV, well above the oxygen radiation barrier. At low pressures, the short decay times of stabilized pinches are markedly lengthened when the discharges are converted to reversed-field pinches. The longest decay times are likely to be dominated by the parameters of the external circuit. Quiet periods in the density fluctuations have been observed for the RFP mode of operation. The occurence of these quiet periods in ZT-40 is in many ways similar to the periods of reduced current fluctuations in Zeta and ETA-BETA II, but the relationship between the two phenomena is yet unclear.

1. S. Ortolani, Los Alamos Scientific Laboratory report LA-8261-MS, Feb. 1980.
2. A. Buffa, et al., 9th European Conf. on Controlled Fusion and Plasma Phys., Oxford, England (1979).

Fig. 12. Single feed. Toroidal current (kA) and voltage (V) vs time (μs) for 20 mtorr (upper traces) and 10 mtorr (lower traces) fill.

TRANSIENT PHENOMENA ON ZT-40*
by
A. R. Jacobson and C. J. Buchenauer

INTRODUCTION

This paper examines two aspects of fluctuations in the ZT-40 reversed field pinch. First, the polarization of the magnetic fluctuations in the outer (vacuum) region is discussed. This in turn provides information on the wavevectors associated with the turbulence. The results provide some clues about the location (in minor radius) of the singular surfaces which are customarily associated with fluctuations. Second, the density fluctuations are studied using a multichord interferometer. We report on the spatial distribution (in major radius) of the chord-averaged fluctuations.

POLARIZATION OF MAGNETIC FLUCTUATIONS AT THE WALL

External magnetic probes have been used to study the time behavior of the magnetic fields close to the shell ($r = r_w = 21.8$ cm), outside the ceramic liner. Both B_θ and B_ϕ are measured simultaneously at two poloidal locations (separated by $\Delta\Theta = \pi$), that is, near the inside and outside in terms of major radius. The common-mode and differential-mode fields are, respectively:

$$\vec{B}^{(0)} \equiv \frac{1}{2} \left\{ \vec{B}^{\text{inside}} + \vec{B}^{\text{outside}} \right\}$$

$$\vec{B}^{(1)} \equiv \frac{1}{2} \left\{ \vec{B}^{\text{inside}} - \vec{B}^{\text{outside}} \right\}$$

We reexpress the differential-mode (mainly fluctuating) field in terms of components parallel and perpendicular to the instantaneous common-mode (mainly equilibrium) field, viz:

$$B_\parallel^{(1)} = \vec{B}^{(1)} \cdot \hat{e}_\parallel \quad ; \quad B_\perp^{(1)} = \vec{B}^{(1)} \cdot \hat{e}_\perp$$

(Note that the "parallel" and "perpendicular" coordinate axes are constantly shifting with the orientation of $\vec{B}^{(0)}$ in the θ-ϕ surface.) We wish to study the polarization ratio, i.e., $B_\parallel^{(1)}/B_\perp^{(1)}$. To exclude the effects of slow offsets, the ratio will actually be determined in terms of the derivatives, i.e., $\dot{B}_\parallel^{(1)}/\dot{B}_\perp^{(1)}$; the two definitions coincide for a single frequency mode. A turbu-

---

70

lence weighting factor $[\dot{B}_\perp^{(1)}]^2$ is used, so that for any given discharge, we calculate

$$\int_\tau \frac{\dot{B}_\parallel^{(1)}}{\dot{B}_\perp^{(1)}} [\dot{B}_\perp^{(1)}]^2 \, dt / \int_\tau [\dot{B}_\perp^{(1)}]^2 \, dt$$

The averaging time τ is a 50 μs interval, centered at peak θ, during which both θ and F are sensibly constant.

The polarization ratio (actually, minus the ratio) is shown in Fig. 1 for a group of 20 mtorr discharges with peak I_ϕ between 300 and 500 kA. The abscissa is F/θ (at peak θ). The first significant feature is that all (but one) of the discharges have __negative__ ratio $\dot{B}_\parallel^{(1)} / \dot{B}_\perp^{(1)}$. It can be shown by simple arguments that this is a property which would be expected of magnetic fluctuations arising from $\vec{k} \cdot \vec{B} = 0$ singular layers in the pinch. That is, the experimental polarization is consistent with resonant ($\vec{k} \cdot \vec{B} = 0$) phenomena, whereas the opposite polarization (i.e., positive $\dot{B}_\parallel^{(1)} / \dot{B}_\perp^{(1)}$) would __not__ be consistent.

The second significant feature of the data in Fig. 1 is the trend toward more parallel fluctuations at deeper reversal (leftward on abscissa). To investigate this, we have considered the effect of a single singular layer mode for the case of a Bessel function equilibrium. The mode has wavevector $\vec{k} (\equiv k_\phi \hat{\phi} + \frac{m}{r} \hat{\theta})$ such that $\vec{k} \cdot \vec{B} = 0$ at $r = r^*$. The computed polarization ratios for a single mode (in the Bessel function equilibrium model) are shown in Fig. 2 for three singular layer locations r^*. Comparison with Fig. 1 shows that the experimental data would be consistent with singular layers ($\vec{k} \cdot \vec{B} = 0$) in the __outer half__ of the pinch, i.e.,

$$\frac{1}{2} r_w < r^*_{exp} < r_w \quad .$$

LOCATION OF ELECTRON DENSITY FLUCTUATIONS

The chord-averaged electron density is measured simultaneously along seven vertical paths, shown in Fig. 3. The data can be differentiated in time to give $\dot{n}_e$ along each chord. The root-mean-square values (in time) of these chord-averaged $\dot{n}_e$'s give an indication of the spatial distribution (in offset major radius, $R - R_0$) of the fluctuations. Figure 4 shows such data averaged over 30 identical stabilized pinch discharges at 20 mtorr (D_2) and I = 400 kA. The 100 μs averaging period is centered around peak current, at which time the toroidal field at the wall is (positive) 1 kG. The chord-averaged fluctuations are

$$-\frac{\left\langle \dot{B}_{\parallel}^{(1)}\ \dot{B}_{\perp}^{(1)}\right\rangle_{WALL}}{\left\langle \dot{B}_{\perp}^{(1)2}\right\rangle_{WALL}}$$

EXPERIMENTAL POINTS: 20 mTorr
DISCHARGES
BETWEEN
#662 AND #1196
AVERAGING TIME: $\Delta T = 50\mu s$
AT PEAK θ

F/θ

$\frac{-B_{\parallel}^{(1)}}{B_{\perp}^{(1)}}$ IN BESSEL FUNCTION
MODEL

$r^* = 1/2\ r_w$

$r^* = 0$

$r^* = r_w$

F/θ
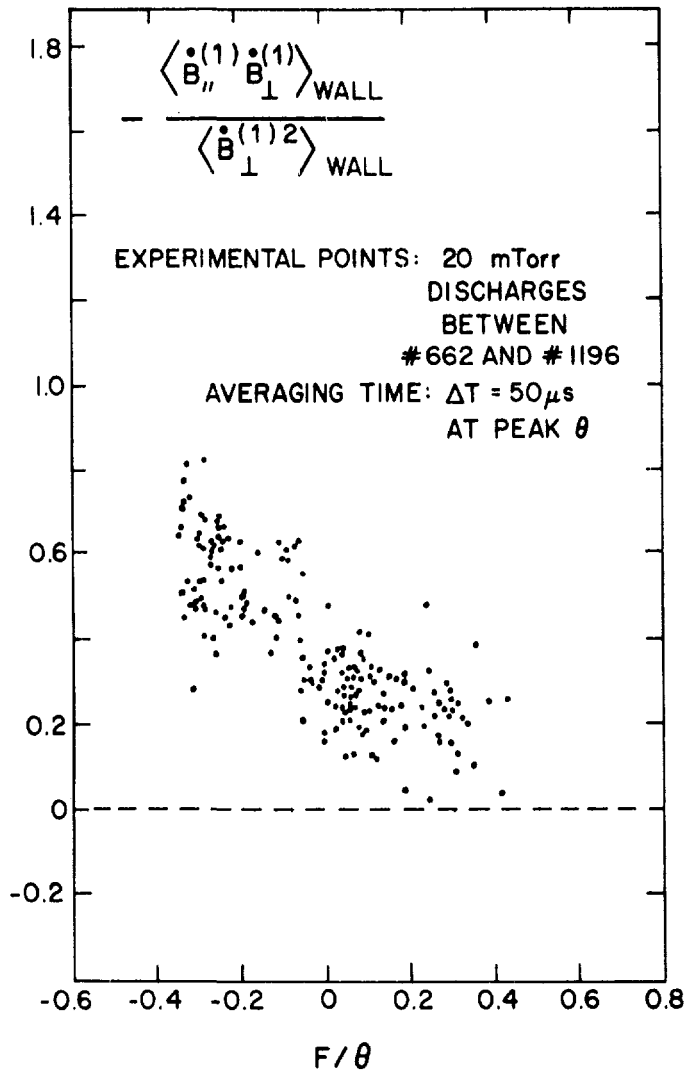
Fig. 1
Experimental polarization ratios as a
fluctuating mode for the case of func-
tion of F/θ (= B_ϕ/B_θ at wall). Each
data point is a separate discharge,
during 50 μs centered around peak θ.
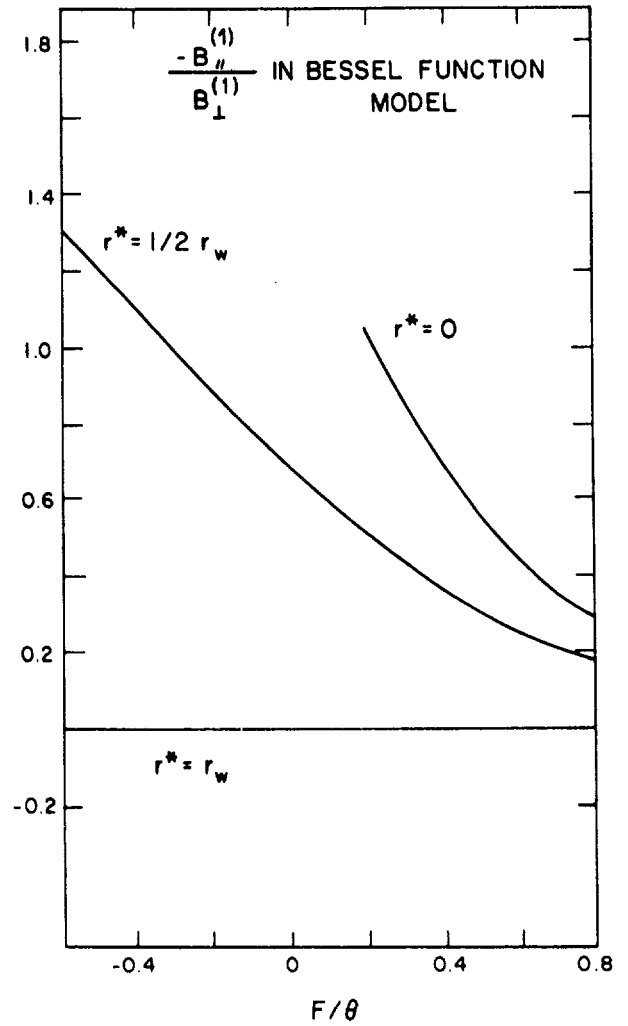
Fig. 2
Polarization ratios for a single
Bessel function equilibrium.

peaked toward the outside; dn/dt is twice as large at $R - R_o = 16.4$ cm as at
$R - R_o = 0.5$ cm. The density profiles (not shown), on the other hand, do not
peak at the edge, but are, instead, flat to within 10%. Thus, the fluctuation
level in terms of $\delta n/n$ is probably higher toward the edge. If the fluctuations
are isotropic, the profile of average $\dot{n}_e$ in Fig. 4 would Abel transform into a
profile even more strongly edge-peaked in minor radius. However, the isotropy

LOCATION OF CHORDS FOR $\int n_e \, d\ell$ MEASUREMENTS
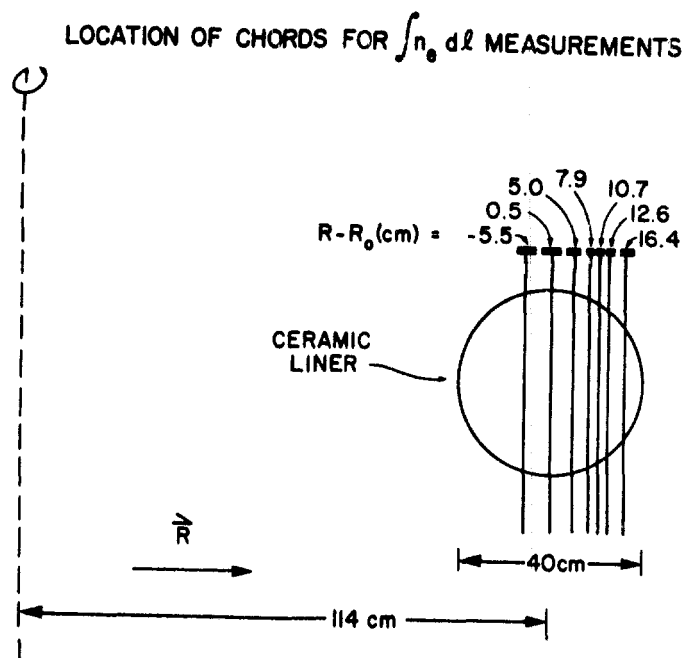
Fig. 3

Arrangement of the 3.39 μm interferometer chords for electron density measurements.

of the fluctuations is unknown, so Abel inversion of the major radius profiles would not be strictly justified.

The same shot-, chord-, and time-averaged data are shown in Fig. 5 for 14 self-reversing pinch discharges at 5 mtorr (D_2). The edge-to-center fluctuation ratio is now about 3. The (hollow) density profiles (not shown) are only about half as edge-peaked; thus the fluctuation level $\delta n/n$ is again probably higher toward the edge.

CONCLUSIONS

External measurements of magnetic fluctuations indicate consistency with $\vec{k} \cdot \vec{B} = 0$ singular layer effects. Comparison with a Bessel function equilibrium implies that the $\vec{k} \cdot \vec{B} = 0$ layers would lie in the outer half of the pinch.

Chord-averaged density measurements indicate edge-peaking of the density fluctuations. The criteria for valid Abel inversion are not met; nonetheless, the profiles (in major radius) of chord-averaged $\dot{n}_e$ are consistent with the density fluctuations being peaked on the outside in minor radius.

RMS $d\bar{n}/dt$ $100 < t < 200\ \mu s$
#1180-#1209 AVERAGED TOGETHER
  20 mTorr
  4 FEEDPLATE
$\langle B_\phi \rangle$= 2.7 kG
$V_{\phi_{BANK}}$ = 7.0 kV

RMS dn/dt $120 < t < 220\ \mu s$
#1225-#1240 AVERAGED TOGETHER
(NO DATA ON #1228, #1234)
4 FEEDPLATE   5 mTorr
$\langle B_\phi \rangle$ = 1.65 kG
$V_{\phi_{BANK}}$ = 8.0 kV
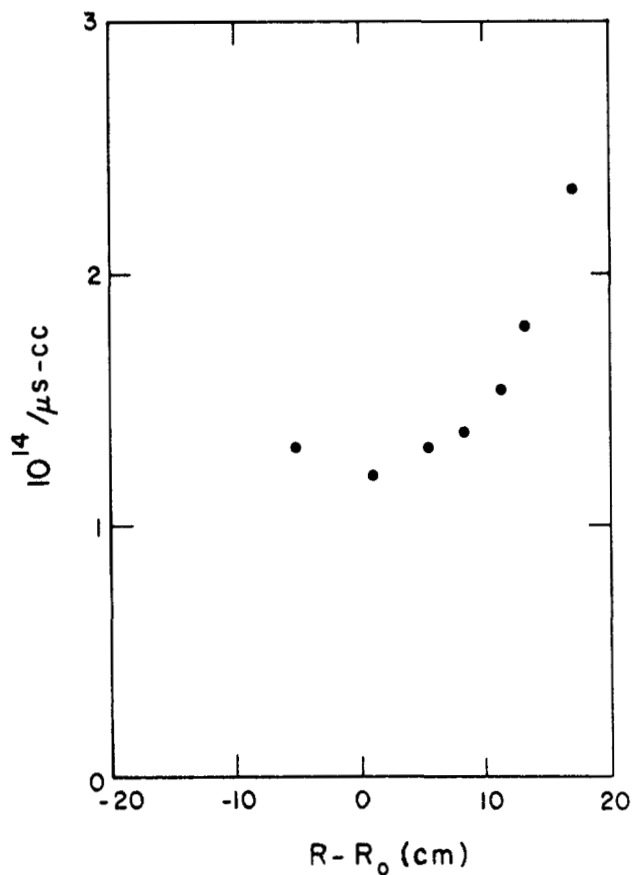
Fig. 4
Chord-, shot-, and time-averaged
$\dot{n}_c$ as a function of offset
major radius for thirty identical
stabilized pinch discharges.
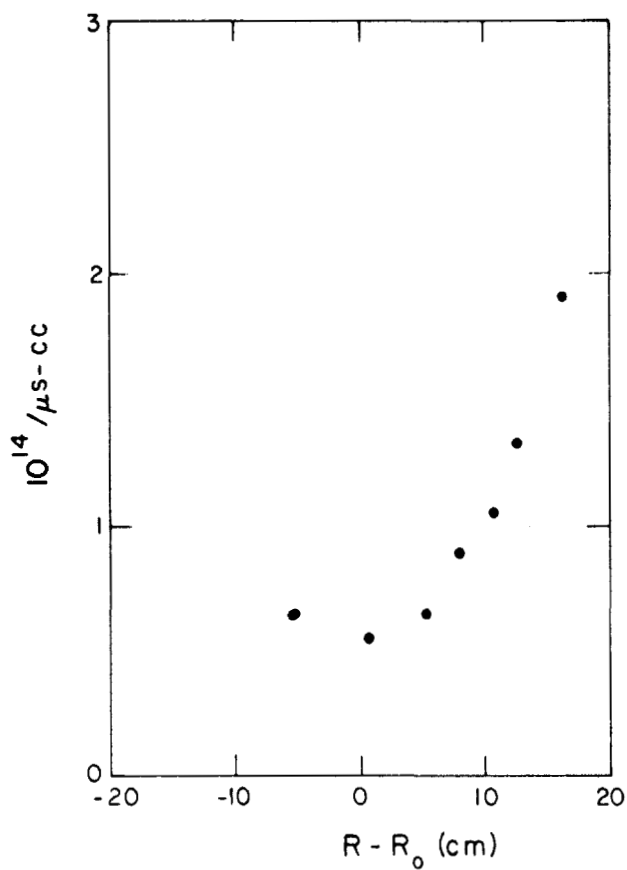
Fig. 5
Chord-, shot-, and time-averaged
$\dot{n}_e$ as a function of offset
major radius for fourteen identical
self-reversing discharges.

74

PROGRESS ON RFP STABILITY PROBLEMS SINCE THE PADUA WORKSHOP

D C Robinson
Culham Laboratory, Abingdon, Oxon, OX14 3DB, UK
(Euratom/UKAEA Fusion Association)

Both linear and non-linear stability problems associated with cylindrical RFP equilibria have been investigated.

I   Resistive instability growth when Rw-Rp/Rw > 0.04 and $\beta \neq 0$ has been investigated (Rw is the conducting wall radius and Rp the vacuum edge of the plasma). Δ' calculations show that both the RFP and spheromak can be tearing mode stable with a vacuum region of up to 4% of the radius. The growth rate calculations have established that a 10% vacuum region gives rise to modes with growth times of $\sim 1/10$ the field diffusion time at modest values of S (4.10^3) and at high θ (~ 2) if the value of β is zero. If the central β value reaches 5% then only a 5% vacuum region is acceptable.

We have also studied tearing mode stable tokamak configurations at low q($\leqslant 2$) and find in this case that Rw-Rp/Rw < 0.4 is acceptable.

II   As described at the Oxford Conference [1], tearing mode stability and the stabilising influence of parallel viscosity on the resistive 'g' mode demands specific parallel and perpendicular current distributions giving $\bar{\beta} \sim 10\%$ for the RFP and $\bar{\beta} \sim 5\%$ for the spheromak. Density gradients apparently give rise to no collisional drift modes but temperature gradient effects have not yet been investigated.

III   Many "resistive 'g' modes" on different rational surfaces have been identified in the Culham Levitron with $T_e \sim 10$ eV, $n_e \sim 10^{12}$ cm^{-3} and no parallel current present. The modes are observed only where $\nabla p < 0$. The modes are thought to be electrostatic ($\beta < m_e/m_i$) ion temperature gradient 'g' modes giving rise to enhanced classical diffusion. Our fluid simulation (Levitron Note 111) of these plasmas show that the 'g' mode which bedevils the RFP is stable in the Levitron for $\beta(0) < 0.4\%$ and $S \approx 5 \times 10^3$ (the value of shear and S as in experiment).

IV   Numerical calculations of the non-linear 'g' mode showed that the mode failed to saturate. It is not yet clear whether the mode was too close to the hydromagnetic domain or that it destabilised the tearing mode. Simple analytic considerations suggest convective saturation at low β or magnetic island formation and saturation if the current distribution is tearing mode stable at high β. Our own calculations on the m=0 non-linear 'g' using the code INSTAB do indicate saturation. The equations are solved using an ADI scheme similar to that used by Waddell et al[2].

The program is run by priming from the linear code RIP4A. For the initial runs the Pitch and Pressure model equilibrium including a vacuum edge has been used. For this model the Suydam Parameter C1 is constant up to and beyond the singular surface and is then taken gradually to zero at the wall (C1 < 1/8 is the Suydam interchange stability criterion). So far two full non-linear runs have been completed. These were conducted for a magnetic Reynolds number, S =1000 and K_z = 0.4 one being with C1=0.1 and the other with C1= 0.05. Both grow with the linear growth rate until the island width approaches the resistive layer thickness. Marked non-linear behaviour then begins to occur, with the growth of the fields and velocities going almost to zero near the 0-pt but continuing near the X-pt at level somewhat less than the linear growth rate.

It is considered that the reduction in growth rate is due to a non-linear decrease in pressure gradient. A flattening in the J_θ current gradient also occurs as in the Rutherford tearing mode saturation mechanism.

At reduced β both Livermore and Culham calculations indicate saturation, when island width is comparable with resistive layer thickness.

Hence
$$\frac{\delta B}{B} \propto S^{-x} \qquad \tfrac{1}{2} < \alpha < \tfrac{2}{3}$$

provided the plasma is tearing mode stable.

If the saturation was purely convective then resultant diffusion is a factor times classical. However island saturation leads to ergodic field lines in high shear systems and non self-consistent theory of this transport problem exists for $\beta \neq 0$.

V   Plasma rotation or electron fluid motion at the diamagnetic drift frequency can make a resistive liner appear as a conducting shell to tearing and ideal MHD modes.

This problem has been investigated analytically and with a new version of the code RIP4A. Though stability can be achieved in this way new instabilities are also produced. For certain modes and current profiles on the TOSCA device this has been found to be the case even though the liner (the only shell) has a vacuum field penetration time of 7μs. A dispersion relation has been obtained for such cases. These results indicate that a full conducting shell may be unnecessary for the RFP.

VI   3D field line tracing calculations are being used to study ergodicity and magnetic islands for q < 1 and > 1. A single mode with $b_r/B_\theta \sim 1\%$ and R/a $\sim$ 3 gives large ergodic regions. Two modes with $b_r/B_\theta < 1\%$ produce large ergodic regions for islands which nearly touch. The Grad-Shafranov equation is solved for 2D free boundary equilibria and small helical perturbations superposed, to obtain approximate magnetic surfaces. Figure 1 shows the results obtained for a tokamak elliptic equilibrium with two modes present. The 'destabilising' nature of high shear and high β has been demonstrated. Similar calculations are underway for RFP equilibria.

REFERENCES

[1]   Hosking R J and Robinson D C, Controlled Fusion and Plasma Physics (Proc. of 9th Euro. Conf. Oxford) 1 (1979) 61.

[2]   Waddell B et al "Non-linear Numerical Alogrithms", Theoretical and Computation Plasma Physics, (ICTP College, 1977), p 79.
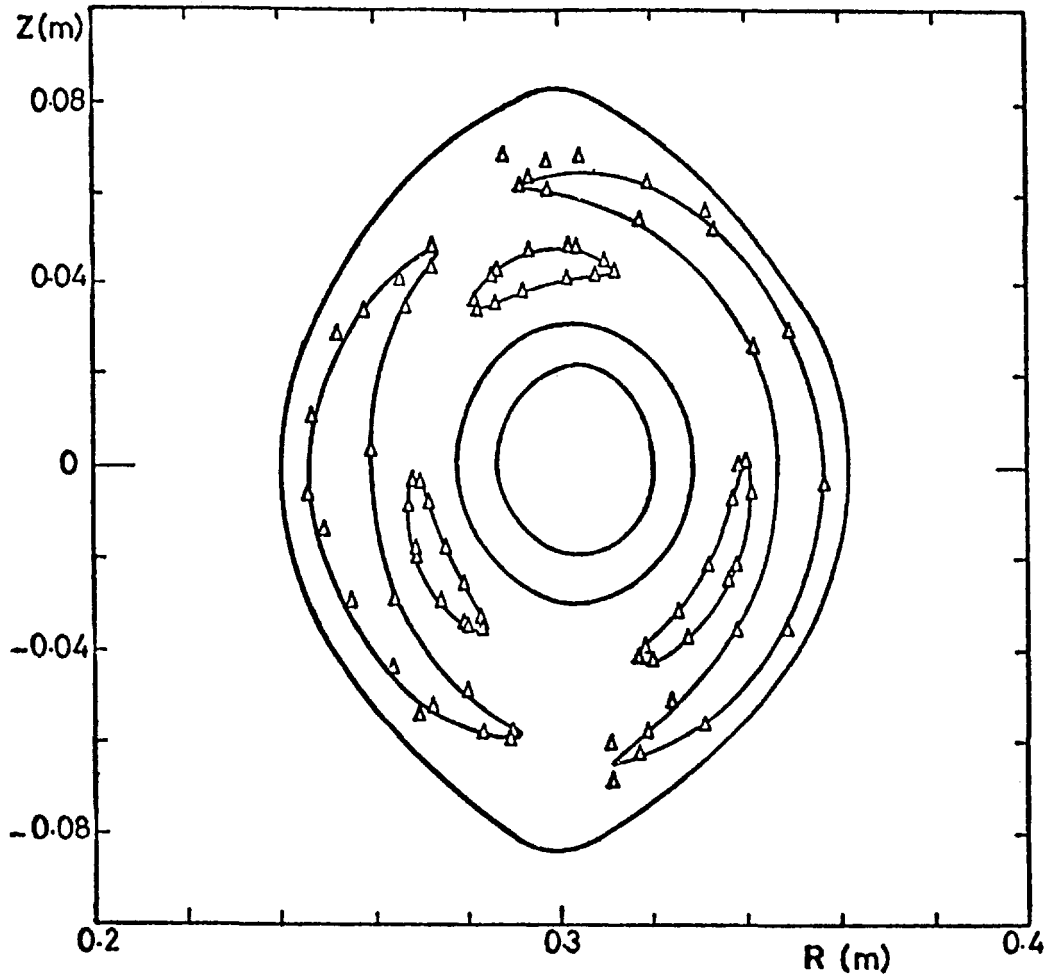
Fig.1

Calculated magnetic surfaces for an elliptical plasma with I_{pl} = 10 kA, I_s = 3.4 kA, β_I = 0.5, q(a) $\sim$ 3.3, q(0) $\sim$ 1.1, $I_{3/2}$ = 1kA, $I_{2/1}^{pl}$ = 0.5 kA. Significant ergodisation has not occurred in this case.

THE KINK TEARING MODE IN THE REVERSED FIELD PINCH

Rostom Y. Dagazian
Los Alamos Scientific Laboratory
Los Alamos, New Mexico 87545

INTRODUCTION

In this work, I examine the kink-tearing stability of a cylindrical equilibrium model, which although more complicated than the Bessel function model,[1] (BFM) still offers itself to analytic treatment. The introduction of extra complication leads to analytic profiles that can match more closely the experimental data.[2] The model consists of three regions, a) a central tokamak-like core of constant longitudinal current density and magnetic field, b) a force-free region in which the pressure is constant and the fields are described by the BFM, and c). a vacuum-like region with constant longitudinal but linearly decaying azimuthal field.

To study the stability of this configuration to kink-tearing, I essentially follow the treatment of Refs. 3 and 4. The central core is assumed to be much denser and hotter than the outer regions. It is then conceivable to consider inertial effects of the bulk of the plasma only in the first region and neglect them far from resonant ($\underset{\sim}{k} \cdot B^{(0)} = 0$) surfaces in the outer regions. In this manner, the perfect conductivity MHD equations can be solved exactly in each region. A dispersion relation is derived by setting the jump of the logarithmic derivative Δ' of the radial magnetic perturbation across the resonant surface equal to that derived in the literature[5] from resistive layer theory. Using, in addition, a simple form for the conductivity that includes electron inertia,[3] I can study the transition from a perfect conductivity kink to tearing and then to collisionless tearing as the temperature of the resonant layer is allowed to vary from very low to very high temperatures. The present treatment admits finite beta effects through the choice of the equilibrium model but it is not at all concerned with pressure driven modes.

II. THE MODEL

Here I consider the system of equations of resistive incompressible MHD. I assume that resistivity is small although finite. Thus, it is important only in

the vicinity of a singular ($\underline{k} \cdot B^{(0)} = 0$) surface; $\underline{k}$ is the wavevector of a given mode and $\underline{B}^{(0)}$ the equilirium magnetic field.

I consider the equilibrium to comprise regions 1, 2, and 3 defined by the internals (o, r_0); (r_0, r_v); (r_v, r_w) respectively; here r_0, r_v, and r_w are the radii of the inner core, the force-free vacuum interface, and of the perfectly conducting wall respectively. The equilibrium mangetic field $(B_\theta^{(0)}, B_z^{(0)})$ is given as

$$B_{\theta 0}\left[r, \ r_0 \ \frac{J_0(r_0)}{J_1(r_0)} \ \right], \ \frac{B_{\theta 0} r_0}{J_1(ro)} \ [J_1(r), J_0(r)], \ \text{and} \ \frac{B_{\theta 0} r_0}{J_1(r_0)} \ [J_1(r_v) \ \frac{r_v}{r}, \ J_0(r_v)]$$

in each region respectively. Here r, θ, z are cylindrical coordinates, $B_{\theta 0}$ is the azimuthal magnetic field at $r = 1$; distance is normalized to a characteristic length a, and the J_n are Bessel functions of the first kind.

Taking advantage of the helical symmetry of the modes under consideration, I employ helical coordinates r, $\tau \equiv m\theta + k_z$, and assume perturbations of the form $f(r)e^{i\tau - i\omega t}$. I then introduce the helical flux functions[6] $\psi(r, \tau)$, $f(r, \tau)$, $g(r, \tau)$ for the magnetic field, current density, velocity, and vorticity respectively to cast the resistive incompressible MHD equations in the form

$$\omega \rho^{(0)} a^2 \tilde{g} = -F^{(0)}\tilde{f} + I^{(0)}\tilde{\psi} \ , \tag{1}$$

$$h\Lambda\tilde{\psi} + \frac{2mk}{h} \ \tilde{f} = -i\eta_0^{-1} \ (F^{(0)}\tilde{\phi} + \omega\tilde{\psi}) \ , \tag{2}$$

$$\omega\rho^{(0)} a^2 \ (h\Lambda\tilde{\phi} + \frac{2mk}{h} \ \tilde{g}) = -F^{(0)}(h\Lambda\tilde{\psi} + \frac{2mk}{h} \ \tilde{f})$$

$$+ \frac{a\tilde{\psi}}{r} \ \frac{\partial}{\partial r} \ (mJ_z^{(0)} - krJ_\theta^{(0)}) + 2kJ_\theta^{(0)} \ \frac{a\tilde{\psi}}{r} - 2kB_\theta^{(0)} \ \frac{\tilde{f}}{r} \ , \tag{3}$$

$$2mk\Lambda\tilde{\psi} - h\Lambda\tilde{f} + 4m^2k^2\tilde{f}/h^2 = i\eta_0^{-1} \left(\omega\tilde{f} + F^{(0)}\tilde{g} + I^{(0)}\tilde{\phi} - \frac{2kB_\theta^{(0)}}{r}\tilde{\phi}\right) \tag{4}$$

where the tilde denotes perturbed quantities and

$$h(r) \equiv m^2 + k^2r^2 \ , \quad \Lambda \equiv \frac{1}{r}\frac{\partial}{\partial r}\frac{r}{h}\frac{\partial}{\partial r} + \frac{1}{r^2}\frac{\partial^2}{\partial \tau^2} \ ,$$

$$F^{(0)} \equiv -\psi_{,r}^{(0)}/r \ , \quad I^{(0)} \equiv -f_{,r}^{(0)}/r \ , \quad \eta_0 \equiv \eta/a^2 \ .$$

III. SOLUTION

It is now possible to derive a second order differential equation for $\tilde{\psi}(r)$ in each region and solve it exactly.[7] To this purpose I have set $\eta_0 \equiv 0$ in each region (except in the vicinity of a singular surface). I also set $\omega = 0$, except in region 1. Two possibilities exist:

1. $r_0 < r_s < r_v$. The pertinent solutions can be put into the form

$$\psi_1(r) = A_1 \ell_1(x_1) \ , \quad r < r_0$$

$$\psi_2^I(r) = A_{21}^I [\ell_2(x_2) + A_{22}^I \partial_2(x_2)] \ , \quad r_0 < r < r_s$$

$$\psi_2^{II}(r) = A_{21}^{II} [\ell_2(x_2) + A_{22}^{II} \partial_2(x_2)] \ , \quad r_s < r < r_v$$

$$\psi_3(r) = A_{31}[\ell_3(x_3)\partial_{3w} - \ell_{3w}\partial_3(x_3)] \ , \quad r_v < r < r_w \tag{5}$$

2. $r_v < r_s < r_\omega$ resonant surface in vacuum-like region. Then I write

$$\psi_1(r) = A_1 \ell_1(x_1) \ , \quad r < r_0$$

$$\psi_2(r) = A_{21}[\mathcal{L}_2(x_2) + A_{22}\mathcal{Y}(x_2)] \quad , \qquad r_o < r < r_v$$

$$\psi_3^I(r) = A_{31}^I [\mathcal{L}_3(x_3) + A_{32}^I \mathcal{Y}_3(x3)] \quad , \qquad r_v < r < r_s$$

$$\psi_3^{II}(r) = A_{31}^{II} [\mathcal{L}_3(x_3)\mathcal{Y}_{3w} - \mathcal{L}_{3w}\mathcal{Y}_3(x_3)] \quad , \qquad r_s < r < r_w \tag{6}$$

Here the notation was adopted

$$\mathcal{L}_n(x_n) \equiv \alpha_n x_n \mathcal{J}_{m-1}(x_n) + m \mathcal{J}_m(x_n)$$

$$\mathcal{Y}_n(x_n) \equiv \alpha_n x_n \mathcal{Y}_{m-1}(x_n) + m \mathcal{Y}_{m-1}(x_n)$$

$$x_n \equiv \lambda_n r$$

$$\alpha_{1,2,3} \equiv (2\alpha-1)^{-1}, k(1-k)^{-1}, -1, \lambda_{1,2,3} \equiv k(4\alpha^2-1)^{1/2}, (1-k^2)^{1/2}, k \tag{7}$$

where $\mathcal{J}_n$ and $\mathcal{Y}_n$ are the Bessel functions or modified Bessel functions of the first and second kind, respectively, as discussed in the text above. The letter subscript on the eigenfunction symbols denote evaluation at the particular radius indicated by that subscript.

Continuity of $\tilde{\psi}$ and integration of Eqs. (1-4) across interfaces gives jump conditions necessary to join up the solutions valid in the various regions. The ratio of the resistive layer density to the inner core density $\hat{\rho}$ can serve as a small parameter to keep the resistive layer width small with respect to the size of the system.[3] Finally, setting the Δ' calculated for these solutions across $r = r_s$ equal to that obtained from resistive theory, the desired dispersion results. A rather small computer program has been written by T. Hewitt to search for solutions.

DISCUSSIONS-RESULTS

Figure 1 shows a typical stability diagram, which was obtained with the aid of the present analysis. It is seen that the case $r_0 = .5$, $r_v = 3.5$, $\hat{\rho} = .5$ is unstable over most of the k, r_w plane. Only very tight aspect ratios could be immune to gross modes (A $\leq$ 1.5). The m = 1 remains unstable even when the wall practically touches the plasma edge.

Figure 2 shows the m = 1 growth rate as a function of k for the same model T_e = 100 eV, r_w = 6.0. It is seen that as the $r_s \rightarrow r_v^-$, the calculated growth rate blows up; it tends to zero, however, when $r_s \rightarrow r_v^+$. For the portion of the vacuum curve that curves down and the part of the force-free curve that blows up the resistive layer width is comparable or larger than $|r_s - r_v|$; hence the theory breaks down. It is more likely that the curve is smooth through the boundary in reality.

Figure 3 shows the temperature dependence of the m = 2 growth rate for various values of k. It is seen that instability persists to very high temperatures (mainly but not solely) due to the presence of electron inertia. However, the growth rate is small as T_e approaches the kilovolt range.

A search is under way to determine whether kink-tearing stable equilibria similar to the ones examined by Robinson[4] do exist for the present model resistive marginal stability can be calculated by estimating $\Delta'(w = 0)$. Kink-tearing growth rates can be calculated reliably for a wide range of situations; the theory generally breaks down when (roughly) the product of the resistive layer width times Δ' greatly exceeds unity. In this limit usual resistive tearing theory also breaks down.[9]

REFERENCES

1. R. D. Gibson, K. J. Whiteman, Plasma Physics, Vol. 10, p. 1101 (1968).

2. S. Ortolani, private communication.

3. O. P. Pogutse, PPL-TRANS-121 (March 1977).

4. D. Monticello, Proceedings on "Theory of Magnetically Confined Plasma," Varenna, Italy, p. 183 (Sept. 1977).

5. Bruno Coppi, John M. Greene, John L. Johnson, Nuclear Fusion 6, 101 (1966).

6. J. L. Johnson, C. R. Oberman, R. W. Kulsrud, E. A. Frieman, MATT Report PM-S-34 (1958).

7. D. Voslamber and D. K. Callebaut, Phys. Rev. <u>128</u>, 2016 (1962).

8. D. C. Robinson, Nuclear Fusion <u>18</u>, 7 (1978).

9. See for example R. D. Hazeltine and H. R. Strauss, Phys. Fluids <u>22</u>, 1007 (1978).
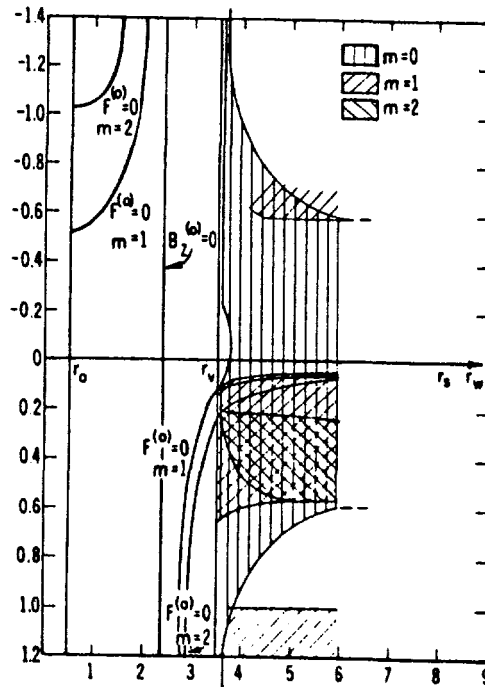
Figure 1

Stability diagram. r_0 = .5, r_v = 3.5, $\hat{\rho}$ = .5, T_e = 100 eV.
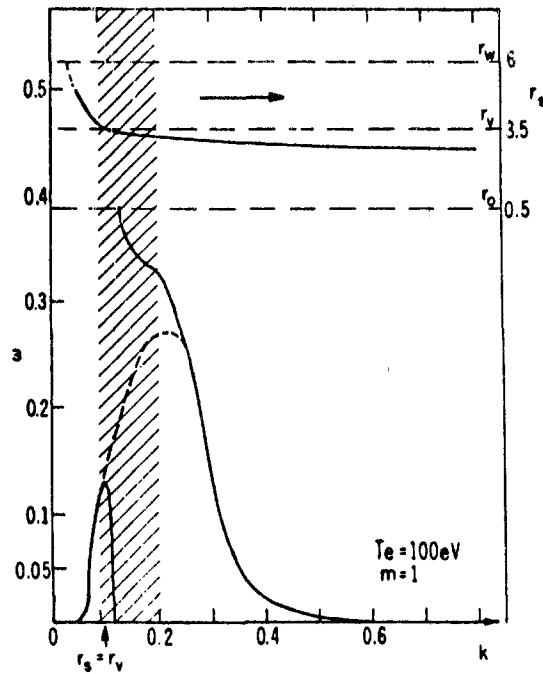
Figure 2

m = 1 growth rate as a function of k. Normalization is to the Alfvén time at r = 1., $n_e = 10^{13}$ cm^{-3}. r_o = .5, r_v = 3.5, r_w = 6.0, T_e = 100 eV.
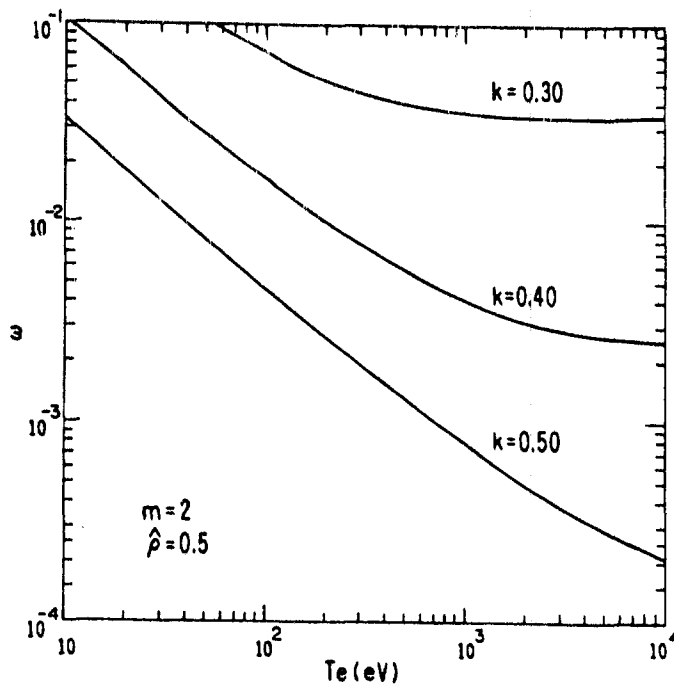

Figure 3

The temperature dependence of the m = 2 growth rate. Normalization is to the Alfven time at r = 1, $n_e = 10^{13}$ cm^{-3}. r_o = .5, r_v = 3.5, r_w = 6.0.

STABILITY ANALYSIS OF PLASMAS LIMITED BY A RESISTIVE WALL OF FINITE THICKNESS

C.F. Nalesso

Centro di Studio sui Gas Ionizzati del C.N.R. - Via Gradenigo 6/A - PADOVA (Italy)

Abstract

Ideal MHD stability analysis of plasmas surrounded by a resistive wall of finite thickness is studied. A boundary condition on the perturbed plasma quantities at the surface of separation of the plasma and vacuum is derived. This allows us to obtain the instability growth rate provided the perturbed quantities can be found either as an analytical solution or as a numerical solution of an eigenvalue problem. An equilibrium configuration with a constant radial profile of the axial current density is assumed as an example and some numerical results for RFP plasmas with the characteristic parameters of η-β 11 and a prototype fusion reactor are presented.

Introduction

Ideal MHD stability analysis has been carried out for many years both theoretically and numerically in very general plasma equilibrium conditions. Usually the assumption of a superconducting cylindrical wall surrounding the plasma is made, and this is reasonably well fulfilled in most of the experiments so far studied. In a fusion reactor device, however, where stability must be assured for times longer than the diffusion time through the conducting material, it could be important to take into account the finite conductivity of the wall (liner). Stability analysis in the approximation of a very thin conducting liner has been carried out in the past using either an energy principle or a normal mode approach. Here we present the stability analysis of an ideal plasma surrounded by a wall of finite thickness and conductivity. Because of dissipation in the conducting wall it turns out that the system of equations, is no longer self adjoint so that the unstable modes are not necessarily purely exponentially growing modes [1]. An approach based on the time Laplace transform of the perturbation is thus assumed and an eigenvalue equation for the perturbed plasma quantities is derived.

The boundary conditions

Let us assume an ideal plasma in equilibrium in a cylindrical region of radius a, surrounded by a vacuum region in $a \le r \le r_o$, by a resistive wall of conductivity σ_o, thickness δ_o of inner radius r_o and finally by an external vacuum region extending to a perfectly conducting wall at r_2. Following the method of [2,3] we will assume every perturbed quantity of the form

$$f(r,\theta,z,t) = f_{m,k}(r,t)\exp i(m\theta+kr) \qquad (1)$$

and will Laplace transform in time the equations.

The problem is then solved by integrating the MHD equations in all the considered regions with the appropriate boundary conditions [4]. In the plasma region for any equilibrium configuration it is always possible, after linearizing the plasma equations, to get the perturbed quantities by solving two first order differential equations, for instance in the perturbed radial magnetic field component b_r and the total perturbed pressure $p^* = p + \bar{B}_i \cdot \bar{b}_i / \mu_o$ where $\bar{B}_i$ is the equilibrium internal field and $\bar{b}_i$ the perturbed one.

Furthermore, the continuity of the tangential component of the electric field and of the total pressure across the surface r=a, impose a relationship between $b_{ri}(a,s)$ and $b_{re}(a,s)$ and between p^* and $b_{ze}(a,s)$.

Moreover, it is shown in reference [2] that the ratio $b_{re}(a,s)/b_{ze}(a,s)$ is a function only of the geometry, the m and k numbers and of the complex variable s and it is given by:

$$\frac{b_{ze}(a,s)}{b_{re}(a,s)} = \pm i \frac{\Delta_2(ak,r_ok)\Psi(z_o)-kG_m(ak,r_ok)(\frac{m}{r_ok}\chi(z_o)+1)}{\Delta_1(ak,r_ok)\Psi(z_o)+k\,_2(r_ok,ak)(\frac{m}{r_ok}\chi(z_o)+1)} = iF(z_o) \qquad (2)$$

where

$$G_m(ak,r_ok) = I_m(ak)K_m(r_ok)-I_m(r_ok)K_m(ak)$$

$$\Delta_1(ak,r_ok) = I'_m(ak)K'_m(r_ok)-I'_m(r_ok)K'_m(ak) \qquad (3)$$

$$\Delta_2(ak,r_ok) = I_m(ak)K'_m(r_ok)-I'_m(r_ok)K_m(ak)$$

and $\Psi(z_o)$, $\chi(z_o)$ are defined in [2] and are functions of s since $z_o = (\mu_o\delta_o\sigma_o s+k^2)^{\frac{1}{2}}$. It is easy then to obtain the expression

$$ika(\frac{m}{a}B_{\theta i}(a)+kB_{zi}(a))\frac{\mu_o p^*(a,s)}{b_{ri}(a,s)}+k(b_{\theta e}^2(a)-b_{\theta i}^2(a))=-a(\frac{m}{a}B_{\theta e}(a)+kB_{ze}(a))^2 F(z_o) \quad (4)$$

We see that, for any equilibrium configuration, it is possible to formulate the stability problem as an eigenvalue problem involving, for instance, a system of two first order differential equations with the usual boundary conditions on the axis and a boundary condition at r=a given by (4). Expression (4) replaces the classical condition $b_r=0$ at a perfectly conducting wall. Furthermore, whenever an analytical solution for $b_{ri}(a,s)$ and $p^*(a,s)$ is possible, (4) gives the dispersion relation.

As an example consider the equilibrium configuration given by

$$\bar{B}_i(r) = B_{\theta 0}(0, \frac{r}{a}, b_i) \quad (0 \le r \le a), \quad \bar{B}_e(r) = B_{\theta 0}(0, \frac{a}{r}, b_e) \quad (a \le r \le r_2) \qquad (5)$$

An analytic solution for the perturbed plasma quantities can easily be obtained [4,5]. The dispersion relation obtained in this case is

$$2ka(m+kab_i)(m^2\beta^2-1)I_m(u) / m\beta(uI'_m(u)+m^2\beta\Gamma I_m(u)) = -(m+kab_i)^2 F(z_o) \qquad (6)$$

where

$$\beta = 2(m+kab_i) /[(m+kab_i)^2+\Gamma^2], \quad u = (1-m^2\beta^2)^{\frac{1}{2}}ka \qquad (7)$$

and $\Gamma = s\tau_A$ (τ_A=azimuthal Alfvén time). The dispersion relation obtained depends on the complex parameter s, but fortunately, with a proof similar to that given in reference [3] it is possible to show that the solutions of equation (6) can only be real or complex conjugate pairs with a negative real part. This implies that the growth rate of the unstable modes need only be studied at real positive values of s with an upper bound given by the case with no resistive wall.

A useful simpler result can be obtained when the instability growth rate ω is such that $r_o\delta_o\mu_o\sigma_o\omega \gg 1$. Then the expressions for $\Psi(z_o)$ and $\chi(z_o)$ can be approximated by [2] $\chi = \omega/r_o k \quad \Psi = -r_o\tanh(\delta_o z_o)$ (8) and the dispersion relation becomes practically independent of r_2 (the position of the perfectly conducting wall). Another interesting case is when $\delta_o^2\mu_o\sigma_o\omega \ll 1 \ll r_o^2\mu_o\sigma_o\omega$. As in this case the resistive wall can be assumed "thin", we can use for Ψ and χ the approximation given in [3] and the results already given in the literature [1,5] are recovered.

Numerical results

The dispersion relation (6) has been solved numerically in two cases, in the first one to analyse the effect of the liner on the RFP plasmas obtained in η-β II [6] and in the second case to study the behaviour of a possible RFP reactor. In figure 1 is shown the instability growth rate as a function of the wavenumber k for the typical parameters of the RFP discharges of η-β II, namely a=6.25 cm, r_o=12.5 cm, r_2=15.5 cm, δ=0.025 cm, liner resistivity = 7.4 10⁻⁷ Ω/m, plasma current of about 200 kA and density of 4 10²⁰ m⁻³.

In figure 2 the dispersion relation for a reactor type RFP plasma is shown. In this case the curve shown is independent of the perfectly conducting wall, except near the marginal stability points, and expression (8) can be used.

Conclusions

In this paper a general treatment of the problem of the stability of an ideal

Fig. 1   Fig. 2
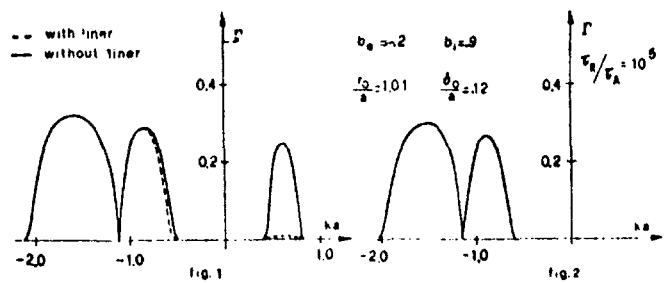
cylindrical plasma with a resistive wall of finite thickness has been given.

It has been shown that, for the considered stability problem, the effect of the region external to the plasma, can be described by a boundary condition (equation (4)) on the perturbed plasma quantities. This condition, allows us to obtain an eigenvalue problem which leads to a dispersion relation for the growth rate of the unstable modes whenever an analytical solution is possible.

If the instability growth time is much shorter than the characteristic diffusion time through the resistive layer $\tau_R = \delta_o r_o\sigma_o\mu_o$, the condition (4) can be simplified, the position of the perfectly conducting wall becomes unimportant and a simpler expression can be obtained. This case applied particularly to a reactor-like machine where the resistive layer (first wall) is reasonably thick.

A particular plasma configuration with a constant axial current density and parabolic pressure is considered as an example and the method is applied to analyse the stability of RFP plasmas with the parameters characteristic of the n-β II experiment and of a prototype reactor.

References

[1] Goedbloed J.P., Pfirsch D., Tasso H., Nuclear Fusion 12 (1972) 649

[2] Nalesso G.F., Costa S., To be published in Nucl. Fusion, vol. 20, n. 4

[3] Nalesso G.F., Costa S., Internal Report Ist. Elettrotecnica ed Elettronica Univ. Padova, UPee 79/12 (1979)

[4] Tayler R.J., Proc. Phys. Soc. B70 (1957) 31

[5] Tanaka H., Tuda T., Takeda T., Nuclear Fusion 12 (1972) 119

DISPERSION DIFFERENTIAL EQUATION FOR A STRAIGHT VLASOV-FLUID RFP WITH SMALL ION GYRORADIUS*†

H. Ralph Lewis
Los Alamos Scientific Laboratory
P. O. Box 1663
Los Alamos, New Mexico 87545

The objectives of this work are to use the Vlasov-fluid model[1] to derive a dispersion differential equation which is valid for rather general equilibrium magnetic field configurations, and to apply the dispersion differential equation to study stability and RF heating of a straight reversed-field pinch. For deriving the dispersion differential equation, a convenient operator technique has been used to solve the ion Vlasov equation in powers of the ratio (thermal ion gyroradius)/(plasma radius). No expansion is made in powers of ω/ω_{ci}, and ω/ω_{ci} is not assumed to be small compared to unity. Also, the parallel streaming derivative that occurs in the ion Vlasov equation is taken into account in lowest order and is not assumed to be small. This solution of the Vlasov equation is a generalization of the method used by Cayton and Lewis for studying stability and RF heating of a sharp-boundary screw pinch.[2] In the present work, in addition to not restricting the size of ω/ω_{ci} and the parallel streaming derivative, the equilibrium profiles are allowed to be diffuse. The dispersion differential equation is obtained by substituting the approximate solution of the ion Vlasov equation into the perpendicular component of the Maxwell $\nabla \times \mathbf{B}$ equation (the pressure balance equation) without further approximation. The final form of the dispersion differential equation is an equation for the Laplace transform of the electron fluid displacement.

I. General Theory of the Perturbation Solution

We use a convenient general formula for the iterative solution of the Laplace transform of the linearized Vlasov equation in which the zeroth order part of the equilibrium Liouville operator is $- B_0 \partial/\partial\phi + i\zeta$, where ζ is real and independent of ϕ, B_0 is the magnitude of the equilibrium magnetic field, suitably scaled, and ϕ is a phase angle around the equilibrium magnetic field of the perpendicular component of the velocity vector; B_0 may be space-dependent. We denote Laplace transforms by a carat ($\hat{\ }$), and write the Laplace transform of the linearized Vlasov equation as

$$(R_0 + \eta R_1)\hat{g} = \hat{\Gamma} ,\tag{1}$$

---

where η is an ordering parameter. We take the zeroth order operator R_0 to be

$$R_0 = - B_0 \frac{\partial}{\partial \phi} + i\zeta - i\omega$$

$$= - B_0 \frac{\partial}{\partial \phi} + i(\zeta - \sigma) + \gamma , \qquad (2)$$

where $\omega = \sigma + i\gamma$, σ and γ are real, and we assume

$$\text{Im } \omega = \gamma > 0 . \qquad (3)$$

Im ω is taken to be positive definite because the contour for inverse Laplace transforms is assumed to lie in the half plane Im $\omega > 0$. If the contour is deformed so that part of it lies in the lower half plane, then the $\hat{g}$ to be used in computing the inverse Laplace transform along that part is the analytic continuation of the $\hat{g}$ determined under assumption (3). The small-gyroradius perturbation solution is based on the assumption that the local ion gyrofrequency, which is represented by B_0, is large compared to each of the frequencies which characterize the action of the operator R_1 on $\hat{g}$ in Eq. (1). In order to ensure that the magnitude of the operator R_0 is bounded from below by the ion gyrofrequency, we assume that the imaginary part of the contour along which the inverse Laplace transform is evaluated is at least as large as the maximum value of B_0. The solution of Eq. (1) can be written as

$$\hat{g} = \sum_{n=0}^{\infty} (-1)^n \eta^n (R_0^{-1} R_1)^n R_0^{-1} \hat{r}$$

$$= R_0^{-1} \sum_{n=0}^{\infty} (-1)^n \eta^n G_n , \qquad (4)$$

where

$$G_0 = \hat{r} \qquad (5a)$$

89

and

$$G_{n+1} = R_1 R_0^{-1} G_n \quad \text{for } n > 1 \, . \tag{5b}$$

It may be verified by direct substitution that this is a formal solution of Eq. (1). The operator R_0^{-1} exists, is unique, and can easily be written explicitly. This formal series solution is used for calculating velocity moments of g; the usefulness of the dispersion differential equation that is derived from it must be assessed a posteriori, especially in the neighborhood of resonances.

II. The Linearized Equations of the Vlasov-Fluid Model

The Vlasov-fluid model is a low-frequency model for an ion-electron plasma in which the ions are treated as collisionless and the electrons are treated as a massless, pressureless fluid. The linearized equations for the model can be written as

$$\underset{\sim}{E}_1 + \underset{\sim}{u}_0 \times \underset{\sim}{B}_1 + \underset{\sim}{u}_1 \times \underset{\sim}{B}_0 = 0 \, , \tag{6}$$

$$[\frac{\partial}{\partial t} + \underset{\sim}{v} \cdot \underset{\sim}{\nabla}_{\underset{\sim}{r}} + (\underset{\sim}{E}_0 + \underset{\sim}{v} \times \underset{\sim}{B}_0) \cdot \underset{\sim}{\nabla}_{\underset{\sim}{v}}] \tilde{f}_1 = - \tilde{f}_0'(\epsilon) \underset{\sim}{v} \cdot \underset{\sim}{E}_1 \, , \tag{7}$$

$$\frac{1}{4\pi} [(\underset{\sim}{\nabla} \times \underset{\sim}{B}_0) \times \underset{\sim}{B}_1 + (\underset{\sim}{\nabla} \times \underset{\sim}{B}_1) \times \underset{\sim}{B}_0] - \tilde{n}_0 \underset{\sim}{E}_1 = \int d^3 \underset{\sim}{v} \, (\underset{\sim}{E}_0 + \underset{\sim}{v} \times \underset{\sim}{B}_0) \tilde{f}_1 \, , \tag{8}$$

where $\tilde{f}_0$ and $\tilde{f}_1$ are normalized distribution functions,

$$\underset{\sim}{u}_0 \times \underset{\sim}{B}_0 = - \underset{\sim}{E}_0 \, , \tag{9}$$

$$\tilde{n}_0(\underset{\sim}{r}) = \int d^3 \underset{\sim}{v} \, \tilde{f}_0(\epsilon) \, , \tag{10}$$

$$\tilde{f}_0'(\epsilon) = \frac{d\tilde{f}_0}{d\epsilon} \, , \tag{11}$$

and ϵ is the total particle energy.

III. Specialization to a Straight Screw Pinch

For a straight screw pinch, a special case of which is a straight reversed-field pinch, we use velocity variables $(v_\perp, v_\parallel, \phi)$ defined by

$$\underset{\sim}{v} = \underset{\sim}{v}_\perp + v_\parallel \hat{\underset{\sim}{b}} \; , \qquad \hat{\underset{\sim}{b}} = \underset{\sim}{B}_0/B_0 \; , \tag{12}$$

$$\underset{\sim}{v}_\perp = v_\perp \hat{\underset{\sim}{v}}_0 \; , \qquad v_\parallel = \hat{\underset{\sim}{b}} \cdot \underset{\sim}{v} \; , \tag{13}$$

$$\hat{\underset{\sim}{v}}_0 = \hat{\underset{\sim}{r}} \cos\phi + \hat{\underset{\sim}{b}} \times \hat{\underset{\sim}{r}} \sin\phi \; . \tag{14}$$

The operators R_0 and R_1 in Eq. (1) are

$$R_0 = - B_0 \frac{\partial}{\partial \phi} + i(\kappa v_\parallel - \omega) \; , \tag{15}$$

$$R_1 = v_\perp \cos\phi \frac{\partial}{\partial r} + i\tau v_\perp \sin\phi + E_{0r}\left(\cos\phi \frac{\partial}{\partial v_\perp} - \frac{1}{v_\perp} \sin\phi \frac{\partial}{\partial \phi} \right)$$

$$+ \left(D_1 v_\perp \sin\phi \cos\phi + D_2 v_\parallel \cos\phi \right)\left(v_\parallel \frac{\partial}{\partial v_\perp} - v_\perp \frac{\partial}{\partial v_\parallel} \right)$$

$$+ \left(D_1 v_\parallel \cos^2\phi - D_3 v_\parallel - D_2 \frac{v_\parallel^2}{v_\perp} \sin\phi - D_4 v_\perp \sin\phi \right) \frac{\partial}{\partial \phi} \; , \tag{16}$$

where

$$\kappa = \frac{m}{r} \hat{b}_\theta + k \hat{b}_z \; , \tag{17}$$

$$\tau = \frac{m}{r} \hat{b}_z - k \hat{b}_\theta \; , \tag{18}$$

91

$$D_1 = \hat{b}_\theta \frac{d\hat{b}_z}{dr} - \hat{b}_z \frac{d\hat{b}_\theta}{dr} + \frac{\hat{b}_\theta \hat{b}_z}{r} , \tag{19}$$

$$D_2 = \frac{\hat{b}_\theta^2}{r} , \tag{20}$$

$$D_3 = 2 \frac{\hat{b}_\theta \hat{b}_z}{r} , \tag{21}$$

$$D_4 = \frac{\hat{b}_z^2}{r} , \tag{22}$$

$$\hat{\underline{b}} = \hat{b}_\theta(r)\hat{\underline{\theta}} + \hat{b}_z(r)\hat{\underline{z}} . \tag{23}$$

The remainder of the derivation of the dispersion differential equation is straightforward and in progress. The result, which will be applied to a straight reversed-field pinch, will be an equation for the electron fluid displacement that will provide finite ion gyroradius corrections to the predictions of the guiding center model.

References

[1] J. P. Freidberg, Phys. Fluids 15, 1102 (1972).

[2] T. E. Cayton and H. R. Lewis, Phys. Fluids 23, 109 (1980).

Low-Frequency Microinstabilities in Cylindrically Symmetric Systems with Arbitrary β and Strong Magnetic Shear

Ralph Linsker

Plasma Physics Laboratory, Princeton University

Princeton, NJ 08544

The microstability analysis of low-frequency modes ($\omega \ll \Omega_{ci}$) in magnetically sheared systems with arbitrary β is of particular relevance to reversed-field pinch theory. I shall discuss a method for the practical calculation of such modes in cylindrical geometry, with particular attention to the strongly sheared case. I will also show that in the electrostatic sheared-slab limit, some recent integral-equation analyses gives incorrect results for the drift eigenmode when the shear and density gradient scale lengths are comparable ($L_s \sim L_n$).

The modes I will consider are radially localized (mode width $\ll$ system size). The unperturbed state may have an arbitrary pitch profile, density gradient, parallel electron current, ion and electron temperature gradients, and β. I consider the collisionless limit. Because I assume cylindrical symmetry, there are no trapped-particle or other toroidal effects in this model. I impose the ordering: (ion gyroradius ρ_i)/(system size and all equilibrium gradient scale lengths) $\sim O(\epsilon) \ll 1$, $\omega/\Omega_{ci} \sim O(\epsilon)$, and $k_\perp \rho_i \sim O(1)$.

The method of solution is as follows: I consider electromagnetic perturbations $(\phi, \vec{A}) \sim \exp[i(kz + \ell\theta - \omega t)]$, choose the gauge to eliminate A_r, solve the linearized Vlasov equation for the perturbed ion and electron distribution functions, and invoke quasineutrality and the parallel and

perpendicular components of Ampere's law to obtain three integral equations

relating $\phi(r)$, $A_{\parallel}(r)$, and $A_{\perp}(r)$. I discretize the Fourier transforms of ϕ

and $A_{\parallel,\perp}$ in radial-wavenumber space, and obtain a matrix equation (LV = 0) of

order 6N relating the Fourier components $\hat{\phi}[\pm k_r(n)]$, $\hat{A}_{\parallel,\perp}[\pm k_r(n)]$, where n = 1

to N labels the discretized radial wavenumber. (V collectively represents

these 6N components.) In the absence of parallel electron current, ϕ and $A_{\parallel,\perp}$

have definite parities and the matrix order reduces to 3N. The matrix L is

a complicated function of ω. I solve numerically the eigenvalue problem

LV = λV , then seek an ω such that $\lambda(\omega)$ = 0 with a corresponding eigenvector

V that is physically meaningful (*i.e.*, not an artifact of the discretization

process nor of the imposed periodic boundary conditions). I then study the

dependence of ω upon $k_{\perp}$, L_s/L_n , T_e/T_i , $L_n/L_{Te,i}$, the parallel electron

current velocity, the pitch profile, and β .

There are several points of departure from previous work. Because the

case $L_s \sim L_n$ (with $T_e \sim T_i$) is of interest, ion Landau damping occurs within

several ion gyroradii of the mode-rational surface. Therefore, the frequently-

used differential formalism (*e.g.*, $\phi'' + Q(x,\omega)\phi$ = 0 for the electrostatic slab

case) is inapplicable. Higher derivatives of   and $A_{\parallel,\perp}$ must be retained,

and an integral-equation approach is appropriate.

There has been recent work[1] concerning an integral formalism for electro-

static drift waves on a sheared slab. If one applies this work to the case

$L_s \sim L_n$, however, an incorrect solution for the eigenmode is obtained. The

problem is that one conventionally takes the ion resonant denominator (in the

perturbed distribution function f_{1i}) to be $[k_{\parallel}(x)v_{\parallel} - \omega]$, where $k_{\parallel}(x) = k_{\perp}x/L_s$

for a sheared slab, and x is the distance from the mode-rational surface.

But an accurate calculation of the particle orbit gives for this denominator

94

$[k_{\parallel}(x_{G.C.})v_{\parallel} - \omega]$ where $x_{G.C.} \cong x + v_{\perp}\cos\alpha/\Omega_{ci}$. The integration of f_{1i} over velocity space is substantially complicated by this extra term. It is, however, possible to do the integration analytically; the result[2] is that a term (in n_{1i})

$$\zeta_i Z(\zeta_i) \int \exp(-b) I_0(b) \exp(ik_r x) \hat{\phi}(k_r) dk_r \quad , \tag{1}$$

where $b = \rho_i^2(k_{\perp}^2 + k_r^2)$, $\zeta_i = (\omega/\sqrt{2}\, v_{Ti})(|L_s/k_{\perp}x|)$, and I_0 is a Bessel function) is replaced by

$$\frac{1}{2\pi} \int dk_r' \exp(ik_r'x) \int dk_r \hat{\phi}(k_r) \exp(-b_1) I_0(b_2) \int dx' \exp[i(k_r - k_r')x']\zeta_i' Z(\zeta_i') \quad , \tag{2}$$

where $b_1 = \rho_i^2(k_{\perp}^2 + \frac{1}{2}k_r^2 + \frac{1}{2}k_r'^2)$, $b_2 = \rho_i^2[(k_{\perp}^2 + k_r^2)(k_{\perp}^2 + k_r'^2)]^{1/2}$, and $\zeta_i' = (\omega/\sqrt{2}\, v_{Ti})$ $\times(|L_s/k_{\perp}x'|)$. This change substantially alters the eigenmode shape within a distance $\sim \rho_i$ of the mode-rational surface, which is significant when $L_s \sim L_n$ and $T_e \sim T_i$ (*i.e.*, when the radial mode width is $\sim$ several times ρ_i). For the cases studied thus far ($k_{\perp}\rho_i\sqrt{2} \sim 1$), the eigenvalue ($\omega/\omega_{*e}$) is only changed by ≤ 0.02 even for $L_s/L_n \sim 3$.

Another feature of the present work is the full incorporation of electromagnetic effects. One is therefore not limited to $\beta \ll 1$, as are treatments that neglect the perturbed $A_{\perp}$.

A preliminary result (for the electrostatic limit) is that for strong shear ($L_s/L_n \sim 6$) and $T_e \sim T_i$, electrostatic drift waves are strongly stabilized for the $k_{\perp}(\sim 1/\rho_i\sqrt{2})$ that have been investigated; and that the damping rate is very insensitive to ion temperature gradient, pitch, and moderate electron current velocities u_c. One requires $u_c \gtrsim (T_e/2m_e)^{1/2}$ to drive the drift mode unstable for $L_s/L_n = 6$. Such a large u_c is compatible with

Ampere's law only at such low densities that $\beta \sim$ electron gyroradius/system size.

Some applications of the method developed here include the study of electromagnetic corrections to these drift-wave results; the calculation of Alfven mode stability at arbitrary β , and of corrections to the Suydam criterion when $k_\perp \rho_i$ is nonzero; and the study of the general question of the stability of current- and temperature-gradient-driven low-frequency modes for arbitrary β and cylindrically-symmetric magnetic configurations. The bulk of the electromagnetic mode for the method described has been implemented and is currently being tested.

The investigation of drift instabilities in the RFP configuration was suggested to me by Dr. F.W. Perkins. I would like to thank Drs. Perkins, A. Boozer, and G. Rewoldt for advice and useful discussions.

[1]L. Chen *et al.*, in *Plasma Physics and Controlled Nuclear Fusion Research, 1978,* vol. I (IAEA, Vienna, 1979), p. 763; Y.C. Lee, L. Chen, and W.M. Nevins, "Stability of Drift-Wave Eigenmodes with Arbitrary Radial Wavelengths," Princeton Plasma Physics Laboratory Report PPPL-1544 (May 1979) and to be published in Nucl. Fusion; W.M. Tang, G. Rewoldt, and E.A. Frieman, "Integral Equation Analysis of Drift Wave Eigenmodes in a Sheared Slab Geometry," Princeton Plasma Physics Laboratory Report PPPL-1627 (Feb. 1980).

[2]After completing this calculation, I learned from Dr. L. Chen that a form equivalent to expression (2) was derived by B. Coppi, M. N. Rosenbluth, and R. Z. Sagdeev, Physics of Fluids $\underline{10}$, 582 (1967). Recent stability proofs and numerical calculations (see Ref. 1) using the integral-equation formalism have, however, been based on expression (1), which cannot properly be used in the strong-shear case that is of interest here.

THE NONLINEAR EVOLUTION OF RESISTIVE INTERCHANGE MODES IN REVERSED FIELD PINCHES* —— D.D. Schnack and J. Killeen, National MFE Computer Center, Lawrence Livermore Laboratory, Livermore, Ca. 94550

1. INTRODUCTION

The linear stability of cylindrical Reversed Field Pinch configurations is well known [1]. It has been found that while stability against ideal MHD modes can be achieved, such equilibria may be susceptable to resistive instabilities [2]. Recently, analytic equilibria have been discovered which are not only stable against tearing modes at zero-β, but which also satisfy the Suydam criterion for values of central β up to 18% [3]. This is achieved by judiciously expanding the pitch $\mu(r)=rB_z/B_\theta$ as a power series in r which approximates the well known Bessel function model (BFM) near the axis. Unfortunately, these equilibria have been found to be unstable to slow resistive interchange modes [4]. These modes are driven by the local pressure gradient at the singular surface and have a growth rate $\omega \sim t_R^{-1/3}t_H^{-2/3}$, as compared with tearing modes which are driven by the gross configuration of the field away from the singular surface, and which grow as $t_R^{-2/5} t_H^{-3/5}$. If these modes are dangerous nonlinearly, they may limit the attainable values of β.

In this paper we present the results of the application of a two dimensional resistive MHD computer code [5] to the nonlinear evolution of resistive interchange modes in tearing-mode-stable RFP equilibria [3]. We find that the m=1 mode is insignificant when the singular surface is outside the field reversal point, and is more active nonlinearly but still fairly localized when the singular surface lies in the inner regions of the plasma. The m=0 mode, which is not present in tokamaks, is found to lead to highly distorted flux surfaces and interchange vortices of large radial extent when β is near the Suydam marginal point. However, if the initial β is sufficiently small, this mode remains localized allowing significant Ohmic heating of the pinch to occur.

2. EQUILIBRIUM AND COMPUTATIONAL MODEL

In cylindrical geometry, the condition for magnetostatic equilibrium can be written in terms of the pitch function $\mu(r)=rB_z/B_\theta$ as

$$\frac{dB_\theta}{dr} = B_\theta \frac{\mu^2/r - \mu\mu' + r\mu'^2 \, C_1}{\mu^2 + r^2}$$

---

where $C_1 = -p'(\mu/\mu')^2/2rB_z^2$, and primes denote differentiation with respect to r. Specific equilibria are found by giving the constant C_1 and the function $\mu(r)$. Note that for $C_1 < 1/8$ the configuration is stable to Suydam modes. Stability against non-localized ideal MHD modes is obtained by either requiring that the pitch length of the magnetic field lines $2\pi\mu$ be greater than the axial wave number of the perturbration, and $\gamma \equiv \mu\mu'/2 > 0$ on axis (as is the case for tokamaks), or that $\mu(r)$ be a monotonically decreasing function of radius which changes sign inside the plasma, and which satisfies $\gamma < -4/9$ (as is the case for the RFP)[1].

In this work we take [3]
$$\mu(r) = 2(1 - r^2/8 - r^4/\lambda - r^6/\delta - r^8/\varepsilon - \ldots)$$

where λ, δ, and ε are constants. The motivation for this choice is to obtain a function $\sigma(r) = \underline{J} \cdot \underline{B}/B^2$ which is small in the outer regions of the plasma and approximately constant near the axis. This assures that the tearing mode driving term σ' is near zero in the central regions of the pinch. With $C_1 = 0$, it has been found [3] that the choice of $\lambda = 400$, δ, $\varepsilon \to \infty$ is optimum in that it yields the most extensive stable region in (k_z, R_w) space. Choosing $C_1 = .1$ results in an equilibrium which is both tearing mode and Suydam stable with a value of central $\beta \approx 18\%$. However, it is now susceptable to pressure driven resistive interchanges, or g-modes.

We study the non-linear evolution of these modes by posing an initial value problem in which the initial conditions consist of the equilibrium quantities described above perturbed by an unstable eigenmode obtained from a numerical solution of the linearized resistive MHD equations [2]. The system is then advanced in time by numerically solving the full set of nonlinear resistive MHD equations in two space dimensions by the method of finite differences [5]. For cases involving axial symmetry (e.g., the m=0 mode), we solve the problem in the (r,z) plane. When m=1, we reduce the dimensionality of the problem from three to two by transforming to the helical coordinate system $(r, \phi = m\theta + k_z z)$.

3. RESULTS

For tearing instabilities at zero β it has been established that the most nonlinearly active mode in both tokamaks and Reversed Field Pinches is characterized by azimuthal mode number m=1 [6,7]. In that case the magnetic island is observed to dominate the central core of the plasma resulting in a final state which is almost asixymmetric. In contrast, we find here that for the resistive g-mode at $\beta = .18$, i.e., near the marginal stability point, the magnetic island for m=1 remains fairly localized near the singular surface. In fact, we find that when the singular surface is outside the field null we are

able to observe only the slightest nonlinear growth before complete saturation occurs. However, when the singular surface is inside the field reversal point, the mode is found to have more robust nonlinear behavior. The island in the saturated state for this case is shown in figure 1. Note that, while the island width has become a significant fraction of the minor radius, it is still fairly localized near the singular surface. This difference in nonlinear behavior between m=1 tearing and resistive interchange modes may be due to the fact that the driving force for the g-mode is centered within the resistive layer at the singular surface, whereas the free energy for tearing modes comes from the magnetic field configuration away from the resistive layer.

The case m=0 requires a field null for its occurance and is therefore unique to the RFP. The m=0 tearing mode at zero β has been found to have relatively benign nonlinear behavior [7]. In contrast, the m=0 resistive g-mode, when it evolves near the marginal point $\beta =.18$, is found to result in large magnetic islands, highly distorted flux surfaces, and interchange vortices of large radial extent. The flux surfaces and flow field near saturation for this case are shown in figures 2 and 3. Note that the vortex motion tends to become concentrated near the reconnection point, which may indicate a cascading of energy to shorter wavelengths resulting in turbulent flow. This behavior may be due to spatially localized coupling to ideal interchange motion. In any case, such a configuration would seem to be highly conducive to enhanced radial transport. Recently, this behavior has been confirmed with an ion PIC code [8].

The above results indicate that the resistive g-mode may place a restriction on the value of β attainable through Ohmic heating. By requiring that the characteristic Ohmic heating time be less than the e-folding time for a resistive g-mode, one finds that $\beta \leq (S/4)^{-2/5}$, where $S=t_R/t_H$ is the magnetic Reynold's number [9]. For $S=10^3$, which characterizes the cases presented above, this requires $\beta \leq 0.1$, while for an initially hotter plasma, $S=10^5$, one finds $\beta \leq .02$. We investigate this behavior by studying the nonlinear evolution of the m=0 resistive g-mode for the case $S=10^3$, $\beta =.078$, which is less than the limit discussed above. Additionally, we require that the total axial current remain constant. In figure 4 we plot the evolution of $T_0(t)/T_0(\emptyset)$, the ratio of the temperature on axis to the initial temperature on axis, and $(W(t)-W(\emptyset))/W(\emptyset)$, the percentage change in magnetic island width. It can be seen that for this value of β the island saturates quickly allowing significant Ohmic heating to take place. It would thus appear crucial that the initial pinch plasma be formed in a low β state.

4. ACKNOWLEDGMENT

REFERENCES

1. D.C. Robinson, Plasma Phys. 13, 439 (1971).

2. J.A. Dibiase, Ph.D. Thesis, Univ. of Calif., Davis, UCRL-51594 (1974).

3. D.C. Robinson, Nucl. Fusion 18, 939 (1978).

4. D.C. Robinson, Eighth European Conf., Prague, Vol. 1, p. 78 (1977).

5. D. Schnack and J. Killeen, J. Comp. Phys. 34 (1980).

6. B.V. Waddell, M.N. Rosenbluth, D.A. Monticello, and R.B. White, Nucl. Fusion 16, 528 (1976).

7. D. Schnack and J. Killeen, Nucl. Fusion 19, 877 (1979).

8. D.W. Hewett and D.D. Schnack, these proceedings.

9. R.A. Gerwin, private communication.

FIGURE CAPTIONS

Fig. 1   Saturated magnetic island for $m=1$, $k_z=-1$, $\beta=.18$, $S=10^3$.

Fig. 2   Highly nonlinear phase of the magnetic island for the case $m=0$, $k_z=.4$, $\beta=.18$, $S=10^3$.

Fig. 3   Velocity field corresponding to figure 2.

Fig. 4   Relative temperature on axis and percentage change in island width for the case $m=0$, $k_z=1$, $\beta=.078$, $S=10^3$.

Fig. 1

Fig. 2

Fig. 3

Fig. 4

A Comparison of the m = 0 Resistive Interchange Mode
as Simulated by Nonlinear Hybrid and MHD Codes

D. W. Hewett, Los Alamos Scientific Laboratory

Los Alamos, New Mexico 87545

D. D. Schnack, Lawrence Livermore Laboratory

Livermore, California 94550

A two and one-half dimensional hybrid simulation code[1] has recently been used to study the occurrence and nonlinear behavior of m = 0 modes in Reversed Field Z-Pinch (RFZP) equilibria. Of particular interest is the nonlinear development of the m = 0 resistive interchange modes. Although other modes have faster linear growth, Schnack[2] has observed with his nonlinear resistive MHD code, that the m = 0 does not saturate at benign levels. The objective in this work is to verify Schnack's result and, further, to investigate the influences of ion kinetic effects on this mode.

The two and one-half dimensional hybrid model naturally includes ion Finite Larmor Radius (FLR) effects through the particle-in-cell representation of the ion component. The electron component is represented as a massless thermal fluid. In the quasi-neutral limit used in this model, the electron momentum equation with resistivity is combined with the radiation-free Darwin limit of Maxwell's equation to provide the electric and magnetic fields along with the electron drift velocity. The density and ion drift velocity are obtained by summing over the ion representation after each explicit time advance. To complete the time advance, the electron/field equation combination is solved implicitly so that the only time step constraints remaining are those normally associated with the explicit time advance of the ion component. The time step must be sufficiently small to resolve field diffusion, Alfvén velocity, and ion thermal and drift velocities on the grid.

The initialization of this code for the m = 0 study of the RFP involves loading the particle ions with the appropriately weighted r, z, v_r, v_θ, and v_z values so as to reproduce the desired RFP density and temperature profiles when these moments of the distribution are determined. The selected profiles for this work are the tearing mode stable profiles of Robinson[3] with finite pressure added (Fig. 1). The precise equilibrium is defined by specifying the pitch $P(r) = rB_z(r)/B_\theta(r) = 2(1 - r^2/8 - r^4/400)$ and the pressure $p(r)$ such that $p' = C_1 rB_z^2 (P'/P)^2$ where the prime denotes differentiation with respect to r.

Increasing the parameter C_1 monotonically increases the β of the equilibrium up to $C_1 = 0.125$ for which the equilibrium becomes unstable to localized Suydam modes. This limiting β is approximately 18% on axis. For the results presented here, we take a relatively large value for C_1 ($\approx 0.1 \rightarrow \beta \approx 15\%$ on axis) to provide, for computational economy, a large linear growth rate for the $m = 0$ mode.

Some of the specific parameters for the results presented here are:

Magnetic field on axis	2.5 kG
Ion temperature on axis	~100 eV
Ion FLR on axis	~0.2 cm
C_1	0.1
Linear growth time for $m = 0$ G-mode	26 μs

Since the expected mode will require a relatively large number of Alfvén times, a perturbation, localized at the singular surface, is added to the drift velocities at $t = 0$. The perturbation approximates the plasma displacement obtained from linearized resistive MHD codes and, consequently, should reduce the computational time required for the unstable mode to emerge from "noise".

The simulation parameters chosen for this run include:

Magnetic Reynold's number	10^3
Grid resolution	40 (radial) x 20 (axial)
Particles	10,000
Period BC's in the z-direction with ($z_{max}-z_{min}$)	80 cm
r_{wall}	20 cm
time step	5 ns

The time evolution of this equilibrium is displayed in a sequence of toroidal flux function $\psi(=rA_\theta)$ contour plots (Fig. 2). Since the initial perturbation is added via a mass flow, the $t = 0$ contour simply displays the equilibrium flux function. The effect of the initial perturbation is evident in ψ at 5 μs but momentarily disappears at 10 μs. At times 15, 20, and 25 μs the mode is observed to grow rapidly through the linear phase and into the nonlinear regime without saturation. Saturation of this $m = 0$ displacement finally occurs between 30 and 35 μs when the mode "hits" the conducting wall.

Comparing this result with an earlier simulation of the same equilibrium by Schnack with a resistive MHD initial-value code, we find striking agreement in the nonlinear character of the instability. (See Fig. 3). Although neither

103

code includes the potentially stabilizing influence due to electron thermal conductivity, both start from identical profiles and similar perturbations. Considering the large differences in the two simulation techniques, the similarity of the results coupled with the disruptive character of the mode provide incentive to make further comparisons and to investigate more extensively the proposed RFP start up procedure. Specifically, the start up technique proposes to circumvent this mode by achieving large S values while maintaining low β. At high S, the interchange mode will be highly localized and will be more strongly stabilized by ion FLR effects.

REFERENCES

1. D. W. Hewett, "A Global Method of Solving the Electron-Field Equations in a Zero-Inertia-Electron-Hybrid-Plasma Simulation Model," J. Comp. Phys. (accepted for publication) 1980.

2. D. Schnack and J. Killeen, "The Nonlinear Evolution of Resistive Instabilities in Finite Beta Reversed Field Pinches," paper 3B 31, Sherwood Theory Meeting, Mount Pocono, Penn. (1979).

3. D. C. Robinson, Plasma Phys. 13, 439 (1971).
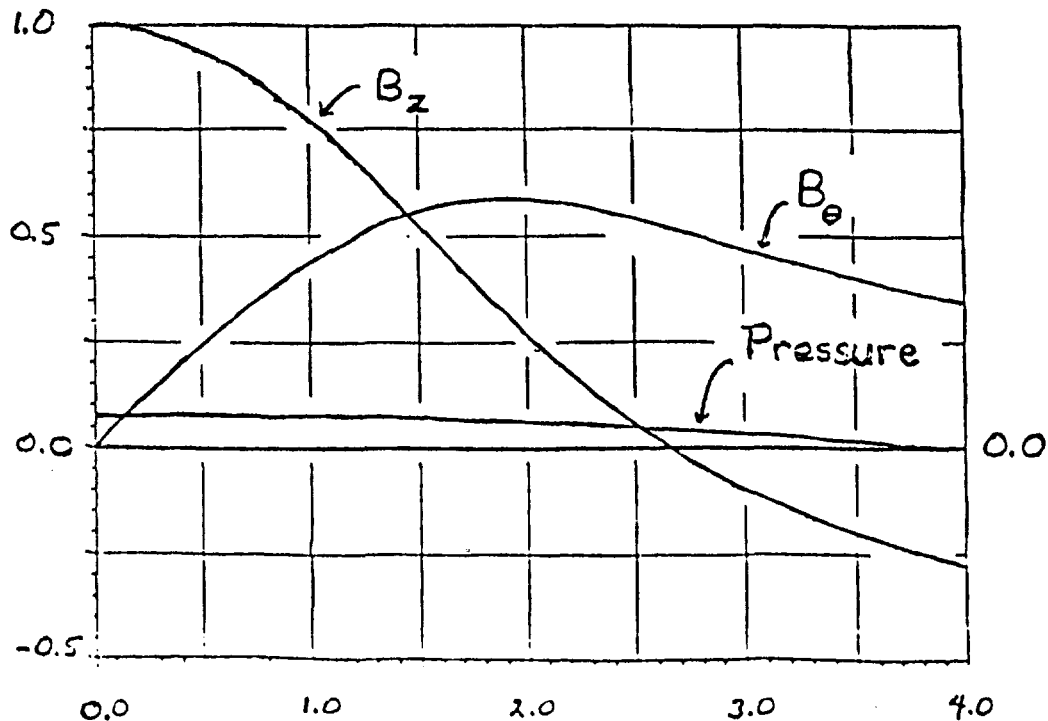
Fig. 1 Robinson's RFP Equilibrium

Fig. 2   Time Sequence of Toroidal Flux Contours from 2-D Hybrid
Simulation of the m = 0 G-modes.
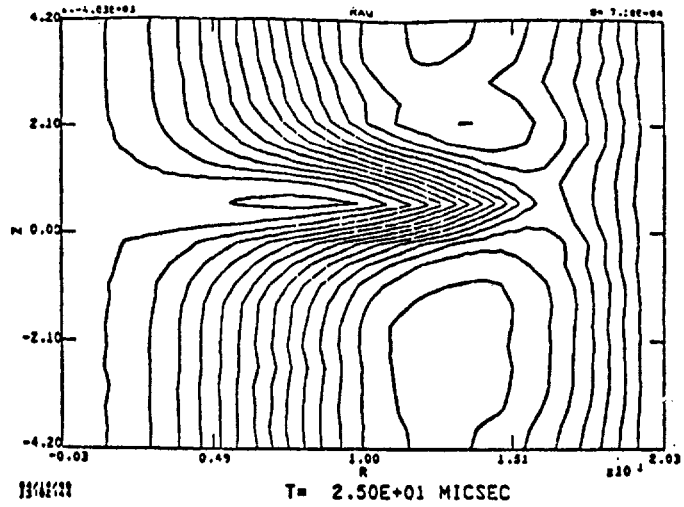
a) 2-D Hybrid Code
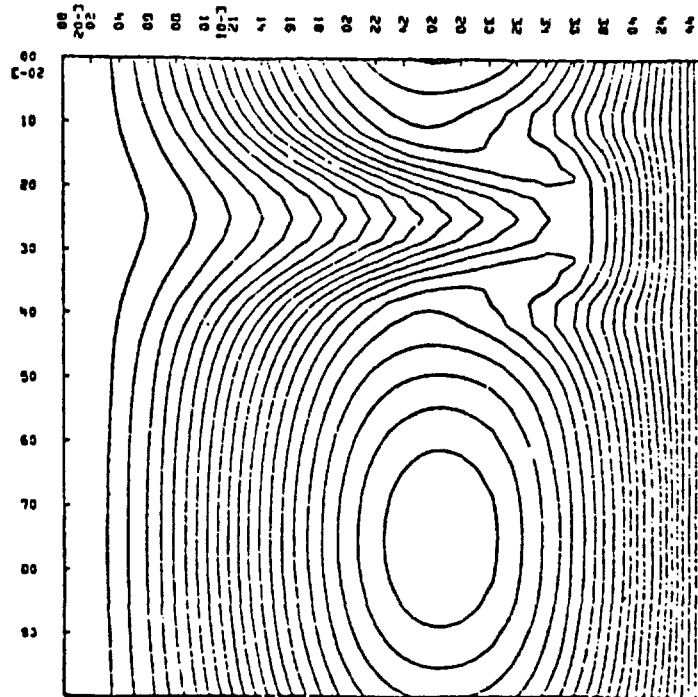
b) 2-D MHD Code

Fig. 3 Toroidal Flux Contours in Nonlinear Regime

ELECTRON TEMPERATURE GRADIENT EFFECT

ON RESISTIVE-G MODE

by

C. L. Chang, N. T. Gladd and C. S. Liu
Department of Physics and Astronomy
University of Maryland
College Park, Maryland 20742

INTRODUCTION The low-frequency interchange instability may be excited in a collisional plasma with magnetic shear if the local magnetic curvature is along the direction of pressure gradient; the so called resistive-g mode[1] localized at bad curvature region with $\nabla B \nabla P > 0$. Recent experiment on Levitron performed by Ainsworth et al.[2] reconfirms the existence of this mode. Remarkably, they find unstable low frequency fluctuations only on the outer edge of the super-conducting ring, and these low frequency fluctuations, which persist for a wide range of magnetic shear, are expected to be the source of observed anomalous particle diffusion across the magnetic field lines.

THEORY Since this low-frequency highly-unstable mode may also play an important role in the machines like Reverse Field Pinch and Spheromak, we examine, in this paper, its stability property in more details by including the effect of electron temperature gradient η_e. The whole analysis is carried out within the context of a slab geometry and, in modeling the electron temperature gradient effect on the electron-ion collisions, a velocity-dependent Lorentz collision model is adopted in our drift kinetic formalism. In addition, this velocity-dependent treatment is extended to include the curvature drifts of electrons and ions by taking the guiding center drift to be proportional to their parallel kinetic energy $mv_\parallel^2/2$. The perturbed electron distribution is then given by the linearized drift kinetic equation

$$\{ \omega - k_\parallel v_\parallel - \omega_{ge}(v_\parallel/v)^2 - i(\nu_c/2)\cdot[\partial/\partial\xi\,(1-\xi^2)\,\partial/\partial\xi]\}\,f_e$$

$$= e\phi\,\{k_y\,(\partial f_{oe}/\partial P_y) + [k_y v_\parallel + \omega_{ge}(v_\parallel/v_c)^2]\cdot(\partial f_{oe}/\partial H)\} \tag{1}$$

where ω_{ge} is the electron curvature drift frequency and ξ is the cosine of pitch angle variable $\xi = v_\parallel/v$. Using the quasineutrality condition $\tilde{n}_e = \tilde{n}_i$, the differential eigenmode equation describing low-frequency electrostatic instability can be cast into the standard form

$$\frac{\partial^2 \phi}{\partial x^2} + Q(x)\,\phi = 0 \qquad (2)$$

with the potential function $Q(x)$ expressed as

$$Q(x) = -\frac{2\tau\,[\,\Sigma + \Lambda + (\,\tau + \omega*/\omega\,)\,\Gamma_0\zeta H(\zeta,\mu)\,]}{\Gamma_0'\,(\,\tau + \omega_*/\omega\,)\,\zeta H(\zeta,\mu)} \qquad (3)$$

where $\zeta = \omega/k_\parallel v_i$, $\mu = \omega_{ge}/\tau k_\parallel v_i$, $\tau = T_e/T_i$ and the functions Σ, Λ and H are defined in Ref. (3). The above eigenmode equation, though complicated, can be solved numerically by the standard shooting techniques.

NUMERICAL RESULTS AND DISCUSSIONS   Physically, the interchange instability arises because the charge seperation, caused by both electrons and ions experiencing curvature drifts in the opposite direction, further enhances the density perturbation itself. It is therefore necessary to short out this charge seperation in order to quench the instability. In the case of sheared magnetic field, this charge neutralization may be achieved by electron thermal motion along the field lines. However, in a region centered around the mode rational surface with $\omega v_c / k_\parallel^2 v_e^2 \lesssim 1$, the electrons behave adiabetically and the unstable charge seperation remains. This is best illustrated in Fig. 1(a) where the numerically solved wavefunction ϕ and potential Q are plotted against the radial distance x/ρ_s. From this figure, we can see that at the mode rational surface $x=0.$, the potential Q forms a well to localize the wavefunction and $\mathrm{Im}Q$ (>0) serves as negative dissipation to drive the instability. Subsequent plots (b), (c) and (d) in the same figure are for $\eta_e = 1.,2.$ and 3. respectively. From these figures, we can see that the electron temperature gradient dramatically destroys the well generated

by the curvature drifts, by forming a potential barrier at the mode rational surface. Indeed, this η_e related potential barrier pushes the wavefunction away from the unstable adiabatic region and consequently stabilizes the resistive-g mode. Figure 2 plots the growth rate γ/ω_* as a function of η_e, we notice from this figure that the temperature gradient effect is more complicated than simply stabilizing. Specifically, the growth rate is mildly enhanced at first by the increasing η_e and then decreases rapidly. To gain a qualitative understanding of the influence of η_e on stability behavior, we proceed further to calculate the potential strength $Q(x)$ at mode rational surface $x=0$

$$Q(x) = \frac{(\omega_{ge}/\omega).(\omega_*/\omega).(1. + \eta_e + \Gamma_0/\tau)}{2\rho_s^2 \; (|\Gamma_0'|/2).(1 + \omega_*/\omega\tau).(\omega_{ge}/2\omega\tau)} \qquad (4)$$

In the case of bad curvature $\omega_{ge}\omega_* > 0$, the sign of $Q(0)$ is determined by the quantity $-1/\omega^2$. Accordingly, the real part of the potential $\text{Re}Q(0)$ forms either a barrier ($\text{Re}Q < 0$) or a well ($\text{Re}Q > 0$) depending on whether $\omega_r > \gamma$ or $\gamma > \omega_r$. Therefore, by increasing η_e, the real frequency increases linearly with the temperature gradient and, as soon as the uprising ω_r exceeds γ, the potential well at $x=0$ becomes repulsive; thus pushing the wavefunction away from the destabilizing region and bringing down the growth rate.

In summary, we have examined the effect of electron temperature gradient on the resistive-g mode. Our numerical results show that with the increasing temperature gradient η_e, the growth rate of this curvature driven mode decreases considerably. This temperature gradient stabilization may be explained analytically by considering the electron dynamics at the mode rational surface.

REFERENCES

[1] Furth H P, Killeen J and Rosenbluth M N, Phys. Fluids 6, 459 (1963)

[2] Ainsworth N R et al., 1979 in Plasma Physics and Controlled Nuclear Fusion Research (Proc. 7th Int. Conf. Innsbruck, Austria 1978) IAEA Vienna , to be published.

[3] Chang C L, "Low Frequency Drift Waves in Sheared Magnetic Field" Ph.D. thesis, Phys. Publication # 80-140, Univ. of Md. (1980)
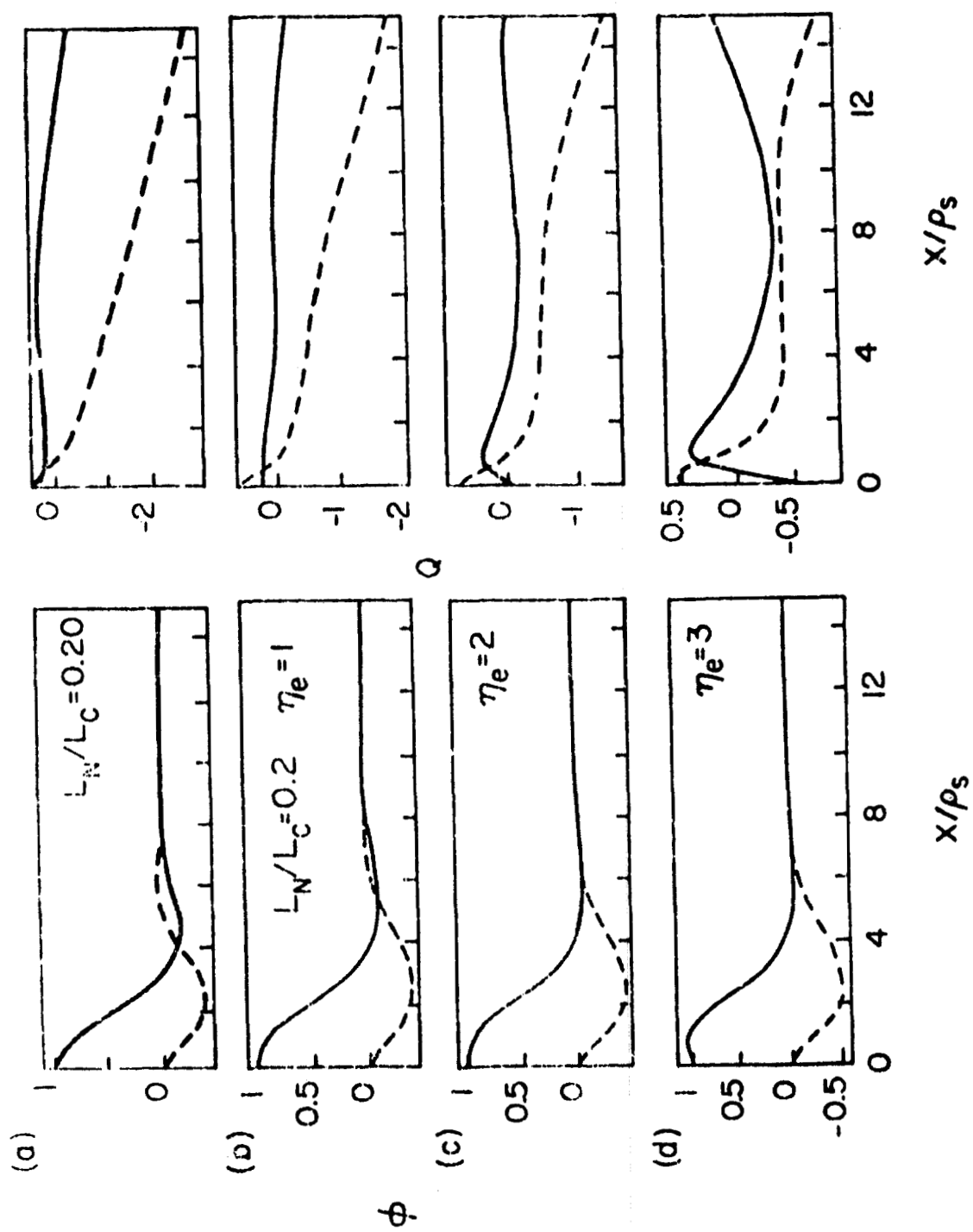
Figure 1
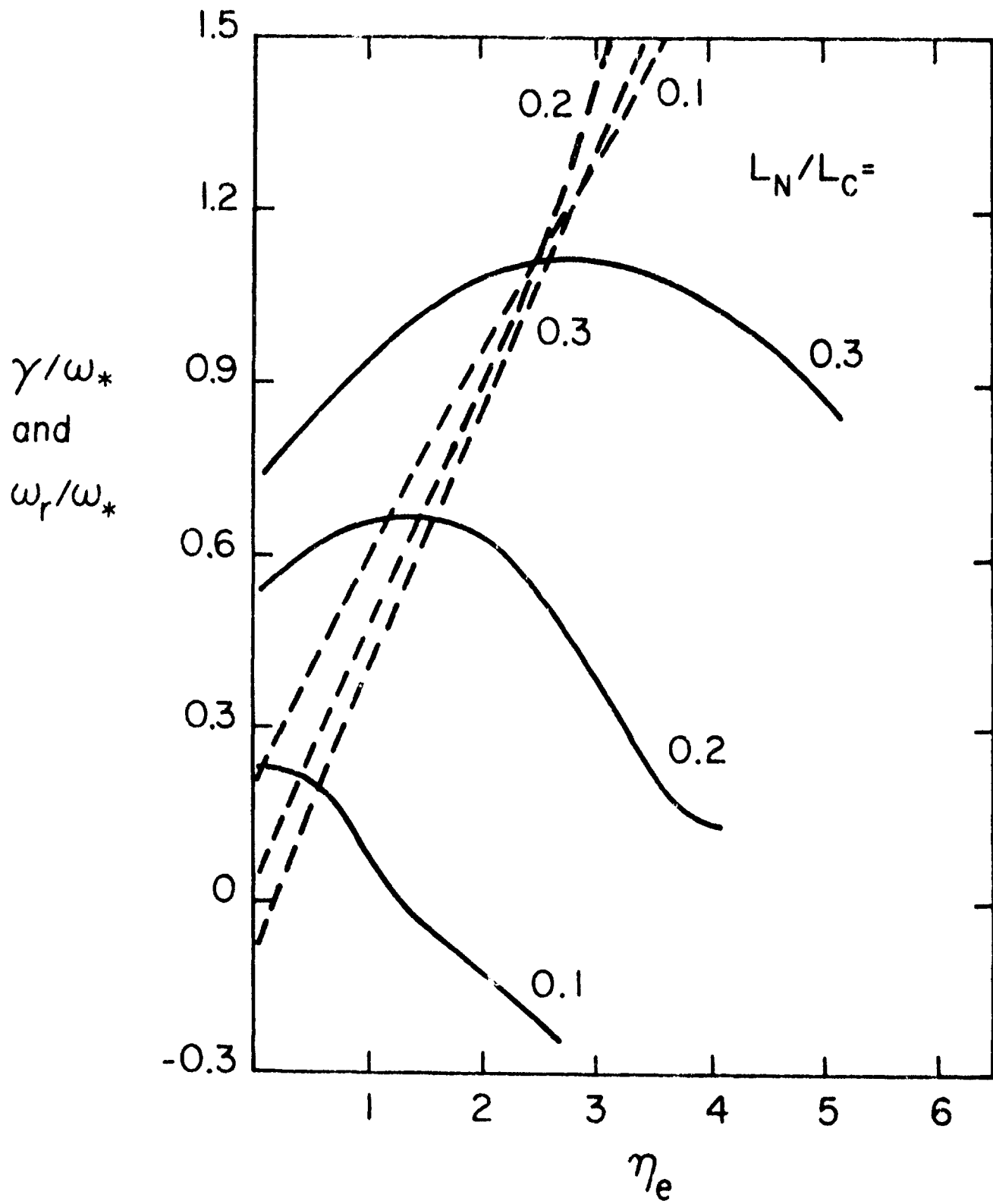
Figure 2.

MHD EQUILIBRIUM AND INTERCHANGE STABILITY OF HELICAL CONFIGURATIONS WITH "PITCH REVERSAL"

M. S. Chu, C. Chu, R. Goforth, F. W. McClain, M. Schaffer, and T. Ohkawa
General Atomic Company

We discuss here the OHTE configuration, a high current, low flux, helically symmetric toroidal pinch configuration with pitch reversal.[1] The configuration consists of a central paramagnetic core and a pitch reversed boundary region. The pitch reversal is the combined result of plasma paramagnetism and the translational transform effect of the external helical fields. The plasma boundary is either determined by a limiter or separated from the outside by separatrices created by the external coils. Although the experimental apparatus is toroidal in nature, in this paper, we discuss the MHD equilibria and interchange stability of this configuration in the straight approximation.

In straight helical equilibria, the magnetic field $\vec{B}$ is given by

$$\vec{B} = f\vec{u} + \vec{u} \times \vec{\nabla}F, \qquad \text{with } \vec{u} = (\hat{z} + \alpha r\hat{\theta})/(1 + \alpha^2 r^2)$$

(r, θ, z) is the usual cylindrical coordinate system and $2\pi/|\alpha|$ is the pitch length of the external coil. The helical flux function F, being a function of radius r and the symmetry variable $u = \theta - \alpha z$, satisfies the helical Grad-Shafranov equation

$$\frac{1}{r}\frac{\partial}{\partial r}\frac{r}{1 + \alpha^2 r^2}\frac{\partial F}{\partial r} + \frac{1}{r^2}\frac{\partial^2 F}{\partial u^2} = -\frac{2\alpha f}{(1 + \alpha^2 r^2)^2} - \frac{ff'}{(1 + \alpha^2 r^2)} - \mu_0 p' \quad (1)$$

The helical current flux f and pressure p are arbitrary functions of F. For a discharge inside a cylindrical chamber, the variation of the flux function F on the chamber surface is determined largely by the external helical coil currents. The separatrix passing through $\vec{\nabla}F = 0$ locations divides the plasma into open and closed field line regions. The closed field lines enclose the central plasma, while the open field lines lead to the chamber surface or may be lead to divertor regions enclosing the helical coils. Thus, the separatrices may form a magnetic limiter for the discharge channel. The discharge may also be limited by a material limiter (located at F_ℓ) inside of the separatrix. The requirement that the current vanish outside of the limiting surface gives the free boundary condition

$$
\begin{cases}
f' = 0 \\
p' = 0
\end{cases}
\quad \text{for} \quad
\begin{array}{l}
F > F_b = \min\,(F_\ell, F_s) \\
\text{or } r > r_{lim}
\end{array}
\tag{2}
$$

In (2), r_{lim} is the limiter location. The differential equation (1) with arbitrary f' and p' satisfying (2) has been solved numerically with the helical flux boundary condition given by realistic external coils. The numerical method[2] utilizes the fact that the differential equation (1) for F is separable in r and u. The free boundary condition (2) is satisfied iteratively by modifying the source term to equation (1).

When the external helical coil current I_h is zero, ordinary (reversed field) pinch equilibria are obtained. For instance, for $f' = -\mu = $ const inside of F_b, and zero plasma pressure, the Bessel function equilibrium $B_z = B_{zo}Jo(\mu r)$, $B_\theta = B_{zo}J_1(\mu r)$ is obtained. We notice that in here axial magnetic field reversal can only develop due to plasma current parallel to the magnetic field. [The development of this reversed field region has been observed experimentally to lead to plasma quiescence[3] and explained qualitatively theoretically[4].]

When the helical coil current I_h is increased, the external flux surfaces are deformed into noncircular shapes. An example of the flux surfaces is given in Fig. 1 for both $\ell = 2$ and $\ell = 3$ configurations. Note that the noncircularity decreases rapidly away from the plasma surface. The separatrix location is determined mainly by the ratio of the plasma current I_p to I_h, with the separatrix radius increasing for increasing plasma current. The various flux surface averaged quantities are shown in Fig. 2 for the
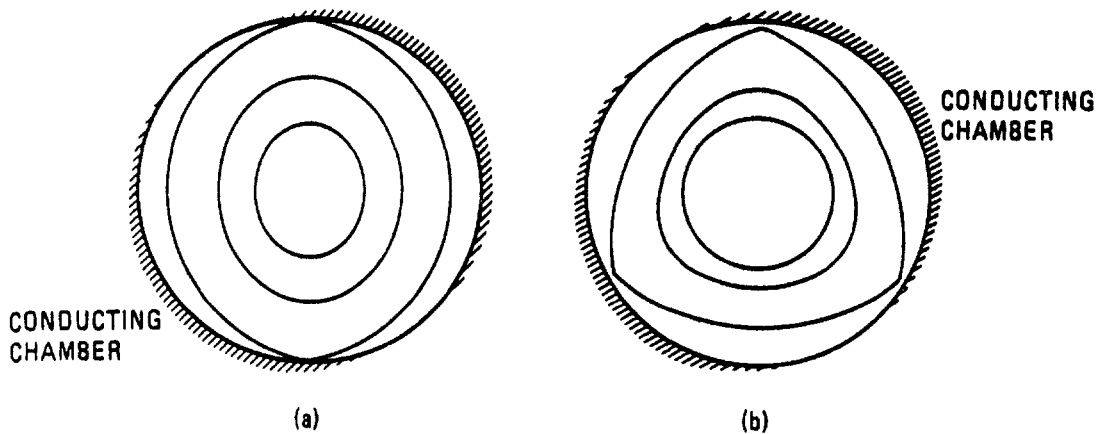
Fig. 1. $\ell = 2$ and $\ell = 3$ helical flux function contours for separatrices just within the chamber. $\langle \mu r_p \rangle = 3$. $I_h = 30$ kA, 45° winding angle, coil radius 0.215 m. For $\ell = 2$, $I_p/I_h = 5.5$, $\langle r_p \rangle = 0.158$m. For $\ell = 3$, $I_p/I_h = 4$, $\langle r_p \rangle = 0.165$m.
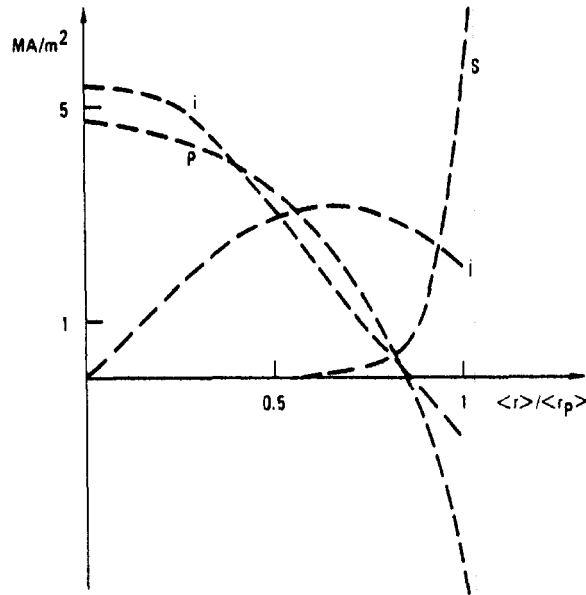
Fig. 2. Flux surface averaged toroidal current
density i, poloidal current density j,
for an ℓ = 3 equilibrium as a function
of averaged radius. Shown also are the
relative profiles of the pitch P and
shear S.

ℓ = 3 case. The interior of the configuration differs little from a
(reversed field) pinch, yet it has quite different characteristics near the
boundary. To demonstrate this properly, we also exhibit the pitch profiles
for three current profiles in Fig. 3.

In current profile A, f' is constant throughout the plasma, as in Figs.
1 and 2. In current profile C, f' is kept constant inside of the pitch
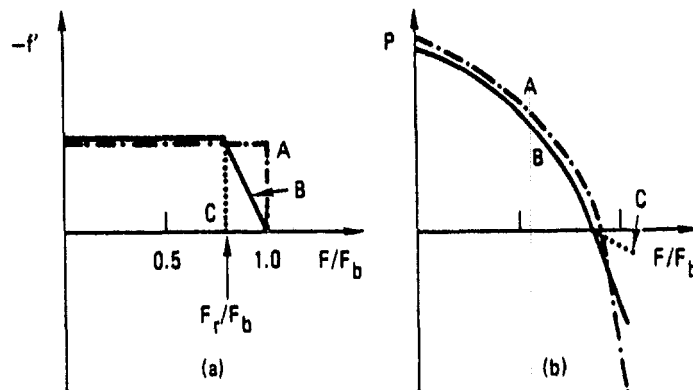
Fig. 3. Current density profiles f' and the corres-
ponding pitch profiles P for helically symmetric
equilibria. F_b is the plasma boundary. F_r is
the reversal point.

115

reversal point and is reduced sharply to zero outside. The pitch reversal
in this case is due entirely to the external helical field, which adds a
translational transform to the magnetic field. Profile A has been proposed
by Taylor[4] to be favorable for its stability to current driven modes. Pro-
file C has been usually assumed for current drive and power input considera-
tions. Finally, profile B has a trapezoidal f' profile, shown in Fig. 3a,
in which f' tapers in the reversed pitch layer from the central value to
zero at the limiting surface. The corresponding pitch profiles are plotted
in Fig. 3b. The translational transform was chosen to enhance the pitch
reversal. Various other profiles with different f' and p', for instance,
cases where f' varies as a power law or exponential function of F have also
been computed. In general, the plasma develops a pitch reversal when the
plasma current to axial flux (pinch) ratio exceeds a value which depends on
the external helical field.

To study the stability of these configurations to localized interchanges,
the stability criterion of Greene and Johnson[5] is used:

$$D_I = Sh + A_1 + A_2 + A_3 \leq 0 \qquad (3)$$

where $Sh = -1/4$ \qquad (4)

$$A_1 = -\frac{V'}{S^2} \left[\left\langle \frac{B^2}{|\nabla F|^2} \right\rangle \mu_0(p'V'' + I'\chi'' - J'\psi'') \right.$$

$$\left. + S \left(f' < \frac{B^2}{|\nabla F|^2} > + \mu_0 p' f \left\langle \frac{1}{|\nabla F|^2} \right\rangle \right) \right]$$

$$A_2 = \frac{\mu_0 p'^2 V'^2}{S^2} \left\langle \frac{1}{B^2} \right\rangle \left\langle \frac{B^2}{|\nabla F|^2} \right\rangle$$

$$A_3 = -\frac{\mu_0^2 V'^2 p'^2 f^2}{S^2} \left[\left\langle \frac{1}{|\nabla F|^2} \right\rangle^2 - \left\langle \frac{B^2}{|\nabla F|^2} \right\rangle \left\langle \frac{1}{B^2 |\nabla F|^2} \right\rangle \right]$$

$$S = \psi'\chi'' - \chi'\psi''$$

with < > indicating average over the flux surface. I and J are the toroidal
and poloidal current flux, V the volume, and ψ, χ are the toroidal and poloi-
dal magnetic fluxes, ' indicates differentiation w.r.t. the helical flux F.
This criterion is to be compared to the Suvdam criterion for circular pinches.
Due to the noncircularity of the flux surfaces, the geodesic curvature terms

are slightly destabilizing near the separatrix. However, the additional translational transform maintains the shear in this region. The explicit value of the various terms in the interchange criterion are shown across the flux surfaces in Fig. 4 for an A profile equilibrium. This particular configuration has a volume averaged β of 18%, (corresponds to $\beta_I = 10^7/\pi$ $\int p dV/I^2 R_0 = 40\%$) and still has stability margin throughout.
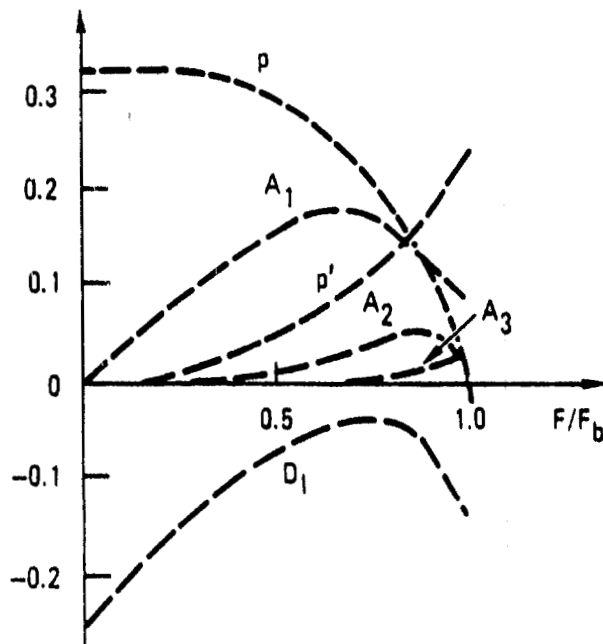
Fig. 4.   Relative value of various quantities in the
interchange criterion across the flux surface.

In conclusion, we have demonstrated the basic equilibrium and interchange stability properties of a high current low flux helically symmetric system.

REFERENCES:

1. T. Ohkawa, et al., GA-A15561 (1980) submitted to Phys. Rev. Letters.
2. F. McClain, et al., DELINV, GA-A15845 (1980).
3. D. C. Robinson and R. E. King in Plasma Physics and Controlled Fusion Research (Proc. 3rd Int. Conf. Novosibirsk, 1968) 1, IAEA, Vienna (1969) p 263.
4. J. B. Taylor, in Pulsed High Beta Plasmas, Pergamon, Oxford (1976), p 59.
5. J. M. Greene and J. L. Johnson, Plasma Physics, 10, 729 (1968).

DYNAMICAL DETERMINATION OF OHMIC STATES OF A CYLINDRICAL PINCH*--D.D. Schnack, National MFE Computer Center, Lawrence Livermore Laboratory, Livermore, CA. 94550

1. INTRODUCTION

One of the fundamental problems in understanding the observed behavior of the Reversed Field Pinch (RFP) is the mechanism for generation and maintenance of the reversed axial field. While the theory of Taylor [1] predicts a relaxation toward such a state, it does not address the problem of the dynamics of its attainment or regeneration. Experimental observations indicate that the mechanism may not be unique [2], and models based on both turbulence [3] and instability [4] have been proposed. In the former case, it is shown that the mean magnetic field evolves from a given initial state to a final force-free steady state consistent with the Taylor theory. In the latter case, the nonlinear interaction of kink modes with different helicity leads to field reversal, which is then sustained by continued unstable activity.

In this paper we address the dual problems of generation and sustainment of the reversed axial field. We show that, if a cylindrical plasma is initially in an axisymmetric state with a sufficient degree of paramagnetism, field reversal can be attained by mode activity of a single helicity. The initial paramagnetism may be due to the method of pinch formation, as in fast experiments [5], or to a gradual altering of the pitch profile resulting from a succession of instabilities [6]. Furthermore, if the total current is kept constant and energy loss and resistivity profiles are included in an ad hoc manner, we find that the final steady state of the helical instability can be maintained for long times against resistive diffusion without the need for further unstable activity. These states, which possess zero order flow and possibly reversed axial field, represent steady equilibria which simultaneously satisfy force balance and Ohm's law, and are termed Ohmic states [7].

2. METHOD OF SOLUTION

We approach the problem of the existence and accessability of Ohmic states by solving an initial value problem in which an initially unstable, axisymmetric cylindrical Z-pinch equilibrium is perturbed with an eigenmode of an $m=1$ resistive kink instability obtained from a linear resistive MHD code. The nonlinear evolution and saturated final state of this configuration is then determined with a nonlinear, two-dimensional MHD code which solves the full set of helically symmetric resistive MHD equations [8]. Specifically, we choose

$$J_z = \frac{4I}{a^2}\left(1 - \frac{r^2}{a^2}\right) \quad , \quad B_\theta = \frac{2Ir}{a^2}\left(1 - \frac{1}{2}\frac{r^2}{a^2}\right)$$

where r=a is the radius of a conducting wall, and the boundary conditions are such that the total current I remains constant throughout the calculation. Since there is initially no azimuthal current, the axial field $B_z(r)$ can be specified arbitrarily. Specific choices are discussed in the next section. More peaked or flattened initial current profiles could be used, but here we consider only the parabolic model given above.

In order to approximate the cool outer regions of the pinch, we employ a scalar resistivity model which is peaked near the conducting wall, i.e., $\eta(r)=1/[\sigma_0+(1-r^2/a^2)^2]$, where σ_0 is a constant which limits the value of resistivity at the wall, and is usualy taken to be 10^{-2}. A more complete calculation would allow for a self-consistent resistivity, or perhaps even $\eta=\eta(\psi)$, where ψ is the helical flux. However, the above model has the gross property of maintaining a peaked current profile throughout the evolution of the pinch, while avoiding the nonlinear computational problems associated with a self-consistent calculation.

Since the total axial current remains constant, a steady state will not be reached unless the resulting Ohmic heating is balanced by an energy loss term, which physicaly may be due to radiation, diffusion to the limiter, etc. For these calculations we choose a loss rate profile $q(r)=\alpha(r/a)^2 p/(\gamma-1)$, which again serves to cool the outer regions of the plasma.

3. RESULTS

For a given value of total current, we allow the instability to proceed to its final saturated helical state where we examine the average value of axial field at the wall, defined be

$$\langle B_{zw}\rangle = \frac{1}{2\pi}\int_0^{2\pi} B_z(a,\theta)d\theta$$

A plot of $\langle B_{zw}\rangle f$, the average value of $B_z(a)$ in the final Ohmmic state, versus $B_{\theta_w}=I/a$, the value of azimuthal field at the wall, is thus equivalent to the familiar F-θ diagram.

Particular results require that the initial axial field profile $B_z(r)$ be specified. The choice $B_z(r)=const.=1$ corresponds to initial conditions which resemble a tokamak, and for a given total current can be made unstable by the proper choice of axial wave number. In figure 1 we plot $\langle B_{zw}\rangle f$ versus B_{θ_w} for this case. Note that, while quite paramagnetic final states are reached, field reversal is not achieved, with $\langle B_{zw}\rangle f \approx .35$ for

$B_{\theta_W} \geq 4$. Helical mode activity does not provide sufficient axial flux amplification in the core to reverse the axial field for this configuration. The helical flux topology and flow field for the Ohmic state corresponding to $B_{\theta_W}=1.5$ are shown in figures 2a,b. Note the presence of the magnetic island which persists in spite of resistive diffusion. In figure 4 we display $\langle B_{ZW} \rangle$ as a function of time for this case, demonstrating the relaxation to a final Ohmic state.

There is experimental evidence that the initial state of the pinch may be highly paramagnetic [5]. This is certainly the case for fast pinches, and may also result in slow pinches from gradual modification of the pitch profile due to a series of instabilities such as that described above [6]. We thus consider an initial axial field profile of the form

$$B_Z = 1 - (1 - B_{ZW_0}) \frac{2r^2}{a^2} (1 - \frac{1}{2} \frac{r^2}{a^2})$$

where B_{ZW_0} is the value of $B_Z(a)$ in the initial state. When $B_{ZW_0}=.5$, field reversed Ohmic states are still not achieved. When $B_{ZW_0}=.02$, transient reversal is obtained for $B_{\theta_W}=1.5$, and a fully reversed Ohmic equilibrium is achieved when $B_{\theta_W}=2$. This is demonstrated in figure 5, where we plot $\langle P_{ZW} \rangle$ versus time. The resulting helical flux surfaces are shown in figure 6. Note that, while the state is helically deformed, no magnetic island is present.

4. DISCUSSION

We have demonstrated qualitatively that, in addition to turbulence and instability, there is a further candidate for the maintenance of the reversed field state, i.e., an Ohmic equilibrium which is maintained against resistive diffusion by the action of zero-order flow. Additionally, such states are accessible as the saturated states of helical instabilities. However, since in our model the resistivity and loss profiles are somewhat arbitrary and not self-consistent, quantitative results are elusive. For example, when proper normalization is taken into account, we find field reversal to occur for values of $\theta = B_{\theta_W}/B_{Z_{ave}}$ in the range $4.4 < \theta < 5.8$, which is considerably larger than predicted by Taylor's theory [1]. This may also be due to the scalar character of the resistivity. In any case, further refinement of the model may be necessary.

5. ACKNOWLEDGEMENT

REFERENCES

1. J. B. Taylor, Phys. Rev. Letters <u>33</u>, 1139 (1974).

2. E.P. Butt, A.A. Newton, and A.J.L. Verhage, in <u>Pulsed High Beta Plasmas</u>, p. 419, D.E. Evans, ed., Pergamon Press, Oxford (1976).

3. G.G. Gimblett and M.L. Watkins, in <u>Pulsed High Beta Plasmas</u>, p. 279, D.E. Evans, ed., Pergamon Press, Oxford (1976).

4. C.W. Gowers, D.C. Robinson, A. Sykes, A.J.L. Verhage, J.A. Wesson, M.R.C. Watts, and H.A.B. Bodin, in <u>Sixth Conference on Plasma Physics and Controlled Nuclear Fusion</u>, Brechtesgaden, IAEA (1976).

5. A.J.L. Verhage, A.S. Furzer, and D.C. Robinson, Nucl. Fusion <u>18</u>, 457 (1978).

6. R.Y. Dagazian, private communication.

7. J.A. Wesson, private communication.

8. D. Schnack and J. Killeen, J. Comp. Phys. <u>34</u> (1980).

FIGURE CAPTIONS

Fig. 1 $\langle B_{ZW} \rangle_f$, the average value of the axial field at the wall, vs. B_{θ_W} for the case $B_{ZW_0} = 1$.

Fig. 2 Helical flux surfaces in the final Ohmic corresponding to $B_{\theta_W} = 1.5$, $B_{ZW_0} = 1$.

Fig. 3 Final flow field corresponding to fig. 2.

Fig. 4 $\langle B_{ZW} \rangle$ vs. time for the case $B_{\theta_W} = 1.5$, $B_{ZW_0} = 1$.

Fig. 5 $\langle B_{ZW} \rangle$ vs. time for the case $B_{\theta_W} = 2.0$, $B_{ZW_0} = .02$. Note that a field-reversed Ohmic state has been attained.

Fig. 6 Helical flux contours in the Ohmic state $B_{\theta_W} = 2.0$, $B_{ZW_0} = .02$. Note the absence of a magnetic island.

Fig. 1

Fig. 2

Fig. 3

Fig. 4

Fig. 5

Fig. 6

ON A HELICAL OHMIC STATE FOR REVERSED FIELD PINCHES

by Rostom Y. Dagazian

I. INTRODUCTION

Experimental evidence[1] leads us to conclude that no violent phenomena are associated with the onset of field reversal in RFPs. The numerical work of Schnack[2] also corroborates to this; it also suggests very strongly that a mode of single helicity maybe completely sufficient to explain all of the phenomena involved. If a single mode by itself cannot produce enough of a paramagnetic effect, it is very easy to imagine a chain of successive modes each rearranging longitudinal flux by a small amount near the plasma edge until the next (generally higher toroidal number mode) becomes excited and until finally a profile is carved that is completely stable to further perturbation.

It is also evident from the work of Schnack that a final saturated state of a mode with paramagnetic behavior is not necessarily geometrically complicated and in some cases it does not really possess a magnetic island. On the other hand, finite flows seem to be instrumental in maintaining such a state.

Single helicity and simplicity of the final state suggest that the problem is amenable to analytic investigation; the presence of flow, however, constitutes a serious complication. In this work, it will suffice to merely give an outline of a method for treating the problem analytically without really presenting any concrete results.

II. THE MODEL

We search for helical, finite beta equilibria, which satisfy the set of _resistive_ incompressible MHD equations

$$\nabla p = \underset{\sim}{J} \times \underset{\sim}{B} - \rho \underset{\sim}{v} \cdot \nabla \underset{\sim}{v} \tag{1}$$

$$-\nabla \phi + \underset{\sim}{v} \times \underset{\sim}{B} = \eta \underset{\sim}{J} \tag{2}$$

$$\nabla \cdot \underset{\sim}{v} = \nabla \cdot \underset{\sim}{B} = 0 \tag{3}$$

$$\underset{\sim}{J} = \nabla \cdot \underset{\sim}{B} \tag{4}$$

where the symbols have their usual meaning.

The inclusion of Ohm's law Eq. (2) and of the $\underset{\sim}{v} \cdot \nabla \underset{\sim}{v}$ term in Eq. (1) is to be noted. It is important in view of the fact that field reversal cannot be maintained in the presence of finite resistiveity in axisymmetry.[3] Here helical symmetry and finite flow are introduced together as effects producing a field reversed state that maintains itself in time.

If one is to believe the experimental and numerical results, one must assume that the amplitude of the helical distortion of the final state will indeed be small although finite. We then think immediately of a small amplitude expansion of Eqs. (1-4), a quasilinear treatment should be appropriate. One has to only go to second order in the amplitude when calculating corrections to $B_z^{(0)}$, the equilibrium cylindrical part of the longitudinal magnetic field. However, examining Eqs. (1-4) more closely, we find that because we set $\partial/\partial t \equiv 0$, singularities will occur when $\underset{\sim}{k} \cdot \underset{\sim}{B}^{(0)} = 0$; $\underset{\sim}{k}$ here is the wavevector of the helical distortion. The singular behavior gets progressively worse as one examines higher order equations in the amplitude expansion.[4]

We are then led to consider the separate regions for the problem, a) the resonant region, i.e., the region near the original mode rational surface in which a completely nonlinear treatment is necessary if well behaved solutions are to be found, b) the rest of the plasma, where a quasilinear treatment is sufficient.

Asymptotic matching of the solutions in the two regions will yield the final answers.

III. OUTLINE OF CALCULATION

We employ helical fluxes ψ, δ, f, g[5] for the magnetic field, flow, current density, and vorticity respectively. Far from the resonent surface, we employ an amplitude expansion of the form

$$\psi(r,\tau) = \psi^{(0)}(r) + \delta\psi^{(1)}(r,\tau) + \delta^2\psi(r,\tau) + \ldots$$

$$\delta \ll 1 \tag{5}$$

Here $r, \tau \equiv m\theta + kz$ are the usual helical coordinates. We further assume weak flows in the external regions

$$\phi^{(0)} \equiv 0 \tag{6}$$

then letting $\psi^{(1)}(r,\tau) = \psi^{(1)}_{(r)}e^{i\tau}$ to be the form of the linear part of the distortion we proceed to calculate first the r dependence of the linear fields from Eq. (1-4) then the second order fields that result because of the interaction of the helical distortion with itself. Assuming rather long wavelength distortions, the second order equations simplify considerably upon neglecting terms of $O(k^2\delta, k\delta^2)$.

The quasilinear treatment of the regions far from the resonant surface is rather straight-forward given the assumptions laid forth above. To attack the problem in the nonlinear region, we assume strong spatial variation and try to solve the complete nonlinear set of Eqs. (1-4) to lowest order in this variation. In addition, being guided by the numerical results, we assume nonlinear behavior to be rather mild and look for essentially helically symmetric solutions even in this region. Eqs. (1-4) now reduce to (assuming $\rho = \rho_0 = const.$)

$$(\psi'\dot f)^{\cdot} - (\dot\psi f')^{\cdot} = \frac{-k\rho_0}{m}(\dot\phi\phi')^{\cdot} \tag{7}$$

$$kr\rho_0\,\frac{\partial}{\partial x}\,\mathcal{P}\,\phi' - kr\,\mathcal{Y}\,\psi'' + m\,\mathcal{F}\,\psi' \tag{8}$$

$$\rho_0\,\frac{\partial}{\partial x}\,\mathcal{P}\phi' = \mathcal{Y}\,\psi'' \tag{9}$$

where

$$\mathcal{P} \equiv \underline{v}\cdot\nabla, \quad \mathcal{Y} \equiv \underline{B}\cdot\nabla, \quad \mathcal{F} \equiv \underline{J}\cdot\nabla$$

$x = r-r_s$, r_s is the resonance radius, the prime denotes differentiation with respect to x and the dot with respect to τ.

We can show now that separable solutions to the system of Eqs. (7-9) do exist and they are of the form

$$\psi(x,\tau) = \psi_x(x)\,\psi_T(\tau) \tag{10}$$

One can in turn derive nonlinear relations between the various fluxes. The details of these calculations will be given in a furture publication. The interesting aspect of the nonlinear behavior here is that it always seems to manifest itself in the form of a nonlinear equation studied by Abel.[6] For a very particular set of assumptions on the constants of separation involved, we can keep terms up to $O(\phi^6)$ to derive for the x-dependence of the flow

$$\int d\phi z_1^2 \left(c_0 - I(\phi)\right) \left[\phi + \left(c_0 - I(\phi)\right) \left(\frac{z_0 z_1}{(w_0)^{1/2}} - \frac{\hat{\gamma}}{2} \phi z_1^2\right)\right]^{-1} = \frac{x - x_0}{2} \tag{11}$$

where $I(\phi) \equiv \frac{4}{\hat{\gamma}} \int \frac{d\phi}{\phi z_1^2}$

and $Z_\nu = Z_\nu \left(\frac{1}{(\hat{\gamma} w_0)^{1/2}} \frac{1}{\phi}\right)$

is a cylinder Bessel function.

Matching a solution of the type of Eq. (11) to the quasilinear solution in the exturnal regions will in turn yield the properties of the helical ohmic state.

IV. CONCLUSION

A plan has been set forth for studying a helical resistive field reversed plasma state analytically. A quasilinear treatment is seen to be appropriate and tractable in the bulk of the plasma. A nonlinear theory is essential in understanding the phenomena in the resonant region.

ACKNOWLEDGEMENT

REFERENCES

1. See for example A. J. L. Verhage, A. S. Furzer, D. C. Robinson, Nucl. Fus. 18, 4 (1978).

2. D. D. Schnack, "Dynamical Determination of Ohmic States of a Cylindrical Pinch," paper...these proceedings.

3. R. A. Gerwin, private communication.

4. M. N. Rosenbluth, R. Y. Dagazian, and P. H. Rutherford, Phys. Fluids 16, 11 (1973).

5. J. L. Johnson, C. R. Oberman, R. W. Kulsrud, E. A. Frieman, MATT. Report No. PM-S-34 (1958).

6. Oeuvres Complètes de N. H. Abel, edited by L. Sylow and S. Lie.

MAGNETIC ISLANDS AND STOCHASTIC FIELD LINES IN THE RFP

by Ross L. Spencer
Los Alamos Scientific Laboratory
Los Alamos, New Mexico 87545

ABSTRACT

The effect of magnetic perturbations on RFP equilibria is considered. Using a Hamiltonian representation for the magnetic field lines, the formation of magnetic islands is discussed. The transition from magnetic islands to stochastic field lines is also discussed. As an example, the effect of the magnetic perturbations caused by pumping ports in ZT-40 is computed using a crude model for the pumping port fields.

I. INTRODUCTION

Good plasma equilibrium and low transport rates require the existence of well defined magnetic surfaces. It has been recognized for some time that magnetic field errors can introduce asymmetries that cause loss of equilibrium and enhanced transport rates.[1] If the field errors are of very small magnitude, they cause the appearance of small, isolated magnetic island chains; as the field errors become larger, portions of the error fields with different harmonic content can interact with the main fields and with each other to produce regions where the magnetic field lines wander randomly.[2-3] Such field lines are called stochastic field lines, and when they occur over a substantial part of the plasma, equilibrium may be lost, or at best, transport in the affected area will be enhanced.[4-5] In this paper these issues will briefly be discussed with reference to the reversed field pinch. An estimate of the field errors due to the pumping ports in the ZT-40 discharge chamber are used as an illustration of the effect field errors can have on a reversed field pinch.

II. MAGNETIC ISLANDS

A simple way to see what magnetic field errors can do to an equilibrium configuration is to use a Hamiltonian description of magnetic field lines. It is possible to make a correspondence between magnetic field lines and the phase space trajectories of a Hamiltonian system. In making this correspondence, it is convenient to use an action-angle description, i.e. the Hamiltonian is taken to depend on the action, J, the angle, α, and the time, t. The corresponding unperturbed magnetic equilibrium is described by the poloidal flux function, ψ, the Hamada poloidal angle θ_H, and the toroidal angle, ϕ. The correspondence between the two systems is made as follows.

$$\theta_H \sim t \tag{1}$$

$$\psi \sim J \tag{2}$$

$$\phi \sim \alpha \tag{3}$$

$$\chi = \int^{\psi} q(\psi')d\psi' \sim H \tag{4}$$

where q is the safety factor and where χ is the toroidal flux function. If the correspondence is made this way, then the condition

$$\frac{\partial}{\partial J}\frac{dJ}{dt} + \frac{\partial}{\partial \theta}\frac{d\theta}{dt} = 0 \tag{5}$$

is the analog of $\vec{\nabla} \cdot \vec{B} = 0$, and the invariance of $\oint dJ d\theta_H$ in time corresponds to flux conservation, $\oint \vec{B} \cdot d\vec{a} = const$. That the Hamiltonian system correctly describes the unperturbed magnetic field lines is seen by writing the Hamilton equations.

$$\frac{d\psi}{d\theta_H} = -\frac{\partial \chi}{\partial \phi} = 0 \tag{6}$$

$$\frac{d\phi}{d\theta_H} = \frac{\partial \chi}{\partial \psi} = q \tag{7}$$

i.e., the field lines remain on the $\psi = const$ surfaces and are described by

$$\phi = q\theta_H + const \tag{8}$$

The Hamada poloidal angle, θ_H, of course, is constructed so that Eq. (8) holds.

To see what effect a magnetic perturbation can have, the Hamiltonian is modified. A particularly simple modification that illustrates the principal effects is given by

$$H = \psi + \psi_1 \cos(m\theta_H - n\phi) \tag{9}$$

where ψ_1 is a constant. This perturbed Hamiltonian produces a helical perturbation field with direction normal to the equilibrium surfaces. Note that this perturbation field is not a self-consistent equilibrium perturbation;

130

indeed, the axisymmetry is broken so it may be that no equilibrium with such a magnetic perturbation exists.

Making a canonical transformation from the variables (ψ, θ_H) to the variables $(\psi, m\theta_H - n\phi)$ produces a new Hamiltonian that is independent of ϕ, allowing the magnetic field topology to be examined analytically. The main effect of adding the perturbation can easily be shown to be the production of a chain of magnetic islands at the resonant magnetic magnetic surface, i.e., at the surface where

$$q = m/n \tag{10}$$

It is also easy to show that the islands have a width given by

$$\Delta\psi = 4 \left(\frac{\psi_1}{dq/d\psi}\right)^{1/2} \tag{11}$$

For the simple case of circular flux surfaces, the width of the islands in radius (if the resonant surface is well away from $r=0$) can be shown to be given by

$$\Delta r = 4 \left(\frac{r \, \Delta B_r}{nB_\theta \, dq/dr}\right)^{1/2} \tag{12}$$

where ΔB_r is the magnitude of the radial helical magnetic field perturbation at the resonant surface. Two such island chains are shown in Fig. 1.

Note that the island width is proportional to the square root of the perturbation amplitude, so a small perturbation can make a large island. Note also that large shear helps to reduce the island width.

III. STOCHASTIC FIELD LINES

Stochastic field lines may be produced if two perturbations of different helicity are superposed, i.e. if the Hamiltonian is of the form

$$H = \psi + \psi_1 \cos(m_1\theta_H - n_1\phi) + \psi_2 \cos(m_2\theta_H - n_2\phi) \tag{13}$$

131

with $n_1/m_1 \neq n_2/m_2$.

Analytic methods are, at present, too weak to allow the trajectories of such a system to be found; the trajectories must be found by numerical integration. If ψ_1 and ψ_2 are small enough, two separate island chains are produced by the sum of the two perturbations, as shown in Fig. 1, but as ψ_1 and ψ_2 are increased, a threshold is reached beyond which further amplitude increases produce stochastic field lines. Figure 2 shows the result of perturbations of magnitude

$$\frac{\Delta B_1}{B} = \frac{\Delta B_2}{B} \simeq .01 \qquad (13)$$

Remnants of the island chains still are present, but the regions previously covered by the island separatrices and their neighboring field lines are now filled with stochastic field lines. Roughly speaking, the threshold for stochasticity is reached when the perturbation amplitudes are large enough that the islands they produce begin to overlap. As the threshold for stochasticity is reached, the separatrices are destroyed and small chains of islands with large toroidal and poloidal mode numbers appear; as the perturbation amplitudes increase, the stochastic region eats away at the field lines on either side of the separatrix. Since the transport properties of such a stochastic region are thought to be bad,[4-5] it is desirable to keep the magnetic field perturbations small if they have resonant toroidal and poloidal mode numbers. The above example shows that "small" may mean considerably less than 1% in relative magnitude.

IV. PUMPING PORT PERTURBATIONS: AN EXAMPLE

One source of magnetic field perturbations in an RFP is the various holes that are cut in the flux conserving shell for pumping and diagnostic access. As an example, consider the pumping ports on ZT-40. There are four of them evenly spaced around the outside of the torus with a ratio of the port radius to the minor radius of the shell of about 1:4. To approximate the magnetic field of such a port, the field of a hole in an infinite plane with a magnetic field parallel to the plane[6] is used to choose a magnetic dipole to represent the pumping port. An infinite array of these dipoles is placed alongside an infinitely long cylindrical RFP equilibrium to crudely represent the effect of the pumping ports on the discharge. The field of the infinite array of dipoles is Fourier analyzed in z and θ and a fairly large number of terms in the Fourier series are used to supply the perturbation fields for the numerical determination of the field lines. The results of such a calculation for a typical RFP profile are shown in Fig. 3. Note the fine structure of magnetic island chains and especially the relatively large islands near the outer edge of the plasma. The islands do not yet appear to overlap and cause stochasticity, but a larger perturbation might.

This computation, though crude, suggests that pumping ports as large as those of ZT-40 may cause loss of plasma quality near the edge. Further studies are in progress to more accurately determine the pumping port fields and to

determine the feasibility of plugging the ports. Future studies will examine other sources of magnetic field perturbations and their possible effects on the behavior of RFP discharges.

REFERENCES

1. D. W. Kerst, J. Plasma Phys. 4, 253 (1962).

2. M. N. Rosenbluth, R. Z. Sagdeev, J. B. Taylor, and G. M. Zaslavski, Nucl. Fusion 6, 297 (1966).

3. G. H. Walker and J. Ford, Phys. Rev. 188, 416 (1969).

4. T. H. Stix, Phys. Rev. Lett. 30, 833 (1973).

5. A. B. Rechester and M. N. Rosenbluth, Phys. Rev. Lett. 40, 38 (1978).

6. J. D. Jackson, Classical Electrodynamics, Second Edition, (John Wiley and Sons, New York, NY) Chapter 5.
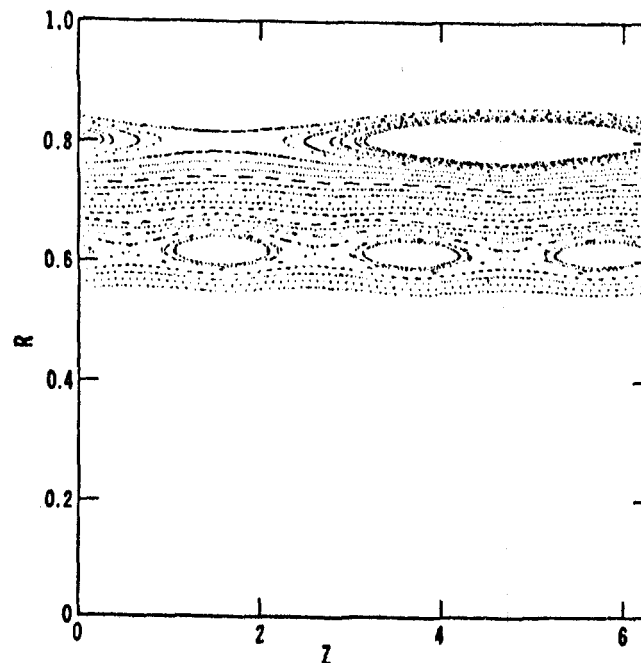
Fig. 1.
The effect of two magnetic field perturbations of form $\Delta B_1 \cos(kz)$ and $\Delta B_2 \cos(\theta - 3kz)$ with $k = 1$ on a cylindrical reversed field equilibrium is shown. The points represent the intersection of field lines with a section of the $\theta = 0$ plane of an infinitely long cylinder. $\Delta B_1/B = \Delta B_2/B = .001$. The unperturbed fields have a field reversal surface at $r = .8$ and a $q = 1/3$ surface at $r = .6$.
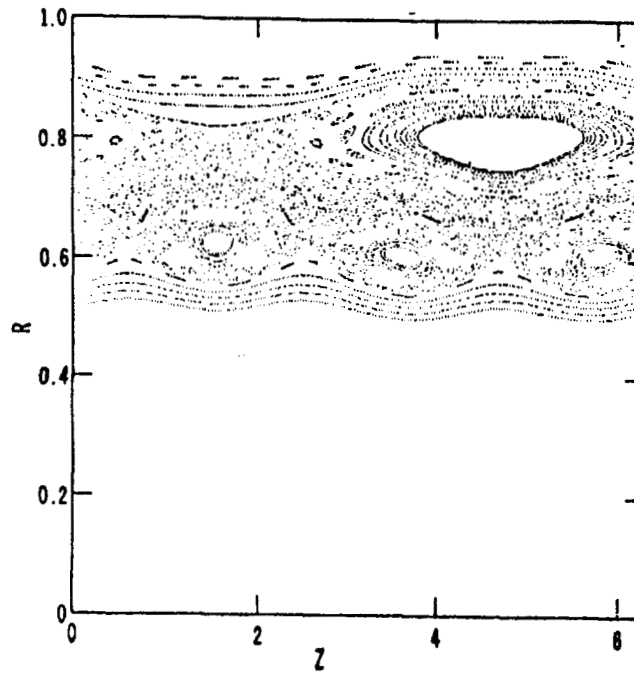
Fig. 2.

The effect of increasing the field perturbations of Fig. 1 to $\Delta B_1 = \Delta B_2 = .01$ is shown.
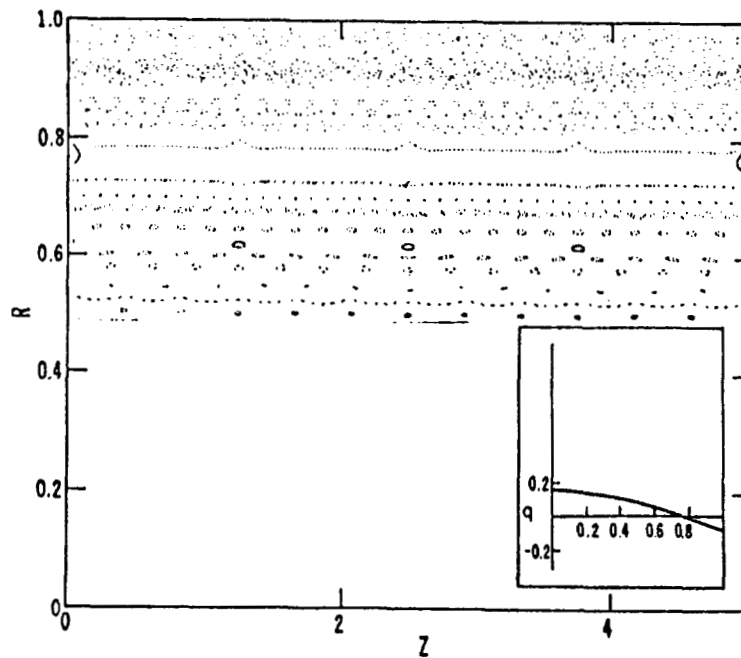
Fig. 3.

The magnetic field lines in a section of an infinitely long cylindrical RFP with dipoles approximating pump ports along the side is shown. The section shown corresponds to ZT-40. The inset shows the q profile. The r and z axes are in the same units, i.e., the aspect ratio is 5.

134

FORCE-FREE EQUILIBRIA IN CYLINDRICAL GEOMETRY

Z. G. An, A. Bondeson, H. H. Chen, Y. C. Lee, C. S. Liu, and E. Ott
Department of Physics and Astronomy
University of Maryland
College Park, Maryland 20742

A stable equilibrium for a plasma must correspond to a minimum value of the energy, subject to all constraints restricting the evolution of the discharge. For a low-beta plasma with small but finite resistivity, the stable equilibria can be found by minimizing the magnetic energy, $\int B^2 \, dV$, while keeping the helicity, $K = \int A \cdot B \, dV$ constant.[1] This leads to the so-called force-free states, for which

$$j = \nabla \times B = \lambda B \qquad (1)$$

and for which the energy is given by $W = \lambda K$ (in a simply connected geometry). Using the readily available force-free states in spherical geometry, Rosenbluth and Bussac[2] showed that a near-spherical plasma is stable to internal tilting, when the equilibrium is slightly oblate, whereas a prolate configuration is unstable.

We report here on an investigation of the minimum energy states in a cylindrical plasma, characterized by the aspect ratio L/R, where R and L are the radius and length of the plasma column. The cylindrical problem differs in one essential aspect from the spherical one, viz. the separable solutions of the force-free Eq. (1) cannot be made to match the boundary condition $B \cdot n = 0$ term by term, except for the axisymmetric solutions. Hence, analytical efforts to construct non-axisymmetric force-free states have failed sofar, and we have had to resort to numerical techniques.

We present the main idea behind our approach for a general geometry, although its successful application may be limited to rather simple cases, such as cylindrical and rectangular. We assume that the magnetic field and the vector potential can be expanded as a sum of normal modes

$$A = \sum_i a_i A_i \; , \qquad B = \sum_i a_i B_i \; , \qquad B_i = \nabla \times A_i \qquad (2)$$

which is <u>complete</u> for B (divergence-free and with zero normal component on the boundary). Clearly, the expansion for A need not be complete, because of the freedom implied by gauge transformations. To minimize W with K constant we introduce a Lagrange multiplier λ and look for the stationary points of

$$\int (B^2 - \lambda A \cdot B) dV = \sum_i \sum_j a_i a_j (\langle B_i \cdot B_j \rangle - \lambda \langle A_i \cdot B_j \rangle) \; . \qquad (3)$$

Taking the variation with respect to the coefficient a_i we get the following hermitian, infinite matrix equation

$$\sum_j a_j [2\langle B_i \cdot B_j \rangle - \lambda (\langle A_i \cdot B_j \rangle + \langle A_j \cdot B_i \rangle)] = 0 \qquad (4)$$

which can be solved numerically for the lowest eigenvalues, since the matrix $\langle B_i \cdot B_j \rangle$ must be invertible. Invoking the completeness of the basis for B one easily proves that any stationary point of Eq. (3) has $A = B/\lambda + \nabla \phi$ which implies Eq. (1), i.e., forcefreeness.

In cylindrical geometry, we can use the conventional TE-TM-mode expansion, which can be shown to be complete. Thus, we take

$$A = -\hat{z}\Psi + \hat{z} \times \nabla\Phi \ , \ B = \nabla \times A \tag{5}$$

where Ψ and Φ are expressed in terms of solutions of Helmholtz' equation:

$$\Psi = \sum_{jn\ell} J_n(\alpha_{nj}\frac{r}{R})[a_{jn\ell}\cos n\phi + \bar{a}_{jn\ell}\sin n\phi] \ \cos\frac{\ell\pi}{L}z$$

$$\Phi = \sum_{jn\ell} J_n(\beta_{nj}\frac{r}{R})[b_{jn\ell}\cos n\phi + \bar{b}_{jn\ell}\sin n\phi] \ \sin\frac{\ell\pi}{L}z \tag{6}$$

where α_{nj} and β_{nj} are the $j-$th zeroes of J_n and J'_n, respectively.

One easily finds that $<B_i \cdot B_j>$ is diagonal and $<A_i \cdot B_j>$ completely off-diagonal with

$$\int B^2 \, dV = \frac{\pi L}{4} \sum_{jn\ell} (a^2_{jn\ell} + \bar{a}^2_{jn\ell})(1 + \delta_{\ell,1})\alpha^2_{nj}J^2_{n+1}(\alpha_{nj})$$

$$\tag{7a}$$

$$+ \frac{\pi L}{4} \sum_{jn\ell} (b^2_{jn\ell} + \bar{b}^2_{jn\ell})[(\frac{\beta_{nj}}{R})^2 + (\frac{\ell\pi}{L})^2](\beta^2_{nj} - n^2)J^2_n(\beta_{nj}) \ ,$$

$$\int A \cdot B \, dV = 4L \sum_{jn\ell}\sum_{j'\ell'} [b_{jn\ell}a_{j'n\ell'} + \bar{b}_{jn\ell}\bar{a}_{j'n\ell'}]$$

$$\ell-\ell' \text{ odd}$$

$$\times \frac{\ell}{\ell^2 - \ell'^2}\frac{\beta^2_{nj}\alpha_{nj'}}{\alpha^2_{nj'} - \beta^2_{nj}} J_n(\beta_{nj})J_{n+1}(\alpha_{nj'}) \tag{7b}$$

$$+ 4\pi \sum_{jn\ell}\sum_{j'\ell'} b_{jn\ell}\bar{b}_{j'n\ell'}\frac{n\ell\ell'}{\ell'^2 - \ell^2} J_n(\beta_{nj})J_n(\beta_{nj}')$$

$$\ell-\ell' \text{ odd}$$

where, in the case $n = 0$, $a^2 + \bar{a}^2$ stands for $2a^2$, etc. Since $<B_i \cdot B_j>$ is diagonal, the truncated Eq. (4) is easily solved for the smallest λ by a standard iteration procedure. Higher eigenvalues can be found by means of the Gram-Schmidt orthogonalization process. If higher states are not required, the TM coefficients $(a,\bar{a})$ can be eliminated from Eq. (4) yielding a numerical scheme which is considerably more effective and requires less storage.

The main numerical result for the cylinder case is that the first axisymmetric state has the lowest energy as long as $L/R \lesssim 1.668$. When $L/R \gtrsim 1.668$, the first $n = 1$ state has lower energy and the axisymmetric equilibrium should be unstable to $n = 1$ perturbations. This instability has been observed in numerical MHD calculations[3], with a threshold value for L/R at about 1.68, in excellent agreement with the eigenvalue calculation. The tilting instability observed in the spheromak experiment at the University of Maryland[4] is also explained; the L/R value is here rather large (~ 3-5) although the boundary condition at the ends $z = 0,L$ is clearly more complicated than $B_z = 0$.

Finally, we briefly discuss some properties of the force-free states

$$\nabla \times B_i^F = \lambda_i B_i^F \tag{8a}$$

or

$$\nabla \times A_i^F = \frac{1}{\lambda_i} \nabla \times (\nabla \times A_i^F). \tag{8b}$$

Since $B \cdot \hat{n} = 0$, the vector potential can always be chosen to be normal at the boundaries of a simply connected volume. Therefore, Eq. (8b) is hermitian, implying that B_i^F and B_j^F are orthogonal if $\lambda_i \neq \lambda_j$. In the case of degenerate eigenvalues, we see from the truncated Eq. (4) (which can be written as an eigenvalue equation for a real symmetric matrix) that to a p times degenerate

eigenvalue correspond p mutually orthogonal eigenstates. Hence, the mapping of a finite subset of the TE-TM basis onto the approximate force-free states is invertible. We expect this to hold also for the complete TE-TM basis, which indicates that the force-free eigenvalues indeed form a complete orthogonal set, as opposed to the proposition in Ref. 5. We point out that the existence of this set may prove useful in, e.g., MHD stability calculations, even if the exact form of the eigenfunctions can only be found by numerical methods.

REFERENCES

1. J. B. Taylor, in Pulsed High Beta Plasmas, Pergamon, Oxford (1976). p. 59.

2. M. N. Rosenbluth and M. N. Bussac, Nucl. Fusion 19, 489 (1979).

3. G. Marklin, in Proceedings of the RFP Workshop (1980).

4. G. Goldenbaum, in Proceedings of the RFP Workshop (1980).

5. G. Vahala, Phys. Fluids 23, 418 (1980).

STABILITY OF A FORCE-FREE CYLINDRICAL SPHEROMAK

G. J. Marklin and C. S. Liu
Department of Physics and Astronomy
University of Maryland
College Park, Maryland 20742

The Taylor-Woltjer variational principle[1] predicts that a turbulent plasma will decay to a state of minimum energy satisfying the force-free equation

$$\nabla \times \vec{B} = \lambda B \quad , \tag{1}$$

with the energy of the state proportional to the eigenvalue λ.

The axisymmetric (n=0) solution to Eq. (1) in a conducting cylinder of length L and radius R is

$$B_r = k \, J_1(\alpha r) \, \sin(kz) \, ,$$
$$B_\phi = \lambda_0 J_1(\alpha r) \, \cos(kz) \, , \tag{2}$$
$$B_z = \lambda \, J_0(\alpha r) \, \cos(kz) \, ,$$

where $\alpha R = j_{1,1}$ (the first zero of J_1), $kL = \pi$ and $\lambda_0 = (\alpha^2 + k^2)^{1/2}$.

A plasma in this equilibrium will be stable to all Ideal MHD modes unless there are non-axisymmetric (n≠0) states with a lower energy, but analytic n≠1 solutions to Eq. (1) in cylindrical coordinates have not been found and a numerical stability analysis is required.

Using a δW formalism, Rosenbluth and Bussac[2] have analyzed the stability of the n=0 force-free equilibrium in a sphere where the n≠0 solutions to Eq. (1) are well known. They found that with a conducting wall boundary, all modes were stable except an n=1 tilt which was marginal, becoming unstable if the sphere is given a prolate deformation. The n=1 tilting instability should be the most important in a cylinder as well and it has been observed on the PS-1[3] which has an equilibrium resembling the one given by Eq. (2).

The stability of the n=0 equilibrium is analyzed by making an n=1 velocity perturbation and numerically integrating the linearized Ideal MHD equations

$$\frac{\partial \vec{V}_1}{\partial t} = \vec{J}_1 \times \vec{B}_0 + \vec{J}_0 \times \vec{B}_1 \ ,$$

$$\frac{\partial \vec{B}_1}{\partial t} = \nabla \times (\vec{V}_1 \times \vec{B}_0)$$

(3)

using a 2-D Eulerian leap-frog scheme. The fastest exponentially growing mode eventually dominates and its growth rate is calculated. This growth rate is normalized to the Alfvén transit time $\iota_A = R/V_{A0}$ (V_{A0} is the Alfvén speed at the center of the cylinder) and is plotted in Fig. 1 for different values of the elongation L/R.
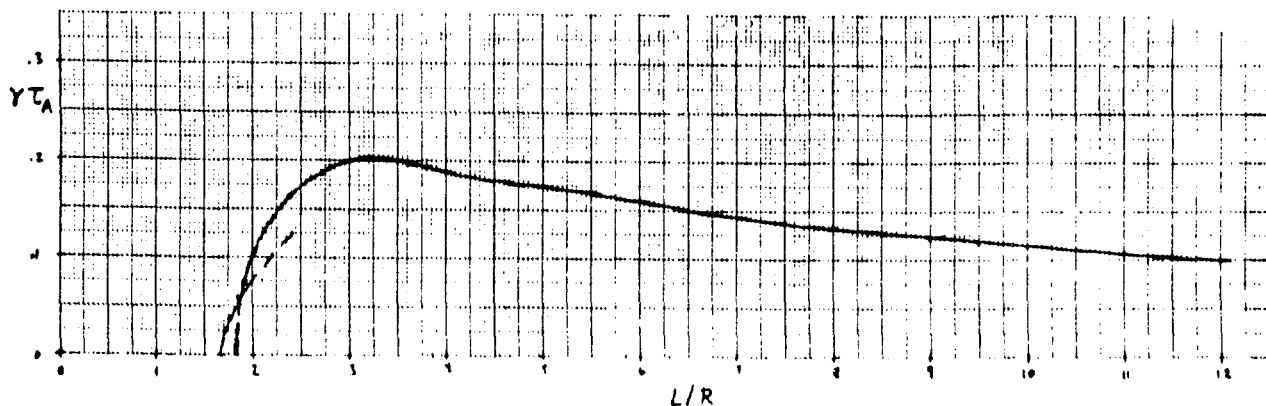
Fig. 1. Normalized growth rate $\gamma\tau_A$ plotted as a function of elongation L/R.

The plasma first becomes unstable when L/R exceeds the threshold value

1.68 ± .03. This is the point where the energy of the n=1 tilted state

becomes lower than that of the n=0 equilibrium. The eigenfunction for this

mode shows the plasma tilting from the n=0 to the n=1 configuration.

In an independent numerical calculation of the solutions to Eq. (1),

An et al.[4] found the crossover in energy between the n=0 and n=1 states

occurring at the critical value L/R = 1.668, in excellent agreement with the

threshold found above.

The fact that this threshold must agree with the crossover of the n=0

and n=1 energies (eigenvalues) can be seen by looking at Eq. (3) at marginal

stability where $\partial \vec{V}_1/\partial t = 0 = \vec{J}_1 \times \vec{B}_0 + \vec{J}_0 \times \vec{B}_1$ and using $\vec{J}_0 = \lambda_0 \vec{B}_0$ to reduce

it to $(\vec{J}_1 - \lambda_0 \vec{B}_1) \times \vec{B}_0 = 0$. This has the solution

$$\vec{J}_1 - \lambda_0 \vec{B}_1 = \lambda_1 \vec{B}_0 , \tag{4}$$

where λ_1 is in general some scaler function of position which has the same

$\exp(i\phi)$ angular dependence as $\vec{J}_1$ and $\vec{B}_1$. Taking the divergence of Eq. (4),

one finds an equation for λ_1:

$$\vec{B}_0 \times \nabla \lambda_1 = 0 . \tag{5}$$

Equation (5) only permits λ_1 to be non-zero on a rational surface where

q=m (m=0, ±1, ±2,...). At L/R=1.68 however, the q value is .95 on the magnetic

axis and it decreases monatonically to .60 on the z-axis and at the wall.

Since there is no rational surface λ_1 must be zero and Eq. (4) reduces to

$$\vec{J}_1 = \nabla \times \vec{B}_1 = \lambda_0 \vec{B}_1 \tag{6}$$

142

Equation (6) says that $\vec{B}_1$ is an $n=1$ solution to Eq. (1) with eigenvalue λ_0. Hence at this value of L/R where the system is marginally stable λ_0, which was defined as the eigenvalue of the $n=0$ force-free state, is also the eigenvalue of the $n=1$ force-free state.

At L/R=1.80, there is another threshold where a second mode appears. At this value of L/R, the q value is increased to 1 on the magnetic axis and Eq. (5) can have a solution with a non-zero λ_1; λ_1 will in fact be a delta function on the rational surface and Eq. (4) will look like

$$\vec{J}_1 = \lambda_0 \vec{B}_1 + \delta[q(\psi) - 1] \exp(i\theta) \vec{B}_0 ,$$

where ψ and θ are the usual flux coordinates. The perturbed magnetic field for this mode is similar to the tilting modes' but the displacement is localized **outside** the rational surface where q<1. This is an "inverted" analog of the kink mode in a tokamak which has its displacement localized <u>inside</u> the rational surface where q<1.

As L/R is increased to 3.1, the q=1 surface moves out to the wall and the displacement is no longer localized. The growth rate is maximum at this point.

For very large L/R the growth rate drops off slightly and the eigen-functions take on a periodic structure in the z-direction.

References

[1] J. B. Taylor, Phys. Rev. Lett. <u>33</u>, 1139 (1974).

[2] M. N. Rosenbluth and M. N. Bussac, Nuclear Fusion <u>19</u>, 489 (1979).

[3] G. C. Goldenbaum, this proceeding.

[4] Z. G. An et al., this proceeding.

Studies of the Formation of Field Reversed Plasma
by a Magnetized Co-Axial Plasma Gun

W. C. Turner, E. H. A. Granneman*, C. W. Hartman,
D. S. Prono, J. Taska

Lawrence Livermore National Laboratory
Livermore, CA 94550

A. C. Smith, Jr.

Pacific Gas and Electric Company
San Francisco, CA 94106

We have continued our experiments on co-axial gun production of field reversed plasma [1]. The emphasis of experiments reported here was to attempt formation of an isolated, reconnected, field reversed plasma by axial translation from the gun.

A schematic of the experimental set-up is shown in Figure 1. The gun injects axially into a drift tank followed by a magnetic mirror. For the experiments reported here, only the guide coils outside the vacuum vessel and solenoids on the plasma gun electrodes were used; the mirror coil was not energized. A stainless steel flux conserver is placed in the mirror throat to prevent the plasma from contacting the nonconducting vacuum wall in the region of the mirror. An axis encircling array of magnetic loop probes includes four diamagnetic loops and a loop which measures the azimuthally averaged outward pointing radial component of magnetic field. These loop probes are stainless steel jacketed and form a flux conserving boundary (at a radius = 30 cm) for plasma emitted from the gun. A five tip probe that can be positioned anywhere along the axis of the experiment is used to measure internal components of magnetic field. Each probe tip contains two small coils; one to measure the axial (poloidal) component of magnetic field and another to measure the component out of the plane of Figure 1 (toroidal component).

The basic idea behind magnetized coaxial gun formation of field reversed plasma [2] is to add solenoid coils to the inner and outer electrodes of an ordinary co-axial gun. Together with the externally applied guide magnetic field, these solenoids form a magnetic cusp at the gun muzzle. Plasma reaching the gun muzzle carries the flux of the inner electrode with it, thus reversing the magnetic field downstream of the cusp. Then one of the two situations shown in Figure 2 can occur. In the first situation the elongated field lines reconnect and an isolated field reversed toroidal plasma is formed. In the second case, the plasma cools by thermal conduction back to the gun electrodes, and the elongated field lines diffuse back into the gun before they can reconnect. Figure 3 shows schematically the behavior of some magnetic probe signals for each of these situations. For axially displaced diamagnetic loops formation of closed

*On leave from FOM-Institute for Atomic and Molecular Physics,
 Amsterdam, The Netherlands

field lines should appear as a propagating pulse. If the field lines remain open and diffuse back to the gun, then the loop furthest from the gun should have the shortest duration and its signal should be the first to disappear. The probe measuring the outward component of radial magnetic field should also show distinctive behavior. If a closed field line plasma is formed then the radial field should have first one sign and then the other. If field lines contract back to the gun then one should observe a signal with the same polarity as the emerging plasma front returning to the gun late in time.

Figures 4 to 7 show some magnetic signals of gun produced plasma. With the five tip probe positioned 68 cm from the gun the spatial profiles of B_z (poloidal) and B_x (toroidal) in Figure 4 have been obtained. For this particular shot the guide magnetic field was 2.2 kG and the axial magnetic field at the center of the plasma is -9 kG. The radius of zero axial field is $R_0 \simeq 10$ cm. Integrating the B_z flux out to R_0 yields an estimated poloidal flux $\psi_{pol.} = 1.5 - 2.0 \times 10^3$ kG - cm^2, about equal to the net flux in the inner electrode of the gun, $\psi_{gun} = 1.6 \times 10^3$ kG - cm^2. The toroidal component of magnetic field exhibits the expected odd symmetry about y = 0 and reaches a maximum value 7.5 kG at 5 to 10 cm off the symmetry axis. Assuming cylindrical symmetry the toroidal current per unit axial length (1 MA/meter) and the total poloidal current (330 kA) have been estimated from the magnetic field profiles. The poloidal current is about one-half the gun discharge current at the time plasma begins to leave the gun. The axial propagation distance of the field reversed plasma shown in Figure 4 has been determined by retracting the five-tip probe on successive shots.

Figure 5 shows the behavior of ΔB_z detected by the center tip of the five tip probe for three conditions. For the first two cases the inner electrode flux was fixed at $\psi_{gun} = 1.8 \times 10^3$ kG - cm^2 and the probe moved from 67 cm to 117 cm from the gun muzzle. As the probe is retracted, the duration of ΔB_z signal decreases from 20 µsec to 3 µsec, and the peak amplitude decreases from 20 kG to 13 kG. For the third case, the probe position was left at 117 cm and the inner electrode flux decreased to $\psi_{gun} = .8 \times 10^3$ kG - cm^2. As a result the peak amplitude $|\Delta B_z| = 20$ kG is regained and the signal duration exceeds 20 µsec again. The plasma behavior on these three shots strongly suggests that the poloidal field lines are not breaking free from the gun. Further evidence of this is indicated in Figures 6 and 7. Figure 6 shows an example of the diamagnetic loop signals 51 cm, 68 cm, 119 cm and 136 cm from the gun. For this shot the total electrical energy delivered to the gun was 180 kJ, the guide field was 3.3 kG and the inner electrode flux $\psi_{gun} = 1.8 \times 10^3$ kG - cm^2. The signals show the behavior sketched in Figure 3 when the poloidal field lines do not reconnect. Figure 7 shows the behavior of the radial component of magnetic field at R = 30 cm, z = 58 cm from the gun for three successive shots. For these shots the guide field was fixed at 3.3 kG the electrical energy input to the gun was 140 kJ and the inner electrode flux was varied, $\psi_{gun} = 1.46 \times 10^3$, 1.88×10^3 and 2.13×10^3 kG - cm^2. As the inner electrode flux was increased, a delayed negative signal indicative of

the plasma front returning to the gun occurred earlier in time. It does not appear in the first of these shots because it occurred after the recording time interval shown in Figure 7. Again this is the behavior sketched in Figure 3 that is expected to occur if the soloidal field lines do not reconnect.

The signals in Figures 4 to 7 are a small subset of our data. In general we have found that propagation distance of field reversed plasma increases with (1) increasing gun bank discharge energy (up to 200 kJ), (2) decreasing inner electrode flux, and (3) decreasing guide field. This is expected from the energetics of poloidal field lines stretching but not breaking free from the gun. In a uniform guide field the plasma translational energy was in all cases insufficient to compress the plasma when it reached the funnel shaped flux conserver at the mirror throat. If the field reversed plasma reached the funnel entrance (170 cm from the gun) it stagnated there and did not propagate into the mirror region. Introducing a negative gradient in guide field $dB/dz \simeq - 0.7$ kG/m at the funnel was sufficient to force field reversed plasma through the funnel ($z = 288$ cm from the gun). In all cases the field reversed plasma would propagate out from the gun in a few μsec and then return to the gun on a much slower time scale of the order 30 μsec. The time behavior of the diagmagnetic loop data plus recent HeNe interferometry at the exit of the gun suggest that slow plasma at the gun muzzle is inhibiting reconnection.

The magnitude of field reversed poloidal flux produced by the gun, the radial size of plasma and the ease with which reproducible plasmas with good symmetry and spatial coherence can be generated are all encouraging for our eventual goal of providing a field reversed target plasma for neutral beam injection. However, in order to obtain adequate lifetime the poloidal field lines must be made to reconnect to avoid excessive thermal conduction back to the gun electrodes. Methods for accomplishing reconnection must inhibit slow plasma from filling the region between the gun and downstream field reversed plasma. At present three methods seem worthy of investigation; (1) a pulsed pinching coil at the gun muzzle, (2) a passive slow plasma diverter near the gun muzzle and (3) reduction of the gas input to the gun substantially below the 50 atm - cm^3 for the experiments reported here. Some successes have been obtained for the first two methods with a mhd plasma simulation code (J. Eddleman and J. Shearer, private communication). The third method has been shown to work experimentally (see paper by T. Jarboe, et al., at this workshop).

References

(1)   W. Turner, C. W. Hartman, J. W. Shearer, J. Taska, Bull. Am. Phys. Soc., 24, 1083 (1979).

(2)   H. Alfven, L. Lindberg, P. Mitlid, J. Nucl. Energy, 1, 116 (1960).
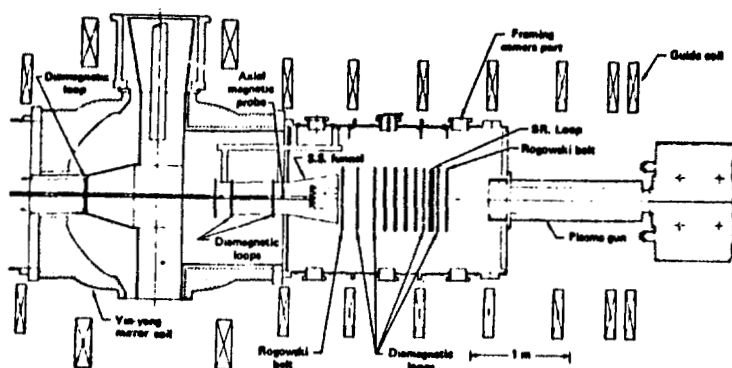
Fig. 1
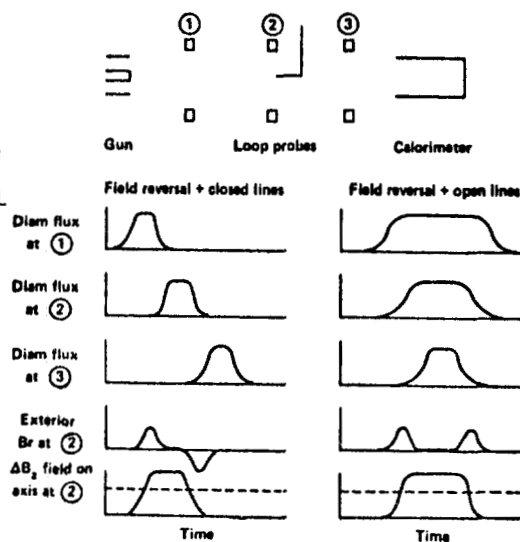
Fig. 3

FIELD REVERSAL SCENARIOS WITH AND WITHOUT
FORMATION OF CLOSED FIELD LINES
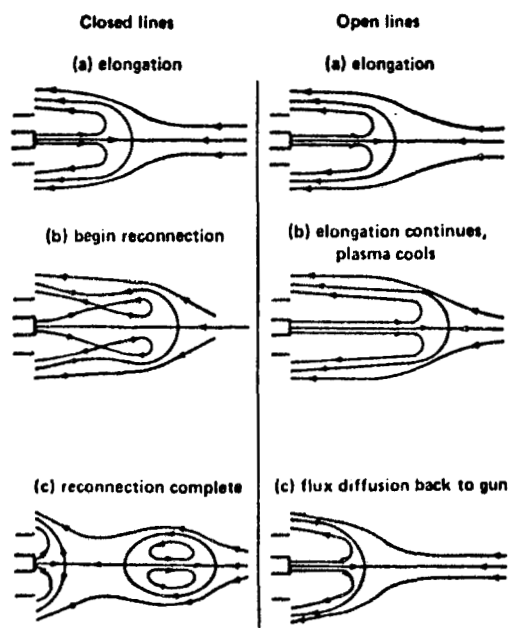
Fig. 2

MAGNETIC FIELD PROFILES AND DERIVED PLASMA CURRENTS
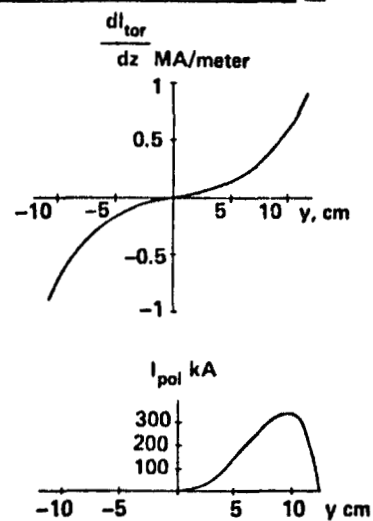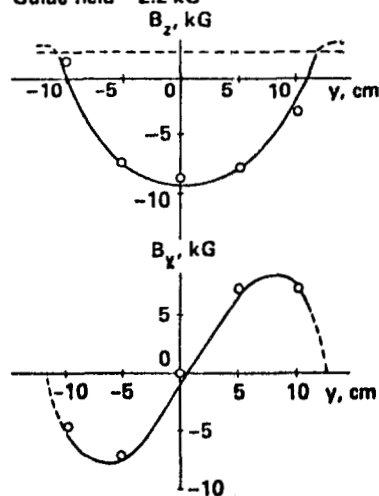
Fig. 4

AXIAL MAGNETIC FIELD STRENGTH

Guide Field $B_0 = 3.3$ kG
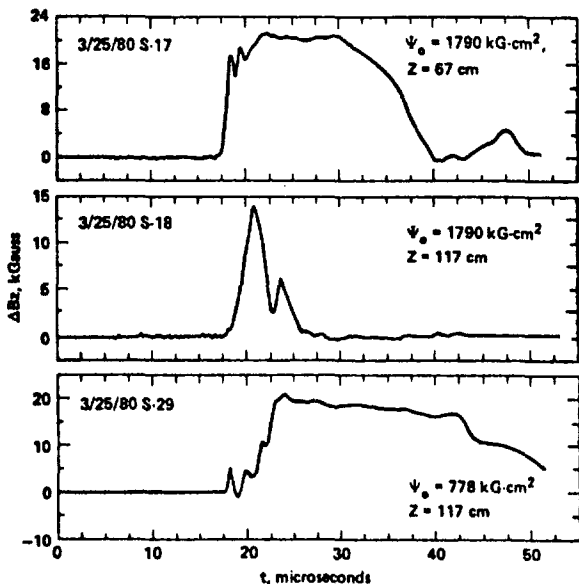
Fig. 5

DIAMAGNETIC LOOP SIGNALS AT FOUR AXIAL POSITIONS FROM THE PLASMA GUN MUZZLE

Guide field = 3.34 kG   3/27/80 S-9
$\Psi_0 = 1780$ kG-cm^2
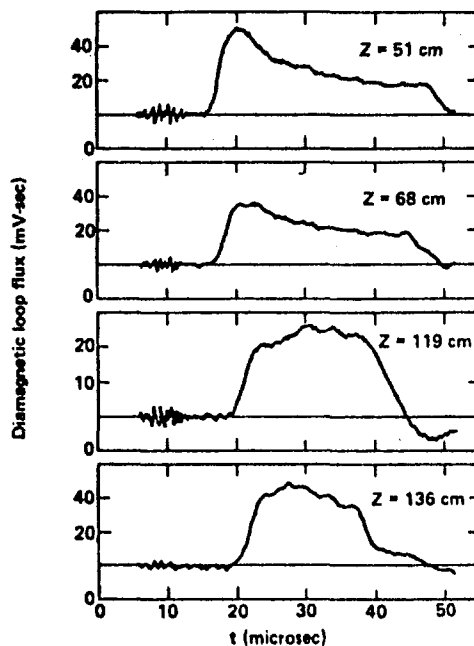
Fig. 6

RADIAL COMPONENT OF MAGNETIC FIELD MEASURED AT R = 30 cm

Fig. 7

148
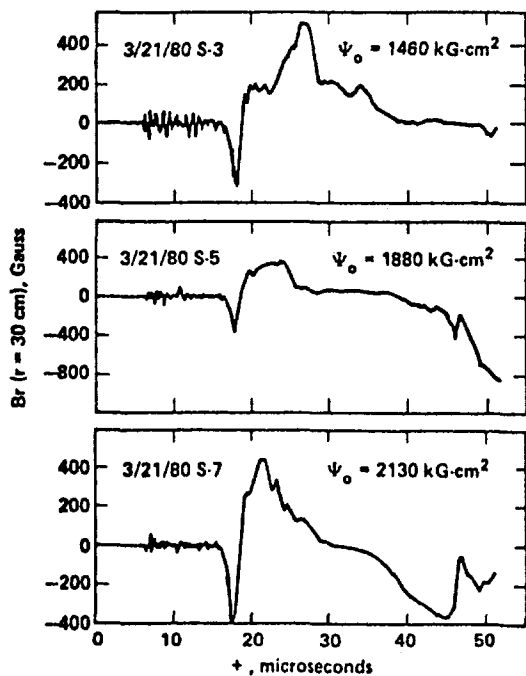
GUN-GENERATED COMPACT TORI AT LOS ALAMOS*

T. R. Jarboe, I. Henins, H. W. Hoida, R. K. Linford,
J. Marshall, D. A. Platts, A. R. Sherwood
Los Alamos Scientific Laboratory, Los Alamos, New Mexico 87545

ABSTRACT

We have generated compact toroids which can be made to come to rest in a cylindrical resistive flux conserver. They are observed to rotate so that their major axis is perpendicular to the axis of the flux conserver. Subsequently they appear to remain stationary and decay with a time constant of about 100 μs. We have also generated compact toroids in an oblate geometry which remain aligned with the axis of the flux conserver and decay with a time constant of 150 μs. The magnetic field reconnection time for compact toroid formation is measured in the latter case to be much shorter than the decay time.

A compact toroid is a toroidal magnetic plasma containment geometry, in which no conductors or vacuum chamber walls pass through the hole in the torus. This latter property could ease the constraints upon the construction and maintenance of a reactor. For example, it would allow the reacting plasma to be translated. A compact toroid could contain both poloidal and toroidal field components. Compact toroids created without the use of toroidal field have been observed in experiments.[1-2] This paper reports the production of compact toroids with toroidal field utilizing in part a technique pioneered by Alfven et al,[3] but extended by us to a higher temperature fully ionized plasma regime. In the present experiment a solenoidal coil is placed inside the inner electrode of a coaxial plasma gun. This coil produces axial magnetic field inside the inner electrode which diverges and becomes a largely radial field in front of the gun muzzle. When the gun is fired, the emerging plasma stretches the radial field lines in the axial direction away from the gun. These elongated field lines reconnect behind the plasma forming the closed poloidal field of the compact toroid, while the magnetic field generated by the gun current becomes the embedded toroidal field. The major axis of the compact toroid will then coincide with the axis of the coaxial gun.

The length of the coaxial gun used in our experiments is 0.70 m, and its inner and outer electrodes have radii of 0.10 m and 0.15 m respectively. For the results reported here, the total D_2 gas puffed into the gun with a fast valve is 0.75 cm^3 atm. About 150 μs after the gas is puffed, the gun is energized with a 37-μF capacitor bank charged to 45 kV. About 2 μs after the initiation of the discharge the current peaks with a value of 0.8 MA, and it reverses in about 4.5 μs. The gun current has fallen to about one-third of its peak value at 3.5 μs when the plasma current sheath reaches the gun muzzle. The gun absorbs almost all of the initial energy in the capacitor bank during the first 2.5 μs of the discharge. The addition of a magnetic

---

149

"bias" field between the gun electrodes parallel to the axis of the gun allows it to be operated with much smaller gas loads and makes the gun discharges more reproducible.

Using this magnetized plasma gun we have produced compact toroids in two different flux conservers. The first is a stainless steel cylinder which is 0.46 cm in diameter, 1.2 m long, and 1.6 mm thick. Both ends are open. This cylinder is aligned to be coaxial with the plasma gun, and it is placed 0.13 m from the muzzle. To make measurements in this flux conserver we have employed as diagnostics: magnetic probes, spectroscopic observation of CV radiation, and an infrared interferometer. When the plasma emerges from the gun muzzle, the magnetic probes sense a disturbance which propagates at a velocity of about 10^6 m/s into the resistive flux conserving shell. For low values of initial axial flux inside the inner electrode of the gun the plasma pushes the plasma-magnetic field configuration completely through the shell and out the other end, whereas for high flux values the configuration barely leaves the gun. For an intermediate value of 0.015 Wb, which was used for the data reported here, the disturbance propagates into the flux conserver and essentially stops; then, within the accuracy of our measurements, reconnection occurs and the configuration remains with little or no axial motion. The compact toroids generated in this flux conserver are observed to rotate so that the axis of the compact toroid is perpendicular to the axis of the flux conserver.[4] See Fig. 1. This tipping has been predicted from a δW calculation which shows that prolate compact toroids are unstable to tipping.[5] After rotation the compact toroid assumes a racetrack shape which is oblate-like. Figure 2 shows the magnetic field on axis and also on a diameter at the midplane of the flux conserver. These data are consistent with a rotated compact toroid where the quantities labeled B_z and B_r are two components of the toroidal field and B_θ is the poloidal field. The poloidal flux can be estimated from these data to be two-thirds of that which was put on the gun initially. Flux loops placed on the outside surface of the flux conserver show that the motion of the compact toroid remains the same when the internal probes are removed. However, the magnetic field decay time increases from 40 µs to 100 µs.

Using a double-pass 3.4-µm HeNe interferometer we have determined that the average density on a diameter at the midplane of the flux conserver is about $10^{14}/cm^3$. The time history of the density is similar to that of the magnetic fields. We observe the existence of CV radiation for over 150 µs if all probes are removed, which implies that there are electron temperatures of over 70 eV throughout much of the compact toroid's life.

We have produced compact toroids when an initial axial magnetic "guide" field was established within the cylindrical stainless steel flux conserver. In the presence of this field the compact toroid was still observed to rotate as described above. However, the characteristic decay time of the magnetic field configuration was only 10-15 µs, i.e., much shorter than comparable conditions without the guide field. We speculate that the rapid destruction in the guide field case is due to reconnection of magnetic field lines in the high shear regions which occur after the toroid rotates, opening previously closed field lines.

In an attempt to stabilize the tipping of compact toroids produced by the magnetized gun, we have generated compact toroids in a second flux conserver having an oblate region incorporated in its geometry. This flux conserver is

150
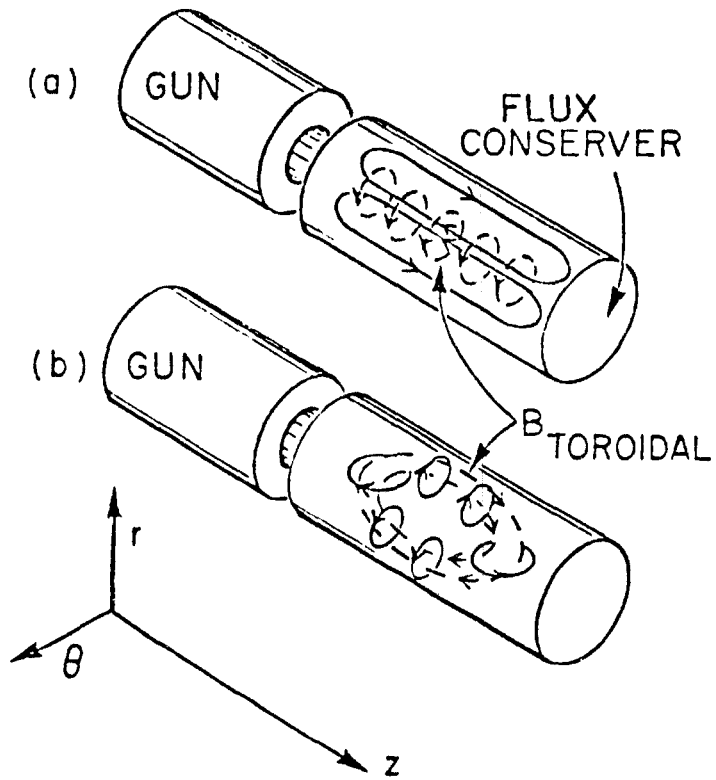
Fig. 1.
Schematic of the compact toroid's positions before and after its major axis rotates 90°.
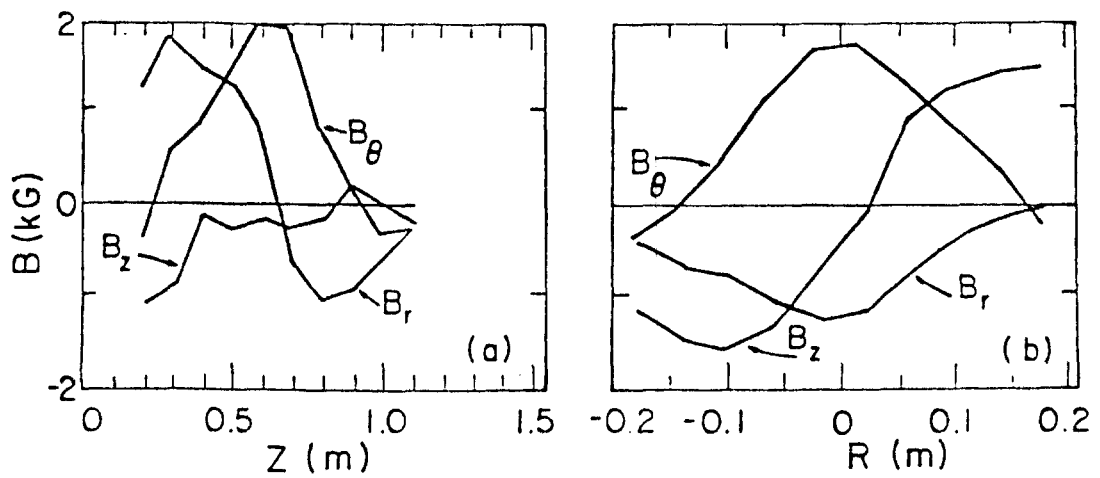
Fig. 2.
Magnetic field profiles on the axis and across the midplane of the prolate flux conserver at 25 μs after the gun is fired.

made of 0.8-mm-thick copper, and a cross section of it is shown in Fig. 3.
The plasma from the magnetized gun is injected from the left through the
0.34-m-diameter entrance cylinder into the confining region. With this
geometry the tipping no longer occurs and the configuration is stable
throughout its life time. We also tried a 0.46-m diameter entrance cylinder
and found that the compact toroid still tipped. With the elimination of the
complication of tipping, three distinct time scales emerge. The first
($\sim$ 1 μs) is the time required to fill the flux conserver with magnetic field
and plasma. The second ($\sim$ 12 μs) is the time for the decay of the fields in
the entrance cylinder. Figure 4a shows this decay. We interpret this decay
as being due to field line reconnection which is completed in about 30 μs.
The third time ($\sim$ 150 μs) is the characteristic time for the decay of the
fields in the flux conserver measured after reconnection has occurred.
Figure 4b shows this decay. It is interesting to observe that the three time
scales 1 μs, 12 μs, and 150 μs have the proper relative values to be an Alfven
time, a resistive tearing time, and a resistive decay time respectively.[6]
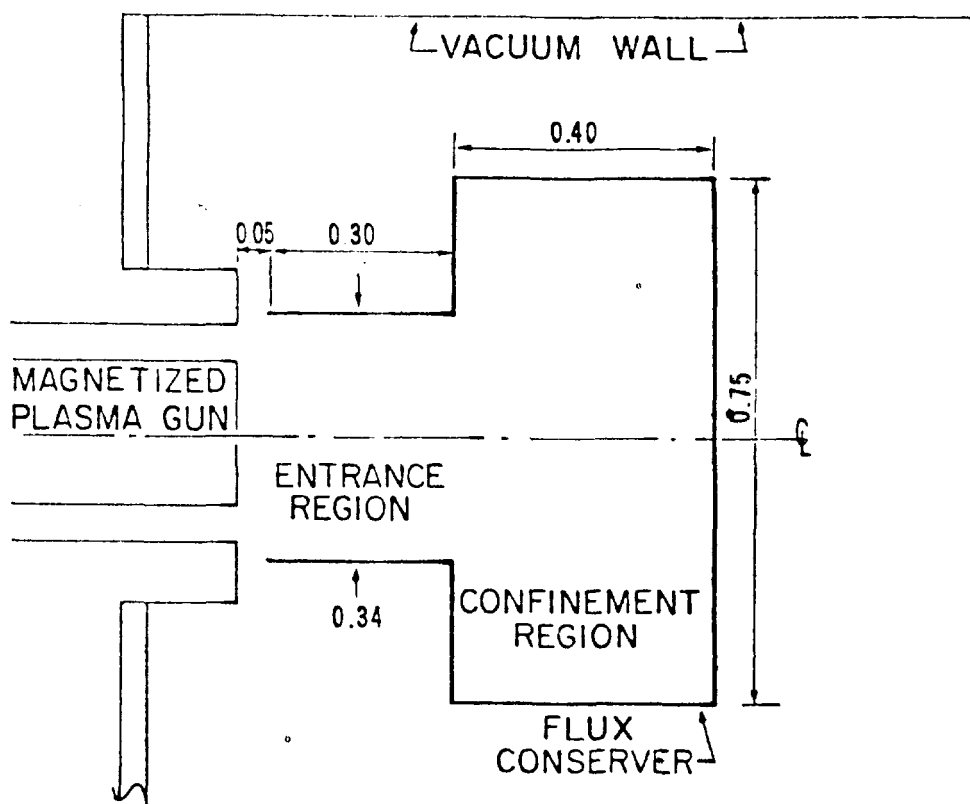
Fig. 3.
Schematic of the geometry for creating a stable compact toroid. It is axially
symmetric with dimensions given in meters.
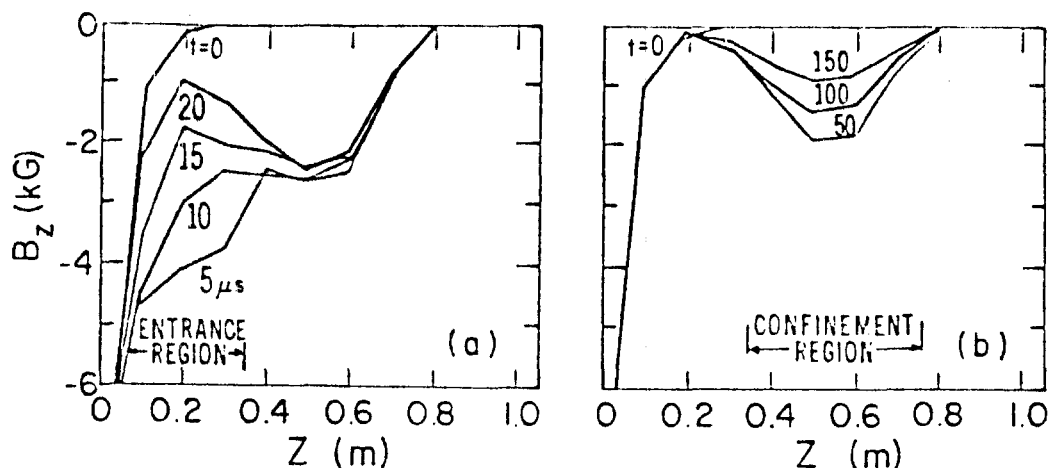
Fig. 4.

Plots of the axial component of the magnetic field on axis at various times. Figure 4a shows plots at various times during the decay of the field in the entrance cylinder. The time elapsed between plots is 5 μs. Figure 4b shows plots at various times during the decay of the compact toroid and the time between plots here is 50 μs. The gun discharge is initiated at t=0 and the plot labeled t=0 shows the value of the axial component of the magnetic field in this region due to the coils which supply the initial axial flux for the plasma gun.

Figures 4b and 2a illustrate the dramatic differences in the fields on the axis of the flux conserver for the stable and rotated toroid. If it does not tip then one expects to have only B_z on axis as is the case in Fig. 4b (the peak transverse components are measured to be less than 15% of the peak B_z and are not shown). When the compact toroid rotates 90° one then expects to have only transverse components on axis. Fig. 2a shows the transverse components (B_θ and B_r) to be much larger than B_z. Thus, the measurement of all components of the magnetic fields on the axis of the flux conserver is a powerful means of determining the extent of tipping.

CONCLUSION

A compact toroidal plasma configuration is generated in a cylindrical resistive flux conserver using a magnetized coaxial plasma gun. If the initial poloidal field strength of the magnetized gun is adjusted appropriately the configuration is observed to stop within the flux conserver. For a straight cylindrical flux conserver the axis of the toroid is observed to rotate so that it is orthogonal to the original axis of symmetry. After this rotation, the deformed toroid appears to be MHD stable and decays away with about a 100-μs time constant. CV radiation is observed throughout the lifetime of the magnetic field structure. Interferometric measurements show an initial value of about 10^{14} cm^{-3} and a lifetime for the plasma density similar to the magnetic field lifetime. When a compact toroid is generated in an oblate flux conserver under proper conditions it does not tip as verified by the fact that the transverse fields on axis are small compared to the axial

field. In this stable case the reconnecting time (12 μs) can be observed and it is much shorter than the decay time of the fields of the compact toroid (150 μs).

REFERENCES

1. R. K. Linford, W. T. Armstrong, D. A. Platts, E. G. Sherwood, "Field Reversal Experiments (FRX)," Proc. Seventh Int. Conf. on Plasma Phys. and Contr. Nucl. Fusion, Innsbruck, 1978, Paper IAEA-CN-37/S-1-1, Vol. II, p. 447.

2. A. Eberhagen, W. Grossmann, Z. Phys. 248 (1971) 130.

3. H. Alfven et al, J. Nucl. Energy, Part C: Pl. Phys. 1, 116 (1960).

4. T. R. Jarboe, I. Henins, H. W. Hoida, J. Marshall, D. A. Platts, and A. R. Sherwood, "The Motion of a Compact Toroid Inside a Cylindrical Flux Conserver," submitted to Phys. Rev. Lett., 1980.

5. M. N. Rosenbluth and M. N. Bussac, Nucl. Fusion 19, 489 (1979).

6. H. P. Furth, J. Killeen, and M. N. Rosenbluth, Phys. Fluids 6, 459 (1963).

Two-Dimensional Modeling of the Formation of the
S-1 Spheromak

S. C. Jardin, H. P. Furth, M. Okabayashi, W. Park, M. Yamada
Plasma Physics Laboratory, Princeton University
Princeton, New Jersey 08544

A two-dimensional (axisymmetric) computational model has recently been developed to solve the resistive MHD equations over the time scale, in the geometry, and with the boundary conditions appropriate to the study of the formation of the S-1 spheromak. Since the unique feature of this device is the induction of both toroidal and poloidal currents into the plasma, the plasma boundary conditions are formulated in terms of electric fields which are coupled into the external circuit equations which are solved simutaneously with the plasma evolution equations.

Figure 1 is a schematic diagram of the components affecting the magnetics of the S-1 spheromak device. There are two top-bottom pairs of equilibrium field (EF) coils located outside of the vacuum chamber at $R = 0.8$ m, $Z = \pm 1.0$ m and $R = 1.5$ m, $Z = \pm 0.825$ m. The skin time of the chamber walls is short compared to the rise time of these coils but long compared to the pulse time of the experiment so that the static fields from the EF coils are effectively "frozen in" the chamber walls.

The flux core is located on the symmetry plane with a major radius of 1.0 meter and a minor radius of 18.0 centimeters. Inside the flux core are the poloidal windings of the toroidal field coil (TC) circuit and the toroidal windings of the poloidal field coil (PC) circuit. These two sets of windings are connected by leads to the PC and TC sets of capacitor banks. Surrounding the flux core is a thin metallic liner of thickness 10 mills and with resistivity 12×10^{-7} Ohm-meters. There are 15 turns in the TC windings and 1 turn in the PC. The TC circuit has a capacitor of 2320 µf charged to 16.3 kV and has 0.772 m-Ohm resistance. The PC circuit has 1870 µf capacitor and 0.340 m-Ohm resistance.

Figure 2 shows the computed currents in the circuits, liner, and plasma as a function of the time t. The EF and PC currents have brought up slowly so that they have the values - 220 kA and 500 kA respectively at time $t = 0$ when the plasma is preionized. At $t = 0$ the TC capacitor banks are discharged and simultaneously the PC circuit current is decreased by charging the PC capacitors. The currents in the TC and PC circuits are crowbared and allowed to decay resistively at time $t = 100$ µsec and $t = 140$ µsec respectively. In response to the changing circuit currents, poloidal and toroidal currents are induced into the liner and plasma as indicated in the figure.

Figure 3(a) shows the computational grid used in the calculation. A nonorthogonal grid was utilized so that cell boundaries align with physical boundaries allowing accurate computation of boundary conditions. Figure 3(b) shows the poloidal magnetic flux distribution at time $t = 0$. Only the contours on the upper half plane are plotted since the device is symmetric about the midplane. The lower part of Fig. 3(b) shows the poloidal flux on the midplane plotted against the major radius R.

Figure 4 shows the distribution of the poloidal magnetic flux, the toroidal current, the toroidal magnetic field, and the poloidal current at time t = 125 µsec . The evolution of these quantities is determined by resistive diffusion combined with the equilibrium constraint which dictates a preferential inward expansion. In Fig. 4(a), the magnetic axis has formed and moved inward to R = 0.6 m and many closed magnetic field lines now exist. A large toroidal current exists in Fig. 4(b) centered about the magnetic axis. From Fig. 4(c)(d) it is seen that the toroidal field also has a maximum at the magnetic axis, and most of the poloidal current is circulating about this point.

Figure 5 shows the fields and currents at time t = 250 µsec after the spheromak configuratin is fully formed. The magnetic axis is now located at R = 0.48 m. This configuration will slowly decay, on a time scale determined by the Spitzer resistivity, and hence the temperature, of the central region. Reasonable estimated of radiative and transport losses suggest a central temperature of several hundred electron volts which would imply a lifetime of several milliseconds.

The calculations presented here have used a subset of the MHD equations obtained by setting the plasma pressure to zero. This force free approximation is valid if the plasma $\beta \sim \mu_0 p/B^2$ is small. The plasma resistivity was that of a 20 eV Spitzer value with extra enhancement up to 10 times near the conductors (where the temperature is expected to be low) and where the streaming parameter V_D/V_{Te} is large. More recent calculations with finite pressure, a full energy equation with radiation losses, ohmic heating, and diffusion, and with a self-consistent plasma resistivity show qualitatively the same behavior.

ACKNOWLEDGMENT

156
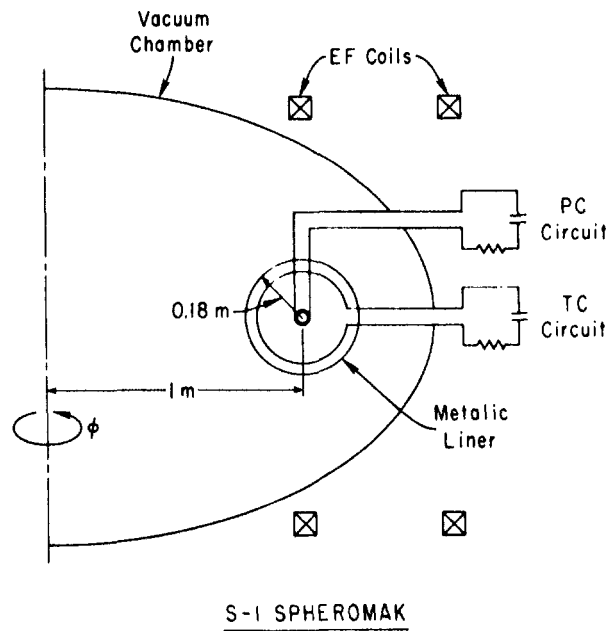
Fig. 1. The magnetic components of the S-1 spheromak.
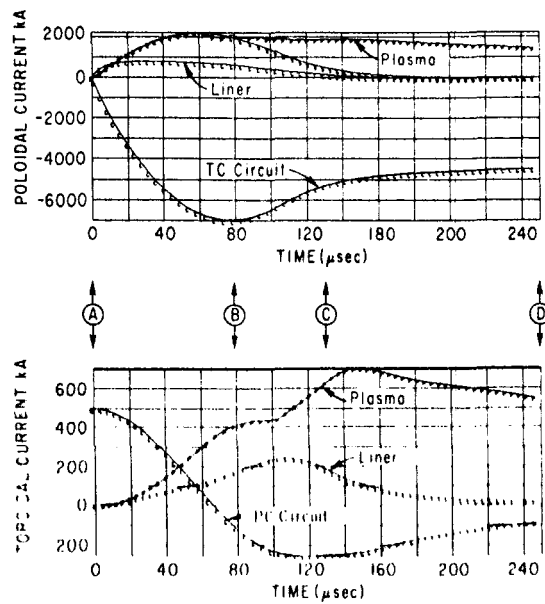
Fig. 2. Time histories of the currents in the circuits, liner, and plasma.

157
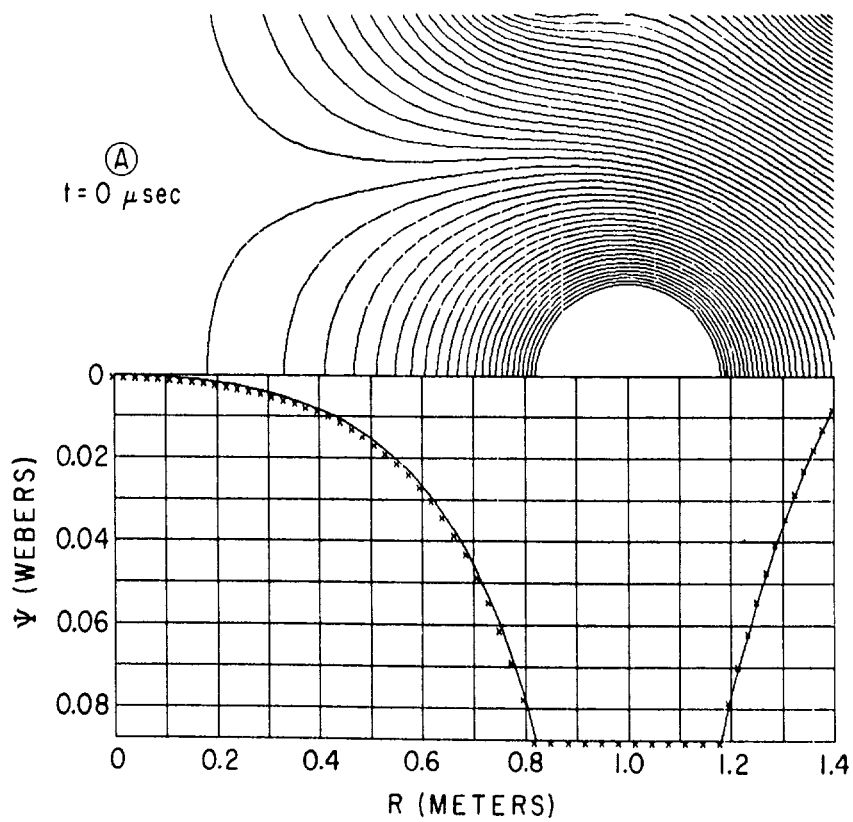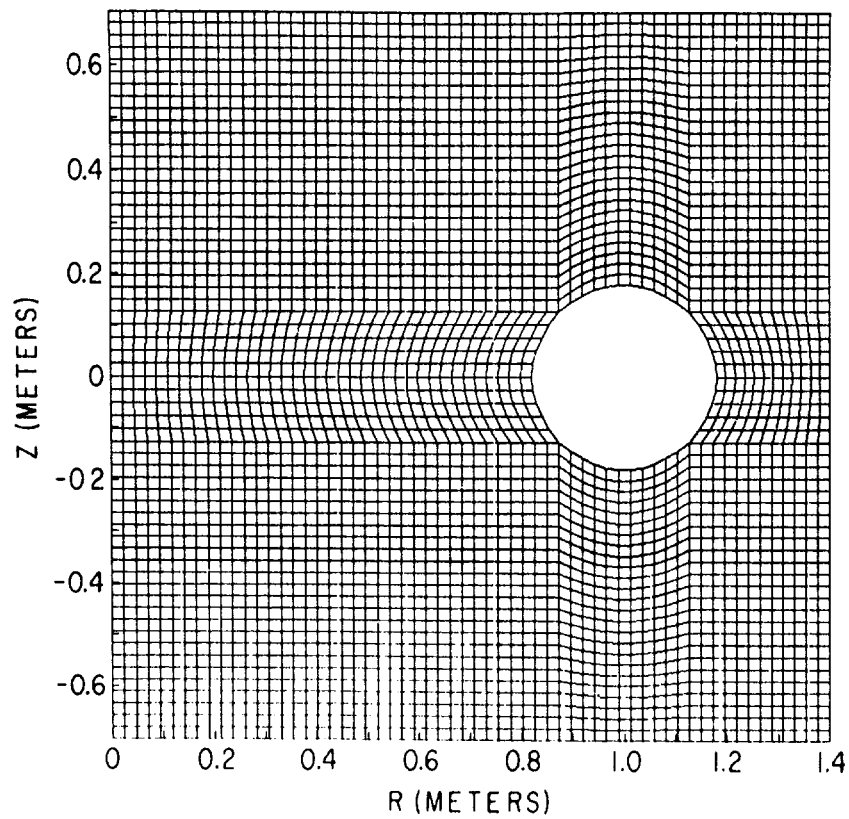
Fig. 3. (a) Computational grid, (b) poloidal flux contours
at time t = 0. Graph shows midplane values.
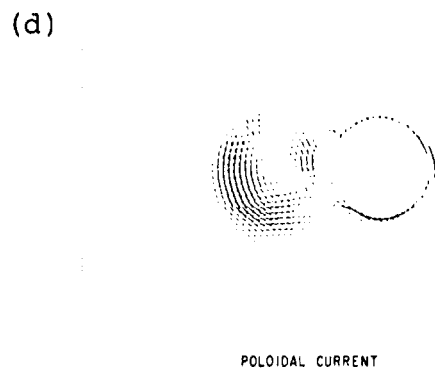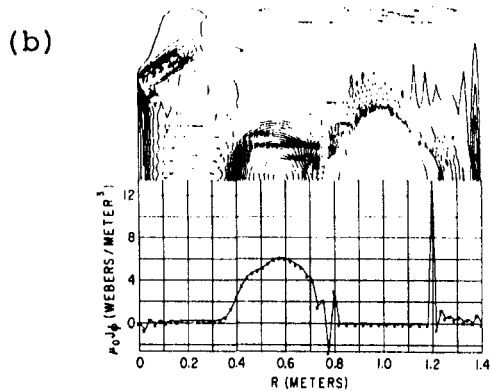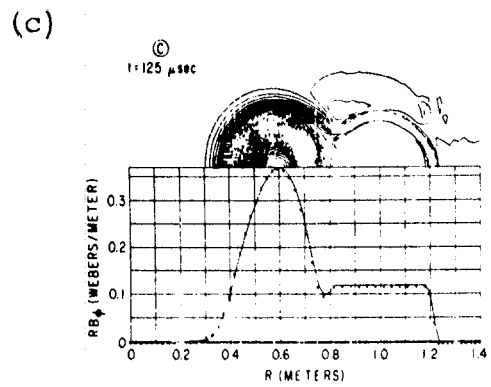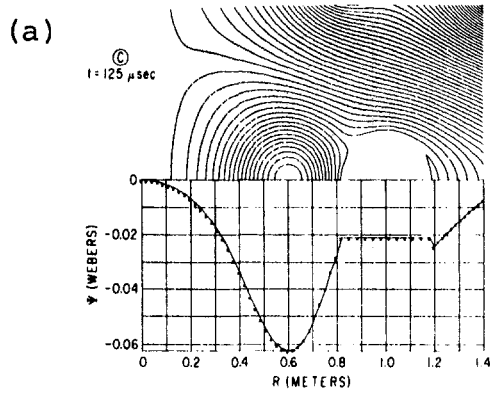
Fig. 4. (a) Poloidal flux, (b) toroidal current,
(c) toroidal field strength and, (d) poloidal current vectors at
t = 125 µsec.
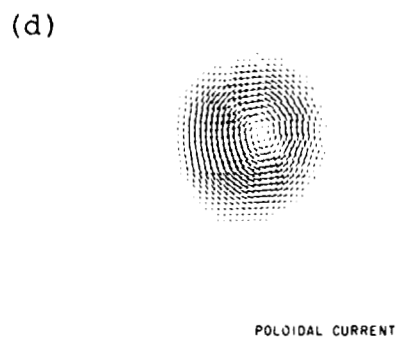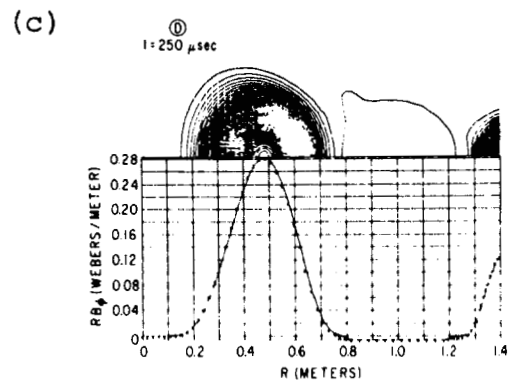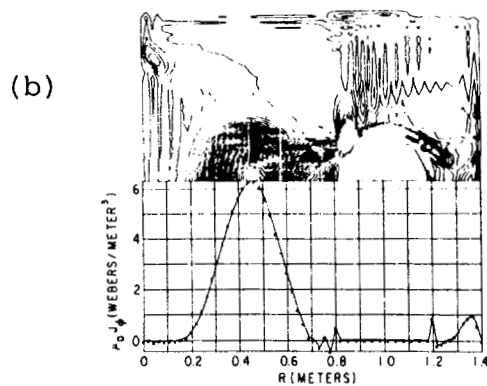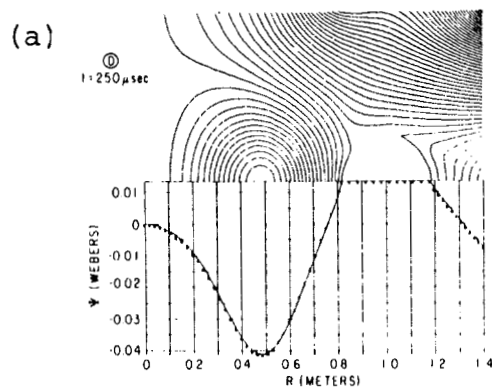
Fig. 5. (a) Poloidal flux, (b) toroidal current,
(c) toroidal field strength and, (d) poloidal current at
t = 250 µsec.

THE OHTE PLASMA CONFINEMENT CONCEPT

M. J. Schaffer, M. S. Chu, C. Chu, R. R. Goforth
R. La Haye, T. Ohkawa, T. Yamagishi

Because it approximates a Taylor equilibrium,[1] the reversed field pinch (RFP) is a very attractive plasma confinment configuration. In practice, transport processes distort Taylor equilibria by overheating the interior[2] and cooling the edge. Interior turbulence associated with the former may be tolerable[3], but the turbulent core must be surrounded by an effective confinement layer. In RFPs this is obtained by reversal of the axial field, and the corresponding Taylor profile has large plasma currents out to a conducting wall. In practice, large current gradients develop near the edge which seriously restrict the parameter range consistent with MHD stability in the critical confinement layer[4,5].

The OHTE configuration[6] attempts to improve the properties of the confinement layer by adding helical windings around the pinch (Fig. 1). This has a number of consequences, the most notable of which is to combine with the predominantly azimuthal field of the pinch to produce an axial or translational transform, also shown in Fig. 1. (This transform is analogous to the well-known rotational transform of a predominantly axial field.[7]) Both theoretical and numerical analyses show that translational transform essentially adds algebraically to field line pitch arising from plasma currents. The transform is only weakly dependent on local currents; it depends on the global plasma azimuthal field and the applied helical winding field. The
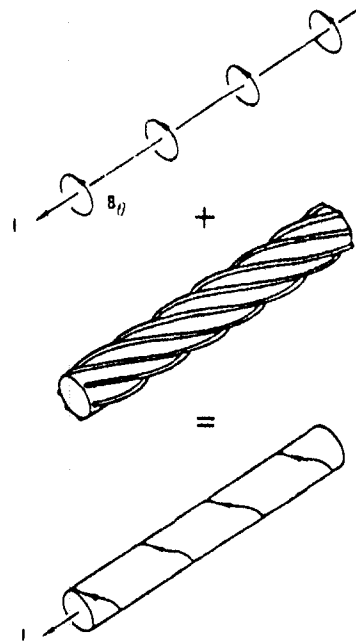
Fig. 1. OHTE plasma confinement configuration in straight geometry

direction of the transform is determined by the winding direction, since field lines are bent toward the winding pitch. Translational transform is quite localized; it decays almost exponentially from the surface with an e-fold distance of about 10% of the average plasma radius. It is always highly sheared near the edge. Therefore, the helical winding in OHTE is used to establish or enhance pitch reversal around a Z-pinch. Current near the edge may be small or zero, consistent with transport. The gradient of $\sigma = \vec{j} \cdot \vec{B}/B^2 = j_{\parallel}/B$, which is a major factor driving surface tearing instabilities,[4,5] is greatly reduced thereby. Numerical evaluation of the stability criterion for local interchange modes in helical geometry[8] confirms that the transform contribution to shear also contributes to stability.

As in other helical configurations, the OHTE configuration possesses a helical separatrix (Fig. 2). Transform is greatest near the separatrix. (It is actually equal to the winding pitch at the separatrix, where the additivity of pitch and transform breaks down. However, the volume of such strongly affected field lines is negligibly small.) Since field lines outside the separatrix intercept nearby structure (e.g., wall, coils, coil leads), the plasma is naturally bounded by its separatrix, which also serves as a magnetic limiter to reduce plasma-wall interaction. (It is noteworthy that preliminary experiments in Doublet III with an axisymmetric magnetic limiter, but not a divertor, have produced substantial reduction in the plasma impurity level[9].) Line tying may help to stabilize the plasma boundary. The electrical power needed to produce a separatrix at a given radius around a pinch core of a given current varies roughly as ℓ^{-2} for a given volume of winding conductor, where ℓ is the number of winding periods in the azimuthal direction. Therefore, $\ell = 1$ and $\ell = 2$ windings are more favorable than $\ell = 3$ and higher in reactor embodiments. Neither the power nor the transform profile depend very sensitively on the winding pitch.

The OHTE-like Taylor equilibrium is obtained by solving the MHD equilibrium equations in helical geometry subject to $\mu_0 \vec{j} = \mu \vec{B}$ with μ a constant. The result is[10]
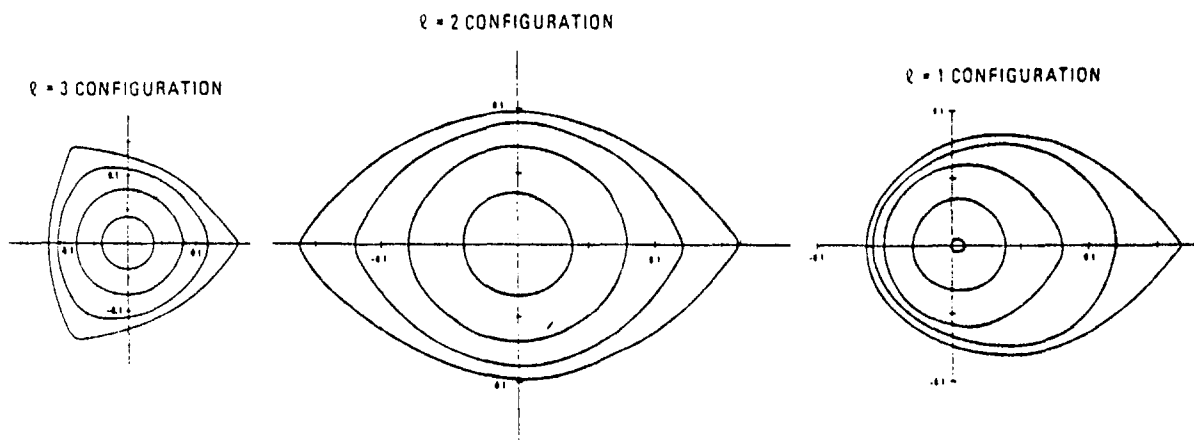
Fig. 2. OHTE flux surfaces in the rz-plane for $\ell = 3$, 2 and 1

$$B_r = - \frac{1}{r} \frac{\partial F}{\partial u} \tag{1}$$

$$B_\theta = \left(\frac{\partial F}{\partial r} + \alpha r f \right) \cdot (1 + \alpha^2 r^2)^{-1} \tag{2}$$

$$B_z = \left(- \alpha r \frac{\partial F}{\partial r} + f \right) \cdot (1 + \alpha^2 r^2)^{-1} \tag{3}$$

$$F = \frac{f_o}{\mu} + \sum_m F_m(r) \cos m(\theta - \alpha z) \tag{4}$$

$$F_m = a_m \left[\gamma J_m(y_m) - y_m J_m'(y_m) \right] \quad , \quad |\gamma| > m \tag{5}$$

$$y_m = |\gamma^2 - m^2|^{1/2} |\alpha r| \tag{6}$$

$$\gamma = \mu/\alpha \tag{7}$$

$$f = f_o + \mu F \tag{8}$$

Here F is the helical flux function, $2\pi/\alpha$ is the winding pitch, and f_o and the a_m are arbitrary constants. For $|\gamma| < m$ the J-Bessel functions become I-modified Bessel functions. As in RFPs, the Taylor state has large $j_\parallel$ currents out to the wall. However, as already pointed out, the OHTE pitch-reversed configuration persists if $j_\parallel$ goes to zero or even reverses slightly in the confinement layer. Numerical equilibria with nonuniform μ are given in a companion paper[11].

Plasma current may also drive ideal MHD kink modes. Helical effects are large in the confinement layer, and a 3-dimensional stability analysis is required in general. The problem reduces to two dimensions in the special case where the mode and winding pitches are equal (synchronous mode). We have analyzed the synchronous mode $m \neq \ell$ in a constant-μ free-boundary plasma of average radius $\bar{a}$ inside a circular conducting cylinder of radius b, using the method of Rosenbluth and Bussac[12]. It is found that: 1) the most unstable mode is an $m = 1$ mode with strong $m \neq 1$ components, and 2) the stability window is the same as for an $m = 1$, $k = \alpha$ mode in a circular equilibrium with $a = \bar{a}$. This is an encouraging result, since the synchronous mode orients itself to resonate with the weakest point in the helical equilibrium. Other wavelengths average over the full configuration and should therefore be more stable. For $\alpha\bar{a} = -0.68$ and $b/\bar{a} = 1.25$ the synchronous mode is stable up to

163

$u\bar{a} = 3.0$. In a toroidal plasma the helical winding may be designed such that n/ℓ is noninteger if $\ell \neq 1$, where n is the number of winding periods in the toroidal direction. Then the lowest synchronous azimuthal mode number is $m = \ell$, rather than $m = 1$.

The effect of magnetic field errors and toroidicity on transform have been investigated. The field errors due to the insulating gap in a conducting shell were modeled, and transform pitch reversal of an otherwise non-reversed model configuration persisted for field errors at the plasma surface of over 7% of the plasma azimuthal field there. Experimental field errors can be kept much lower than this level. Toroidicity has been investigated by field line tracing with simple plasma models for the $\ell = 3$, $n = 16$ winding of the experiment described below. As in stellarators[13], toroidicity causes the loss of some of the outer field lines and reduces the amount of transform that can be achieved in practice. These effects are minimized by either adjusting the plasma radial position, by suitable choice of the helical current distribution, or by a combination of both. The effect of β is to shift the optimum plasma position by few mm ($0 \lesssim \beta_\theta \lesssim 1$, $a = 150$ mm, $R_0 = 1240$ mm).

In order to treat toroidal effects with a more realistic plasma model and to interpret magnetic probe signals from the toroidal experiment, the plasma equilibrium has been expanded as a Fourier series:

$$F = \text{Re} \sum_{mn} F_{mn}(r) \exp(im\theta - in\alpha R_0 \phi) \quad , \text{ etc.} \quad (9)$$

where a quasicylindrical coordinate system (r, θ, ϕ) of major radius R_0 is used. The principal toroidal-helical effects are given by sideband terms $m = \ell \pm 1$, which are calculated by integrating functions of the lower order terms $(0,0)$, $(1,0)$ and (ℓ,n).

The OHTE Confinement Test Experiment presently under construction is illustrated in Fig. 3. It has a major radius of 1.24 m, stainless steel bellows vacuum chamber with turbomolecular pumping, a 15 mm thick aluminum conducting shell of inner radius 199 mm, and a 45° average helical winding with $\ell = 3$, $n = 16$. Plasma currents up to 600 kA with rise times of 1-3 msec are anticipated with a 2.85 weber (unidirectional current) induction coil. Net toroidal field is provided by supplying unequal currents to positive and negative helical windings. The vertical field which accompanies this technique is cancelled by a vertical field coil, which also provides the equilibrium field during long plasma discharges. The filling gas breaks down near the toroidal axis as a small (minor) radius stellarator with opposed rotational and current transforms. As the poloidal field approaches the toroidal field strength, the plasma becomes OHTE-like. Further increase in current causes the separatrix to expand. Toroidal flux is conserved by the conducting shell during the startup sequence.
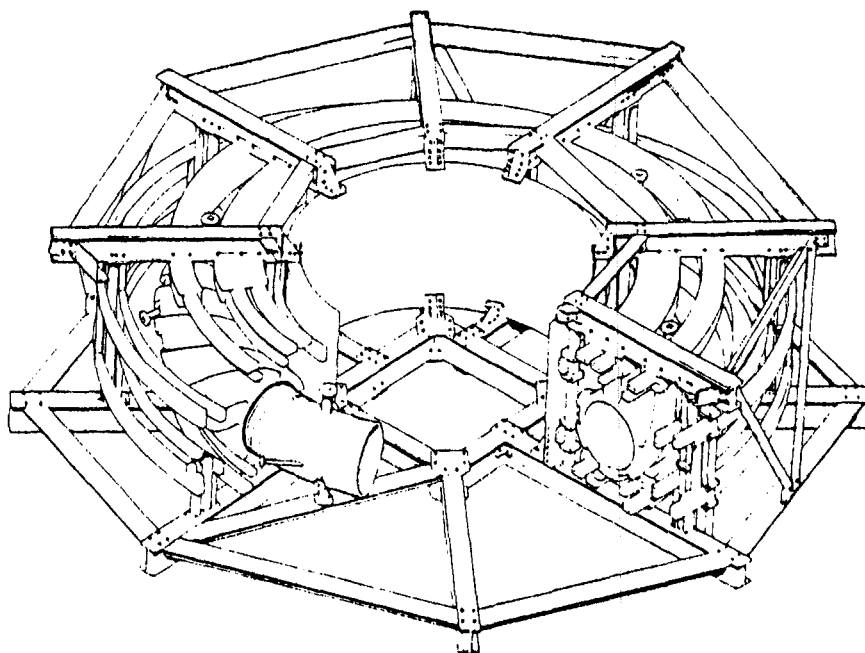
Fig. 3. OHTE confinement test experiment

REFERENCES

1. J. B. Taylor, Phys. Rev. Letters 33, (1974) 1139.
2. J. P. Christiansen and K. V. Roberts, Nucl. Fusion 18, (1978) 181.
3. D. C. Robinson and R. E. King, Plasma Physics and Controlled Nuclear Fusion Research (Conf. Proceedings, Novosibirsk, 1968), vol 1, 263.
4. D. C. Robinson, Nucl. Fusion 18, (1978) 939.
5. P. H. Sakanaka and J. P. Goedbloed, Phys. Fluids 17, (1974) 919.
6. T. Ohkawa, et al., General Atomic Report GA-A15561 (1980). Submitted to Phys. Rev. Letters.
7. L. Spitzer, Jr., Phys. Fluids 1, (1958) 253.
8. J. M. Greene and J. L. Johnson, Phys. Fluids 5, (1962) 510.
9. T. Tamano, private communication.
10. D. Correa and D. Lortz, Nucl. Fusion 13, (1973) 127.
11. M. S. Chu, et al., this workshop.
12. M. N. Rosenbluth and M. N. Bussac, Nucl. Fusion 19, (1979) 489.
13. A. Gibson, Phys. Fluids 10, (1967) 1553.

SETTING UP REVERSED FIELD PINCHES

A A Newton and J W Johnston
UKAEA, Culham Laboratory and Oxford Polytechnic
(Euratom/UKAEA Fusion Association)

Abstract

Self-reversal is the dominant physical process in the setting up stage of RFP when the toroidal flux is conserved by a closed shell. 0-D and 1-D simulations are described. Other modes of setting up are possible in which the self reversal effect may be reduced or enhanced.

INTRODUCTION

The reversed field pinch magnetic field distribution (RFP) appears complicated (see Fig 1) compared to other plasma containment configurations. It may be thought difficult to set up but the self reversal process, which is driven by instabilities tending to minimise the plasma energy, ensures that the distribution arises. Although the setting up stage is complex and many physical processes are at work, we consider the dominant one to be self reversal. Data on the mode used on ZETA where a closed shell conserved toroidal flux is summarised in the experimental paper.[1]

This paper presents two types of calculations. Firstly, 0-D calculations which cross-link the θ and ϕ circuits enabling us to predict the circuit current. The second calculation uses a 1-D code with a dynamo formulation (assuming average axisymmetry) to predict the evolution of the field.

0-D CODE[2]

This code represents the plasma as a 4 terminal network connecting the θ and ϕ circuits. The magnetic field is assumed to evolve through a given series of relaxed states. The toroidal flux and magnetic energy are found by solving:

$$d\phi/dt = -V_\theta \quad \text{and} \quad dW_m/dt = V_\phi I_\phi - V_\theta I_\theta - \eta \int J.J \, d^3x$$

and these quantities are used to determine θ, I_ϕ and I_θ etc. The plasma resistivity, η, is assumed to be radially independent and to have a time variation:

$$\eta(t) = \eta_2 + (\eta_1 - \eta_2)/(1 + \exp[(t - t_s)/t_w])$$

This simulates the observed decrease of resistivity from a high value η_1 to η_2.

Any set of field configurations can be used provided that I_ϕ, $B_\phi(a)$ and $\int J^2 d^3x$ are known as functions of ϕ and W_m. We have chosen a model similar to the BFM but with the current density reduced in the region $0.7 < a/r < 1$; this gives an F-θ curve similar to experiment.

The relaxation invariant, $K_o = \int A.B\ d^3x$ could have been used in place of W_m. When the BFM is used as the relaxed state this does not change the results.

0-D CODE RESULTS AND MODES OF SETTING UP RFP

The code has been used to make predictions for existing and proposed RFPs. Figure 2 shows the predicted waveforms of ETA BETA II which are close to those observed.[3]

Various modes of forming RFP have also been investigated. The ZETA mode uses self reversal which is turbulent with energy loss to the wall. Other modes with more or less turbulence and losses may exist requiring different volt seconds and having different wall interaction. Alternatives can be envisaged, all with similar I_ϕ waveshapes and different I_θ programming. In one, I_θ is matched to the self reversal to make the liner a virtual flux conserver (this is a sub-case of the ZETA mode). The effect of varying the liner to the shell spacing, measured by λ, the ratio of inductance outside the liner to the inductance inside the liner with no plasma, is to double the V_ϕ flux consumption as λ increases from 0 to unity.

Pitch convection should minimise the self reversal activity by creating a field configuration with minimum energy by continuously raising the I_ϕ and I_θ currents together. The plasma cannot be fully stable until reversal is achieved but MHD activity should be smaller than in the ZETA mode (and the necessary continuous injection of gas should protect the wall).

The constant θ mode requires strong self reversal. It begins with a seed plasma at some fraction of the peak current to give the required θ and then I_ϕ is raised. Self reversal generates additional positive flux inside the plasma and unwanted negative flux is removed at the outside with I_θ being driven to maintain F to correspond with the desired θ. In principle a high β configuration can be maintained throughout setting up (although the losses due to self reversal fluctuations may preclude this in practice).

Table 1 summarises examples of these modes for a device with R/a = 1.8/0.6m for the same plasma model and I_ϕ circuit drive (14.4MJ at 3kV). The demands of

167

the constant θ mode are clearly shown with a lower peak current and a higher flux consumption, measured by the volt seconds factor, $\int_0^{\tau_r} V_\phi dt/\psi$, where ψ is the poloidal flux. Pitch convection is the most favourable and requires a contribution to the poloidal flux from the self reversal processes in order to give a volt seconds factor less than 1. The final circuit parameters were chosen by trial and error - a similar procedure to that used in experiment and have not been optimised. Also, the fact that a higher flux consumption may be associated with higher plasma resistivity, due, say, to more impurity release has not been taken into account; thus, the differences between the modes may be larger in experiment.

Table 1

Comparison of Setting Up Modes

	ZETA Mode	Constant θ	Pitch Convection
Current rise time (ms), τ_r	5.5	6.1	5.2
Peak current (MA)	2.23	2.17	2.42
θ/F at peak current	1.83/-0.66	1.82/-0.64	1.87/-0.73
Volt second factor	1.14	1.61	0.86
I_θ circuit energy (MJ)	0	4.8	3.8
I_θ circuit voltage (V)*	0	80.0	800.0

* Simple C, L and R drive circuits are used with values referred to one turn.

1-D CODE

The basic theoretical pinch equilibrium is the minimum energy state with Bessel function fields (BFM) which is ideal and resistive MHD stable. This is force free and has reversal when $\theta > 1.2$ (it can then be stable with a small vacuum region) and has $\mu = j/B$ constant across the plasma. In a practical situation, even without a vacuum region, $j \to 0$ at the walls (see Fig 3) and there must be a layer predisposed to tearing instabilities driven by $d/dr(j/B)$ when $\beta \sim 0$ although stable configurations with $j \to 0$ have been found. These equilibria and the BFM have high magnetic shear and thus with small modification could contain finite β: it is these equilibria which are important for fusion. The main residual MHD instability may be resistive pressure driven (g-mode).

Knowledge of local criteria for various instabilities and the resulting transport would in principle permit calculations of plasma evolution: this has been attempted for Suydam modes in the central plasma.[4] However, since the

modes driving self reversal are not clearly identified we make, on heuristic grounds, the assumption that $\mu(r)$ tends to become uniform. This is the basis of the 'mean μ model' in which we take a field diffusion equation:

$$\frac{d\underline{B}}{dt} = -\nabla \times \left[\alpha \underline{B} - \frac{1}{\mu_o} (\eta + \eta_T) \underline{\nabla} \times \underline{B} \right]$$

with the dynamo term:

$$\alpha = \mu \left(\frac{\eta_T}{\mu_o} \right) + F(\bar{\mu} - \mu)$$

where f is any positive weighting function, $\bar{\mu}$ is the spatial average of μ with weighting $f|B|^2$ and η_T is a turbulent resistivity which provides the energy to drive the dynamo. It can be shown that, for low values of β, a dynamo of this form satisfies the Taylor conditions of reducing the magnetic energy with K_o constant and the magnetic field, therefore, relaxes towards the BFM.

The 1-D code is a variant of ATHENE with the boundary conditions modified to $dP/dr(a) = 0$ and $V_r(a) = E \times B/B^2$ to ensure j parallel to B near the edge. Mesh points are added or removed as the plasma moves inwards or outwards. Figure 4 shows F-θ curves for $\tau_r/\tau_\eta = 10$ and $\tau_\alpha/\tau_\eta = 1/50$ (where $\tau_\eta = \mu_o a^2/\eta$ and $\tau_\alpha = \eta a^2/\eta_T$) showing the self reversal effect. For comparison a curve with no dynamo shows FFPM-like behaviour.

HEAT LOSS

The fluctuations producing self reversal also give an enhanced perpendicular heat loss.[5] A simple argument gives a scaling law $(\delta B/B) \propto S^{-\frac{1}{2}}$ for the fluctuation level required to drive a dynamo maintaining the field configuration against resistive decay (S is the Lundquist number). When coupled with a model of electron thermal conductivity along perturbed field lines using the same δB and scale lengths this gives a classical scaling for the temperature and β in collisionless conditions.

REFERENCES

[1]   A A Newton and E P Butt: this Workshop

[2]   J W Johnston: to be published

[3]   A Buffa et al: Proc EPS Conf, Oxford, 2 (1979) p544.

[4]   A A Newton et al: in "Pulsed High Beta Plasmas" ed D E Evans, Pergamon (1976) and J P Christiansen and K V Roberts: Nucl Fusion 18 (1978) 181.

[5]   P G Carolan et al: Proc EPS Conf, Oxford, 1 (1979) p100.
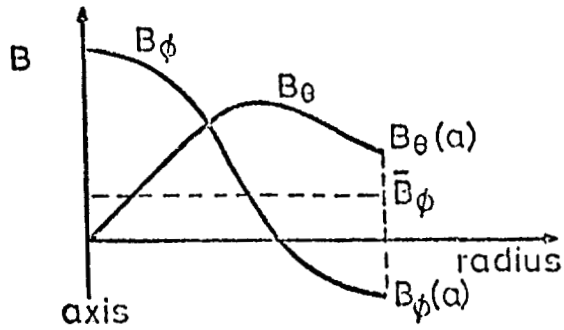
Fig 1 A reversed field configuration with J → 0 at the edge.
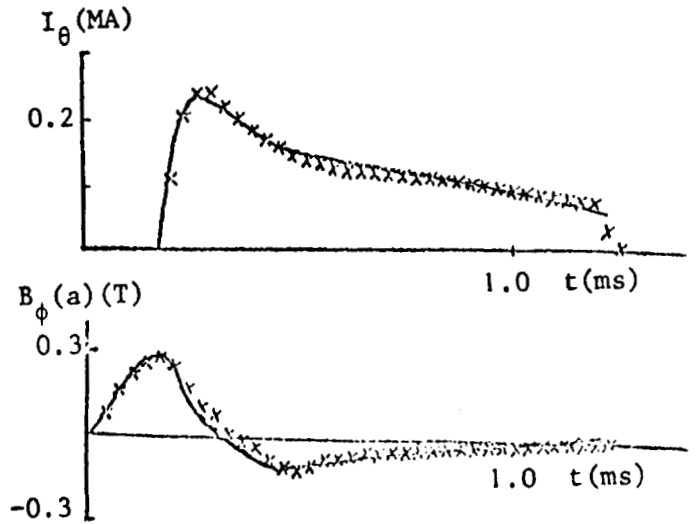
Fig 3 0-D simulations of ETA BETA II waveforms with the experimental results shown xxxxx.
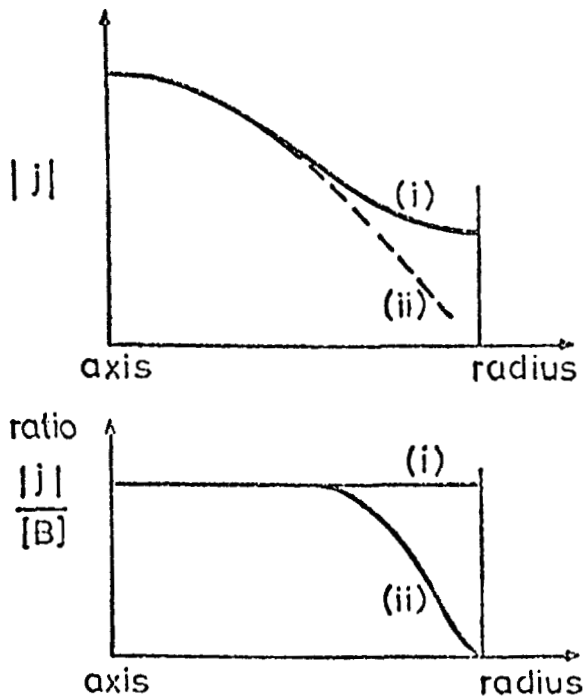
Fig 2 The current density $|J|$ and the ratio $|J|/|B|$ for the relaxed field configuration assumed the 0-D model.
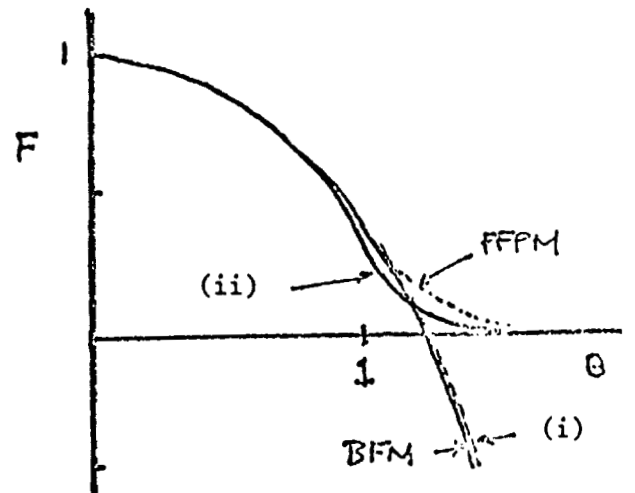
Fig 4 F-θ curves for 1-D simulations of the current rise phase with (i) and without (ii) the dynamo.

D. A. Baker, L. W. Mann, T. A. Oliphant, and J. A. Phillips
Los Alamos Scientific Laboratory
Los Alamos, New Mexico
Los Alamos Scientific Laboratory, Los Alamos, N.M. 87545

I. INTRODUCTION

An earlier paper[1] showed that under rather general conditions, the setting up of uniform current density plasma columns by means of axial currents, which rise to their final constant value in a short time compared to plasma compression and plasma field diffusion times, involves either an energy loss and/or plasma pressure at the wall in order to reach the final equilibrium state. This theorem is based upon general conditions of energy and pressure balance and cylindrical symmetry. The purpose of the present paper is to first extend the general global analysis to the opposite case of long current risetimes and second to compare the implications of these global considerations with the results of computer calculations and experiments on reversed field pinch (RFP) configurations.

II. LOWER BOUNDS ON THE ENERGY LOSS ASSOCIATED WITH SETTING UP AN RFP THROUGH A SERIES OF TAYLOR LOWEST ENERGY STATES

A. Model

Consider a cylindrically symmetric plasma column surrounded by a B_z flux conserving conducting cylinder of radius a. (See Fig. 1). There is an initial longitudinal field B_{zo} and a current I(t) rises from zero slowly enough to allow the plasma-field configurations to continuously follow a series of relaxed states. For the purposes of this paper these states are assumed to be the Taylor lowest energy states.[2] In the spirit of Ref. 1 bounds on the energy losses associated with this type of RFP setup are investigated.

B. Taylor Lowest Energy States

The Taylor lowest energy states satisfy the force free equation

$$\vec{\nabla} \times \vec{B} = \alpha \vec{B} \tag{1}$$

where the force free parameter α is independent of radius r. For the cylindrically symmetric z independent case $\vec{\nabla} \cdot \vec{B} = 0$ implies $B_r \equiv 0$ and solutions of Eq. (1) are

$$B_z = B_o J_o(\alpha r), \quad B_\theta = B_o J_1(\alpha r) \tag{2}$$

with the coefficients B_o being independent of r; J_o and J_1 are Bessel functions of the first kind. Since the analysis is restricted to cylindrically symmetric states, we will only consider α values for the range[2] $\alpha a \leq 3.2$. The time dependences of α and B_o as I(t) rises are determined by two conditions:

(1) Maxwell's Equation $\vec{\nabla} \times \vec{B} = \mu_o \vec{J}$ yields

$$B_\theta(a,t) = \mu_o I(t)/2\pi a \tag{3}$$

(2) B_z flux conservation requires

$$\phi_z = \int_0^a B_z(r,t) 2\pi r dr = \pi a^2 B_{zo} = \text{constant} \tag{4}$$

The desired fields then become

$$B_z(r,t) = [\theta B_{zo}/J_1(2\theta)] J_o(2\theta \, r/a) \tag{5}$$

$$B_\theta(r,t) = [\theta B_{zo}/J_1(2\theta)] J_1(2\theta \, r/a) \tag{6}$$

where the pinch parameter θ is given by

$$\theta(t) = B_\theta(a)/\langle B_z \rangle = \mu_o I(t)/2\pi a B_{zo} = \alpha a/2 \; . \tag{7}$$

A family of curves showing the time evolution of these field profiles is given in Figs. 2 and 3.

C. Field Energy

The field energy per unit length at any time is given by

$$W_F \equiv W_\theta + W_z = \int_0^a (B_\theta^2/2\mu_o) 2\pi r dr + \int_0^a (B_z^2/2\mu_o) 2\pi r dr. \tag{8}$$

Using Eqs. (5) and (6) yields

$$W_\theta = \left[W_{zo}/(2J_1^2(2\theta)) \right] \int_0^{2\theta} J_1^2(x) x dx, \tag{9}$$

$$W_z = \left[W_{zo}/(2J_1^2(2\theta)) \right] \int_0^{2\theta} J_o^2(x) x dx \; . \tag{10}$$

Fig. 1. Geometry for derivation of energy and pressure balance.
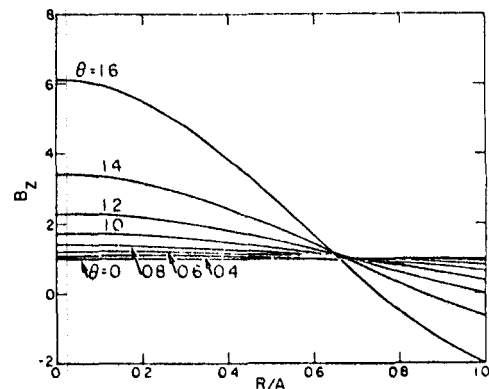
Fig. 2. B_z profile evolution for flux conserving Taylor states.

171
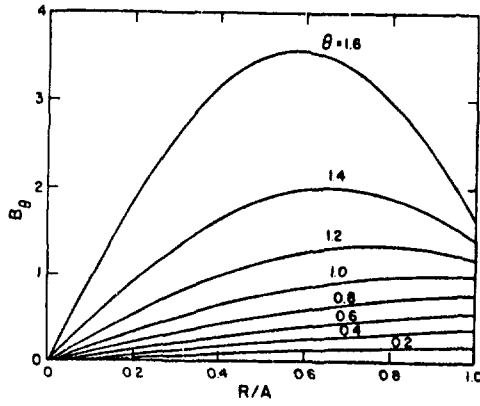
Fig. 3. B_θ evolution corresponding to Fig. 2.

where $W_{zo} = \pi a^2 B_{zo}^2/2\mu_o$. These energies are plotted vs θ in Fig. 4.

D. Energy Input

To compute the energy input to the pinch during the current rise, Faraday's Law $\oint \vec{E} \cdot d\vec{s} = - \dot{\phi}$ is applied to path 2 of Fig. 1
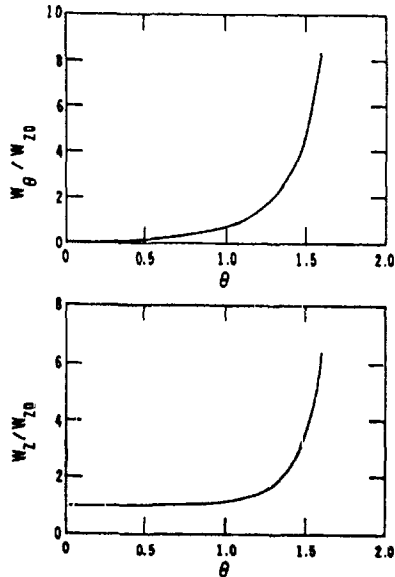
Fig. 4. Field energies calculated from Eqs. (9) and (10).
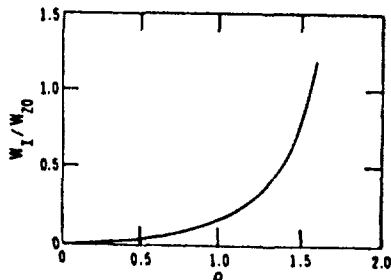
Fig. 5. W_I as calculated from Eq. (13).

$$E_z(0,t) - E_z(a,t) = -\dot{\phi}_\theta; \qquad \phi_\theta = \int_0^a B_\theta dr \qquad (11)$$

for use with Poynting's theorem. The Poynting energy input W_{in} per unit length in a time T is then given by integrating over the cylindrical surface $r = a$:

$$W_{in} = \int_0^T \int_S (\vec{E} \times \vec{H}) \cdot d\vec{S} dt = \int_0^T E_z(a,t)H_\theta(a,t) 2\pi a dt$$

or from Eqs. (3), (4), and (11) and $\vec{B} = \mu_o\vec{H}$

$$W_{in} = \int_0^T \dot{\phi}_\theta I(t)dt + \int_0^T E_z(o,t)I(t)dt \qquad (12)$$

$$\equiv W_I + W_E$$

The W_I term that follows from Eq. (6) is given by

$$W_I = W_{zo} \left\{ 2\theta \frac{[1-J_o(2\theta)]}{J_1(2\theta)} - \int_0^{2\theta} \frac{[1-J_o(x)]}{J_1(x)} dx \right\} \qquad (13)$$

and is plotted vs θ in Fig. 5. A calculation of the W_E term requires the electric field on axis. If a simple Ohm's law $E_z = \eta J_z$ is assumed on axis the following expression is obtained

$$W_E = \int_0^T \eta(0,t)J_z(0,t)I(t)dt \quad . \qquad (14)$$

Making use of $\nabla \times \vec{B} = \alpha\vec{B} = \mu_o\vec{J}$ we obtain

$$\vec{J}(r,t) = (\alpha/\mu_o)\vec{B}(r_z t) \quad . \qquad (15)$$

Substituting from Eq. (5) the current density on axis is:

$$\vec{J}_z(0,t) = 2B_{zo}\theta^2/[\mu_o a J_1(2\theta)] \quad . \qquad (16)$$

Substituting the expressions for $J_z(0,t)$ and $I(t)$ obtained from Eqs. (7) and (16) into Eq. (16) gives

$$W_E = (4\pi B_{zo}^2/\mu_o^2) \int_0^T \eta(0,t)[\theta^3/J_1(2\theta)]dt \quad . \quad (17)$$

Unlike the W_I term this expression depends upon the time history of the current rise both through η and θ. For η classical ($\eta \sim T^{-3/2}$) and a sinusoidal current rise in time τ_R (i.e., $\theta(t) = \theta_{max}\sin(\pi t/2\tau_R)$) W_E is calculated numerically. Some specific examples of W_E for this case assuming only bremsstrahlung and oxygen line radiation losses have been calculated for ZT-40 using a zero dimensional code.[3] The results are shown for two current risetimes and several oxygen impurity levels are shown in Fig. 6.

E. Energy Balance

Energy conservation applied at the end of the time interval $0 < t < T$ requires

$$\underset{\text{initial plasma energy}}{W_p(0)} + \underset{\text{plasma field energy}}{W_F(0)} + \underset{\text{and field energy input}}{W_{in}(T)} = \underset{\text{plasma energy}}{W_p(T)} + \underset{\text{field energy}}{W_F(T)} + \underset{\text{energy loss}}{W_L(T)}$$

$$\qquad (18)$$

For the case under consideration $I(0) = 0$ we have $W_F(0) = W_{zo}$. The energy dissipated W_{diss} in the plasma during $0 \le t \le T$ goes either into additional plasma heating or losses so that $W_{diss} = W_p(T) - W_p(0) + W_L(T)$. Grouping these terms in Eq. (18) and using Eq. (12) we obtain

$$W_{diss} = W_{zo} - W_F + W_I + W_E \quad . \qquad (19)$$

For the case of a dissipative Ohm's law the W_E integral of Eq. (14) is positive implying $W_{diss} > W_{zo} - W_F + W_I$. The right hand side of this
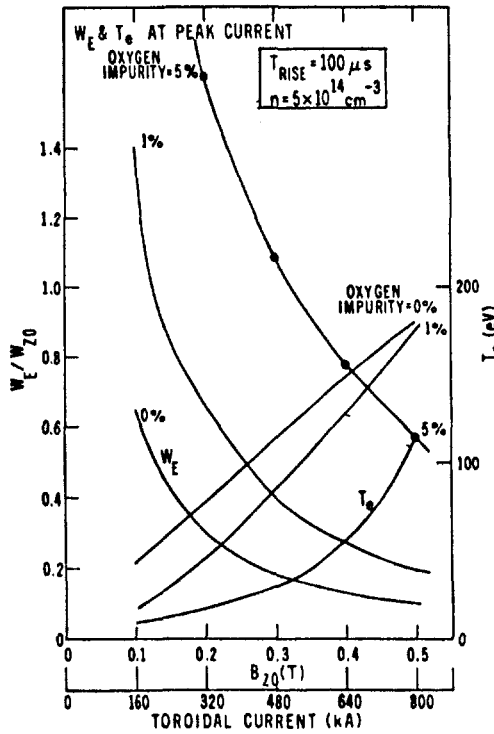
(a)
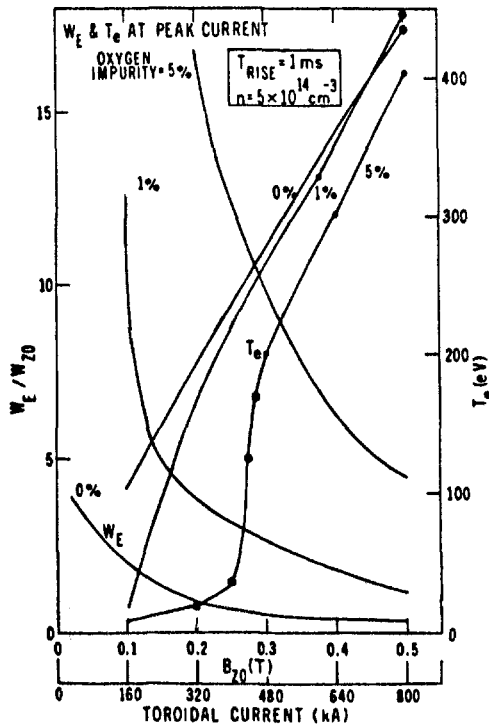
(b)

Fig. 6. W_E and T_e as a function of the peak value of the current which rises sinusoidally in a time τ_{rise} for ZT-40 dimensions. (a) $\tau_{rise} = 100$ μs, (b) $\tau_{rise} = 1$ ms.

inequality is plotted in Fig. 7. This lower limit on the energy dissipated increases with θ up to $\theta = 1.34$ where W_{diss} is equal to approximately the initial field energy. Since the Taylor state is force-free it cannot sustain a plasma pressure gradient implying that either the energy dissipated goes into plasma heating with the wall containing the plasma pressure or some or all of it is lost. In the latter case since plasma losses are irreversible, we have shown that for $\theta \geq 1.34$ at least an amount of energy equal to the initial field energy must be lost in order to reach the Taylor state. For $\theta = 1.34$ (see Fig. 4b) this energy amounts to approximately one third of the final poloidal field energy. As the sample calculations shown in Fig. 6 indicate, in practice this loss may be considerably higher since the W_E term can add a significant amount.

F. Conclusion

It has been shown that for slow startups, as well as the fast ones of Ref. 1 the energy dissipation during formation is a serious consideration since it can lead to significant energy losses and/or plasma pressure at the walls. The most questionable assumptions which leave a possible escape from these conclusions are those of cylindrical symmetry and Ohm's law on axis; assymetries may invalidate the above Poynting vector calculations of the energy input and Ohm's law on axis may be invalid due to e.g., turbulence, dynamo activity, and electron runaways, so that W_E may not always be positive. The global energy and pressure balance arguments can be applied to other specifications of the relaxed states. It is expected that departures from the force-free model used will not significantly alter the conclusions about the energy dissipated.

III. COMPUTER CALCULATIONS FOR VARIABLE CURRENT RISETIMES

The energy loss requirement to satisfy both equilibrium and poloidal beta restrictions for MHD stability as a function of current risetime has been examined using the 1-D-time-dependent, non-ideal MHD code RAVEN.[4] Calculations for ZT-40 dimensions were made assuming the following characteristics:

$$I_\phi = 6 \times 10^5 \sin\left(\pi t/2\tau_e\right) \text{ A}, \quad t < \text{risetime} \left(\tau_R\right)$$
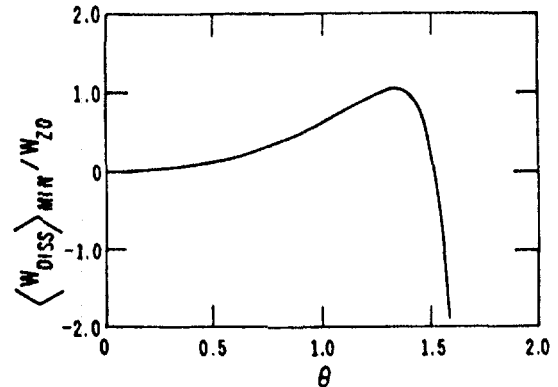
Fig. 7. Lower limit on the energy dissipated as obtained from Eq. (19) without the W_E term.

and

$$I = 6 \times 10^5 A, \quad t > \tau_R$$

$$B_{\phi wall} = 0.2 \cos\left(\pi t/\tau_R\right) + 0.1 \ T \quad t < \tau_R$$
$$= -0.1 \ T \quad t > \tau_R$$

The plasma conditions were: $T_i = T_e$; $\eta = 10 \times n(T_e = 10eV)$ (constant in time); and plasma mass density 8.3×10^{-6} kg/m^3. Plasma losses were zero and thermal conductivity was allowed inside the plasma but not to the wall. Under these conditions, the theorem of Ref. 1 implies, that for sufficiently short current risetimes, the plasma will exert pressure on the wall as the fields diffuse.

In Ref. 1 the energy input term [W_I of Eq. 12 in this paper] was integrated by parts to yield

$$W_I = \phi_\theta(T)I(T) - \int_0^T \dot{\phi}_\theta I dt \qquad (20)$$

and the last term was called $W_{\theta p}$. This expression was useful in deriving the theorem because $W_{\theta p} \to 0$ as the risetime of current became short compared to the rise of ϕ_θ due to diffusion and/or compression. Several current risetimes in the interval 0.2-20 μs were considered and in Fig. 8 is shown the results for the 10 μs risetime. The terms $W_{\theta p}$ and $\phi_\theta I$ behave as expected while the field annihilation on axis term, W_E, begins to become significant at ~ 3 μs. The computed β_θ reaches a value of unity at 6.5 μs, before the current maximum at 10 μs.

The results showing the effect of varying current risetimes are shown in Fig. 9. Here normalized times for a given event, i.e., time divided by the current rise time τ_R, are plotted versus τ_R. For a τ_R, for example, of 2 μs, the plasma boundary which initially moved radially inward started to expand, i.e., velocity becomes positive, at a normalized time of ~ 0.3. B_θ flux reached the axis at 0.9, $\beta_\theta = 1$ at ~ 1.3, and
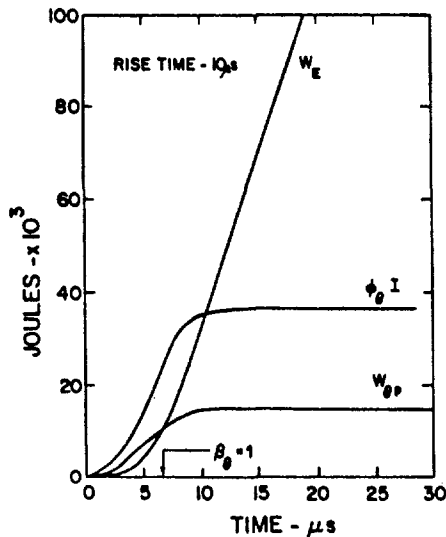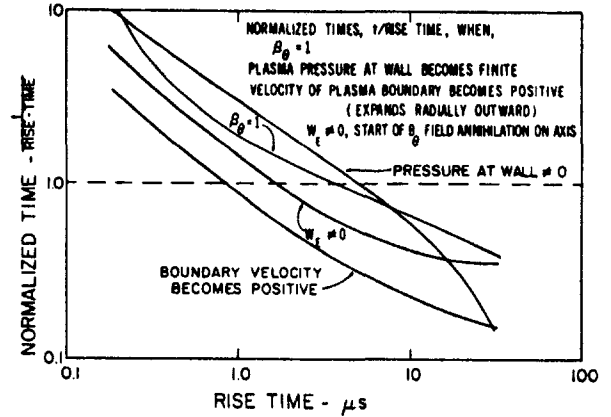
Fig. 9. Normalized times when the plasma boundary velocity >0, $\beta_\theta = 1$, $W_E \neq 0$ and wall pressure $\neq 0$ for different rise times.

plasma pressure on the wall became nonzero at ~ 2.0.

These calculations lead to the following conclusions:

1) For the cases considered with diffusion of magnetic fields, the predictions of the theorem are confirmed by the code, i.e., without losses:

(a) Plasma energy rises with time and the discharge expands to the wall by the time the current density has diffused through the column.

(b) Wall pressure or plasma energy losses are required for energy and pressure balance by the time the field diffusion is complete.

(c) For short current risetimes β_θ reaches unity early in the rise time limiting radial compression.

2) The longer risetimes require greater energy losses (due to an increase in W_E). Even if the losses resulting from field diffusion are large the rise time might be adjusted so that the rate of energy loss can be tolerated by the wall without excessive release of impurities. This possibility involves obtaining a favorable tradeoff between the negative $W_{\theta p}$ term and the positive W_E term in the energy input.

Examination of the theorem shows that to meet the energy and pressure balance conditions and minimize losses,

(1) the magnitude of term $W_{\theta p}$ should be increased. This might be done by starting the discharge on axis and allowing it to expand radially.

(2) the magnetic fields and gas injection could be programmed to establish the required profiles with minimal field diffusion.

IV. FLUX INPUT TO ZT-40 WITH VARIABLE RISETIMES

The current risetime in ZT-40 has been varied between 33 and 240 μs by: (1) raising the charge voltage on the toroidal current bank in discrete steps, 5.0, 7.5 and 10 kV, and firing the crowbar switch at 90°, 45°, and 30° in the first quarter cycle (four feedpoint operation) and, (2) by reconnecting the I(t) circuit for one feedpoint operation. The peak I(t) was roughly the same, 360 kA, for all risetimes. The value of θ was between 1.2 and 1.4 for the 33, 40 and 100 μs

Fig. 8. Energy terms computed by code RAVEN for a 10 μs current risetime.

risetimes and varied between 0.4 and 1.4 for the 240 µs time. These discharges were nonreversed field pinches.

The poloidal flux input per quadrant, $\int_0^T V_f dt$, where V_f is feedplate voltage was calculated up to peak current for all cases and shown in Fig. 10 as a function of filling gas pressure. With the fastest risetime, 33 µs, the flux input is relatively constant with pressure and is somewhat less than that for a fully diffused uniform current channel with pinch radius, $r_p = 14.5$ cm, calculated from the magnetic field ignoring plasma pressure. With longer risetimes the flux input increased which is interpreted as an increase in flux annihilation on axis, as suggested by the computer code results. As the filling pressure is reduced, however, the flux input drastically increases with the longer risetimes. This behavior correlates with the observations on ZT-40 that at the lower pressures there are large fluctuations in density, magnetic fields and discharge current; strong anomalous resistivity effects might be expected.

These results indicate that in all cases the fields have diffused to the axis by the time of peak current and a sizeable fraction of the input energy to the plasma must be lost if there is to be no plasma pressure on the wall. Absolute measurements of radiation, particle losses and wall pressure could support this conclusion.

V. PLASMA HEATING IN ZT-40

A preliminary run on ZT-40 has been made to determine the magnetic field profiles, in the radial interval 10-20 cm, as a function of time using a magnetic probe. The discharge was driven at one feedpoint. An inventory of the components of the flux input was calculated, Fig. 11. The components are as follows:

(1) $2\pi R \int_{10}^{20} B_\theta$ dr is the integrated poloidal flux in the measured radial interval 10-20 cm.
(2) the flux in the cables and stray inductances.
(3) the volt-seconds lost in the circuit resistances.
(4) the poloidal flux inside $r = 10$ cm assuming a uniform current distribution within this radius.

The difference between the sum of these components and the input volt-seconds is due to plasma resistance, 3.9 mΩ, which is approximately a constant up to peak current. Assuming a pinch compression of 2 and uniform current density inside the plasma resistivity is 1.6×10^{-3} ohm-cm and the average $T_e = 15$ eV, which is not unreasonable from the electron temperature measurements for this mode of operation and low peak toroidal current, 360 kA. Using the value of plasma resistance, ohmic heating implies a $\beta_\theta \simeq 1$ and $T_e = T_i = 270$ eV just before peak current with no losses. These calculations suggest that either $\simeq 90\%$ of the input energy has been lost or there is appreciable wall pressure at this time which is consistent with the theoretical conclusion discussed above.

REFERENCES
1. D. A. Baker and J. A. Phillips, Phys. Rev. Letters 32, 202, (1974).
2. J. B. Taylor, Phys. Rev. Letters 33, 1139 (1974).
3. S. Ortolani, Los Alamos Scientific Lab Report LA-8261-MS(1980).
4. T. Oliphant, "Simulation Results of RFP Boundary Motion," these proceedings.

RUNS 1585-1617, MODE (1) (1) V_ϕ-47 kV, V_θ-8kV, P=20mtorr
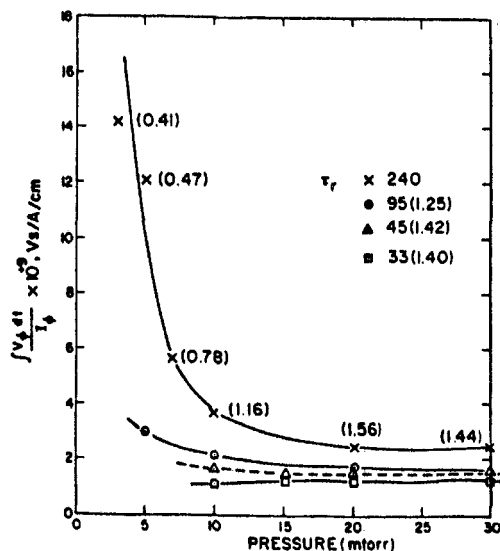
Fig. 10. Input volt-seconds at peak current as a function of fill pressure for different current risetimes. (θ values are given in parentheses.)
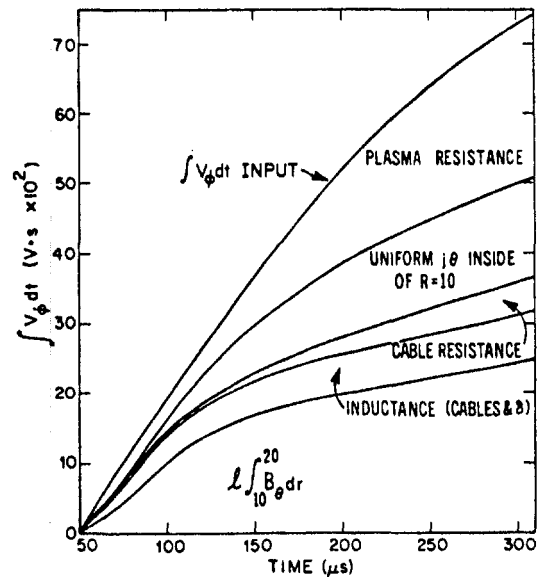
Fig. 11. Inventory of input volt-seconds as a function of time for one feedpoint operation.

175

RELAXATION, FLUX CONSUMPTION AND QUASI STEADY STATE PINCHES

by

M.K. Bevir and J.W. Gray

Culham Laboratory, Abingdon, Oxon., OX14 3DB, UK
(Euratom/UKAEA Fusion Association)

INTRODUCTION

In toroidal containment devices an accurate estimation of the poloidal flux swing required is important. In Tokamaks the estimate is usually made by adding together the individual fluxes required by various parts of the circuit and stages of the pulse. Since there is considerable experimental information available a reliable estimate can usually be made in spite of uncertainties about the plasma resistance and behaviour.

In pinches the situation is different. There are fewer experimental results (see Newton and Butt[1] for information on Zeta) and less understanding of the plasma behaviour from the circuit view point. The poloidal and toroidal currents are connected by the plasma in a way that appears to be more complex than it is in Tokamaks and a number of plasma models have been suggested to represent it. Here we wish to point out that one of the consequences of a model that has been used at Culham (see, for example, Newton and Johnston[2]) is that with certain circuit programming arrangements an effective mean (time averaged) toroidal voltage is obtained without a mean expenditure of flux (ie with a zero mean toroidal voltage). This effective mean voltage can be used to set-up or maintain the pinch.

It is likely that this effect will occur with other models in which the circuit interactions are sufficiently subtle. It is important to realise that there is no fundamental limitation on flux requirements (as there are with energy requirements) and the apparent limitations are due to the simplicity of plasma models used up till now and, in the case of Tokamaks, perhaps, to their (relatively) simple behaviour. Pinches may well be sufficiently complex to allow the effect predicted by this model.

THE PLASMA MODEL

The plasma model described here is based on a time dependent version of the theory of plasma relaxation proposed recently by J.B. Taylor[3]. In that theory a pressureless plasma of high conductivity containing magnetic fields is assumed to achieve a relaxed state inside an infinitely conducting torus. This state is the one in which the magnetic energy

$W = \frac{1}{2\mu_o} \int B^2 d\tau$ has a minimum for all possible fields $\underline{B}$ subject to fixing the

constraints that the total toroidal flux Ψ_z and the quantity $K = \int \underline{A}.\underline{B} \, d\tau$ (where $\underline{A}$ is a vector potential of the field $\underline{B}$ such that $\underline{B} = \text{curl } \underline{A}$). The field distribution $\underline{B}$ in the relaxed state is defined by the two quantities Ψ_z and K and can be deduced from them; in the case of a circular straight pinch the field profiles are Bessel functions and relationships such as the "F,θ" curve can be calculated.

We define two magnetic fluxes by integrating the vector potential $\underline{A}$ the short and long way around the surface of the torus:

minor cross-section: $\int \underline{B}.\underline{dS} = \int \underline{A}.d\ell_\theta = \Psi_z$ (1)

central hole: $\int \underline{B}.\underline{dS} = \int \underline{A}.d\ell_z = \Psi_\theta$ (2)

In order that K be uniquely defined by $\underline{B}$ within the torus it is necessary to specify Ψ_θ. In[3] Ψ_θ (or A_z, its equivalent in cylindrical geometry with r variation only) was taken to be zero. Here we use a modified form of the invariant K which does not require any specification of Ψ_θ and is compatible with the original convention, namely

$$Ku = \int \underline{A}.\underline{B} \, d\tau - \Psi_z \Psi_\theta$$ (3)

This has a unique value for any $\underline{A}$ satisfying curl $\underline{A} = \underline{B}$ within the torus volume and may be used in time dependent situations in which $\underline{A}$, Ψ_z, Ψ_θ etc may vary. If the calculation of the minimum energy W subject to Ψ_z and K being fixed with the above convention for Ψ_θ (or A_z) is repeated with Ψ_z and K_u fixed the same force free distributions of $\underline{B}$ are obtained without the need for any specification of Ψ_θ.

We evaluate $\dfrac{dKu}{dt}$ using (3) and the equations

$$\frac{\partial \underline{B}}{\partial t} = - \text{curl } \underline{E} \, , \quad \frac{\partial \underline{A}}{\partial t} = - \underline{E}$$

and find $\quad \dfrac{dKu}{dt} = - 2 \Psi_z \dfrac{d\Psi_\theta}{dt} - 2 \int\limits_{\text{torus}} \underline{E}.\underline{B} \, d\tau$ (4)

If we use the equation for the force free minimum energy state

$$\text{curl } \underline{B} = \mu \underline{B} \quad (\mu \text{ uniform})$$ (5)

we can obtain further equations. The dissipation integral in (4) becomes, using Ohm's law in the form $\underline{j} = \sigma (\underline{E} + \underline{v} \wedge \underline{B})$,

$$\int \underline{E}.\underline{B} \, d\tau = \int \frac{1}{\sigma}\underline{j}.\underline{B} d\tau = \frac{1}{\mu}\int \frac{1}{\sigma} j^2 d\tau = \frac{D}{\mu}$$ (6)

where the permeability of free space has been taken as unity.

Denoting $\dfrac{d}{dt}$ by a dash, these equations are

$$2W\mu' = I_\theta I_z' - I_z I_\theta'$$ (7.1)

$$W' + D = I_z V_z - I_\theta V_\theta$$ (7.2)

$$K_u' + \frac{2D}{\mu} = 2 \Psi_z V_z$$ (7.3)

$$K_u = \frac{2W - I_\theta \Psi_z}{\mu}$$ (7.4)

and we also have the relations

$$I_z = \mu \Psi_z \qquad (7.5)$$

$$\frac{d\Psi_z}{dt} = - V_\theta \qquad (7.6)$$

$$\frac{d\Psi_\theta}{dt} = - V_z \qquad (7.7)$$

(7.3) is (4) written slightly differently and one of the relations (7.1) to (7.4) is redundant since it can be deduced from the other three. Ψ_θ and V_z are not determined by the magnetic field, but with the help of (7.5) can be eliminated from (7.2) and (7.3), along with the dissipation D, to give

$$K_u' - \frac{2W'}{\mu} = - \frac{2I_\theta \Psi_z'}{\mu} \qquad (7.8)$$

(7.8) together with (7.4) and (7.5) can be written in terms of non-dimensional variables which are all functions of μ alone (dashes now denoting $\frac{d}{d\mu}$) :

$$\frac{I_z}{\Psi_z} = \mu \qquad (8.1)$$

$$\mu\left(\frac{K_u}{\Psi_z^2}\right) = 2\left(\frac{W}{\Psi_z^2}\right) - \left(\frac{I_\theta}{\Psi_z}\right) \qquad (8.2)$$

$$\left(\frac{I_\theta}{\Psi_z}\right)' = -\left(\frac{K_u}{\Psi_z^2}\right) \qquad (8.3)$$

$$\text{or} \quad \mu\left(\frac{K_u}{\Psi_z^2}\right)' = 2\left(\frac{W}{\Psi_z^2}\right)' \qquad (8.4)$$

These functional relationships must be obeyed by any of the variables calculated using the field profiles determined by the solutions of (5) in any torus together with $\underline{B}.d\underline{S} = 0$ on the torus surface. It is unlikely there are more since the functional form of the variables would then be determined without a knowledge of the shape of the torus.

We may note that the energy equation (7.2) implies that once relaxed no energy is dissipated in the continuous relaxation that is assumed to take place from then on as the plasma parameters vary, other than that required to balance the ohmic dissipation calculated from the current distribution that maintains the relaxed field profiles. The energy equation (7.2) and (7.6) have been used as a basis for a circuit analysis code[2] by Johnston. Where the field profiles are solutions of (5), for example Bessel functions, the results are the same as using equation (7.3) instead of (7.2), but will differ when different profiles are assumed. Mondino[4] has also in effect used the energy equation together with field profiles given by Ortolani and Rostagni[5], and found that the equivalent circuit equations required artificial voltage sources in the V_z circuit to satisfy the energy equation.

178

$$\frac{dK_u}{dt} = 2 \, \Psi_z \, V_z - \text{dissipation term} \qquad (9.1)$$

$$\frac{d\Psi_z}{dt} = - V_\theta \qquad (9.2)$$

Apart from estimates of the dissipative terms these equations are not dependent on relaxation phenomena and define K_u and Ψ_z entirely in terms of voltages applied at the plasma surface - however the currents required in the circuits can only be calculated using further assumptions: for example that the plasma is always in the relaxed state corresponding to the value of K_u and Ψ_z obtaining at any moment.

We can see from equation (9.1) that in the absence of dissipation $K_u \propto \int V_z \, dt$ only when Ψ_z is held constant, but that if Ψ_z is varied in time then K_u can be created or built-up without the expenditure of voltseconds in the mean. Alternatively the decay of K_u due to dissipation can be counteracted.

Consider, for example, this second situation whereby we attempt to maintain the plasma in a steady or quasi steady state without continuing volt second consumption. Compare this with the normal mode of operation in which the toroidal flux Ψ_z is kept constant with value Ψ_0 and a constant voltage V_{zo} is found necessary to maintain the discharge. Then (9.1) gives

$$\frac{dK_u}{dt} = 0 = 2 \, \Psi_0 \, V_{zo} - \text{dissipation terms}$$

$$\Psi_z = \Psi_0$$

This is to be compared with a mode of operation in which

$$V_z = V_\omega \cos \omega t$$

$$\Psi_z = \Psi_0 + \delta\Psi \cos \omega t$$

Substituting these in the equation for $\frac{dK_u}{dt}$, assuming the dissipation is the same corresponding to the same mean current and averaging over time with the requirement that $\left[\frac{dK_u}{dt}\right]_{average} = 0$

we find

$$V_\omega = 2 \, V_{zo} \left/ \frac{\delta\Psi}{\Psi_0} \right. \qquad (10.1)$$

and

$$V_\theta = \omega \, \delta\Psi \, \sin \omega t \qquad (10.2)$$

These equations imply that the oscillating voltage in the Z direction must be larger than the mean voltage it replaces by the factor $2 \left/ \frac{\delta\Psi}{\Psi_0} \right.$. For $\frac{\delta\Psi}{\Psi_0} \sim 30\%$, i.e. a factor of 2 to 1 on Ψ, $V_\omega \sim 6 V_{zo}$. The frequency ω should be higher then the inverse classical diffusion time, and perhaps lower then the inverse relaxation time, whatever that may be, if the pinch is to be always relaxed. However equations (9) still apply if the time variations are much faster than the relaxation time, and it is

conceivable that the dissipation term may then be less important. The circuit currents would be different from those predicted by the relaxation theory and would probably be much larger. The estimate of the dissipation based on a relaxed current profile is crucial to the arguments advanced above because (4) applies equally to the cases of a solid conducting rod and to an infinitely conducting plasma. In the first case the current distribution would not be 'relaxed' and oscillating voltages applied at the plasma surface would result in decoupled oscillating currents. In the second case radial motion at the boundary is implied and the effect of suppressing this in a plasma of high conductivity and low density is not yet clear.

Equations (9) imply the least amount of flux is consumed in setting up a pinch by starting with as high a value of the toroidal flux Ψ_z as possible, firing the V_z banks and crowbarring them, and then reducing Ψ_z to its working value. This will give a high K and correspondingly high plasma current. Alternatively a pinch could be set up in a conventional way with relatively modest fields and then gradually built up by applying the oscillating voltages of the previous section, with due attention to gradually increasing Ψ_z and balancing resistive losses in the landings. It is interesting that the results from ηβII(6) indicate that a plasma can be set up with a relatively low flux swing in the air core of 1.1 times the poloidal flux in the plasma.

If the suggestion of this theory, namely that the application of out-of-phase oscillating voltages to the poloidal and toroidal circuits of a pinch produce an effective mean voltage in the toroidal direction, are borne out by experiment and computation we can envisage the construction of a quasi steady-state pinch. In such a device the oscillating voltages would be applied by suitable external circuitry in such a way that the current was maintained or gradually increased. In the steady state mode the pinch would have a plasma current with a fluctuating component some fraction of the mean current and there is some hope that a passive shell would exert an (albeit weakened) stabilising effect indefinitely. There is no room to list here all the properties that such a pinch might possess nor to discuss the engineering parameters. The currents and voltages necessary in such a pinch would be rather less than in the setting up phase of a standard pinch, but required for much longer times. Many physics questions would be raised, not least the effect on the transport - however such a device could be run in combination of different modes; for example in the oscillating voltage mode to get the current in and in a fixed voltage mode (positive or negative) to control the plasma behaviour.

References

1) A.A. Newton and E.P. Butt, this conference proceedings, p

2) A.A. Newton and J.W. Johnston, this conference proceedings, p

3) J.B. Taylor, Pulsed High Beta Plasmas, Pergamon Press 1976, p.59

4) P.L. Mondino, Proceedings 9th Symposium on Fusion Technology 1976, p.149

5) S. Ortolani and G.Rostagni, Pulsed High Beta Plasmas, Pergamon Press 1976, p.335

6) A. Buffa et al, 9th European Conference on Controlled Fusion and Plasma Physics, 1979

THE EDGE REGION OF RFP AND SPHEROMAK PLASMAS

F. W. Perkins
Princeton University
Princeton, NJ 08544

E. J. Caramana
Los Alamos Scientific Laboratory
Los Alamos, NM 87545

I. Introduction

In this paper we explore the effect of the edge region on the slow, field-programming formation mode of RFP's and Spheromaks. In the ideal field programming or pitch-programming scenario both poloidal flux ϕ_p and toroidal flux ϕ_t are simultaneously introduced into the plasma by toroidal E_ϕ and poloidal E_θ electric fields respectively. These fields are frozen into the conducting plasma, which is assumed to be continuously created at the edge, and convected toward the interior with the $\vec{E} \times \vec{B}$ drift velocity (see paper—this conference). Since in the ideal model there is at most a small resistivity, this creates a nearly force-free equilibrium. The assumption of a small resistivity near the edge of the plasma may not be valid due to impurity cooling or microinstabilities. We explore the effect of a small resistive layer near the plasma edge on the ideal pitch-programming scenario.

II. Physics Model

We assume a cylindrical geometry with periodic length $2\pi R$ (R = major radius) and minor radius a, and cylindrical symmetry so that all quantities depend only on the radial coordinate r. The formation time T defined by ϕ_p/E_z is taken to be much longer than the Alfvén transit time across the minor radius T_A so that the plasma evolves through a series of equilibrium states. The parallel resistivity $\eta_\parallel$ is assumed to be large only near the edge.

Using the above assumptions we can write an equation governing the magnetic flux diffusion near the edge. First, note that

$$\dot{\phi}_p = 2\pi R E_z c = V_z = 2\pi R B_\theta U \quad , \quad \dot{\phi}_t = -2\pi a E_\theta c = -V_\theta = -2\pi a B_z U \quad ,$$

where U is the plasma velocity at the edge. It follows that

$$\frac{-\dot{\phi}_t}{\dot{\phi}_p} = \frac{V_\theta(t)}{V_z(t)} = q(t) = \frac{a}{R} P(t, r = a) \quad ,$$

where $P = rB_z/aB_\theta$ is the toroidal flux per unit poloidal flux or pitch of a field line. It is convenient to discuss the diffusion and convection of the magnetic field in terms of the pitch. Defining the independent variable ϕ by $\phi = \int_r^a B_\theta dr$ the evolution equation for P can be written as[1]

$$\frac{\partial P}{\partial t} + \dot{\phi}_p \frac{\partial P}{\partial \phi} = \frac{\partial}{\partial \phi} D \frac{\partial P}{\partial \phi} \quad , \tag{1}$$

where $D = c^2 \eta_\parallel B_\theta^2/4\pi$. The boundary condition on this equation at $\phi = 0$ follows from toroidal flux conservation and Eq. (1) and can be written as

$$E_\theta + E_z \frac{B_z}{B_\theta} \equiv E_z(P - P_0) = \frac{D}{c} \frac{\partial P}{\partial \phi} \quad , \tag{2}$$

where $P_0 = -E_\theta/E_z$ is the applied pitch at the plasma edge.

The steady state solution of Eq. (1) is given by $E_z = 0$, $P = P_0 = $ const. Suppose we now introduce more flux into the system so that $E_z = $ const. > 0. Then we can define $P_0(t) = P_0 + \delta P_0(t)$, $\delta P = P - P_0$, in terms of which Eqs. (1-2) become

$$\frac{\partial}{\partial t} \delta P + c E_z \frac{\partial}{\partial \phi} \delta P = D \frac{\partial^2}{\partial \phi^2} \delta P \quad , \tag{3}$$

$$E_z(\delta P - \delta P_0) = \frac{D}{c} \frac{\partial}{\partial \phi} \delta P \quad , \tag{4}$$

where we have now taken D to be constant. Introducing the nondimensional variables $\eta = cE_z\phi/D$, and $\tau = c^2E_z{}^2t/D$, Eqs. (3-4) become

$$\frac{\partial}{\partial \tau} \delta P = -\frac{\partial}{\partial \eta} \delta P + \frac{\partial^2}{\partial \eta^2} \delta P \tag{5}$$

$$\delta P - \delta P_0 = \frac{\partial}{\partial \eta} \delta P \tag{6}$$

Equations (5) and (6) govern the plasma response to applied electric fields described by δP_0. They can be solved by the method of Laplace transforms. Taking the solution of Eq. (5) which decays towards the plasma interior the answer is

$$\delta P = \frac{1}{2\pi i} \int_{-i\infty}^{i\infty} e^{\gamma\tau - K\eta} \frac{\delta P_{0\gamma}}{1 + K} d\gamma \quad , \tag{7}$$

where $\gamma = K + K^2$ and $\delta P_{0\gamma}$ is the Laplace transform of δP_0. Let us suppose that $\delta P_{0\gamma}$ is large only for $\gamma \ll 1$, then $K = \gamma$, which from Eq. (7) yields $\partial \delta P/\partial \tau = -\partial \delta P/\partial \eta$. Then iterating on Eq. (6) gives

$$\delta P = \delta P_0 - \frac{\partial}{\partial \tau} \delta P_0 \tag{8}$$

which also applies to the interior region $\eta < \tau$ since the decay of δP away from the wall $\sim e^{\gamma\eta}$ is small. So the relative departure of δP from the applied δP_0 is $\sim 1/\delta P_0 \, \partial \delta P_0/\partial \tau \sim \gamma \ll 1$. (Note that for $\eta > \tau$, $\delta P = 0$. This says that the initial pitch $P = P_0$, which is now in the region $\phi > cE_zt$, is unperturbed, i.e., can only move adiabatically.)

The assumption that $\gamma \ll 1$ means that

$$\frac{1}{\gamma} = \frac{c^2 E_z^2 T}{D} = \left(\frac{4\pi a^2}{c^2 n_\parallel T}\right) \left(\frac{c^2 E_z^2 T^2}{a^2 B_\theta^2}\right) \gg 1 \quad,$$

or since

$$cE_z T/aB_\theta \sim 1, \text{ it follows that } \quad T \ll \frac{4\pi a^2}{c^2 n_\parallel} \equiv \tau_R \quad .$$

This means that the formation time τ_R scale must be fast compared to the diffusion time scale measured in terms of the edge resistivity. For the resistive theory used here to apply we must require $T \gg \tau_{ei}$, where τ_{ei} is the collision time. Since $\eta \sim m_e/ne^2\tau_{ei}$, these two inequalities can be conveniently summarized by the requirement that

$$\left(\frac{\omega_{pe}^2 a^2}{c^2}\right)_{edge} = \left(\frac{n_e}{6\times 10^8 \text{cm}^{-3}}\right) \left(\frac{a}{20\text{cm}}\right)^2 \gg 1 \quad,$$

which is easy to satisfy.

Let us now consider the relative size of the parallel and perpendicular electric fields. From $E_\parallel/E_\perp \sim \vec{E}\cdot\vec{B}/\vec{E}\times\vec{B}$ we have

$$\frac{E_\parallel}{E_\perp} = \frac{P_0 - P}{1 + PP_0} \sim \frac{\delta P_0 - \delta P}{1 + P_0^2} \sim \gamma \ll 1 \quad .$$

So we see that $E_\parallel$ is much smaller than $E_\perp$. We can estimate the size of $E_\parallel$ from

184

$$E_{\parallel} \sim E_z \frac{(\delta P - \delta P_0)}{(1 + P^2)^{1/2}} \sim \frac{\delta P_0 E_z \gamma}{(1 + P^2)^{1/2}} ,$$

which gives $E_{\parallel} \sim \frac{cB_\theta}{4\pi a} \eta_{\parallel} \sim \eta_{\parallel} j_{\parallel}$. Thus, the parallel electric field generated is just that required to maintain the current against resistivity.

Although $E_{\parallel}$ is small compared to $E_{\perp}$ it may still be large enough to create runaway electrons and an associated anomalous $\eta_{\parallel}$. To prevent runaway electrons we must satisfy the inequality

$$\frac{eE_{\parallel}\tau_{ei}}{m\bar{v}_e} = \frac{cB_\theta}{4\pi ena\bar{v}_e} \simeq \frac{v_d}{\bar{v}_e} < 1 \quad \text{or} \quad ,$$

$$n > 3 \times 10^{12} \text{cm}^{-3} \left(\frac{B_\theta}{5KA}\right) \left(\frac{20cm}{a}\right) \left(\frac{100ev}{T_e}\right)^{1/2} .$$

Therefore, there is a very real possibility of driving runaway electrons near the edge.

III. Conclusions

1. With appropriate formation time scale T $\tau_R \gg T \gg \tau_{ei}$ and good conducting plasma at the edge, the edge magnetic field adjusts itself to be perpendicular to the applied electric field.

2. The parallel electric field is just that needed to sustain currents required by the force-free equilibrium against resistivity. A large skin current does not appear.

3. The pitch profile $P_0(t)$ [or q(t) profile] is convected away from the edge region by the $\vec{E} \times \vec{B}$ velocity and trapped in the plasma by the frozen-in-flux condition.

4. RFP's and spheromaks are devices to be filled with flux, not current.

5. Anomalous resistivity due to a runaway electric field may be important near the edge and provides for rapid edge heating.

REFERENCE

1. E. J. Caramana and F. W. Perkins, PPPL-1626, Jan. 1980.

STARTUP OF THE RFP IN A QUASI-ADIABATIC MODE

E. J. Caramana
Los Alamos Scientific Laboratory
University of California
Los Alamos, NM 87545

ABSTRACT

The equations describing the purely adiabatic formation of the reversed-field pinch are solved. This method of formation in principle remedies the problem of flux consumption during the startup phase of this device.

1. INTRODUCTION

It is well known that diffuse, stable reversed-field pinch (RFP) equilibria exist at a relatively high value of beta[1,2]. However, difficulty remains in accessing these states.

The usual manner in which a RFP discharge is initiated is to begin with a large toroidal bias field; then the toroidal current is raised as the toroidal field is reversed. This necessarily places the toroidal current exterior to the positive toroidal bias field. Consequently, a diffuse current profile can only result from current diffusion across this field. Approximately one third of the magnetic field energy is lost during this diffusion and the discharge is very turbulent[3]. If this energy is retained as plasma internal energy the plasma beta would be larger than could be contained[4] (It does not matter if the current penetration is due to an anomalous resistivity since the amount of heating depends only on the initial and final states of the plasma). Also, in scaling to large devices the ratio of the energy lost to the vacuum wall area becomes greater. It is thus difficult to believe that a RFP reactor could be initiated in this diffusive manner.

The loss of energy due to current diffusion, and also the associated global turbulence of the discharge, can in principle be avoided by raising the toroidal magnetic field and the toroidal current together on a time scale long compared to the Alfven transit time (so that magnetohydrostatic equilibrium is maintained), but short compared to the magnetic field diffusion time (so that a small plasma beta results at the end of the formation). This is known as pitch-programming and has been mentioned in qualitative terms for some time[5]. It is a formation senario which requires adiabatic compression of the plasma but does not require resistive heating as a consequence of a diffuse current profile.

II. ADIABATIC FORMATION

Consider the ideal MHD equations with the inertia neglected,

$$\frac{\partial n}{\partial t} + \underline{\nabla} \cdot \underline{V}n = 0 \quad , \tag{1}$$

$$\frac{\partial \underline{B}}{\partial t} - \underline{\nabla} \times \underline{V} \times \underline{B} = 0 \quad , \tag{2}$$

$$\frac{\partial T}{\partial t} + \underline{V} \cdot \underline{\nabla} T - \frac{1}{3} T \underline{\nabla} \cdot \underline{V} = 0 \quad , \tag{3}$$

$$\underline{\nabla} p = \underline{J} \times \underline{B}/c \quad , \tag{4}$$

where $p = nT$. In one dimension and in cylindrical geometry, which is the case considered here, these equations retain only the radial component of the velocity $\underline{V}$. This component, V_r, is determined implicitly by Eq. (4) and since we consider no dissipation is driven solely by the applied electric field at the boundary (we assume that plasma exists all the way to the wall radius $r = a$). Progress can be made analytically in solving Eqs. (1-4) by transforming them into a normalized poloidal flux representation and changing the dependent variables.

We define the new independent variable x by

$$x = \int_0^r \chi(r', t) dr' \quad , \quad \chi = B_\theta(r, t)/\phi_{PT} \quad , \tag{5}$$

where $\phi_{PT} = \int^a B_\theta(r, t) dr$. With $\phi \equiv \phi_{PT}(t)/\phi_0$ and $\dot{\phi} \equiv \partial_t \phi_{PT}/\phi_0$, where $\partial_t \phi_{PT} = E_z(r \stackrel{Q}{=} a, t)$ and ϕ_0 is a reference poloidal flux, we define the new dependent variables,

$$Y \equiv r^2/a^2 \quad , \quad Y' \equiv \frac{\partial Y}{\partial x} = \frac{2r\phi_0 \dot{\phi}}{a^2 B_\theta} \quad , \tag{6a,b}$$

$$\tilde{P} \equiv \frac{rB_z}{aB_\theta} \dot{\phi} \equiv P\dot{\phi} \quad , \tag{7}$$

$$\tilde{N} \equiv \frac{n}{n_0} Y' \equiv N\dot{\phi} \quad , \tag{8}$$

$$\tilde{\xi} \equiv \left(\frac{T}{T_0}\right)^{3/2} Y' \equiv \xi\dot{\phi} \quad , \tag{9}$$

with n_0 and T_0 as a reference density and temperature. The Eqs. (1-3) in one dimension have the same form when expressed in terms of these variables, namely,

$$\frac{\partial U}{\partial t} = \frac{\partial}{\partial x} \frac{\dot{\phi}}{\phi} \times U , \qquad\qquad (10a,b,c)$$

$$\frac{\partial^2 Y}{\partial x^2} = \frac{Y'(\tilde{P}^2 + 2Y\phi^2)' + \frac{1}{2} Y'^{1/3}(\tilde{\tilde{N}}\tilde{\xi}^{2/3})'}{2(\tilde{P}^2 + Y\phi^2) + 5/6Y'^{1/3}\tilde{\tilde{N}}\tilde{\xi}^{2/3}} . \qquad\qquad (11)$$

The boundary conditions on Eq. (10) are that known values of $\tilde{P}(t)$, $\tilde{N}(t)$, and $\xi(t)$ be given at $x = 1$. The condition $V(r = x = 0) = 0$ in defining the transformation assures that the regularity condition on P, N and ξ at the origin is satisfied. For Eq. (11) we have that $Y(x = 0) = 0$ and $Y(x = 1) = 1$.

Since Eq. (10) is a linear first-order hyperbolic equation we can solve it exactly. By considering ϕ in place of t as an independent variable and defining $v = xU$, Eq. (10) becomes $\phi \, \partial v/\partial \phi = x \, \partial v/\partial x$. Thus the solution is $v = f(x\phi)$, where f is any arbitrary function of the characteristics $x\phi = \text{const}$.

Since values of v propagate unperturbed along the lines $x\phi = \text{const.}$, from Eqs. (7-9), so do the quantities P, N, and ξ. These are the pitch of a field line (safety factor q/aspect ratio), the density per poloidal flux, and the entropy per particle. We thus have a solution for P, N, and ξ along the characteristics, and Eq. (10) is now defined over the whole domain $0 \leqslant x < \infty$ converting an initial-boundary value problem into a pure initial value problem. As an example, consider the force free Bessel function model (BFM) given by

$$B_z(r) = B_0 J_0(\mu \frac{r}{a}) , \quad B_\theta(r) = B_0 J_1(\mu \frac{r}{a}) . \qquad\qquad (12a,b)$$

We can find all previous adiabatic states by forming the quantity $P(x, \phi = 1)$ at the final time for this model. At $\phi = \phi_1$, $(\phi_1 < 1)$ we have $P(x, \phi = \phi_1) = P(x/\phi_1, \phi = 1)$. Then Eq. (11) can be solved numerically to obtain the configuration $Y(x)$ corresponding to $P(x, \phi_1)$ (we can likewise include N and ξ). Since $x = 0$ is a characteristic we see that the initial state $\phi \rightarrow 0$ is one where $P(x)$ is a constant over $0 \leqslant x \leqslant 1$ given by $P(x = 0, \phi = 1)$. This is a similarity solution of the adiabatic problem, and is possible because there is only one time scale, the formation time, in these equations.

To specify $\phi(t)$ we must know $E_z(a,t)$, the z electric field at the wall. We see that as long as $E_z(a,t)$ remains positive, flux will propagate along the characteristics and into the plasma region. In Fig. (1) we show the electric fields $E_z(a,t)$ and $E_\theta(a,t)$, which if applied at the plasma chamber wall yield a BFM with $\mu = 2.7$. We have chosen $E_z(a,t)$ to be a parabola and have computed $E_\theta(a,t)$ using the fact that $P(x = 1, \phi(t)) = E_\theta(a,t)/E_z(a,t)$.

Two important features of a nearly force-free adiabatic startup should be noted:

189

a) The sign the total Poynting vector at the plasma wall depends only on the sign of $E_z(a,t)$ as long as the total toroidal current remains positive. (This is seen from Fig. 1, or equivalently, from $\underset{\sim}{E} \cdot \underset{\sim}{B} = 0$ and the expression for the Poynting flux.)

b) The toroidal current and the toroidal magnetic field at the wall both reverse direction when $E_\theta(a,t)$ changes sign.

This model implies that plasma be created at the wall in order to freeze in the magnetic flux so that it can be convected inward. Thus a source for this plasma may have to be provided near the wall by the injection of neutral gas during startup. Atomic physics processes are thus expected to be important in the edge region. There is also the possibility of driving runaway electrons[6].

In Fig. (2) we show the trajectory of the force free adiabatic startup of Fig. (1) with reference to the BFM as a function of F and θ $\left(F = B_z(a)/<B_z> \, , \right.$ $\theta = B_\theta(a)/<B_z> \right)$. These states have higher energy than BFM states[7]. We consider the decay to BFM states of two states on this adiabatic curve corresponding to $\phi = 1/3$ and $\phi = 2/3$. The resistive decay is assumed to conserve the toroidal flux and the magnetic helicity $K = \int dV \, \underset{\sim}{A} \cdot \underset{\sim}{B}$ as proposed by Taylor[7]. The BFM states that are found under these conditions show a shift toward increasing θ and decreasing F. A flattening of the total current and a transfer of magnetic energy from the poloidal to toroidal magnetic field occur. About .5% of the magnetic energy is converted into internal energy of the plasma, a rather small amount. During the decay approximately 7% of the poloidal flux is lost. We thus see that such a decay can take place without catastrophic consequences.

The short dotted curve in Fig. (3) shows the range of initial states on the F-θ diagram where one must start to arrive adiabatically at BFM states with θ in the range 1.2 to 1.6. We see that the initial θ is about .8, which means that the plasma must start in a pinch like state.

IV. CONCLUSION

We have shown how the electric fields and the plasma density at the wall of the containing vessel during a nondissipative RFP startup can be analytically calculated as a function of time to give a desired final plasma and magnetic field profile — information of importance to experimentalists. It has been shown that if the states through which the plasma adiabatically evolves decay resistively, subject to reasonable constraints, that the magnetic energy lost is small.

REFERENCES

1. D. C. Robinson, Plasma Phys. 13 439 (1971).
2. D. C. Robinson, Nucl. Fus. 18 939 (1978).
3. E. P. Butt, A. A. Newton, Pulsed High Beta Plasmas, Pergamon Press 1976, p. 425.
4. D. A. Baker, J. A. Phillips, Phys. Rev. Lett. 32 202 (1974).
5. A. A. Newton, private communication.
6. F. W. Perkins, E. J. Caramana, The Edge Region of RFP's and Spheromaks, RFP workshop, LASL, April 1980.
7. J. B. Taylor, Phys. Rev. Lett. 33 1139 (1974).
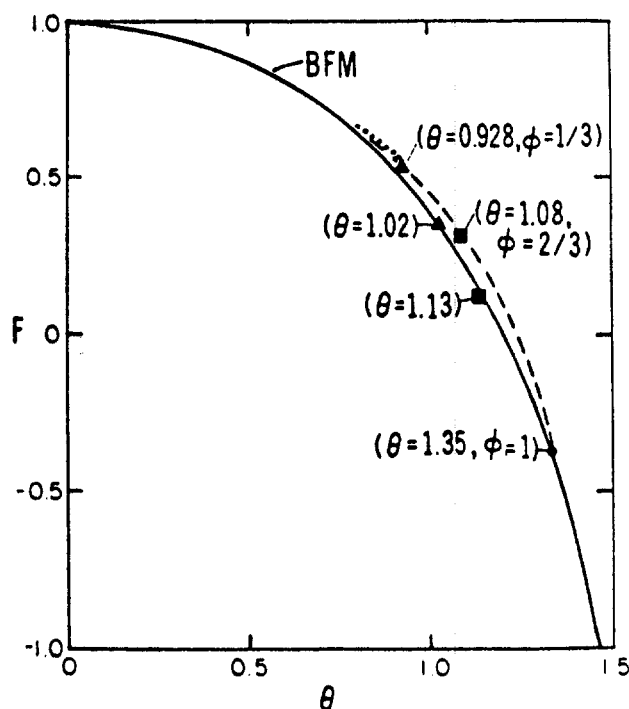
Fig. 1

The electric fields E_z and E_θ that must be applied at the wall of the device to effect a purely adiabatic startup whose result is a BFM state with $\theta = 1.35$ ($\theta = \mu/2$) are given as a function of time in arbitrary units.
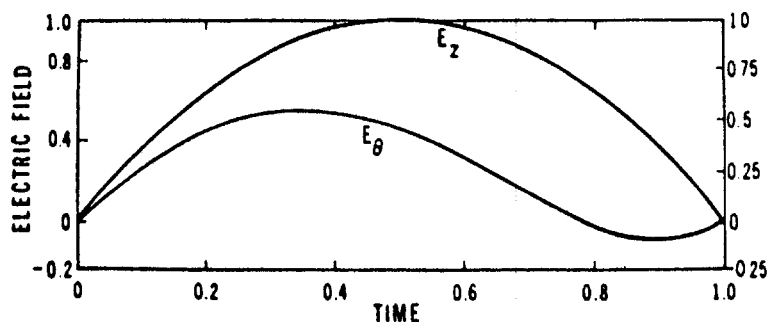
Fig. 2

Shown is the BFM trajectory (solid line) as a function of F and θ. Also shown (dashed) line) is the trajectory followed by a plasma on a purely adiabatic startup ending in a BFM state with $\phi = 1/3$ and $\phi = 2/3$ respectively. On the solid curve these symbols indicate the lower energy BFM states to which these states may resistively decay. The dotted line indicates the range of initial values of F and θ for a plasma to evolve adiabatically to a BFM state with θ in the range 1.2 to 1.6.

ZT-40 STARTUP CALCULATIONS WITH VARIOUS ANOMALOUS TRANSPORT MODELS*
PREPARED FOR THE LOS ALAMOS RFP WORKSHOP
27 APRIL - 1 MAY, 1980

R. N. Byrne and C. K. Chu**
Science Applications, Inc., La Jolla, CA 92014

The purpose of this work is to attempt a 1D numerical simulation of the start up phase of ZT-40, starting from the post-implosion time. We begin with a cold low density plasma with modest toroidal embedded field, since we are prohibited from calculating the breakdown, due to code shortcomings. We aim to calculate plasma buildup and heating, and evolution of both componants of field and current to a final state.

Since our code has no model for the self field reversal which can be induced in this machine, we have chosen to simulate a discharge with forced reversal. We shall explore the effects of various simple transport enhancements on the assembly. As a tool, we use the G2M code(1), run in 1D mode for the sake of economy. The only additional information from 2D would seem to be a better estimate of the mirroring, which would not affect the transport during this phase. Another simplification is the elimination of impurity transport and the solution of rate equations from the model. We merely assume a constant fractional contamination by oxygen, or, in some runs, oxygen and silicon. The impurities are assumed to be in coronal equilibrium, and radiation rates are taken from the PPPL/LLL package of Post et al (2).

The plasma is assumed to be introduced as aneutral flux at the wall, except for an already ionized initial density of about 1/10 final. After all the plasma has been introduced, the neutral flux from the wall is just the negative of the plasma flux, i.e., ions striking the wall are neutralized and reflected with unit albedo.

All the transport models used so far have used Braginskii's(3) classical results as a base upon which other effects are piled. This transport, due to the toroidal geometry, gives rise to the Pfirsch-Schlueter enhancement, but this and other neoclassical effects are small in the early phase upon which we shall focus our attention. One effect of the classical transport which survives to plague us in the simulations is the thermoelectric current, which becomes large near the wall of this device at late times in our model. This gives rise to numerical difficulties and terminates some of the runs.

To this basic transport we add various anomalous enhancements. These include use of an effective collision frequency which is a simple multiple of classical, Alcator scaling, Chodura resistivity, and the Christiansen/Roberts prescription (4) for transport driven by Suydam instabilities.

For input we use smoothed experimental values of total toroidal current, poloidal field at the wall, and total plasma content, as functions of time. They are fairly realistic, except that the toroidal field is taken to rise, at fifty microseconds, from 1500 gauss rather that the somewhat lower values actually used. This is an attempt on our part to allow for field penetration during the breakdown phase when the resistivity is still high. The neutral flux at the wall is taken to be that necessary to force the total electron number in the machine to follow experiment. We calculate on a toroidal flux surface grid with ZT-40 dimensions.

The initial variation in toroidal field is purely geometric, being merely the 1/R variation across the ZT-40 bore, and the current densities vanish. This code cannot handle very low temperatures, so we take 5 eV (peak) as a starting temperature. The density is taken almost flat, at 10**14.

Our first observation is, not surprisingly, that classical transport fails badly to reproduce experiment. The temperature and current spike sharply off-axis, shorting out the bulk of the plasma and giving much too low loop voltage and much too high peak temperatures.

We conclude that we need more transport, and try multiplying classical by 100. The same problem occurs, however, so clearly something better is needed.

We already know something better: the prescription given by Christiansen and Roberts, which represents the effect of small scale turbulence due to Suydam modes. Their model enhances transport of particles and heat by a factor proportional to the local excess of pressure gradient to its Suydam limit. This works somewhat better, for the late time problem, as described in their work. Therefore, we adopt this transport model as basic to RFP, and return to our task of start up simulation.

We still find poor current penetration, due to the tendency of the low density region to overheat, and therefore add Chodura's model(5) of anomalous transport, as used by Sgro and Nielson(6) in their simulations of the (fast) ZT-S machine. This same model has been used by Park and Chu(7).

The model distinguishes parallel and perpendicular resistivities, and turns on when the respective drift velocities exceed a fraction of the sound speed. The parallel resistivity acts to allow field interdiffusion, thus it is responsible for pitch change on a flux surface. The perpendicular resistivity causes cross-surface particle and energy slippage. These collision fre-

quencies are used when- and where-ever they exceed the classical ones.

Now we have a model that gets us in the general realm of experiment. At ten microseconds into the calculation the current profiles no longer peak, nor do the temperatures. The central core is compressed in spite of the extra resistivity at the edge, with the toroidal field rising above the vacuum field. This latter has risen from the initial 1500 gauss to about 1800 due to the programmed increase; the actual field is about 2400, with the excess due to compression. The loop voltage is about 8000 now.

The density profile shows broad wings due to the mechanism supposed to represent buildup, namely, evolution of neutrals from the wall.

At 20 microseconds, the loop voltage is 13000. The vacuum toroidal field has not changed much, yet the central field is up to about 4000 gauss over the central twenty centimeters. The current profiles are, as intended, very broad, as are temperature and density.

By 50 microseconds the field has reversed. The density has become almost flat, as is the ion temperature. The electrons have been heated to almost 600 eV, far above the ions. The toroidal current has become almost flat, giving a poloidal field which is linear in radius. The resulting dip in $B**2$ is filled by the temperature peak.

This model produces adequate current penetration, and eliminates the skin problem but has two new difficulties. First, the loop voltage tends to be about a factor of two above that observed in ZT-40, and second, the anoalous resistance heats the electrons to very high temperatures, even though we have assumed substantial contamination with impurities (1% oxygen, 1/2% silicon).

Noting this, we proceed to try another model, which we call Alcator scaling. In this model, we add a term to the electron heat conductiviy chi, particle diffusitivity D, each term being proportional to the inverse of the electron density. Using $5x 10**19$ for chi and 1/10 that for D reduces the maximum temperature to 400eV, using $5 x 10**20$ brings it down to about 350.

Finally, removing the Chodura terms and leaving the Alcator ones also produces current penetration, though the current does not get all the way in. This gives a very cold result, with the maximum electron temperature just 25eV (at 100 microseconds). The loop voltage is around 5000 at this time, which is probably closer to experiment that the voltages obtained using Chodura resistivity.

We conclude that a mixture of Chodura and Alcator transport (plus Christiansen-Roberts) can give both temperatures and voltages that are not unreasonable, at least for the discharge considered, whereas either alone gives rise to difficulties. There are of course a large number of models considerably less ad hoc that the one used here which may be as good as or better that this one at fitting experiment, such as a dynamo model, or the reconnection being developed by Dr. Caramana for the LASL code. We hope to be able some day to predict the results of any ZT-40 shot from first principles, but for now we do have models that can be made to fit existing data.

1) Byrne, R. N., Klein, H. H.,
   Journal of Computational Physics, 26(1978)352.

2) Post, D. E.,   Jensen, R. N.,   Tarter, C. B.,
   Grasberger, W. H., Lokke, W. A.,
   Atomic Data and Nuclear Tables 20(1977)399.

3) Braginskii, S. I.,
   Reviews of Plasma Physics, 1,(1965), New York

4) Roberts, K. V., Christiansen, J. P., Long, J. W.,
   Computer Physics Communications 10(1975)264.

5) Chodura, R.,
   Nuclear Fusion 15(1975),55

6) Sgro, A. G., Nielson, C. W.
   Physics of Fluids 19(1976),126.

7) Park, W., Chu, C. K.,
   Nuclear Fusion 17(1977),1100

IDEAL MHD STABLE START-UP*

by

R. A. Nebel, R. W. Moses[†] and G. H. Miley
Fusion Studies Laboratory
University of Illinois

Introduction

One of the most important unsolved problems for the Reversed Field
Pinch is how to initially set up the required field profiles. Baker and
Phillips[1] have shown that diffusive start-up processes generally require
large energy losses to reach an equilibrium in the post-implosion phase.
Also, this approach generally results in a high β post-implosion plasma
which does not have enough current to significantly heat the plasma
further.

Consequently, it is desirable to find a non-diffusive start-up technique
which maintains MHD stability to insure minimal energy loss. Newton[2]
originally suggested such an approach based on a convective start-up
technique. This procedure satisfies the necessary stability criterion
that the pitch ($\underline{P} \equiv rB_\phi/B_\theta$) of the field lines does not have a minimum[3].
We have extended Newton's technique using RFPBRN[4] (a transport and stability
code) and have found a start-up scenario that theoretically maintains
ideal MHD stability to global and local modes during both the start-up and
burn phases.

Technique

It is easily shown that for an ideal plasma, conservation of toroidal
and poloidal magnetic flux implies that pitch is also conserved. Conse-
quently, if plasma is fed in at the wall and the fields are simultaneously

[†]Los Alamos Scientific Laboratory

programmed, the pitch initially present in the plasma will be conserved as the plasma is compressed. This condition is also approximately true for a resistive plasma and consequently, the shape of the pitch profile can be controlled externally.

A natural boundary condition for a Lagrangian code like RFPBRN is the placement of the plasma boundary. Since convective start-up involves a plasma compression, we have chosen to model it by starting the plasma boundary initially at ten times the vessel radius and then moving the boundary inward as the simulation moves forward in time. The fields and gas feed rate at the wall are then monitored to determine what programming would be required to do this on an experiment. The equation chosen for the boundary is:

$$r_p = \begin{cases} 10a \left(0.9 \left((\tau_R - t)/\tau_R\right)^4 + .1\right) & t < \tau_R \\ a & \geq \tau_R \end{cases} \qquad (1)$$

where a is the vessel radius, τ_R is the rise time, and t is the present time in the simulation.

The profiles necessary to maintain stability during the heating and burn phases are known, so the question is how to properly program the fields to arrive at these desired profiles. Since start-up is approximately an adiabatic compression, the initial profiles (when the virtual plasma boundary is at ten times the vessel boundary) are arrived at by adiabatically expanding the desired post-implosion profiles to ten times the vessel radius. This insures that the final profiles will be near the desired ones.

Results

Using the programming procedure described above, a start-up scenario has been found which has ideal MHD stability to both local (Suydam)[5] and

197

gross modes during the start-up and burn phases. The gas feed rate and
toroidal and poloidal fields at the wall sufficient for stability are
shown in Figure 1. Start-up is achieved in 1 msec. although slower times
are possible.
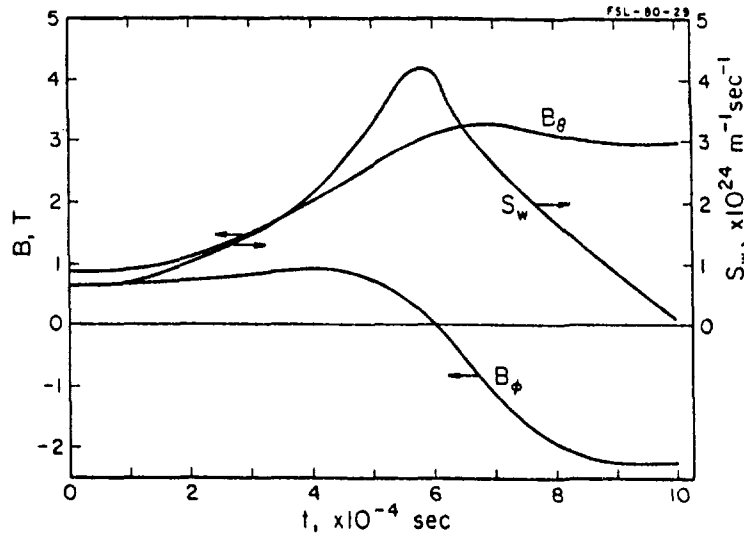
Figure 1. Gas feed rate and magnetic fields at the wall during start-up.

Maintenance of stability during start-up and burn requires peaking
both the toroidal current density and the particle density off axis.
Peaking the particle density off-axis leads to an off-axis pressure peak
which stabilizes interchange modes in the weakly sheared central plasma
region. Peaking the current density off-axis stabilizes gross current
driven kinks in the prereversed state.

Figure 2 shows the initial, start-up termination, and final (end of
burn) current profiles for the RFP. Note that the toroidal current does
diffuse into the central plasma region, but not fast enough that it spoils
the plasma's stability characteristics. However, the toroidal current
remains slightly peaked off-axis during the entire burn.
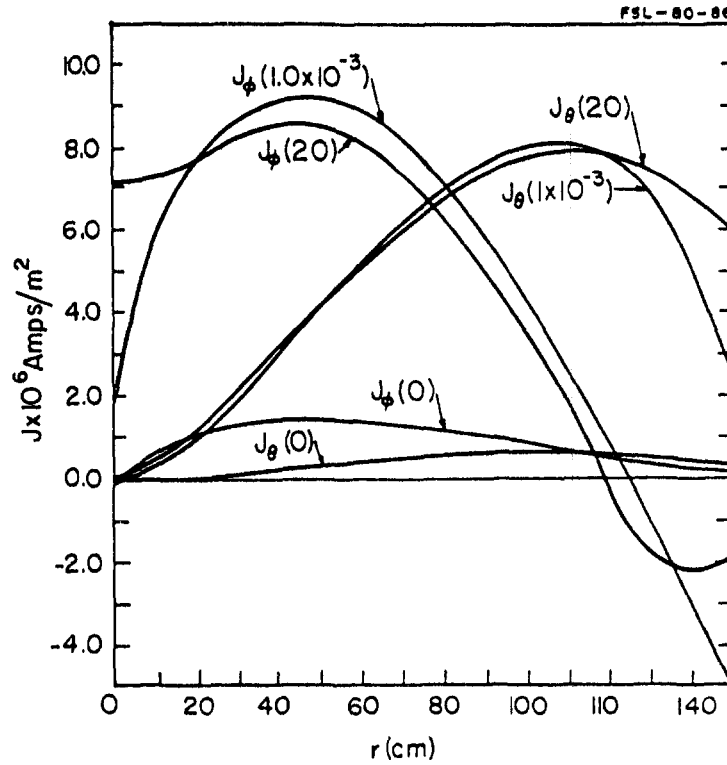
Figure 2. Current density profiles initially, at
the end of start-up, and at the end of
the burn.

Since the toroidal current profile is not an input parameter to RFPBRN,
peaking the current density off-axis was accomplished by flattening the
toroidal field on-axis. The toroidal field profile sufficient to do this
is

$$B_\phi = B_{\phi_0} \left[\frac{2r/r_p}{1+r/r_p} J_0(\alpha r) + \frac{1-r/r_p}{1+r/r_p} \right] \qquad (2)$$

where $\alpha = 2.405/(.93\ r_p)$. Bessel function fields alone were found to be
violently unstable.

Flattening the toroidal field is a stabilizing influence on the plasma
since it decreases the poloidal field near the axis which drives the insta-
bility. Even though the Bessel function profile satisfies the necessary
criterion of not having a pitch minimum, the large poloidal field caused by
the diffuse current profile makes it unstable. Consequently, this is a more

199

stringent stability criterion than just maintaining a minimum-free pitch profile.

The above characteristic appears to have been qualitatively verified on ZT-40.[6] Results of field programming indicate that much better plasma performance is achieved when the poloidal circuit rise lags the toroidal circuit. This implies that putting a seed toroidal field in the plasma leads to better stability which is what the simulations predict.

Summary

A start-up scenario which theoretically predicts ideal MHD stability for both local and global modes during the start-up and burn phases for an RFP reactor has been found. Toroidal current density must be peaked off-axis in the prereversed phase in order to maintain stability. This is consistent with experimental observation. Density and pressure are peaked off-axis in order to stabilize Suydam modes in the weakly sheared plasma interior during the burn phase.

References

1. D. A. Baker and J. A. Phillips, Physical Review Letters, 32, 5, 202-205 (1974).

2. A. A. Newton, "Pitch Convection," HBTXII Workshop (1974).

3. D. C. Robinson, Plasma Physics, 13, 434-462 (1971).

4. R. A. Nebel, et al., "Comparison of Zero-Dimensional and One-Dimensional Thermonuclear Burn Computations for the Reversed Field Pinch Reactor (RFPR)," Los Alamos informal report LA-8185-MS (1980).

5. B. R. Suydam, "Stability of a Linear Pinch," p. 1354, USA (1958).

6. R. B. Howell, private communication.

Classical Transport in the Reversed Field Pinch

Allen H. Boozer

Plasma Physics Laboratory, Princeton University

Princeton, New Jersey 08544

Classical transport coefficients critically depend on the number of symmetry directions. Since theorists concentrate on symmetric idealizations, the high sensitivity of the transport coefficients to symmetry breaking terms has not been generally appreciated. Remarkably, the transport coefficients for the physical situation--no absolute symmetry directions--is the simple sum of three contributions, gyromotion, banana, and ripple transport. With one symmetry direction, as in a perfect torus, there is banana and gyromotion transport. With two symmetry directions, as in a circular cylinder, there is only gyromotion transport. The usual model of the reversed field pinch is a circular cylinder so only gyromotion effects have been included in the model.

Both the toroidicity of the reversed field pinch and the noncircularity of its pressure surfaces break the poloidal symmetry and cause banana-type transport. If the poloidal symmetry breaking is small, the resulting enhancement of the transport coefficients depends only on the variation in the magnetic field strength in a constant pressure surface. The standard analytic model of banana transport[1] assumes there is only one Fourier component to the field strength variation in a pressure surface; so the field strength can be written

$$B = B_o \left[1 + 2\epsilon \sin^2 (\theta/2) \right]$$

with B_o and ϵ constant in the pressure surface.

There are four banana transport effects. First, there is the enhanced particle and energy transport coefficients. The banana diffusion coefficients scale as

$$D_B \simeq \sqrt{\epsilon} \, \rho_p^2 \, (B_T/B)^2 \, \nu$$

with ρ_p the poloidal gyroradius--the gyroradius in the poloidal field alone--B_T the toroidal field strength, and ν the collision frequency. The exact numerical value for the various diffusion coefficients can be obtained by comparing to the well-known

tokamak limit,[1,2] $B_T/B \to 1$. Second, there is an enhanced parallel resistivity

$$\eta_B \simeq \eta_{||} (1 + \sqrt{\varepsilon}) .$$

Third, there is a parallel current induced by the pressure gradient

$$j_{||} \simeq \sqrt{\varepsilon} \, (c/B_p)(B_T/B)(dP/dr)$$

with B_p the poloidal field strength. Finally, a toroidal electric field gives an enhanced radial drift called the Ware pinch

$$v_r \simeq -c\sqrt{\varepsilon}(E_{||}/B_p)(B_T/B) .$$

The factors B_T/B in the reversed field pinch transport formulae are ignored in the standard neoclassical papers. The required modifications are easily demonstrated provided the correct form for the radial drift is used. Using the standard form for a toroidally symmetric magnetic field

$$\vec{B} = g(\psi)\vec{\nabla}\phi + \vec{\nabla}\phi \times \vec{\nabla}\psi$$

one can show the radial drift is

$$\vec{v}_D \cdot \vec{\nabla}\psi = v_{||} \frac{\vec{B} \cdot \vec{\nabla}\theta}{B} \left[\frac{\partial}{\partial\theta} g\rho_{||}\right]_{E,\mu,\psi,\phi}$$

from the expression[3]

$$\vec{v}_D = (v_{||}/B)(\vec{B} + \vec{\nabla} \times \rho_{||}\vec{B}) .$$

In a revised field pinch, the banana transport will dominate only near the magnetic axis where it will flatten the profiles.

A real reversed field pinch does not have perfect toroidal symmetry and even toroidal asymmetries of 1/2% can have important transport effects. This enhancement of the transport, called ripple transport, is caused by the banana orbits not closing as they would if there were perfect symmetry. An important feature of ripple transport is that like-particle collisions contribute to the transport and the transport fluxes depend on the radial

electric field.[4] Both gyromotion and banana transport of particles vanish if only like-particle collisions are present, and they are independent of the radial electric field. This difference in behavior is due to momentum conservation in symmetry directions.

Some analytic work has been done on ripple transport. However, the reversed field pinch is in a much lower collisionality regime than a tokamak. In the collisionality regimes of most interest for reactors, the only real information has come from a Monte Carlo simulation of transport.[5] The reversed field pinch Monte Carlo runs made by Gioietta Kuo-Petravic and me are illustrated in the figure. The code simulates the banana and the ripple transport but not the gyromation transport.
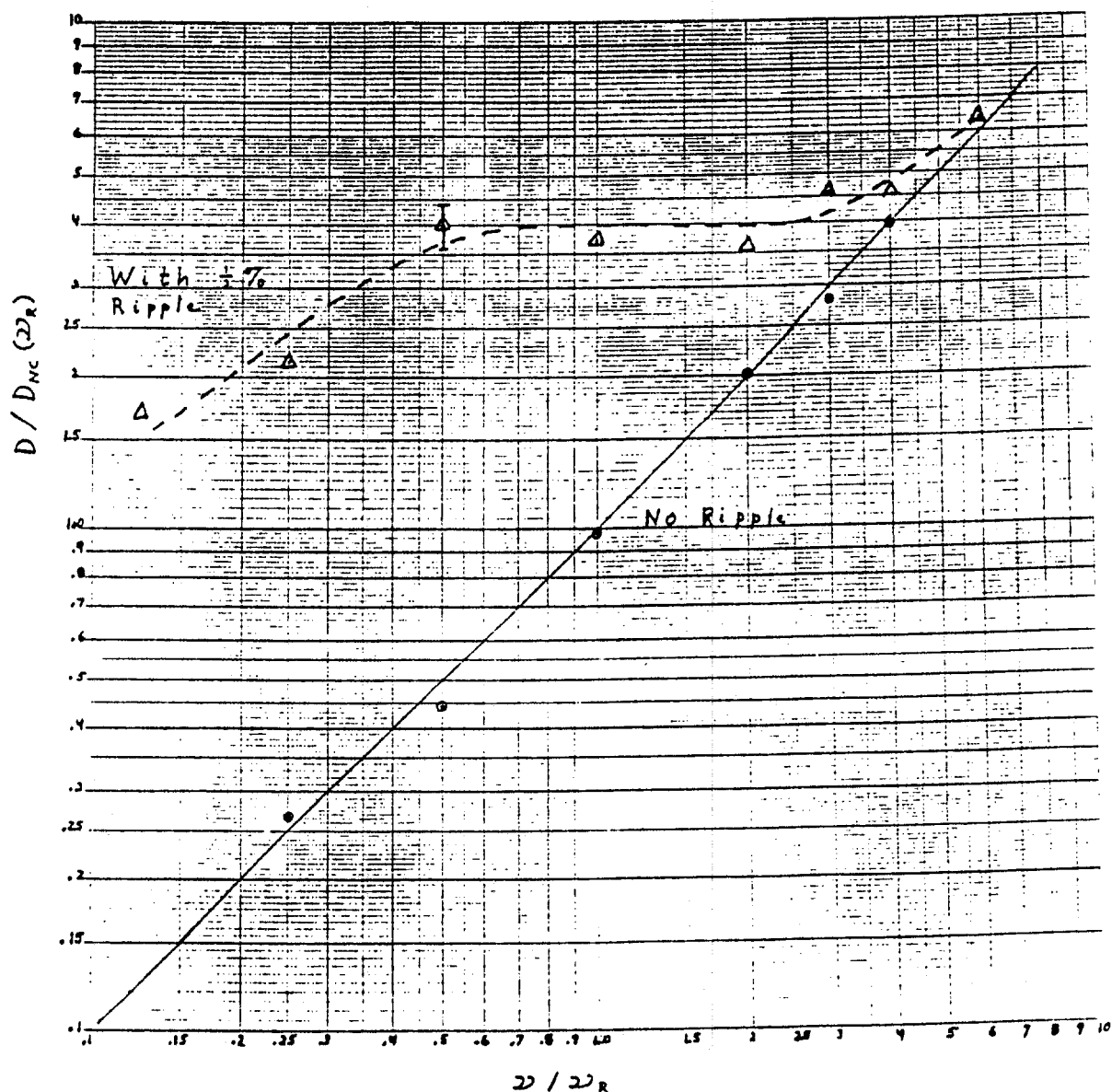
The diffusion coefficient of a thermal test particle is illustrated with 1/2%, N = 10, toroidal ripple, and with no ripple. The no ripple case gives the standard banana regime transport. The collision frequency ν is scaled by ν_R in the figure with ν_R the collision frequency for a thermal particle at 10 keV and 10^{14} particles/cm^3. The diffusion coefficient is normalized by the neoclassical (banana) transport at $\nu = \nu_R$. We assume the plasma radius is 100 cm and the aspect ratio is 7. The flux surface on which the transport is studied is half way out in toroidal flux, the safety factor $q = 1/7$ on that surface, and B is assumed to be 15 kG. The magnetic field strength in the surface is assumed of the form

$$B = B_o [1 + 2\varepsilon \sin^2 (\theta/2) + \delta \cos N\phi]$$

with $\delta = 0.005$. Clearly, a small ripple gives a large effect at low collisionality (note the log-log scale) and a more detailed study of ripple transport in reversed field pinches is important.

Small asymmetries have other important effects. In systems with at least one symmetry direction, magnetic field lines lie in exact surfaces and the conserved canonical momentum in the symmetry direction assures long time particle confinement in the absence of collisions. In an asymmetric plasma, magnetic field lines form islands if the perturbing field resonates with the unperturbed field lines. The radial extent of these islands is

$$\Delta \approx \left| \frac{q}{dq/dr} \frac{RB_1}{B_T} \right|^{1/2}$$

with q the safety factor. The radial component of the perturbation has been assumed of the form

$$B_r = B_1 \exp[i(n\phi - m\theta)] \quad .$$

The island is centered about the surface where q = m/n. If there are sets of islands about a number of surfaces and the islands from the various sets overlap, the magnetic field lines cover a finite volume (become ergodic) giving rapid electron heat transport.

Long term confinement of α particles in the trapped particle regimes of phase-space is questionable in asymmetric geometries. However, in ordinary drift orbit theory passing α's are confined provided the poloidal and toroidal gyroradii are small compared to the system size and there are good magnetic surfaces.[4]

In the past, people have assumed plasmas would self-shield against externally applied ripple. This is certainly not the case, in general. We have looked at the case where $\vec{j} = k\vec{B}$ with k constant and find the plasma instead of reducing the ripple actually intensifies it over the vacuum case.

Acknowledgment

REFERENCES

1. M. N. Rosenbluth, R. D. Hazeltine, and F. L. Hinton
    Phys. Fluids 15, 116 (1972).

2. S. P. Hirshman
    Oak Ridge Report ORNL/TM-6481.

3. A. H. Boozer
    Phys. Fluids 23, 904 (1980).

4. A. H. Boozer
    Princeton Lab. Rept. PPPL-1619 (1980).

5. A. H. Boozer and G. Kuo-Petravic
    Princeton Lab. Rept. PPPL-1703 (1980).

Current Decay and τ_E Scaling Laws Applied to

RFP Transport Calculations

J.P.Christiansen and K.V.Roberts

1. Introduction

Previous performance predictions for RFP devices like HBTX1A and RFX [1] have been based on calculations in which the toroidal current is assumed constant during the sustainment phase. It has also been assumed that electron thermal losses can be described by an anomalous electron thermal conductivity scaling proportional either to the classical or to the Bohm diffusion coefficients. In this paper we describe the effects on the results of transport calculations when different assumptions are made:

(1) The toroidal current is allowed to decay on a characteristic timescale τ_I, i.e. $I \sim e^{-t/\tau_I}$ and

(2) The electron thermal losses are described by an empirical scaling law for the energy confinement time τ_E obtained from Tokamak experiments.

The calculations are carried out with the 1-D equilibrium-transport code ATHENE 1 and the details of the model used are given in [1].

2. Empirical scaling laws for τ_E

At present there is a substantial amount of experimental information [2-3] about losses in Tokamak experiments whereas little information is available from RFP experiments. The scaling laws given in [2-3] differ in their dependance upon plasma parameters. In particular the Alcator na^2 scaling law predicts $\tau_E \sim N$ where N is the line density; such a scaling law would not be beneficial to RFP experiments in which N is usually assumed to be a constant, independent of current and radius.

We have chosen an adaptation by Sheffield of the Hugill-Sheffield scaling law [2] given as

$$\tau_E^{HS} = x_1 \, n^{x2} \, I^{x3} \, R^{x4} \, A^{x5} \, a^{x6}$$

in which n, I, R, A, a have their usual meaning and $x_1 - x_6$ are constants; 3 sets of values for $x_1 - x_6$ are available. The electron thermal losses are now modelled by an anomalous diffusion coefficient

$$D_a(r) = c_a r^2 / \tau_E^{HS}(r). \tag{1}$$

The effect of replacing a Bohm or classically-scaled anomalous diffusion coefficient by the choice (1) can be seen in Figure 1. The electron temperature profile is shown for a calculation in which $D_a = c_B \, D_{BOHM}$ (full curve) and for a calculation in which D_a is given by (1). The parameters for the two calculations are identical, with c_a and c_B being adjusted to produce approximately the same

$\tau_E \approx \tau_E^{HS}$. The strong radial dependence of (1) produces a cooler outer region and this in turn lowers the configuration time τ_c compared with the values obtained for Bohm scaling. The confinement time is calculated as

$$\tau_E(t) = W(t)/L(t),$$

W,L being the total plasma energy and total loss rate respectively. Since steady states are not reached (unlike in Tokamaks), τ_E varies with time and usually reaches a maximum at $t=\tau_c$. The time τ_c is defined as the time at which the RFP configuration is judged to be gross-MHD unstable based on the F,Θ diagram of Robinson [4]. Thus provided that

$$\tau_c/\tau_E(t=\tau_c) > 1 \qquad (2)$$

then

$$\tau_E(t=\tau_c)/\tau_E^{HS} = 1 \qquad (3)$$

can be achieved by adjusting c_a. Figures (2) and (3) show the ratios (2) and (3).

3.   Decay of Toroidal current

If the toroidal current I is not held constant by a suitably-applied electric field the evolution of the RFP configuration becomes quite different from that of the constant-current case. If I is constant the route in the Robinson diagram usually leads to high β - high Θ configurations which eventually are judged to be m = 1 gross-kink unstable. Such a route establishes a reasonably accurate estimate for τ_c when Θ reaches Θ_{max}.

For a decaying current the characteristic timescale τ_I becomes an important parameter. If $\tau_I >> \tau_c$ the evolution ressembles the $\tau_I \to \infty$ case. However if $\tau_I \sim \tau_c$ corresponding to the peaked current-time profiles observed in ZETA and Eta-Beta II the following evolution is established by the calculations. The balance between the build-up of β and the maintainence of constant I is lost and plasma piles up on the outside of the discharge. As I decays, Θ decays and β increases towards β_{max} (the gross Suydam limit). The convection of plasma across the discharge cools the outside and lowers τ_E as well as τ_c. However it now becomes more difficult to estimate τ_c since the RFP configuration should be tested for gross-MHD stability before β reaches β_{max}.

Furthermore the convection of plasma across the discharge tends to push the reversed field out towards the liner. Thus the advantage of maintaining E_θ, as proposed for RFX, is lost and this would make RFX behave more like ZETA.

[1]   J.P.Christiansen,K.V.Roberts, Nucl.Fusion 18(1978)187
      J.P.Christiansen,K.V.Roberts,J.W.Long, Comp.Phys.Comm.14(1978)423
[2]   J.Hugill,J.Sheffield,Nucl.Fusion 18(1978)15
      J.Sheffield, Private Communication, Jan.1977
[3]   C.C.Daughney, Nucl.Fusion 15(1975)967
      M.M.Murakami, H.P.Eubank, Physics Today May 1979
      Pfeiffer,Waltz,Nucl.Fusion (1979)
[4]   D.C.Robinson et al. 6th IAEA Conf. 1 (1977) 429.
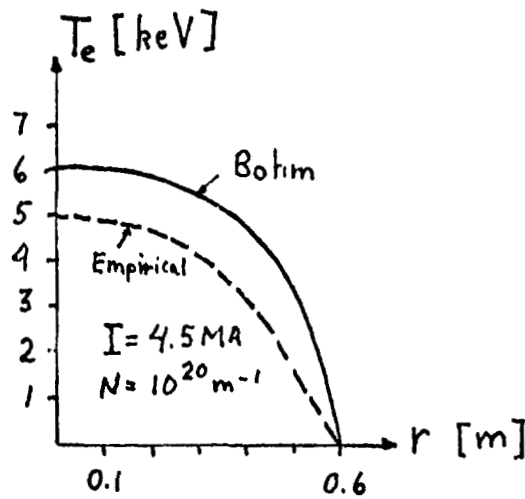
Figure 1. Temperature profiles resulting from using a Bohm diffusion coefficient and D_a of (1).
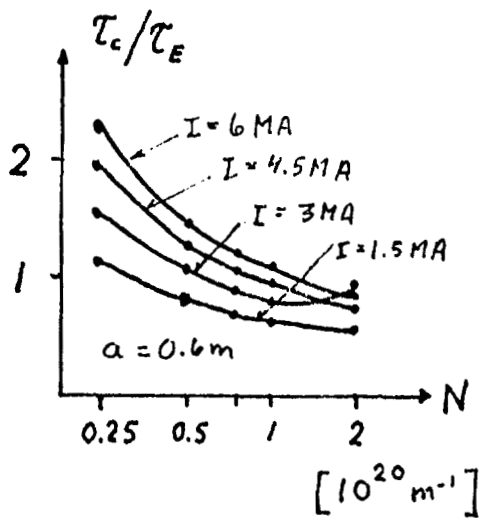
Figure 2. Ratio between configuration time and confinement time.
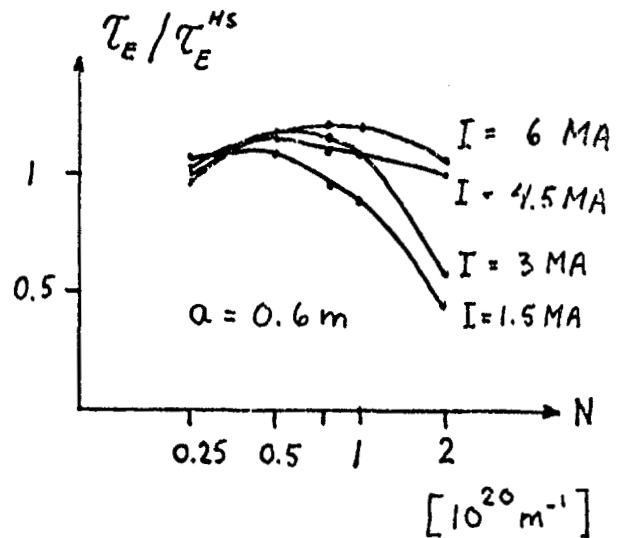
Figure 3. Ratio between actual confinement time and empirical confinement time.

Effects from Impurities in RFP discharges

V. Piotrowicz   and   J.P.Christiansen

(Euratom/UKAEA,Culham Laboratory,Abingdon,Oxon,UK)

1.   INTRODUCTION

The experimental evidence available from measurements on RFP discharges suggest that these are subject to some level of impurity contamination, notably Oxygen and Iron impurities have been observed by spectroscopic measurements. The effects from impurities on Tokamak discharges are significant and although they are not completely understood there is a substantial effort in describing impurity behaviour in Tokamak transport calculations. This paper describes an impurity model used for calculations on RFP discharges. The emphasis in the model has been put on a full time-dependent description of all ionization levels of a given specimen, because RFP discharges unlike Tokamak discharges do not generally reach a steady state. In the next section we describe the model and the last section outlines results from calculations on RFX discharges which are assumed to involve certain levels of Oxygen concentration.

2.   Impurity model

The model used to describe impurities assumes that the plasma of an RFP evolves through a sequence of quasi-static processes which can be split into two categories

I   Entropy generating processes

II   Adiabatic processes

This model can thus be used in combination with the 1-dimensional equilibrium and transport code ATHENE1 [1] . The equilibrium calculations of [1] is described in [2] and can in a straightforward manner be applied to the impurities. Hence we only concern ourselves with entropy generating processes.

We consider a plasma consisting of electrons and various ion components whose fractional abundancies are

$$f_j = n_j/n_i$$

n_j being the number density and n_i the total ion number density. Any quantity ψ depending on atomic mass and charge numbers can then be expressed by the average

$$< \psi > = \sum_j f_j \psi_j \quad .$$

All ions are assumed to share the same temperature T_i. Ions like H, D, T, ^{3}He are described via the equations given in [1] whereas heavier impurities, e.g. Oxygen, are treated as follows: An impurity specimen of density n_j denoted by n for brevity will comprise ionisation stages of densities $(n_1, n_2 \ldots n_z) = \underline{n}$. The atomic physics processes and the transport of these stages are expressed in terms of the equation

$$\frac{\partial n_k}{\partial t} + \nabla \cdot \underline{F}_k = (\underline{\underline{A}})_k n_k n_e \tag{1}$$

In (1) $\underline{F}_k$ is the flux of ions of ionisation stage k and the matrix $\underline{\underline{A}}$ contains the ionization and recombination rates [3].

For $\underline{F}_k$ we use

$$\underline{F}_k = - D_k \nabla n_k + \underline{V}_k n_k \tag{2}$$

where D_k is a diffusion coefficient describing diffusion in a reference frame following the host plasma. This diffusion coefficient is given by the neoclassical expression [4]

$$D_k = (1+q^2) \rho_k^2 \nu \quad , \tag{3}$$

but any anomalous diffusion can be included if required. The ambipolar drift velocity $\underline{V}_k$ is expressed as

$$\underline{V}_k = (k-1) D_k \left(\frac{1}{n_i} \nabla n_i - \frac{1}{2T_i} \nabla T_i \right) \tag{4}$$

Equation (1) is solved numerically by a technique which avoids any influence on the timestep Δt from the space-time variations of n_k. This is necessary since a general calculation involving several aspects of RFP physics should not be delayed by the advance of every single ionization stage. The solution of (1) is solved by a fractional steps method [4]: Atomic physics is first advanced $\frac{1}{2}\Delta t$ in time. Then diffusion takes place over an interval Δt and finally atomic physics recurs over an interval $\frac{1}{2}\Delta t$. We start from

$$\frac{\partial \underline{n}}{\partial t} = n_e \underline{\underline{A}} \, \underline{n}$$

setting

$$\underline{n} = \sum_k \underline{v}_k \exp (\lambda_k n_e t) \tag{5}$$

210

we find the eigenvalues and eigenvectors from

$$(\underline{\underline{A}} - \lambda_k \underline{\underline{I}}) \underline{v}_k = 0$$

Equation (5) advances $\underline{n}$ $\frac{1}{2}\Delta t$ in time.

The diffusion stage

$$\frac{\partial \underline{n}}{\partial t} = -\nabla \cdot \underline{\underline{F}}$$

is treated by a fully implicit method which advances $\underline{n}$ Δt in time. The next and last step finds a new solution (5) and this completes one step in the cycle of calculation of ATHENE1.

Because of the large variations in space of the fluxes (2) it is possible for (5) to produce negative values n_k especially in the wall region. This phenomena is well known in Tokamak impurity calculations [5]. The cure used in Tokamak calculations [5] is also applied here: whilst $D_k \nabla n_k$ (2) can be spatially centred $\underline{V}_k n_k$ cannot, the straight forward average

$$(n_k)_j = \tfrac{1}{2}((n_k)_{j-\frac{1}{2}} + (n_k)_{j+\frac{1}{2}}),$$

which may lead to negative n_k is replaced by

$$(n_k)_j = f_j (n_k)_{j-\frac{1}{2}} + (1-f_j)(n_k)_{j+\frac{1}{2}}$$

and the weighting factors chosen so as to ensure

$$\left| \Delta t \cdot \nabla \cdot \underline{F}_k \right| << n_k.$$

After the atomic physics and transport have been calculated we evaluate the ionization loss

$$P_A = n_e \sum_k n_k S_k \chi_k, \tag{6}$$

the line radiation loss

$$P_L = n_e \sum_k n_k \sum_\ell X_{k,\ell} \, \Delta E_{k,\ell} \tag{7}$$

and the recombination radiation loss

$$P_R = n_e \sum_k n_k \left[R_k^1 (\chi_{k-1} + \frac{3}{2}kT_e) + R_k^2 (\chi_{k-1} + \delta E_{k-1}) \right].$$ (8)

In these expression S, R^1, R^2 denote ionization, radiative recombination and dielectronic recombination rates; χ_k is the ionization potential, $X_{k,\ell}$ the excitation rate coefficients with associated energies $\Delta E_{k,\ell}$; δE_{k-1} is the energy of the resonant transition involved in dielectronic recombination. P_A, P_L, P_R, are then included in the electron energy equation. Care is taken to ensure that the total energy balance between ions, electrons and impurities is maintained.

3.   Results

   We consider calculations on RFX with a toroidal current of $I = 1MA$. In these calculations we vary the line density N as N_o, $2N_o$, $3N_o$ where $N_o = 2.5 \ 10^{19} m^{-1}$ the approximate ZETA line density. The anomalous electron transport is described via the empirical scaling law (Hugill Sheffield) for the confinement time τ_E and we study what happens if I is held fixed or allowed to decay as $\sim e^{-t/\tau_I}$ with $\tau_I = 50$ msec. Two levels, 1% and 3%, of Oxygen impurities are studied for a plasma which otherwise consists of a 50-50 D-T mixture. Initially the impurity concentration is assumed to be proportional to the hydrogen density.

   The results from these calculations are compared with results from earlier calculations ,both sets having identical parameters; the differences are hence due to the time-dependent atomic physics calculation. results indicate that ionization effects dominate spatial diffusion of Oxygen. Recombination radiation dominate s in the hot core region, while the wall region is controlled by line radiation. It is perhaps somewhat surprising that by including time-dependent atomic physics calculation only minor changes to the central temperatures T_{eo}, T_{io} and the configuration time τ_c occur: the increase in total loss (thermal wall loss, radiation loss, ionization loss)increases of course with both N and the concentration of Oxygen, but is balanced by a corresponding increase in the net circuit input. The changes in T_{eo}, T_{io} are of +5%, $\pm$1%, -3% for $N=N_o, 2N_o, 3N_o$ respectively with slightly higher values for τ_c. At low line density the increase is due to Z_{eff} enhancement while at higher N the decrease is caused by higher collision rates.

For the case of a decaying current we find again that including the impurity model only leads to small changes: the configuration τ_c (not too accurately predicted) increases slightly as do the central temperatures. the increase in τ_c arises because the ionization in the centre takes a finite time of order several msec. Thus the fall in electron density during the expansion is partially compensated by the increase in n_e due to time dependent ionization.

In conclusion, it would appear that a time-dependent treatment of low-z atomic physics does not greatly affect the results obtained by prescribing a time-independent Z_{eff}. However this only applies when spatial impurity diffusion is small, when there is no supply of impurities from the wall (sputtering) and of course it only applies to the field-configurations considered (high current).

[1] J.P.Christiansen, K.V.Roberts, J.W.Long, Comp. Phys. Comm. 14(1978)423

[2] K.V.Roberts, J.P.Christiansen, J.W.Long, Comp. Phys. Comm. 10(1975)264

[3] Description of TFR code MAKOKOT

[4] T.Tazima et al. Nucl. Fusion 17(1977)419

[5] M.H.Hughes, M.L.Watkins. Private Communication (1979-80).
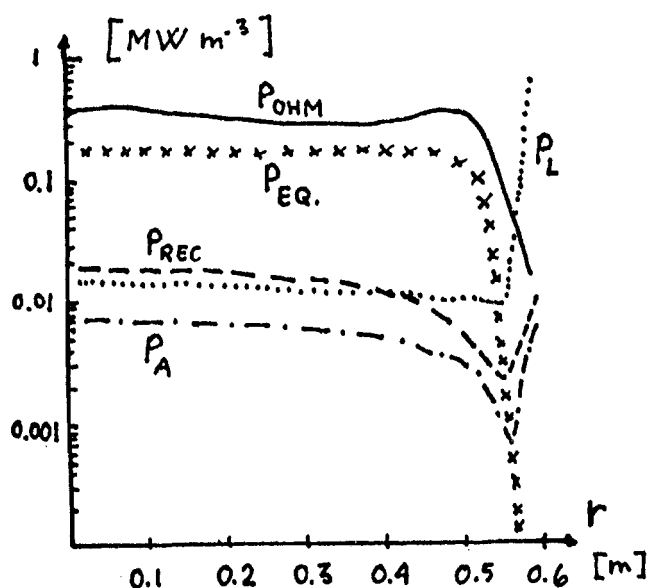
Fig.1. Ohmic input (P_{OHM}), equipartition rate (P_{EQ}), recombination radiation (P_{REC}), line radiation (P_L), Ionisation loss (P_A), against radius for RFX I=1MA, N=2N$_o$, 3% Ox. at t =57msec
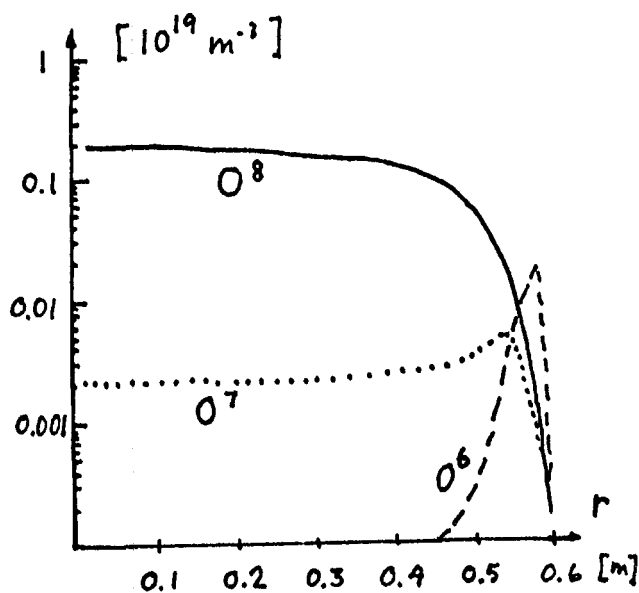
Fig.2. Oxygen concentration at t=57msec. O^8 is fully ionised same RFX parameters as in Fig.1.

213

The Simulation on Formation of RFP Plasmas

H. Matsuda, S. Ido[*] and I. Kawakami
Department of Physics
College of Science and Technology
and
Atomic Energy Research Institute
Nihon University, Tokyo 101, Japan

§1. Introduction

Computational studies have been made to investigate MHD activities of plasmas during formation of reversed field pinch configuration, and behaviors of plasmas after the toroidal field B_T is reversed near the wall. Emphasis is placed upon effect of thermal conductivity, κ , and electric resistivity, η , which are included in the nonlinear MHD equations involved. These transport coefficients are classical or anomalous. In addition to these coefficients, we are forced to include some loss mechanisms in the equations to obtain agreement with experimental results of ETL-TPE-1R.[1] Physical origins which the anomalies of the coefficients and the losses come from are not discussed here.

Some preliminary results are obtained on 3D nonlinear stability of reversed field cylindrical plasma. For high n modes, plasma kinetic energy increases and the modes show nonlinear instability. For low n modes, plasma seems to be stable.

§2. The Model and Numerical Method

The model of computation is described by a set of nonlinear MHD equations. The plasma is a single fluid. The continuity equation, the equation of motion, the equation of kinetic pressure and the equation for magnetic field are used. The current is defined as $\mu_0 \mathbf{j} = \nabla \times \mathbf{B}$, as usual. The electric field, $\mathbf{E}$, is given by simple Ohm's law, $\mathbf{E} + \mathbf{v} \times \mathbf{B} = \eta \mathbf{j}$. The thermal conductivity is not necessarily scaler, but tensor, and expressed by perpendicular $\kappa_\perp$, and parallel, $\kappa_{//}$, components to the magnetic field. The resistivity, η , is assumed isotropic, $\eta_{//} \simeq \eta_\perp$.

When we are considering turbulence in plasma, which may be brought about by microinstabilities of waves, or by MHD instabilities, transport in plasma will become enhanced beyond classical level. This effect can be taken into account by anomalous increase of collision frequency, ν_e. In pinch plasma, we consider that anomaly is caused by strong poloidal current. Characteristic growth rate of current driven instabilities is taken to be the ion plasma frequency, ω_{p_i} , and anomalous collision frequency, ν_e^a, for fully developed turbulence is $\nu_c^a \sim \omega_{p_i}$. When classical collision

---

[*] Present Address: The Institute of Laser Engineering, Osaka University, Suita, Osaka 565

frequency is exceeded by anomalous one, the collision frequency is v_e^a, otherwise $v_e \sim v_c$, where v_c is classical collision frequency.

In order to supress anomalous piling up of kinetic energy found in the numerical model, we have been making use of loss terms which are proportional to pressure, p , and to $(r/a)^2$ where a is minor radius.[2] The latter factor is proportional to volume, so that effective in the outer region of toroidal or cylindrical plasma. These loss terms may be explained as radiation loss or something else, but we do not enter into detail here. We have only to enphasize that these terms are necessary to reproduce experimental results.

For numerical purpose, the artificial viscosity due to von Neumann and Richtmyer[3], $Q_{vis} \propto \rho(\mathrm{div}\ u)^2$ when $\mathrm{div}\ u < 0$, is used. This is needed to suppress numerical fluctuations coming from discretization of continuous plasma fluid.

The numerical method used in our computation is described in ref. 4. This is somehow modified version of ICED ALE[5] - Inplicit Continuous Eulerian, Arbitrary Lagrangian and Eulerian. We are developing another method of numerical solution of nonlinear MHD equations, which are extension of ICED ALE and of finite element method, FEMALE - Finite Element Method for Arbitrary Lagrangian and Eulerian elements. However, the results of computation here are obtained by ICED ALE. The 2D and 3D codes are written in Olympus system[6,7] called ORION.

Difference between our method and ICED ALE is mainly layout of physical quantities. In our method, the position x, the velocity v and the magnetic field B are assigned to vertices, while density n, pressure p, temperature T, current j and the electric field E are assigned to geometrical center of cell. Algorithm has to be changed in consequence.

In 2D simulation, geometry is toroidal. Initially, plasma has constant density and temperature, confined by toroidal magnetic field. At this instant, t = 0, poloidal field start growing, reaching maximum value at t > 0. During growth of the poloidal field, the toroidal field change its direction to negative value at the wall. We assume the boundary condition shown in Fig. 1. From the toroidal current in this figure, the poloidal field at the wall is derived analytically as the boundary condition. The density and temperature are fixed at the wall. The plasma at the wall is at rest throughout computation.

For the 3D simulation, we start computation from equilibrium state of Bessel function model, on which imposing some perturbation of m = 1 and n > 0 modes, since we are interested in nonlinear stability of reverse field plasma. The boundary condition is the same one as the 2D cases.

Our purpose of simulation is mainly focused to investigate the plasma properties of experiment ETL-TPE-1, so parameters of device are: R(major radius) = 50cm, a (minor radius) = 10cm, n_o (initial plasma density) = $10^{15} cm^{-3}$, T_o (initial temperature) = 1eV, I_p (maximum toroidal current) = $10^5 A$, B_T (toroidal field at the wall) = 2.4 K gauss to - 0.2 K gauss.

§3. Computational Results

(1) For general references, we first consider the case where η is classical and isotropic. η is taken from ref. 8 where $\eta_{//} \approx \eta_{\perp}$. κ is also classical and $\kappa_{//} \gg \kappa_{\perp}$. The loss terms, $-p(r/a)^2/\tau_L$, are also included, where $\tau_L \approx 1$ µsec. Results are shown in Fig. 4. At 6 µsec, when B_T was reversed at the wall 2 µsec before, the toroidal current and temperature are peaked near the wall, contrary to the experiment. The field is almost flat around the axis. These show the diffusion is poor in this case, suggesting the resistivity, η , must be anomalous.

We examined another case by enhancing the classical resistivity by factor 5. In this case, toroidal current is slightly diffused, but the peaking of the temperature enhanced because of increase of Ohmic heating. The toroidal field has profile not so much different from the case of pure classical resistivity. The F-θ diagram is shown in Fig. 2 for the pure classical case. Simulation points goes down along the Bessel function model line. After the reversal of field, the F-θ values stay, not going to the large θ value region.

(2) To investigate the effect of anisotropy of the thermal conduction, the case where $\kappa_{\perp}$ is set equal to classical $\kappa_{//}$ is examined. The total toroidal magnetic flux, Φ for the cases of $\kappa_{\perp} \ll \kappa_{//}$ and of $\kappa_{\perp} = \kappa_{//}$ is shown in Fig. 3. Experimentally, Φ is almost constant, and support the anisotropy of κ , $\kappa_{\perp} \ll \kappa_{//}$.

(3) The result of computation with the pure classical resistivity showed that the plasma must be more resistive. We examined the resistivity, η , which is anomalous. The anomaly of the resistivity is assumed to come from the velocity driven microinstabilities, such as Bunemann instability, ion acoustic wave instability, or lower hybrid wave instability. To take into account of these instability phenomenologically, we replace the classical collision frequency, $\nu_{e,a}^c$ simply by the anomalous one, ν_e^a, when $\nu_e^c < \nu_e^a$ in the plasma. ν_e^a is defined as $\nu^a = f_1 \omega_{pi} (1 - \exp(-v_D/f_2 v_{th}^e))$, v_D is a drift velocity derivable from P_i the current, and v_{th} is an ~~electron~~ thermal velocity. f_1 and f_2 are constants of order of magnitude of unity. ν_e^a will exceed ν_e^c when and where $v_D \gg v_{th}$. The profile of the temperature, the toroidal current and magnetic fields are computed and shown in Fig. 5. Diffusion of the toroidal current and the magnetic field is observed. The temperature is also diffused, but not sufficient, in comparison of experiment. In Fig. 2, the F-θ diagram shows the failure of setting up of equilibrium of reversed field configuration for this case of the anomalous resistivity. The value of θ goes to the right, increasing indefinitely.

(4) These results of the computation show

(i) The thermal conductivity has to be naturally anisotropic with respect to the direction of the magnetic field.

(ii) The resistivity is anomalous at the setting up phase of reverse field pinch configuration, since the classical resistivity can not reproduce diffused profile of the current and the magnetic field. However, the anomaly of the resistivity could not reproduce the diffused profile of the

216

temperature. On the contrary, the large value of the resistivity enhance the temperature due to Ohmic heating, thus reducing the resistivity itself near the wall. In addition to the profile of the temperature, the F-θ diagram showed that the failure of reaching stable reverse field configuration. Hence it is expected that after the field reversal, the resistivity is rather classical than anomalous.

(5) Heretofore, we have been considering the 2D simulation. We now consider the 3D simulation. In the 3D simulation, the cylindrical plasma is assumed, with the periodic boundary condition along the axis. The period is $2\pi R/n$, where R is a major radius of torus, and n is a toroidal node number. As initial condition, we assume the Bessel function model for the toroidal and poloidal magnetic field. Thus, the current is force free. The pressure is tentatively assumed sinusoidal profile with maximum value at the axis, $p = p_0 \cos(\pi r/2a)$. Upon this quasi equilibrium, we impose small perturbation of (m, n) mode. The resistivity is constant throughout computation and over whole plasma region. The boundary values of plasma parameters are fixed to the values given at initial time. The parameters given in this way correspond to $S \sim 5 \times 10^3$. The q-value varies from 0.154 to - 0.042, rather small, over plasma.

The evolution of kinetic energy is shown Fig. 6. The vortices are formed corresponding to the (m,n) values. For m = 1 and n ≤ 5, we could not observed the growth of kinetic energy, showing nonlinear stability. For high n modes, n ≥ 10, the plasma is initially stable, showing the decrease of kinetic energy. However, suddenly become rapid growth of kinetic energy. For intermediate values of n , we have not yet investigated complicated behaviors of perturbations.

References

1) TAMARU, T., et al., Plasma Physics and Controlled Nuclear Fusion Research (Proc. 7th International Conference, Innsbruck, 1978) Vol. 2, IAEA, Vienna (1979) 55.
2) Robinson, D. C., private communication.
3) Richtmyer, R. D. and Morton, K. W., "Difference Methods for Initial Value Problems", 2nd edition, Interscience Pub., 1967.
4) IDO, S., Thesis at University of Tokyo (1978).
5) Brackbill, J. U., "Numerical Magnetohydrodynamics for High Beta Plasmas", in Methods in Computational Physics Vol. 16, Academic Press (1976).
6) Roberts, K. V., Computer Physics Communications 7, 237 (1974).
7) Christiansen, J. P., and Roberts, K. V., Computer Physics Communications 7,245 (1974).
8) Braginskii, S. I., "Transport Processes in a Plasma", in Review of Plasma Physics, Vol. 1, Consultants Bureau, 1967.
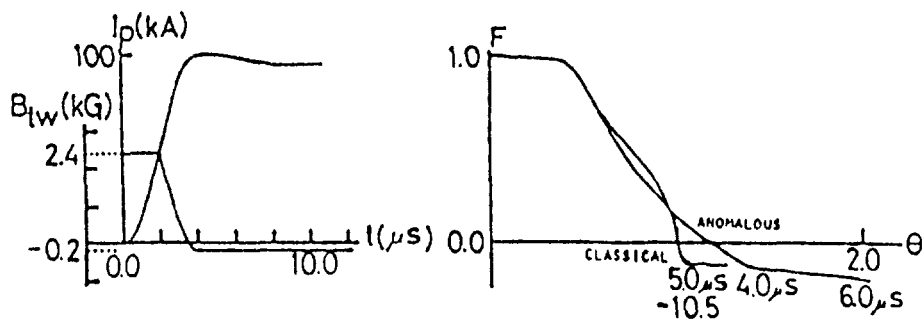
Fig. 1

Fig. 2
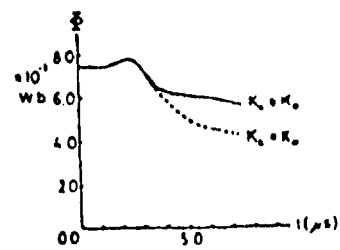
Fig. 3
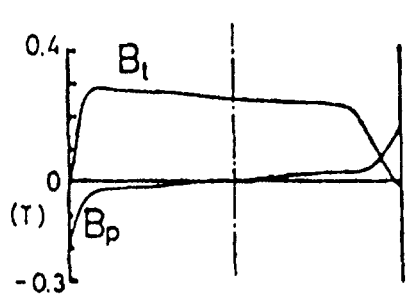
Fig. 4-a
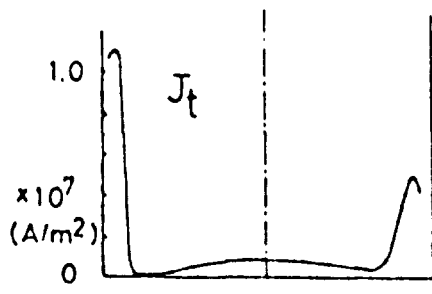
Fig. 4-b
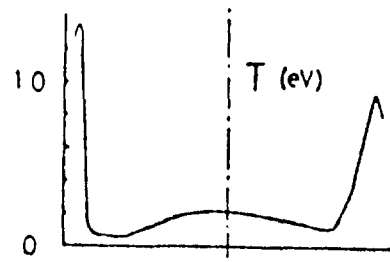
Fig. 4-c
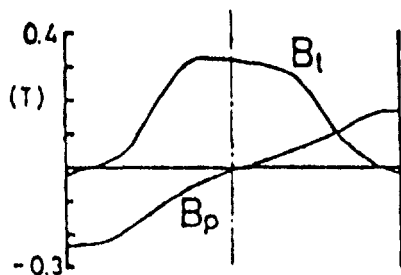
Fig. 5-a
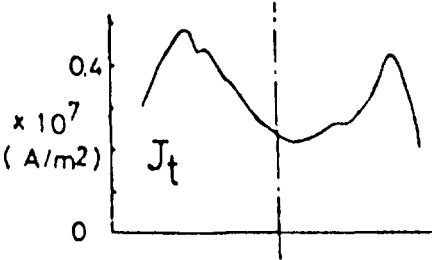
Fig. 5-b
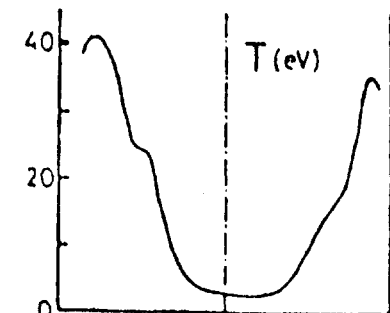
Fig. 5-c
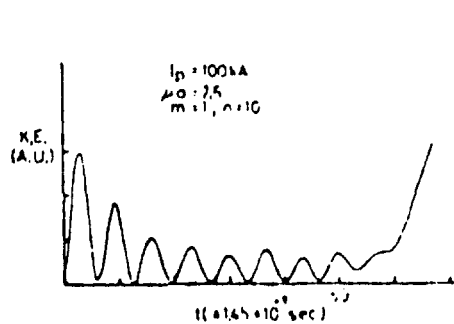
Fig. 6-a
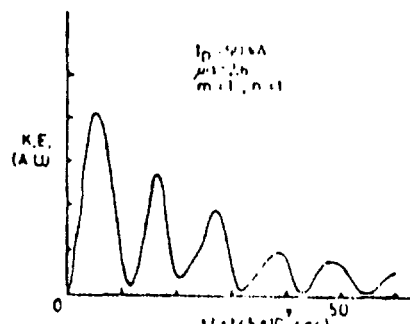
Fig. 6-b

MEAN FIELD ELECTRODYNAMICS
APPLIED TO THE REVERSED-FIELD
PINCH: ANISOTROPIC EFFECTS

S. N. Rasband
Department of Physics and Astronomy
Brigham Young University
Provo, Utah 84602
U.S.A.

ABSTRACT

The implications of anisotropy in the "α" and "β" effect of mean field electrodynamics for a steady-state, reversed-field solution of the induction equation is studied. The anisotropy considered is that imposed by the assumption of cylindrical symmetry.

1. INTRODUCTION

It has been suggested that the methods and concepts of mean field electrodynamics may be useful in understanding the behavior of plasmas confined in reversed-field pinch (RFP) machines.[1,2] In particular, the so-called "α effect" of turbulent dynamo theory has been shown to be capable of giving self-reversal of the toroidal magnetic field. [1]

In this communication we extend previous kinematic studies to include anistropy. The perspective is that of kinematic dynamo theory: We prescribe the velocity field and study the resultant magnetic field behavior. We make no attempt in the current work to consider a dynamic equation for determination of the fluid velocity and the turbulence parameters.

2. THE INDUCTION EQUATION

For a discussion of the basic assumptions, validity criteria, and a general exposition of "mean field electrodynamics," the reader is referred to Moffatt.[3] For our purposes we begin with the induction equation of mean field electrodynamics,

$$\frac{\partial \vec{B}}{\partial t} = \nabla \times (\vec{U} \times \vec{B} + \vec{E}) + \eta \nabla^2 \vec{B}. \tag{1}$$

η is the plasma resistivity, assumed to be spatially homogeneous, isotropic, and time independent. We recognize that the effects of anisotropic resistivity can be significant and may arise from many sources, quite independent of plasma turbulence. Nevertheless, we ignore all contributions to anisotropic resistivity except that due to turbulence as included below. In equation (1) $\vec{U}$ and $\vec{B}$ are the mean velocity and mean magnetic field respectively. $\vec{E}$ is the effective electric field and we write the cartesian components of $\vec{E}$ in the expanded form

$$E_i = \alpha_{ij} B^j + \beta_{ijk} \frac{\partial B^j}{\partial x^k} . \tag{2}$$

We confine our attention to a cylindrical conducting fluid contained within a conducting shell of radius $\underline{a}$. We will also consider only azimuthally symmetric situations; $\vec{B}(r,t) = \hat{\theta} B_\theta(r,t) + \hat{z} B_z(r,t)$ and $\vec{U}(r,t) = \hat{r} U(r,t)$.

In deference to the global, geometric symmetry, and as a generalization of the isotropic case, where $\alpha_{ij} = \alpha g_{ij}$ and $\beta_{ijk} = \beta \epsilon_{ijk}$, we assume a preferred direction along the axis of the cylinder given by the unit vector $\vec{e} \equiv \hat{z}$. In this case α_{ij} and β_{ijk} can be written as

$$\alpha_{ij} = \alpha_\perp (g_{ij} - e_i e_j) + \alpha_\parallel e_i e_j + \bar{\alpha} \epsilon_{ijk} e^k , \tag{3}$$

and

$$\beta_{ijk} = \beta_0 \epsilon_{ijk} + \beta_1 \epsilon_{mjk} e^m e_i + \beta_2 \epsilon_{imk} e^m e_j \tag{4}$$
$$+ \beta_3 \epsilon_{ijm} e^m e_k + \tilde{\beta}_1 e_i g_{jk} + \tilde{\beta}_2 e_j g_{ik} + \tilde{\beta}_3 e_k g_{ij} + \tilde{\beta}_0 e_i e_j e_k .$$

The tensors g_{ij} and ϵ_{ijk} are the usual metric and Levi-Civita (permutation) tensors. The quantities $\alpha_\perp$, $\alpha_\parallel$ and $\tilde{\beta}_0, \ldots, \tilde{\beta}_3$ are pseudo-scalars and the remaining $\beta_0, \ldots, \beta_3$, $\bar{\alpha}$ are pure scalars. All are spatially independent from the assumption that the statistical properties of the fluctuating fields are homogeneous.

We note that anisotropic turbulence leads to anisotropic resistivity. We define $\eta_\perp \equiv \eta + \beta_0 + \beta_1$ and $\eta_\parallel \equiv \eta + \beta_0 + \beta_2$. To achieve a dimensionless form for equation (1) we scale distances in terms of the radius of the cylinder and times in terms of the parallel resistive diffusion time. Specifically we let: $x = r/a$, $\tau = \eta_\parallel t/a^2$, $\delta = \eta_\perp/\eta_\parallel$, $s_\perp = a\alpha_\perp/\eta_\parallel$, $s_\parallel = a\alpha_\parallel/\eta_\parallel$, and $v = aU/\eta_\parallel$. Equation (1) in component form then becomes

$$\frac{\partial B_\theta}{\partial \tau} = -s_\parallel \frac{\partial B_z}{\partial x} - \frac{\partial(v B_\theta)}{\partial x} + \delta\left(\frac{\partial^2 B_\theta}{\partial x^2} + \frac{1}{x}\frac{\partial B_\theta}{\partial x} - \frac{B_\theta}{x^2}\right), \tag{5}$$

$$\frac{\partial B_z}{\partial \tau} = \frac{s_\perp}{x}\frac{\partial(x B_\theta)}{\partial x} - \frac{1}{x}\frac{\partial(x v B_z)}{\partial x} + \frac{\partial^2 B_z}{\partial x^2} + \frac{1}{x}\frac{\partial B_z}{\partial x}. \tag{6}$$

3. STEADY-STATE SOLUTION

The parameter δ clearly is a measure of the anisotropy in the resistivity due to turbulence, in so far as β_{ijk} quantifies this effect. We define $\zeta = s_\perp/s_\parallel$ which then represents a similar measure of the anisotropy in the "α effect."

In order to focus on anisotropy we set the velocity equal to zero. Furthermore, to facilitate comparison, we model our notation after that of reference 1.

As boundary conditions we assume for equations (7) and (8) that the toroidal flux is $\pi a^2 B_0$ and the value of B_θ at the wall is $I_0 a$. We define the

usual pinch ratio $\theta = I_o a/B_o$ and the parameter $\epsilon = (s_\perp s_\parallel/\delta)^{1/2} = s_\perp(\zeta\delta)^{-1/2}$.

The components of the mean magnetic field are

$$B_z(x)/B_o = 1 - 2\theta\delta\zeta/s_\perp + \theta(\zeta\delta)^{1/2} J_o(\epsilon x)/J_1(\epsilon) , \qquad (7)$$

and

$$B_\theta(x)/B_o = \theta J_1(\epsilon x)/J_1(\epsilon). \qquad (8)$$

Assuming that this steady state satisfies $\nabla P = \vec{J} \times \vec{B}$ with $P(a) = 0$, we obtain the pressure profile:

$$P(x) = \frac{B_o^2}{2\mu} \{2(2\theta\delta\zeta - s_\perp)\theta\epsilon^{-1}[J_o(\epsilon x) - J_o(\epsilon)]/J_1(\epsilon)$$
$$+ (1 - \zeta\delta)\theta^2[J_o^2(\epsilon x) - J_o^2(\epsilon)]/J_1^2(\epsilon)\} . \qquad (9)$$

The usual poloidal beta given by the ratio of the average kinetic pressure to the pressure of the poloidal magnetic field at the wall is found to

$$\beta_\theta^* = 2(2\theta\delta\zeta - s_\perp)J_2(\epsilon)/(\epsilon\theta J_1(\epsilon)) + (1 - \zeta\delta) . \qquad (10)$$

From equation (7) we readily obtain a condition on the three parameters $s_\perp$, θ, and ϵ for B_z to equal zero at $x = x_o$. We find $0 < \epsilon < \gamma_1$, and

$$s_\perp^{-1} = \theta[2\epsilon^{-2} - \epsilon^{-1}J_o(\epsilon x_o)/J_1(\epsilon)] . \qquad (11)$$

Equation (11) represents a threshold condition for field reversal in the steady-state solutions of equations (7) and (8). Among the implications of equation (11) we find that smaller amounts of the "α effect" can still lead to reversal in the steady state, if the resistivity is sufficiently anisotropic. For example taking $x_o = 1$, with the parameter choices $s_\perp = 1.0$, $s_\parallel = 1.0$, $\theta = 1.5$, and $\delta = .0912$, equation (11) is satisfied. This gives $\eta_\parallel \approx 11\eta_\perp$ and for the parameters of this example, $\beta_\theta^* = 0.26$. This reduction in the required magnitude of the "α effect" for field reversal, through anisotropy in the turbulent resistivity, may be physically important since it reduces the helicity, or lack of mirror symmetry, required for the fluctuating part of the velocity field. This is evident from the expressions for $\eta_\perp$ and $\eta_\parallel$ where we see that turbulent resistivity depends on scalars as

opposed to pseudo-scalars. We also see from equation (20) that for $x_o \gtrsim .63$, reversal requires that $s_\perp > 0$.

Figure 1 illustrates the type of changes in the $(s_\perp - \theta)$ parameter space which result from anisotropy. The upper bound for $s_\perp$ is established solely by the requirement that $P(x) \geq 0$ for $0 \leq x \leq 1$. The shaded regions denote possible parameter choices with field reversal. We note that anisotropy can considerable reduce the low beta region available with field reversal.

REFERENCES

[1] GIMBLETT, G. G., WATKINS, M. L., 7th European Conference on Controlled Fusion and Plasma Physics (1975), Vol. 1, 103.
[2] GIMBLETT, G. G., WATKINS, M. L., in Third Topical Conference on Pulsed High Beta Plasmas, ed. D. E. Evans, Pergamon Press (1976).
[3] MOFFATT, H. K., Magnetic Field Generation in Electrically Conducting Fluids, Cambridge University Press, Cambridge (1978).
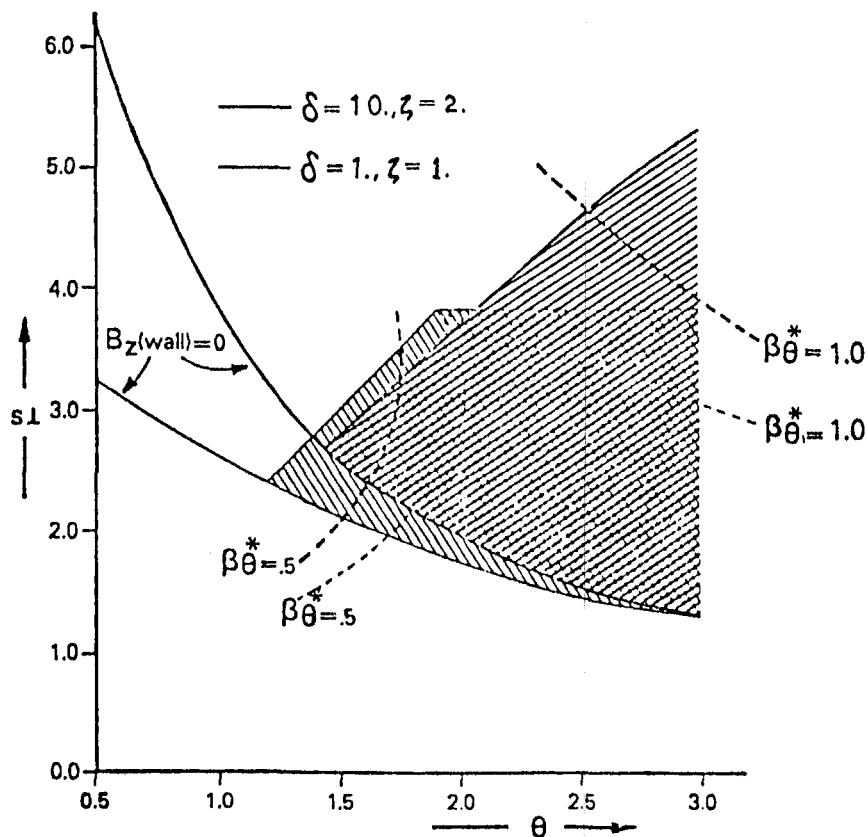
THE ROLE OF IMPURITIES IN PRODUCING THERMAL INSTABILITY IN THE RFP

E. J. Caramana and F. W. Perkins

I. Introduction

A plasma can become thermally unstable due to the temperature dependence of the heating and cooling functions, whereby a small increase in temperature about an equilibrium leads to an increase in the heating function and a decrease in the cooling function. This instability can occur as a consequence of plasma transport.

II. Thermal Instability

a) Physics Model

We consider the MHD fluid equation with the inertia neglected and assume cylindrical symmetry (all quantities depend only on the radial coordinate r). The equations are:

$$\frac{\partial n}{\partial t} + \vec{\nabla} \cdot \vec{V}_r n = 0 \tag{1}$$

$$\frac{\partial \vec{B}}{\partial t} - \vec{\nabla} \times (\vec{V}_r \times \vec{B}) = \vec{\nabla} \times c\ddot{\eta} \cdot \vec{j}, \tag{2}$$

$$\frac{3}{2} \frac{\partial n T_e}{\partial t} + \frac{3}{2} \vec{\nabla} \cdot \vec{V}_r n T_e + n T_e \vec{\nabla} \cdot \vec{V}_r = - \vec{\nabla} \cdot \vec{q}_e - \frac{3 n_i e^2 n^2}{M} (T_e - T_i) + \ddot{\eta} \cdot \vec{j}^2 - K n^2 T_e^\alpha, \tag{3}$$

$$\frac{3}{2} \frac{\partial n T_i}{\partial t} + \frac{3}{2} \vec{\nabla} \cdot \vec{V}_r n T_i + n T_i \vec{\nabla} \cdot \vec{V}_r = - \vec{\nabla} \cdot \vec{q}_i + \frac{3 n_i e^2 n^2}{M} (T_e - T_i), \tag{4}$$

$$\vec{\nabla} p = \frac{\vec{j} \times \vec{B}}{c} \left(p = n(T_e + T_i) \right), \tag{5}$$

$$\vec{j} = \frac{c}{4\pi} \vec{\nabla} \times \vec{B}, \tag{6}$$

where $\vec{q}_e$, $\vec{q}_i$, and $\ddot{\eta}$ are the electron and ion heat flux and the resistivity tensor respectively.

Classical transport coefficients in the strong field limit are assumed. We include in the electron temperature Eq. (3) a term which models energy loss from impurities $K n^2 T_e^\alpha$, where K is a constant and $\alpha = \alpha(T_e)$.

b) Physical Explanation of the Thermal Instability

Note the following relationships among the physical processes contained in Eqs.(1)-(6).

$$\gamma_{PD} = \beta^2 \gamma_{OH} \qquad\qquad \gamma_{ETC} = \beta^2 \gamma_{OH}$$

$$\gamma_{MD} = \beta \gamma_{OH} \qquad\qquad \gamma_{ITC} = \beta^2 \left(\frac{M}{m}\right)^{1/2} \gamma_{OH}$$

$$\gamma_{EI} = \Lambda\, \beta^2 \gamma_{OH}$$

where

γ_{PD} = particle diffusion rate
γ_{MD} = magnetic field diffusion rate
γ_{DH} = ohmic heating rate
γ_{EI} = electron-ion temperature equilibration rate
γ_{ETC} = electron thermal conduction rate
γ_{ITC} = ion thermal conduction rate
Λ = (plasma radius/ion gyroradius)^2

For low β we see that the fastest plasma process is the ohmic heating γ_{OH} and that the dominant transport process is the magnetic field (current) diffusion γ_{MD}.

A thermal instability can occur due to current diffusion into a region of lower resistivity (higher temperature), which aides the ohmic heating in that region, further depressing the resistivity and causing more current diffusion.

This process is depicted schematically in Fig. 1 where the oxygen radiation barrier can be surmounted at Point "A" by allowing the plasma to follow the ohmic heating curve $j_{\parallel} \sim n^{-1} (\gamma_{OH} \sim n)$ instead of $j_{\parallel} \sim$ const. ($\gamma_{OH} \sim n^{-1}$. These two heating curves are the possible steady state solutions to Eq. (2) (V_r is negligible). The plasma switches from the $j_{\parallel} \sim$ const. to the $j_{\parallel} \sim n^{-1}$ heating curve via current diffusion and can thus overcome the radiation barrier at isolated spatial points. As this occurs the density profile remains almost unchanged since γ_{PD} is small.

This instability has been previously considered by Kadomtsev[1] for the case of a weak current along a strong magnetic field ("superheating instability"). We consider the case of a strong current along a strong magnetic field and also a non-equilibrium electron temperature and the presence of impurities.

The physics contained in Eqs. (1)-(6) is represented more clearly by transforming these equations into a normalized poloidal flux representation where the dependent variables are adiabatic invariant quantities.[2] This representation is useful for both numerical and analytical work.

The new independent variable is defined as

$$x = \int_o^r B_\theta\, dr / \phi_{PT} \quad , \qquad \phi_{PT} = \int_o^a B_\theta\, dr \quad ,$$

where a is the plasma radius. The new dependent variables are

$$Y = r^2/a^2 \qquad , \qquad Y' \equiv \frac{\partial Y}{\partial x} = \frac{2r\phi\phi_o}{a^2 B_\theta} \qquad ,$$

$$P = \frac{aB_z}{2\phi_o} Y' \qquad , \qquad N = \frac{n_e}{2n_o} Y' \qquad , \qquad \theta_e = \frac{T_e}{T_o} Y'^{2/3} \qquad , \qquad \theta_i = \frac{T_i}{T_o} Y'^{2/3} \qquad ,$$

where $\phi = \phi_{PT}/\phi_o$ and ϕ_o, n_o, and T_o are reference quantities. Using this representation we perform a linear stability analysis on Eqs. (1)-(6) assuming low plasma beta. We assume

$$P' = P_o' + \epsilon P'_1(x,\tau) \quad (\epsilon \ll 1) \qquad ,$$

$$\theta_e = \theta_{eo}(\tau) + \epsilon\theta_1(x,\tau) \qquad ,$$

$$\theta_i = \theta_{io}(\tau) \qquad ,$$

where P_1', $\theta_1 \sim e^{ikx+\omega t}$, P_o' is a constant, and τ is time measured in units of γ_{MD}^{-1} (note $j_\parallel \sim P'$). We assume γ_{ITC} to be large so that no perturbation in the ion temperature can develop. The result of this stability analysis yields

$$\frac{\partial}{\partial \tau} P_1' = \frac{\partial^2}{\partial x^2} \left[c_1 n_o \left(\frac{P_1}{Y_o}\right)' - \frac{3}{2} c_1 n_o \left(\frac{P_o}{Y_o}\right)' \zeta \right] \qquad , \tag{7}$$

$$\frac{\partial \zeta}{\partial \tau} = \frac{c_2 n_o}{2\theta_{eo}} (P_o/Y_o)'^2 \zeta + c_3(1-\alpha)\theta_{eo}^{\alpha-1} \zeta + c_4 n_o\left(\frac{3}{2} - \frac{5}{2}\frac{\theta_{io}}{\theta_{eo}}\right) \zeta \qquad , \tag{8}$$

$$\frac{\partial \theta_{eo}}{\partial \tau} = c_2 n_o\left(\frac{P_o}{Y_o}\right)'^2 - c_3\theta_{eo}^\alpha - c_4 n_o(\theta_{eo} - \theta_{io}) \qquad , \tag{9}$$

where $\zeta = \theta_1/\theta_{eo}$ and c_1-c_4 are quantities constant in time. In arriving at Eqs. (7)-(9) the electron thermal conduction term, the perpendicular current, the density equation, the pressure balance equation, and consequently all terms in Eqs. (1)-(4) containing V_r have dropped out. The relevant quantity driving the instability is ζ, the relative electron temperature perturbation, as can be seen from Eq. (7). The effect of a spatially uniform energy loss term is to increase ζ by reducing the growth of the zeroth order electron temperature θ_{eo}. For the equilibrium case $\theta_{eo} =$ const., the growth rate ω of this instability

226

approaches the ohmic heating rate γ_{OH}, which is the fastest time scale in Eqs. (1)-(6).

In Fig. 2 we present results of a numerical simulation using ZT-40 parameters (I_z = 500 kA, a = 20 cm). There is a uniform plasma density of $1 \times 10^{14} cm^{-3}$ and, except for the inner 4 cm, a 10%, 2.5 cm wavelength initial current perturbation that is assumed to remain from the formation phase. The initial temperature is a uniform 10 eV. The parallel current and the electron temperature are shown as a function of radius at the initial time and for three cases at 100 μs: impurity free, 2% oxygen, and 4% oxygen. From Fig. 2 we note the following:

1) θ_0 is above the 25 eV oxygen radiation barrier for all cases.
2) $\delta j_{\parallel}$ grows even for 0% ox. due to the temperature equilibration term.
3) temperature wells for the 4% ox case are caught on the ox rad. barrier leading to large $\delta j_{\parallel}$.

We see from this figure the large effect that a small amount of oxygen can have on an initial current perturbation.

The classical damping mechanism for this instability is seen to be the ion thermal conductivity, which is effective in damping the electron temperature perturbation once the ion temperature $\theta_{io} > \frac{3}{5}\theta_{eo}$. However, this can take a time on the order of milliseconds to happen.

III. Anomalous Transport

Since the current and temperature perturbations grow by a large amount before they are damped by a classical mechanism, we must expect that some anomalous mechanism will provide the damping.

The anomalous damping mechanism must be such that the resultant $\chi_{\perp e}/\eta_{\parallel}$ is greatly enchanced over the classical case.

The observed electron thermal conductivity in tokamaks is 100 times classical. When simulations were performed with this value of $\chi_{\perp e}$ the initial current perturbation decays. Since tokamaks have amounts of impurities that are in the range of those used in these calculations, it is interesting to speculate that there could be some connection between the thermal instability and the anomalous electron conductivity observed in tokamaks.

IV. Conclusions

1. The RFP can be thermally unstable at low beta due to the interaction of current diffusion and ohmic heating.

2. Initial current perturbations remaining from the formation phase may be expected to grow rapidly with only modest amounts of plasma impurities present.

3. Such perturbations will be damped by some anomalous mechanism which increases $\chi_{\perp e}/\eta_{\parallel}$ above the classical value.

References

1. B. B. Kadomtsev, Reviews of Plasma Physics, Vol. 2, p. 153.
2. E. J. Caramana and F. W. Perkins, PPPL-1626, 1980.
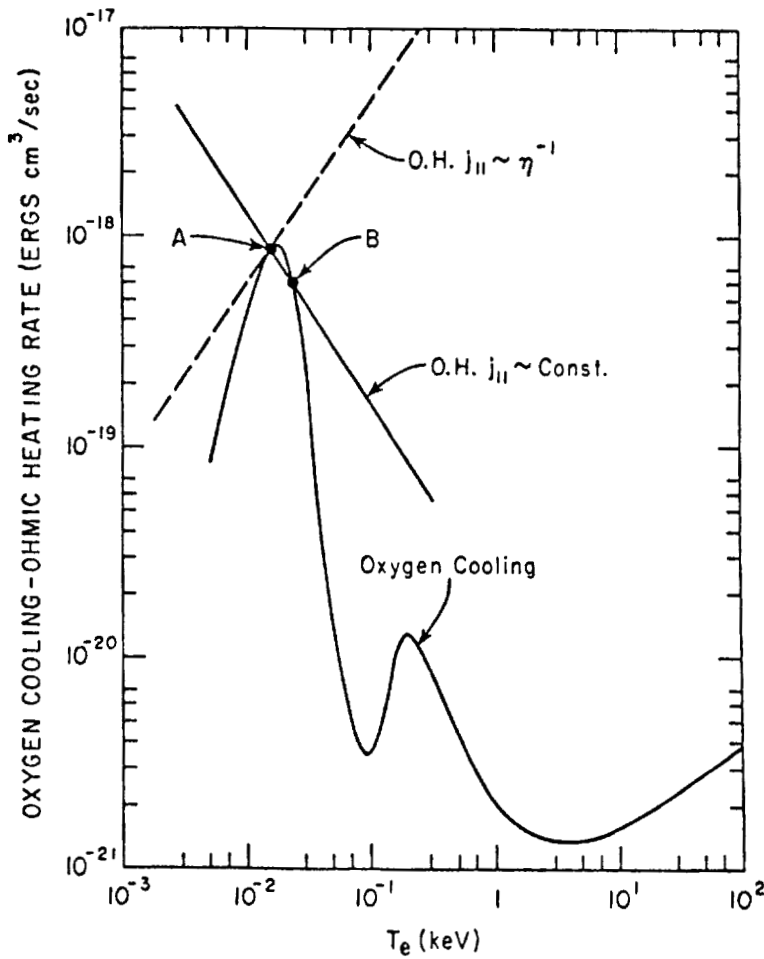
Figure 1
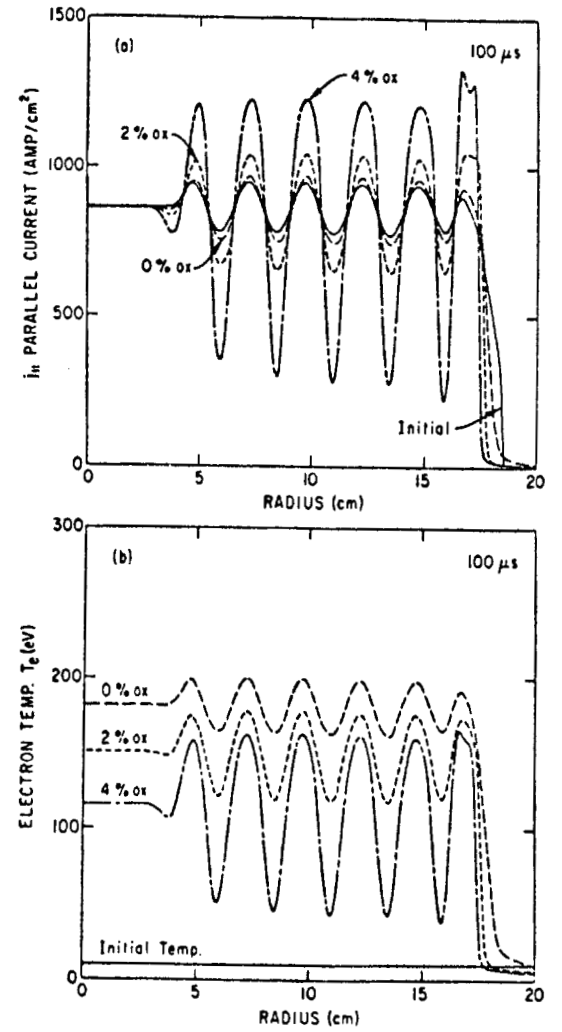
Figure 2

Fig. 1. The radiation cooling rate due to oxygen is given as a function of temperature assuming coronal equilibrium. Also drawn are the ohmic heating rate for a constant current density (solid line), shown to intersect this curve at points A and B, and the ohmic heating rate for $j \sim \eta_{\parallel}^{-1}$ (dashed line), shown to intersect the cooling curve at point A.

Fig. 2a. The parallel current is shown at the initial time, with a 10%, 2.5 cm wavelength perturbation from 4 cm to 17 cm using ZT-40 parameters, and at 100 μs for oxygen impurity concentrations of 0%, 2%, and 4% of the deuterium density ($1 \times 10^{14} cm^{-3}$).

Fig. 2b. The electron temperature is shown at the initial time and at 100 μs.

228

NUMERICAL MODELING OF PLASMA MOTION
IN
RFP EXPERIMENTS

by

T. A. Oliphant

Los Alamos Scientific Laboratory

Los Alamos, New Mexico

A numerical 1-D, cylindrical model for the dynamic and quasi-equilibrium motion of plasmas in RFP and other related experiments has been developed and discussed in an article to appear soon.[1] It is possible to cast the methodology in a clearer and more general form and this is done in the following.

The one space dimension is the radial variable $r(x,t)$ expressed in terms of the Lagrangian space variable x and time t where x is related to the initial configuration by

$$x = \frac{r(x,o)^2 - r(o,o)^2}{2} \tag{1}$$

Thus, the inverse compression $V(x,t)$ is given by

$$V(x,t) = \frac{\partial}{\partial x}\left(\frac{r^2}{2}\right)\Big|_t \tag{2}$$

and the transformation to Lagrangian coordinates by

$$\frac{\partial}{\partial r}\Big|_t = \frac{r}{V}\frac{\partial}{\partial x}\Big|_t \tag{3}$$

$$\frac{\partial}{\partial t}\Big|_r = \frac{\partial}{\partial t}\Big|_x - \frac{ur}{V}\frac{\partial}{\partial x}\Big|_t \tag{4}$$

[1] T.A. Oliphant, "Dynamic and Quasi-Equilibrium Langrangian MHD in 1-D" *J. Comp. Phys.* to be published.

where the velocity u is given by

$$u = \frac{dr}{dt} \tag{5}$$

The Lagrangian equations of motion in the single temperature approximation are

$$\frac{du}{dt} + \frac{r}{\rho_o} \frac{\partial}{\partial x}\left(p + \frac{B_z^2}{2\mu_o}\right) + \frac{1}{\rho_o r} \frac{\partial}{\partial x}\left(\frac{r^2 B_\theta^2}{2\mu_o}\right) = 0 \tag{6}$$

$$e_T \frac{dT}{dt} + \frac{TP_T}{\rho_o} \frac{dV}{dt} - \frac{1}{\rho_o} \frac{\partial}{\partial x}\left(\frac{r^2 \kappa}{V} \frac{\partial T}{\partial x}\right) + \dot{e}_D - \dot{e}_{br} = 0 \tag{7}$$

$$\frac{\partial}{\partial t}\left(\frac{VB_\theta}{r}\right) = \frac{\partial}{\partial x}\left(\frac{\eta^{zz}}{\mu_o V} \frac{\partial(rB_\theta)}{\partial x}\right) - \frac{\partial}{\partial x}\left(\frac{r\eta^{\theta z}}{\mu_o V} \frac{\partial B_z}{\partial x}\right) = 0 \tag{8}$$

$$\frac{\partial}{\partial t}\left(VB_z\right) = \frac{\partial}{\partial x}\left(\frac{r^2\mu^{\theta\theta}}{\mu_o V} \frac{\partial B_z}{\partial x}\right) - \frac{\partial}{\partial x}\left(\frac{r\eta^{\theta z}}{\mu_o V} \frac{\partial(rB_\theta)}{\partial x}\right) = 0 \tag{9}$$

where most of the variables are obvious, but e_T and p_T are temperature derivatives of specific energy and pressure, $\dot{e}_D$ and $\dot{e}_{br}$ are Joule heating and bremsstrahlung loss terms, κ is the thermal conductivity and the η coefficients are from the resistivity tensor. Note that the magnetic field diffusion equation (8) and (9) are in flux-conserving form.

The above set of four PDE's are differenced straight-forwardly in the fully forward, implicit approximation. A splitting method was devised to solve for the adiabatic parts of the coupled difference equations and then to solve separately for the diffusive effects. As an example of how this technique can be generalized, consider a partially ionized plasma with different ion and electron temperature. The free-electron density n_e is given in terms of the atom number density by

$$n_e = fn_a \tag{10}$$

This gives rise to a continuity equation for t with a source term. Since there are now two energy equations, there are a total of six difference equations which can be abbreviated as follows:

$$F_i^f (X_j) = 0 \tag{11}$$

$$F_i^r (X_j) = 0 \tag{12}$$

$$F_i^{Ta} (X_j) = 0 \tag{13}$$

$$F_i^{Te} (X_j) = 0 \tag{14}$$

$$F_i^{Bz} (X_j) = 0 \tag{15}$$

$$F_i^{B\theta} (X_j) = 0 \tag{16}$$

where X_j represents the indexed independent variables $(f_{j+\frac{1}{2}}, r_j, T_{a,j+\frac{1}{2}}, T_{e,j+\frac{1}{2}}, B_{z,j+\frac{1}{2}}, B_{\theta,j+\frac{1}{2}})$/

Upon applying Newton's method and differentiating (11) - (16), this whole set of equations can be expressed as a block-tri-diagonal system in the independent variables. The block elements are 6x6 matrices. Various splitting techniques can be used for solving this system of equations. a new version of the RAVEN code has been developed by splitting into three 2x2 block-tri-diagonal systems. The previous paper[1] discussed elimination of adiabatic variables to form a simple tri-diagonal system.

Any of these splitting methods can be made fully implicit by an outer loop which checks general self-consistency.

As an example relevant to this RFP conference the ZT-40 implosion has been calculated with the time-dependent boundary fields shown in Fig. 1. The motion of the plasma boundary relative to the containing wall is shown in Fig. 2.

FIGURE 1
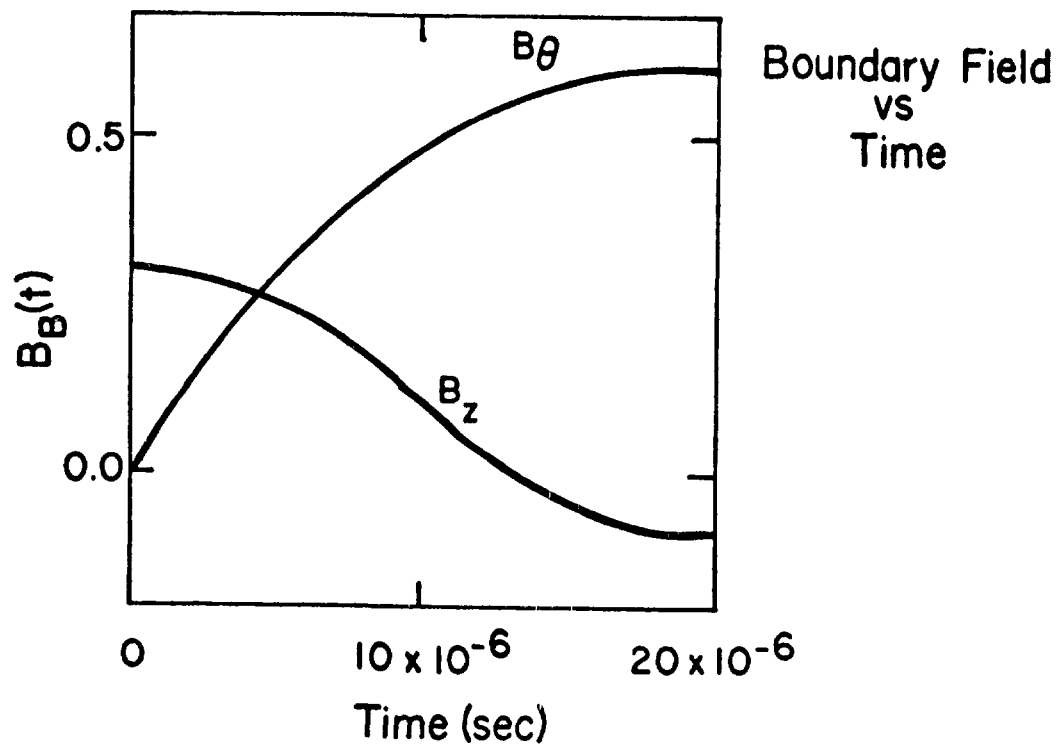
TIME DEPENDENT, IMPOSED BOUNDARY FIELD.

FIGURE 2
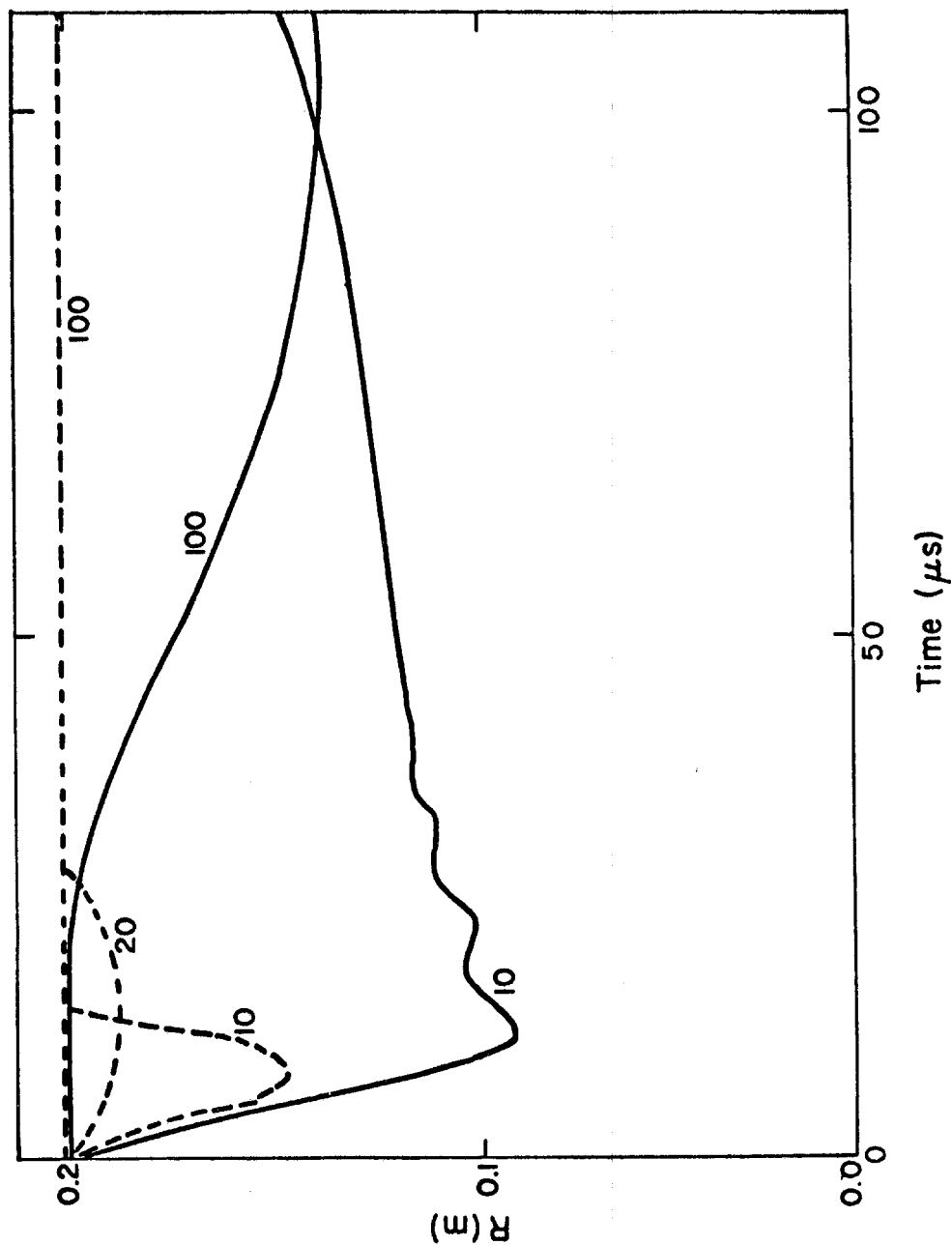
MOTION OF OUTER PLASMA RADIUS VS TIME FOR DIFFERENT RISE TIMES.
THE SOLID CURVES ARE FOR CLASSICAL AND THE DOTTED CURVES FOR
ANOMALOUS RESISTIVITY.

THE BOUNDARY PROBLEM IN RFP DIFFUSION - Richard Christian, Purdue University

In calculations of classical transport in the reverse field pinch it is necessary to assume boundary or interface conditions. This frequently has been accomplished by simply assuming limiting values (floors or pedestals) for the bounding temperatures, pressures, etc. In many cases of interest the plasma behavior in the bulk of the plasma is relatively insensitive to the particular values chosen at the plasma edge. On the other hand, it is of primary importance if one wishes to program the plasma temporal behavior by means of electric fields applied at the plasma edge. It is the purpose of this paper to examine possible mathematical expressions of the boundary conditions for self-consistency and physical plausibility.

We shall assume throughout that axial symmetry holds and the classical transport prevails. For convenience and to a good approximation for the parameter regime of interest, we shall use a one-fluid(i.e. one-temperature) model, neglect thermal forces and use the large B field values (Braginskii's) for the transport coefficients. To start we write the dimensionless and scaled equations that obtain in a cylindrical geometry. These we compare with those obtained for a 1½-D treatment in toroidal geometry.

The cylindrical or 1-D form of the equations are (using a diffusion time scaling and letting $x=r^2$) :

$$\rho_t + (V\rho)' \propto R' \equiv 0$$

$$b_t + (Vb)' = X'$$

$$g_t + (Vg)' = Y'$$

$$p_t + Vp' + \gamma pV' = (\gamma-1)(Z' + Q)$$

where $b \propto B_z$, $g \propto B_\theta/r$, $' = \partial/\partial x$; and with $B^2 = b^2 + xg^2$, $\Delta\eta = \eta_{||} - \eta_\perp$ we have

$$X = 4x/T^{3/2}(\eta_{||} b' + \Delta\eta bp'/2B^2)$$

$$Y = 4/T^{3/2}(\eta_{||} (xg)' + \Delta\eta xgp'/2B^2)$$

$$Z = K_\perp(\rho^2 x/B^2 T^{\frac{1}{2}})T'$$

$$Q = \eta_{||} j_{||}^2 + \eta_\perp j_\perp^2 = 4/(B^2 T^{3/2}) [\eta_{||} (xgb' - (xg)'b)^2 + \eta_\perp x(p'/2)^2]$$

where $\eta_{||}$, $\eta_\perp$ and $K_\perp$ are numerical factors of order one. At $x=0$, b, g, ρ and p are finite while $V=0$. b(x) in general goes through zero, g(x) does not, and ρ, p and T are positive. Furthermore, with the choice $R'=0$ as indicated above V becomes the mass flow velocity. It is more useful for the RFP configuration to use the poloidal flux velocity given by $U=V - Y/g$. The equations then are

$$\rho_t + (U\rho)' = -(\rho/g \cdot Y)'$$

$$g_t + (Ug)' = 0$$

$$b_t + (Ub)' = (X - b/g \cdot Y)'$$

$$p_t + Up' + \gamma pU' = (\gamma-1)(Z' + Q) - (p/g \cdot Y)' - (\gamma-1)p (Y/g)'$$

We now introduce adiabatic variables $\mu = p/g^\gamma$, $\nu = b/g$, $\xi = \rho/g$ and eliminate the explicit dependence upon U, by using the convective derivative, $d/dt = \partial/\partial t + U\partial/\partial x$, with the result

$$d\mu/dt = (\gamma-1)(Z'/g + Q)/g^\gamma - \gamma\mu Y'/g - Y\mu'/g$$

$$d\nu/dt = (X - \nu Y)'/g$$

$$d\xi/dt = -(\xi Y)'/g$$

and, $\qquad (\mu g^\gamma)' + (gv)(gv)' + g(xg)' = 0 \qquad$ for equilibrium.

Next we give the Grad-Hogen 1½-D formulation appropriate for the RFP config-
uration when extended to anisotropic resistivity. The surface averaged equations
for the poloidal, ψ, and toroidal, χ, fluxes are

$$\chi_t + U\chi' = \eta_{\shortparallel} K(\chi'/A)' - (p'\chi'/(\psi')^2)(\eta_{\shortparallel}\tau^2/A - \Delta\eta\langle(rB_\chi/B)^2\rangle) := X$$

$$\psi_t + U\psi' = \eta_{\shortparallel}/A(K\psi')' - (p'/\psi') (\eta_{\shortparallel}\tau^2/A - \Delta\eta\langle(rB_\chi/B)^2\rangle) := Y$$

where now $'=\partial/\partial V$. The pressure and density equations are

$$p_t + Up' + pU' = (\gamma-1)(\lambda_* T')' + (\gamma-1)(\eta_{\shortparallel} j_{\shortparallel}^2 + \eta_\perp j_\perp^2) := (\gamma-1)(Z'+Q)$$

$$\rho_t + (U\rho)' = 0$$

and for equilibrium $\Delta^*\psi = -r^2(dp/d\psi) - f(df/d\psi)$
where the surface averaged quantities are

$$\langle 1/r^2 \rangle = A, \langle r^2 \rangle \langle 1/r^2 \rangle - 1 = \tau^2, \quad fA = \chi'$$

$$U = \langle \vec{u}\cdot\nabla V\rangle, \quad K = \langle|\nabla V|^2/r^2\rangle, \quad \langle\Delta^*\psi/r^2\rangle = (K\psi')'$$

With ψ as the independent variable, we let $\psi' = \alpha$, $\mu = p/\alpha^\gamma$, $v = \partial\chi/\partial\psi \equiv \dot{\chi}$ and $\xi = \rho/\alpha$.
These quantities satisfy

$$d\mu/dt = (\gamma-1)(\dot{Z} + Q)/\alpha^\gamma - \gamma\mu\dot{Y} - \dot{\mu}Y$$

$$dv/dt = (X - vY)^{\cdot}$$

$$d\xi/dt = -(\xi Y)^{\cdot}$$

$$\alpha(K\alpha)^{\cdot} + (\mu\alpha^\gamma)' + (v\alpha)(v\alpha/A)^{\cdot} = 0$$

From the above we can see that the toridal corrections are smaller than the
corrections for anisotropic resistivity. For nearly cylindrical cross-sections
K is proportional to r^2 (=x), and for small aspect ratios A is nearly constant.
Thus one can determine very accurately the classical transport using a 1-D formu-
lation.

There are two somewhat different techniques available for obtaining the
time evolution of a plasma from the preceeding equations. In both cases one
starts with   initial profiles defined by giving two of the three profiles,p,
g, or b and obtaining the third from pressure balance. For the RFP configura-
tion we have found it convenient to specify the pitch or v and then choosing the
pressure to fractionally satisfy the Suydam criterion as well as pressure balance.
After the initial conditions have been obtained the system is allowed to diffuse
for a short time after which the equilibrium condition is again imposed so that
the system essentially remains in equilibrium at all times. In the second method
the boundary requirements are somewhat more specific. From the equations of
motion we find that the flow velocity satisfies

$$(\gamma p + 2B^2)V' + \int_0^x V(g^2)' = Z' + Q + 2xgY' + 2bY' + 2\int_0^x g^2 V' - \partial/\partial t(p+B^2)\big|_{x=0} := W$$

From the flow velocity we can compute the poloidal velocity, $U = V - Y/g$, and
then evaluate the Jacobian $\qquad J_t(x,x_o) = 1 - \int_0^t \partial U/\partial x_o$

and the new fields from the relation. $g(x,t) = g(x=x_o,t=0)/J_t(x,x_o)$

As an exercise let us imagine the position of the free interface specified
as a function of time $x_1 = x_1(t)$. Or more directly write $V(x_1) = dx_1/dt$. Then
we see that V(x) satisfies the integral equation. $(p* := \gamma p + 2B^2)$

$$V(x,t) = \int_o^x W/p* - \int_o^x 1/p* \int_{x'}^{x'} V(g^2)'$$
$$+ (\int_o^x 1/p*)/\int_o^{x_1} 1/p*)[V(x_1,t) + \int_o^x 1/p* \int_{x'}^{x_1} V(g^2)' - \int_o^x 1/p*]$$

Next we can relate the flow velocity to the electric drift (ie, Poynting flux) velocity. This drift velocity in dimensionless units is

$$V_E(x) = -b/B^2 \int_o^x \partial b/\partial t - xg/B^2 [\int_o^x \partial g/\partial t + 4\eta_{\|}g(0)/T^{3/2}(0)]$$

The desired relation follows directly from the equations of motion and is

$$V(x) = V_E(x) - 2x/(B^2 T^{3/2})(\eta_\perp p')$$

We now see that a partial "handle" on controlling the plasma is available, by giving

$$e_\theta(x) = -\int_o^x \partial b/\partial t, \text{ and } e_z(x) = \int_o^x \partial g/\partial t + 4\eta_{\|}g(0)/T^{3/2}(0)$$

as a function of time.

A fully crowbarred configuration corresponds to $e_\theta(x_1) = e_z(x_1) = 0$. In this case the toroidal flux is conserved and the poloidal flux is depleted and appears as a resistive voltage drop on axis.

The remaining conservation or balance equations are those of particle,

$$\int_o^x \partial p/\partial t + Vp|x=x_1 = 0, \text{ and energy conservation}$$
$$d/dt \int_o^x (3/2p+B^2) + [2V_E B^2 + 5/2pV - K_\perp(\rho^2 x/(B^2 T^{1/2}) T'] x=x_1$$

We proceed on the basis that these balance equations must be satisfied as a minimal requirement for any numerical procedure that solves the transport. We may allow anomalous behavior in the magnitude or scaling dependence of the transport coefficients themselves but the balance equations remain inviolate. For the cases of our concern the pressure and density will be assumed to vanish at a free interface thus conserving particles, or the flow velocity will be outward at a fixed wall allowing the loss of particles.

The most important quantity available to the experimenter is the Poynting flux. The experimentalist wishes to know what voltage (E_θ and E_z or E_χ and E_φ) schedule to apply at the gaps in a conducting wall. The theorist has at best a schedule of plasma interface position that maintains equilibrium and stability. These two specifications are separated by a "vacuum" region in which atomic physics plays the key role. It does not appear likely that progress in predicting and calculating plasma behavior in this region will be forthcoming soon. It must therefore be our intent to understand the limits of influence from this region on the plasma behavior so as to minimize any adverse effects.

In general one considers initial profiles chosen consistant with pressure balance. Only those profiles that do not change rapidly on the diffusion time scale are acceptable initial profiles. We have lately used the following parametrization of the initial profiles. First we specify the pitch; $\nu = P_o(1-x)^N - P_1 x$, with parameters P_o, P_1 and N. We exploit the Suydam criterion in the form $p' + \alpha g^2 x/2(\nu^1)^2 = 0$ where α is a parameter generally less that unity. This allows the heated plasma to remain with Suydam limits. Thus we find the equation

$$(g^2)' (\nu + x) + (g^2) [(\nu^2)' + 2 - \alpha(\nu')^2] = 0$$

for a unique g and hence p and b profiles.
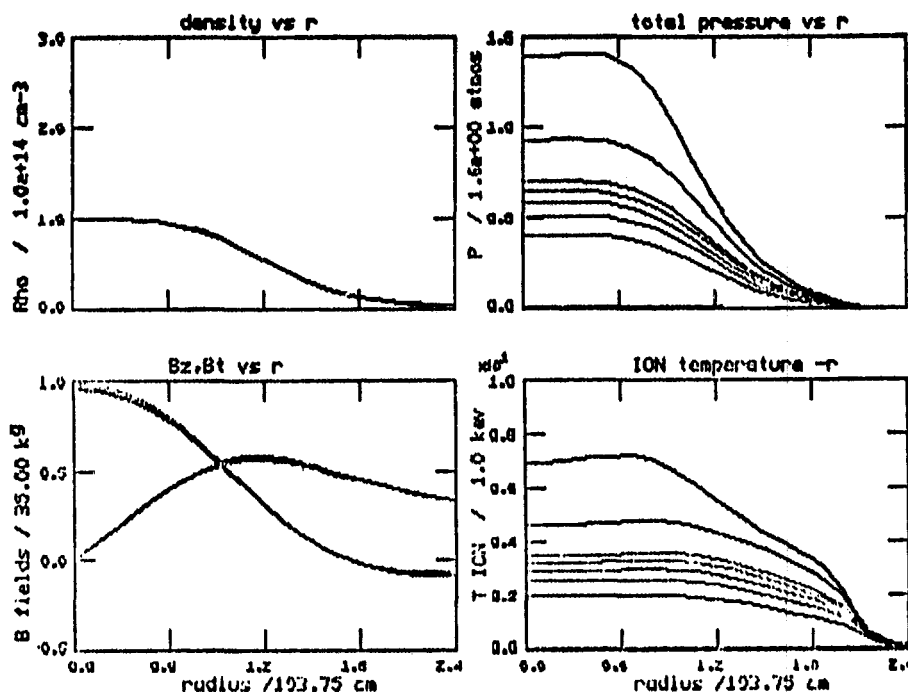
Fig. 1. Plasma profile evolution with time in units, $4\pi\sigma r^2/c^2$. These profiles include brems strahlung loss and D-T energy gain. Note the almost total lack of plasma movement and the small depletion of the magnetic fields. For these profiles the Suydam criteria is satisfied at all radii and for all times. (There is a limited range of profiles that exhibit this "nice" behavior.)

A problem remaining is the treatment of the plasma edge. Let us list some of the possibilities:

1. **Plasma leans on a wall** and the system is crowbarred. This system has $E = V = p' = T' = \rho' = b' = (xg)' = 0$. It is the easiest to program and no numerical difficulties occur and has been extensively used to study the evolution of proposed profiles (see figure 1). A major result of this study is that to avoid the overheating problem j_u must be small in the outer plasma regions (where ρ is small). This requirement is acheived by setting $N \simeq 2$ (rather than $N \simeq 1$) in the pitch profile. This boundary condition is of limited interest since it puts the entire burden of plasma control into the setup phase, therefore we continue to list:

2. **Plasma leans on a wall** initially, but the **Poynting flux is inward** so that in general we expect a squeezing of the plasma (ie, very slow pinch). Now one needs an explicit interface model. If for example, the product $(\eta_\perp p')$ is zero there is no penetration of flux into the plasma since the Poynting flux velocity and the flow velocity are the same at the plasma edge. We consider this case in 5, below while $(\eta_\perp p')$ finite is treated in 6 and 7.

3. **Surface current model.** In this model we stipulate that some finite fraction of the plasma current flows in a sheet on the surface. Thus, the plasma pressure and "tangential B" may be discontinuous. To use this model we will need to find a selfconsistant formulation.

3. **The anomalous $\eta_\perp$ model.** We stipulate that although p' vanishes at the plasma edge $\eta_\perp$ becomes anomalous in such a manner that the product $(\eta_\perp p')$ remaines finite. The aim of this model would be to mock the atomic physics but it is difficutl to see how the atomic physics brings about the desired limit to the quantity $(\eta_\perp p')$.

5. **The current goes to zero at the surface model.** From the Taylor form at the plasma edge we calculate the index. Let us denote the distance from the plasma edge $x_0(t)$ to a point in the plasma by $u=(x_0-x)/x_0$. We consider that the temperature floats. The minimum index for the density is thus 2. We find:

237

$\rho = \rho_2 u^2 + \dots$, $T = T_0 u^0 + \dots$, $p = p_2 u^2 + \dots$, $b = b_0 + b_2 u^2 \dots$, $(xg) = (xg)_0 + (xg)_2 u^2 + \dots$

The reason that no linear terms in u appear in the expressions for the field is that for a floating temperature $(\eta j^2)/\rho$ must remain finite and hence $j_\perp$ and $j_\parallel$ must be linear in u. This model is self-consistent and remains self-consistent as the profiles evolve. It has $(\eta_\perp p') =$ zero and has the drawback mentioned above (see model 2).

6. **The non-vanishing current at surface model A.** In this case we still assume that the temperature floats but that the pressure is linear in u. The current is finite and the temperature at the plasma edge will tend to rise at an unbounded rate. We must therefore impose some ad hoc remedy. We could for example, impose an anomalous thermal conductivity to remove the heat or allow that (due to microinstabilities) the excess energy is absorbed in turbulent plasma behavior.

7. **The non-vanishing current at surface model B.** In this case we assume that while the temperature itself is unbounded at the plasma edge, more measurable quantities such as the pressure or density vanish at the plasma edge. We make the ansatz that at the plasma edge, $\rho = \rho_e u^{1+\alpha} + \dots$, $T = T_e u^\beta + \dots$, $b = b_0 + b_e u^d \dots$ $(xg) = (xg)_0 + (xg)_e u^e + \dots$,
and attempt to determine α, β, d and e. To satisfy pressure balance we require that $[(1+\alpha+\beta) = d$ and $e > d]$ or $[(1+\alpha+\beta) = e$ and $d > e]$. We assume $(1+\alpha+\beta) = d = e$. Next we calculate that at the plasma edge, $\mu = \mu_0 u^{1+\alpha+\beta}$, $v = v_0$, $\xi = \xi_0 u^{1+\alpha}$
$Y' = Y'_0 u^{\alpha-\beta/2}$ and $X' = X'_0 u^{\alpha-\beta/2}$

The indicial equations for v and ξ are satisfied if $\alpha = \beta/2$. The calculations for determining the μ equation give

$$Z' = (\gamma-1) K_{\perp 0} \chi T_e^{\frac{1}{2}}/B_0^2 \ (1+3/2\beta) u^{\frac{3}{4}\beta} := F_a \beta (1+3/2\beta) u^{\frac{3}{4}\beta} \qquad u'^{\frac{3}{4}\beta}$$

$$Q = (\gamma-1)4/(B_0^2 \ T_e^{3/2}) \ (\eta_\parallel \ ((xg)_0 b_e - (xg)_e b_0)^2 + \eta_\perp x (p'/2)^2) := F_b (1+3/2\beta)^2 u^{\frac{3}{4}\beta}$$

$$d\mu_0/dt \ u^{1+\frac{3}{4}\beta} = (\beta F_a + (1+3/2\beta) F_b)(1+3/2\beta) u^{\frac{3}{4}\beta} + O(u^{1+\frac{3}{4}\beta})$$

and thus requires that $(\beta F_a + (1+3/2\beta) F_b) = 0$. For β we write $\beta = -2/(3+2F_a/F_b)$ In applications $F_a/F_b \ll 1$ we choose to write $\beta = -2/3 + \epsilon$ and summarize the edge results: $\rho = \rho_e u^{2/3+\epsilon/2}$, $T = T_e u^{-2/3+\epsilon}$, $b = b_0 + b_e u^{3/2\epsilon}$, $xg = (xg)_0 + (xg)_e u^{3/2\epsilon}$. Thus $p' = -\frac{3}{4}\epsilon p_e T_e u^{-1+\frac{3}{4}\epsilon}$ and $(\eta_\perp p') = -(\eta_\perp \frac{3}{4}\epsilon \ p_e T_e^{-\frac{1}{2}})$ is in general non-zero, positive and remains finite at the plasma edge, allowing the penetration of flux into the plasma. This result means that the (p') term always contributes in such a way as to expand the plasma $(V > 0)$.

It appears in summation that we must modify the classical transport scaling near a plasma interface. If one insists upon using strictly classical scaling then, indeed, numerical calculations show the development of unphysical profiles.

At this point we may ask. "What can be done if the classical model is simply inadequate? Can we find, for example, a model evolving on the diffusion time scale which models the gross features of microscopic phenomena evolving on a much faster time scale?" Let us face these problems in a workshop session.

RELAXATION REVISITED

J. B. Taylor

Culham Laboratory, Abingdon, Oxon., OX14 3DB, UK
(Euratom/UKAEA Fusion Association)

Introduction

The original theory[1] of plasma relaxation was based on simple concepts and has proved remarkably successful in describing the general behaviour of toroidal pinches. It seems appropriate, therefore, to review these concepts as a background and a guide for more recent developments.

Relaxation Theory

The motivation for the theory was the observation that, when the pinch parameter θ exceeds some critical value, toroidal pinches frequently relax to a state which does not depend on initial conditions and in which a spontaneously generated reverse field appears. It seemed to me that one could liken this to a flexible conductor in a viscous medium. Since viscosity can only dissipate energy the flexible conductor comes to rest when its energy is a minimum subject to the inductive constraint LI = constant. (This is a state of maximum inductance, see below.)

Now the plasma resembles an infinite number of interlinked flexible conductors and the problem is to identify the appropriate constraints. If the plasma is _perfectly_ conducting the fluid moves precisely with the magnetic field and each field line maintains its identity. The number of closed field lines interlinked with any other closed line is also maintained. These properties are expressed mathematically by the statement that $\int \underset{\sim}{A}.\underset{\sim}{B}$ is an invariant for each infinitesimal closed flux tube. However, minimising the energy, subject to all these constraints certainly does not lead to a universal final state. On the contrary, the final state depends crucially on the initial state and this is not what is observed.

On the other hand, if the resistivity is non-zero, however small, topological properties of the field are not preserved and lines of force can reconnect. As $\eta \to 0$ the region over which resistivity acts and reconnection occurs gets smaller, but the rate of reconnection _does not diminish as fast as_

η (and may not diminish at all). Consequently, when a real plasma is set in motion we should expect it to preserve only those invariants which do not depend on the identity of lines of force. For a plasma in a conducting toroidal shell there are only two such invariants; the toroidal flux ψ and $K = \int \underset{\sim}{A}.\underset{\sim}{B}$ over the total volume. The state of minimum energy subject to these two constraints _is_ universal and described by the pinch parameter θ alone.

The relaxed states calculated in this way show remarkable agreement with observation[2] including (i) the fact that there is a relaxed state, independent of initial conditions and described by θ alone, (ii) the main features of the magnetic fields observed in this state, (iii) the appearance of a reverse toroidal field when $\theta \gtrsim 1.2$, (iv) the appearance of a helical deformation when $\theta \gtrsim 1.6$ (v) the onset of current limitation when $\theta \gtrsim 1.6$ (the application of higher loop-voltage does not produce significantly more current; instead the plasma inductance increases - c.f. the flexible conductor model!).

In the final analysis this theory requires only that $K = \int \underset{\sim}{A}.\underset{\sim}{B}$ change more slowly than does the energy $W = \int B^2/2$ and the topological constraints. I have already noted that viscosity reduces W but has no effect on K, and that an infinitesimal resistivity permits the topological constraints to be violated but need produce no significant effect on the global K. Even resistivity alone can provide the required mechanism, for in terms of Fourier modes

$$\frac{dK}{dt} = \eta \sum \underset{\sim}{k}.B_k \times B_{-k} \quad , \quad \frac{dW}{dt} = \eta \sum k^2 B_k.B_{-k}$$

so that in any process occurring over short lengths, i.e. at large wave-number, resistivity will have a much larger effect on W than on K.

Plasma Pressure

The fact that the relaxed state has zero pressure (or more precisely zero pressure gradient) has led to some confusion and to the belief that plasma pressure was neglected in the theory. This is not so. In the full theory pressure is included but does not alter the result; the final state has $\nabla p = 0$. This should be expected because if one envisages that lines of force break and reconnect then one must equally envisage that while

reconnection is taking place plasma may flow from one flux tube to another and so equalise the pressure. Hence zero pressure gradient is not an approximation; it is a consequence of relaxation. Of course one can argue that plasma flow is slower than magnetic reconnection and so one might arrive at states which are almost fully relaxed in the magnetic sense but only partially relaxed in the pressure sense. Furthermore we know that starting from a relaxed state it is possible to raise the pressure to a finite, sometimes very significant, value before the onset of instabilities which trigger a new relaxation (see tokamaks below).

Gauge Invariance

Another point of confusion concerns gauge invariance. It may be surprising that the important invariant involves the vector potential $\underset{\sim}{A}$ which is not usually an observable. However, K itself is gauge invariant. For single valued gauge functions in a complete toroidal shell this is obvious, but if one wishes to consider situations in which there are azimuthal and toroidal cuts in the shell, and the gauge may not be single valued, then the appropriate form for the invariant K is

$$K = \int \underset{\sim}{A}.\underset{\sim}{B} \; d\tau - \oint \underset{\sim}{A}.d\underset{\sim}{\ell} \; \oint \underset{\sim}{A}.d\underset{\sim}{s}$$

where $\oint A.ds$ and $\oint A.d\ell$ are integrals round closed circuits the short and long way around the bounding toroidal shell. Using this form one can discuss the effect of voltages applied across the azimuthal and toroidal cuts to sustain the plasma[3].

Tokamaks

I mentioned that to initiate relaxation it seems necessary for the plasma to be first set into fairly violent motion. This is to enable a very small resistivity to work its effect and destroy the purely topological constraints. This presumably explains why relaxation is an almost universal phenomena in pinches - where there are many possible modes of instability and a violent plasma production phase - but not in tokamaks where there are fewer modes of instability and experimenters usually manage to avoid them. Nevertheless, there are relaxed states for the tokamak regime and probably the so-called "disruption" in tokamaks is simply their form of relaxation. Certainly the expansion of the current channel, the near uniform final current and the

negative voltage-spike are all what one calculates for the relaxed state of a tokamak.

Shaped Cross Sections

An interesting point concerns the influence of the shape of the minor cross section on relaxation. In a cross section with acute angled corners, e.g. an equilateral triangle, the pitch of the lines of force will tend to infinity (as at a separatrix) as one approaches the wall and it may appear that this must interfere with relaxation in some way. However this is not so; there are relaxed states for such shapes[4]. The pitch does indeed tend to ∞ as the corner is approached but as the pinch parameter θ is increased the effect of the corner is restricted to an increasingly narrow boundary layer until at the critical θ for field reversal it disappears. On further increasing θ the boundary layer reappears with the pitch now tending to -∞ . It is easy to calculate the critical value for this reversal to occur (analagous to θ = 1.2 for circle), but it is very difficult to calculate the second critical value (analagous to θ = 1.6). The interesting point about these relaxed states with "corners" is that there is frequently a minimum in the pitch at some intermediate distance between the axis and the wall. In circular systems this is a recipe for serious instability, but in the present case, being fully relaxed states, these plasmas are m.h.d. stable despite the pitch minimum.

Summary

In this talk I have tried to explain, in intuitive rather than mathematical terms, the concepts behind the theory of relaxation. The principal one is that once a real, as opposed to an ideal, plasma is set in motion, lines of force may reconnect. Consequently from the infinity of constraints which exist in an ideal toroidal plasma only the two global ones are effective.

As for the usefulness and correctness of the theory, the situation seems to be that it describes remarkably well the relaxed state which is observed in most toroidal pinches (and occasionally in tokamaks!). What is required now is some way of predicting when relaxation will occur, or re-occur; how rapidly it will proceed and what losses occur during relaxation.

References

(1) J.B. Taylor   Phys. Rev. Lett. $\underline{33}$, 1139 (1974).

Fifth International Conference on Plasma Physics and Controlled
Fusion (Tokyo 1974) IAEA Vol. I p.161.

(2) J.B. Taylor   in Pulsed High Beta Plasmas, Ed. D. Evans, Pergamon
Press (1975) p.59.

(3) M.K. Bevir   Proceedings of this Workshop.

(4) The relaxed state for a rectangular section was calculated some time ago
by C. Gimblett and myself. Recently we, and others including C. Chu and
M-S. Chu, have considered different shapes - triangular, lenticular,
pear-shaped etc. If the corner angle in these shapes is less than $\pi/2$
the pitch tends to infinity as $\log |\psi - \psi_{wall}|$. However near the centre
the effect of the wall is not felt and the pitch diminishes outwards as
in a circular section. Consequently, if $\theta < \theta_c$ for reversal, there is
usually a minimum in the pitch at some intermediate radius. These
properties are relevant to the concept of pitch control by external
windings.

INCOMPLETE RELAXATION AND FINITE BETA PLASMAS

Leaf Turner[*]   and   J. P. Christiansen
University of California,   UKAEA/Euratom, Culham Laboratory
Los Alamos Scientific Laboratory   Abingdon, Oxfordshire
Los Alamos, New Mexico, 87545, USA   OX14 3DB, United Kingdom

I. Introduction

The setting-up phase of toroidal discharges is generally believed to involve complex turbulent processes which cannot be described in detail even by large 3-D MHD codes. However, the interest within the CTR community centers on describing the gross features of the plasma configuration which result from and which are sustained by turbulent processes.

The treatment of plasma relaxation presented in this paper is a natural generalization of the earlier treatment of Taylor[1] and yields predictions of finite beta plasma confinement. The analysis yields predictions for global reversed-field pinch (RFP) parameters such as β_θ, F, and Θ. In qualitative accordance with the experimental evidence that RFP discharges have a cool outer region of high resistivity, we present a plasma model which permits vanishing wall values of pressure and current density.

II. The Green's Function

We consider the magnetic vector potential in the Coulomb gauge for a simply-connected (spheromak) or a multiple-connected (toroid, infinite straight cylinder) domain bounded by a perfect conductor. The vector potential may be decomposed into two solenoidal parts $\vec{A} = \vec{A}^\Phi + \vec{A}^J$. The curl of $\vec{A}^\Phi$ yields a vacuum magnetic field bearing the constrained magnetic fluxes. $\vec{A}^J$ arises solely from the presence of volume current density $\vec{j}$ within the plasma and satisfies $\hat{n} \times \vec{A}^J|_{b'dy} = 0$, which ensures that $\vec{B} \cdot \hat{n}|_{b'dy} = 0$. Note that $\vec{A}^\Phi = 0$ for simply-connected geometries. Our procedure is the vector analog of the procedure used to derive the electrostatic scalar potential of a charge distribution in a domain bounded by a perfect conductor. Indeed, one may note that the magnetic counterpart of the electrostatic energy is $\varepsilon_M = \frac{1}{2c} \int \vec{A}^J \cdot \vec{j} d^3 r$ after subtracting off the constant energy of the flux-determined vacuum magnetic fields. Note the lack of explicit dependence on the surface current density.

244

As in the electrostatic case, a Green's function may be defined. For the case of a domain having a straight cylindrical conducting boundary with circular cross section of radius r_0 containing a magnetic flux $\pi r_0^2 B_0$ and current density $\vec{j}(\vec{r})$

$$\vec{A}^{\Phi}(\vec{r}) = \frac{1}{2} B_0 r \, \hat{\theta} \quad ,$$

$$A_i^J(\vec{r}) = \frac{1}{c} \int d^3r' \, G_{ik}(\vec{r},\vec{r}')j_k(\vec{r}') \quad , \tag{1}$$

where $\left[\nabla^2 \, \ddot{G}(\vec{r},\vec{r}')\right]_{ij} = -4\pi\delta_{ij} \, \delta^{(3)} (\vec{r} - \vec{r}')$. If we define the complete set of solenoidal expansion vectors for $\vec{A}^J$ satisfying the boundary condition, orthonormal on $\int\frac{d^3r}{2\pi L}$

$$\vec{\chi}^{m\ell n}(\vec{r}) \equiv \left[\frac{2}{(\gamma_{mn}r_0)^2 - m^2}\right]^{1/2} \frac{1}{|J_m(\gamma_{mn}r_0)|}$$

$$\times \left[\frac{im}{r}J_m(\gamma_{mn}r)\hat{r} - \gamma_{mn}J_m'(\gamma_{mn}r))\hat{\theta}\right] \exp i(m\theta + k_\ell z) \quad , \tag{2a}$$

$$\vec{\Xi}^{m\ell n}(\vec{r}) \equiv \frac{2^{1/2}}{\nu_{mn}\kappa_{m\ell n}r_0|J_m'(\nu_{mn}r_0)|}$$

$$\times \left[ik_\ell\nu_{mn}J_m'(\nu_{mn}r) \, \hat{r} - \frac{mk_\ell}{r} J_m(\nu_{mn}r)\hat{\theta} + \nu_{mn}^2 J_m(\nu_{mn}r)\hat{z}\right]$$

$$\times \exp i(m\theta + k_\ell z), \tag{2b}$$

where $J_m'(\gamma_{mn}r_0) = J_m(\nu_{mn}r_0) = 0$, $\kappa_{m\ell n} = (\nu_{mn}^2 + k_\ell^2)^{1/2}$, $\lambda_{m\ell n} = (\gamma_{mn}^2 + k_\ell^2)^{1/2}$, and where $k_\ell = \frac{2\pi\ell}{L}$ (L being the longitudinal period length); then

$$G_{ij}(\vec{r},\vec{r}') = \frac{2}{L} \sum_{m,\ell=-\infty}^{\infty} \sum_{n=1}^{\infty} \left[\frac{\chi_i^{m\ell n}(\vec{r})\chi_j^{*m\ell n}(\vec{r}')}{\lambda_{m\ell n}^2} + \frac{\Xi_i^{m\ell n}(\vec{r})\Xi_j^{*m\ell n}(\vec{r}')}{\kappa_{m\ell n}^2}\right] \quad . \tag{3}$$

245

One should note that $\vec{\chi} \propto [\vec{\nabla} \times \hat{a}\phi(\vec{r})]$ and $\vec{\Xi} \propto \vec{\nabla} \times [\vec{\nabla} \times \hat{a}\Psi(\vec{r})]$ where ϕ and Ψ satisfy scalar Helmholtz equations and $\hat{a} = \hat{z}$. (For a spherical boundary, $\hat{a} = \hat{r}$.)[2]

III. Hypothesis of Incomplete Relaxation

Without loss of generality, we shall confine our attention to the case of cylindrical symmetry. (Extension to the helically symmetric case is straightforward.) Equations (1)-(3) yield $A_\theta(r) = \frac{1}{2}rB_0 + \sum_{n=1}^{\infty} a_n J_1(\gamma_{on}r)$ and $A_z(r) = \sum_{n=1}^{\infty} b_n J_0(\nu_{on}r)$ which imply the following complete, orthogonal representation of the magnetic fields: $B_\theta(r) = \sum_{n=1}^{\infty} b_n \nu_{on} J_1(\nu_{on}r)$ and $B_z(r) = B_0 + \sum_{n=1}^{\infty} a_n \gamma_{on} J_0(\gamma_{on}r)$. The expansion of the magnetic field is in terms of eigenvectors of the resistive diffusion operator for the case of an isotropic homogeneous resistivity η. Therefore, one can associate with each eigenvector a diffusion time scale $t_n = 4\pi\Lambda_n^2/\eta c^2$, where $\Lambda_n = \nu_{on}^{-1}$ or γ_{on}^{-1}.

In a quasi-steady state, we envisage unspecified turbulent processes occurring on a time scale τ which culminate in a dynamo or "α-effect"[3] that opposes resistive diffusion of spectral modes with $t_n \gtrsim \tau$. A direct cascade of magnetic energy through an "inertial" range of the magnetic energy spectrum, due to nonlinear magnetic field-velocity interactions, is thereby resistively dissipated at a Kolmogorov-like scale length $c(\eta\tau/4\pi)^{1/2}$.[4]

The α-effect is then calculable without the customary recourse to kinematic assumptions if one invokes a hypothesis of incomplete relaxation of the plasma: the magnetic energy ϵ_M of a resistive plasma bounded by a perfect conductor selectively decays with respect to the magnetic helicity K.[5] As a result, the incompletely relaxed state (IRS) of the plasma has the minimum ϵ_M compatible with constant magnetic flux Φ and constant K, as well as with the resistive truncation of the spectrum.

This hypothesis is implemented by setting

$$a_n = 0, \; n > N_z; \; b_\ell = 0, \; \ell > N_\theta \qquad . \qquad (4)$$

The additional requirements

$$\frac{\delta(\epsilon_M - \mu K)}{\delta a_n} = 0, \; n < N_z; \; \frac{\delta(\epsilon_M - \mu K)}{\delta b_\ell} = 0, \; \ell < N_\theta \qquad (5)$$

246

determine the remaining coefficients.

The resulting IRS has

1) a non-vanishing β_θ, calculated from

$$\beta_\theta \equiv \frac{16\pi}{r_o^2} \{ \int_0^{r_o} r \, dr [p(r) - p(r_o)] / B_\theta^2(r_o) \},$$

where r_o = wall radius and $\vec{\nabla} p$ is taken to be $\frac{1}{c}\vec{j} \times \vec{B}$,

2) $\vec{j}(r_o) = 0$, and

3) an α-effect calculable from the steady-state condition:
$$\vec{E} = -\ddot{\alpha}(r) \cdot \vec{B}(r) + \eta \vec{j}(r) = 0.$$

The global RFP parameters β_θ, F, and Θ describing the IRS are found to be consistent with experimental data; e.g., β_θ is a monotonically increasing function of Θ in the relevant domain. See Figs. 1 and 2.

IV. Discussion

Associated with partial relaxation is a net confinement of plasma energy; i.e., $\beta_\theta > 0$. The associated pressure profile is found to be qualitatively sensitive to the choice of N_θ and N_z. This sensitivity may be attributable to any of the following causes:

1) the presence of localized instabilities that are required to maintain the IRS,

2) the neglect of pressure and velocity fields in Eq. (5),

3) the sharpness of the resistive truncation of Eq. (4), and

4) the neglect of a turbulent current-field interaction, $\frac{1}{c}\delta\vec{j} \times \delta\vec{B}$, whose ensemble average can contribute to $\vec{\nabla} p$.

We have considered various physical mechanisms that lead to smoothed pressure profiles, including a gradual resistive truncation procedure motivated by a suggestion of K. V. Roberts. The dynamics determining the actual resistive truncation is unknown as is also the dynamics governing the approach to the IRS.

Application to helical modes in an RFP is straightforward. The present formulation permits ready evalution of the properties of the IRS for a variety of geometries.[6] We wish to re-emphasize that the theoretical anatomy of an RFP differs from that of a simply-connected spheromak only by the presence of a non-vanishing time-independent $\vec{A}^\phi$. Extension of our analysis to cases of anisotropic and inhomogeneous resistivity requires some further analysis.

References

1. J. B. Taylor, Phys. Rev. Lett. __33__, 1139 (1974).
2. Cf. D. Montgomery, L. Turner, G. Vahala, Phys. Fluids __21__, 757 (1978).
3. E. N. Parker, Astrophys. J. __122__, 293 (1955).
4. D. C. Leslie, <u>Developments in the Theory of Turbulence,</u> (Clarendon Press, Oxford, 1973).
5. D. Montgomery, L. Turner, "Selective Decays in MHD Turbulence," 1978 RFP Workshop, Padua.
6. See also S. N. Rasband and L. Turner, Los Alamos Scientific Laboratory report LA-UR-79-2316, to be published.
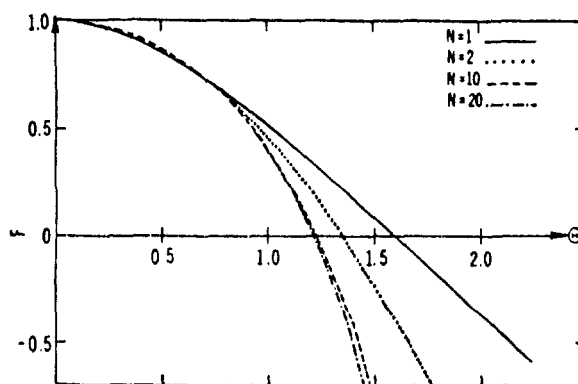
Fig. 1. F as a function of Θ for the cylindrically symmetric minimum energy state. The cases $N=N_\theta=N_z=1,2,10,20$ are depicted.
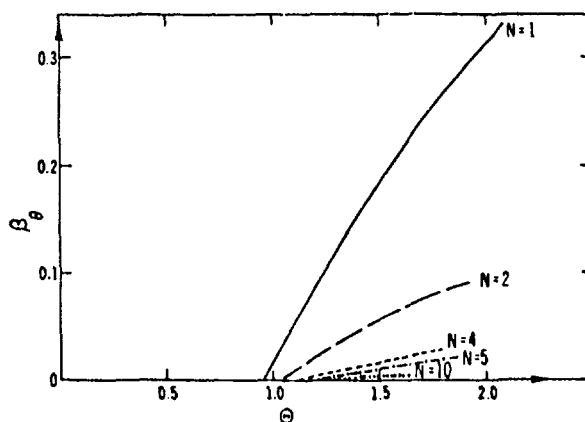
Fig. 2. Poloidal beta as a function of Θ for the cylindrically symmetric minimum energy state. The cases $N_\theta=N_z=1,2,4,5,10$ are depicted.

STATISTICAL MECHANICS OF TURBULENT TOROIDAL DISCHARGES

Guthrie Miller

Los Alamos Scientific Laboratory

Macroscopic turbulence is an experimental fact in toroidal discharges with $q \lesssim 1$. Another experimental fact is the tendency for the plasma to be in a force-free state (j/B = const). This includes the phenomena of self-reversal of the toroidal field. A natural question is to ask whether the two phenomena are related. To attempt to answer this question a theory of turbulence is needed. Such a theory also provides a useful framework for the experimental observations, which, in the case of turbulence, consist of quantities whose time variation is erratic. Clearly a theory encompassing turbulence must be probabilistic and speak of mean values (time averages), mean square deviations and so on.

The subject of this paper is the statistical mechanical approach to magnetohydrohynamic turbulence following that of Montgomery, Turner, and Vahala.[1] The fundamental ideas are first re-examined, and we then complete the calculations.

It is possible to place a a statistical mechanical theory on a somewhat different footing than in Ref. 1. The single essential, as pointed out in the landmark work of Lee,[2] is to have a phase space $\{x_i\}$ in which it is possible to prove a Liouville theorem, $\sum_i \partial \dot{x}_i / \partial x_i = 0$. By assuming ergodic motion in phase space, this leads to a distribution function ρ which is constant in (phase) space as well as time. Any other set of phase coordinates, $\{y_i\}$, that allow a Liouville theorem also leads to constant ρ, so the Jacobean of the transformation $x \rightarrow y$ must be constant.

The foregoing statistical mechanical arguments thus lead to a solution of the problem which can be restated as follows: the distribution function ρ is constant over the sub-manifold of phase space where the system moves ergodically. This manifold is reduced in dimensionality from the unrestricted phase space because of the constancy of certain additive integrals of the motion, H, K.... We therefore obtain

$$\rho = \text{const } \delta(H-\sum_i H_i)\ \delta(K-\sum_i K_i)\ldots \tag{1}$$

Equation (1) as it stands is not very useful because it gives the detailed dependence of ρ on all phase coordinates. What is needed is the integral of Eq. (1) over unused phase coordinates, the vast majority, showing the dependence on only a few coordinates. Generalizing the method given in Khinchin[3] to more than one constant of the motion, this integration results, to a very good approximation, in a Gibbs distribution. The Gibbs distribution was obtained in Ref. 1 apparently by finding the maximum entropy distribution, which, although a simpler calculation, is conceptually more difficult.

In applying these general ideas to magnetohydrodynamics, the equations of motion are taken to be those of incompressible flow. This assumption is valid only for the periods of less violent turbulence observed experimentally (specifically, the "quiet" periods observed in ZT-40).

The phase coordinates $\{\xi_s, \eta_s\}$ are defined by expanding B and v with respect to a complete orthonormal set of vector functions A_s satisfying $\nabla \times A_s = \lambda_s$, where $s = \{\ell, m, n, \iota\}$, with m,n, and ι giving the θ, z dependence, $\cos(m\theta - nz/R + \iota)$, and ℓ a radial mode number. The quantity R is the major radius of the torus–assumed of large aspect ratio–and ι is a phase angle, equal to 0 or $\pi/2$. The vector potential is assumed of the form $A = A_0\hat{z} + \sum \xi_s A_s$.

The boundary condition on A_s is $A_r(a) = 0$ when $m^2 + n^2 > 0$, where $r = a$ is the minor radius of the torus. This implies $A_\theta(a)/A_z(a) = const = - mR/(na)$ and gives a discrete spectrum of λ values. For $m = n = 0$, the choice of a boundary condition is less clear. The choice $A_\theta(a)/A_z(a) = const$, as made in Ref. 1, insures orthogonality. The value of this constant can be expressed as $J_1(\lambda_o a)/J_o(\lambda_o a)$, where λ_o (assumed positive), is the smallest positive λ in the $m = n = 0$ spectrum.

Because of the property $\nabla \times A_s = A_s$, and orthonormality, the equations of motion are easily written in terms of ξ_s and η_s. The Liouville theorem is found to be satisfied-if there is no viscoscity or resistivity. We consider the motion to be constrained only by the constancy of energy and magnetic helicity. This leads to the following Gibbs distribution for the magnetic field (as obtained in Ref. 1):

$$\rho = const \exp\left[-\sum_s \left\{ \left(\frac{\alpha}{2} \lambda_s^2 + \beta\lambda_s\right)\xi_s^2 + \beta A_o\zeta_\ell \xi_{\ell 00}\right\}\right] ,\qquad (2)$$

where ζ_ℓ is a known normalization constant.

Equation (2) provides the solution to the problem. The most interesting feature of Eq. (2) is that the Gaussian distribution for the $\xi_{\ell 00}$ magnetic field components is shifted so these components have nonzero mean value. Before calculating this mean value it is essential to note the $\alpha\lambda_s^2 + 2\beta\lambda_s$ must be positive for all s. This condition first appeared in performing the integration of Eq. (1), but it is also obvious from the result, Eq. (2). This condition implies that β is of the form

$$\beta = -\frac{\alpha}{2} \lambda_o(1-\epsilon) ,$$

with $0 < \epsilon < 1$. In terms of ϵ, some interesting mean values calculated using Eq. (2) are as follows:

$$\bar{\xi}_{\ell 00} = \frac{\zeta \ell \lambda_o A_o (1-\epsilon)}{2\lambda_{\ell 00}[\lambda_{\ell 00} - \lambda_o(1-\epsilon)]} \quad ,$$

$$\overline{(\xi_s - \bar{\xi}_s)^2} = \frac{1}{\alpha \lambda_s [\lambda_s - \lambda_o(1-\epsilon)]} \quad .$$

Thus, fluctuations are small (quiesence) if α is large. but independently of the value of α there exists a mean magnetic field $\bar{B}$. The limit $\epsilon \to 0$ requires $\alpha \to \infty$, so this case is necessarily quiescent.

The expression for $\bar{B}$ contains the denominator $\lambda_{\ell 00} - \lambda_o(1-\epsilon)$ which suggests a solution to the Helmholtz equation. By carrying through the calculations we find $\nabla \times \bar{B} - \lambda_o(1-\epsilon)\bar{B} = 0$ for r in $(0,a)$ so that the mean field is force free. There are discontinuities at $r = a$ which imply δ-function currents at the wall. We find that only when ϵ is small are the wall currents negligible. For small ϵ, $\epsilon \sim 1 - I/(\lambda_o \psi)$, where I is the toroidal current and ψ the toroidal flux.

Magnetic fluctuations are also calculable. We imagine an m,n pickup coil selecting a definite θ,z dependence and obtain,

$$\overline{(B - \bar{B})^2} = \sum_\ell G_\ell \cos^2(m\theta - nz/R + 1)$$

at the wall. There are two noteworthy features of the actual expressions. First $GV\alpha \to 1$ (or $1/2$ if $m = n = 0$) for $\lambda \to \infty$, where V is the volume of the torus, so the summation over ℓ does not converge. The result is therefore given by $(\delta B)^2 = N/(V\alpha)$ where N is the number of terms in the sum. Thus, not

unexpectedly, we cannot ignore large wavenumber modes. The second important feature is the presence of a denominator $\lambda_{\ell mn} - \lambda_0(1-\varepsilon)$, which can vanish. This occurs whenever the axisymmetric configuration is unstable, in which case $\lambda_{\ell mn}$ of the unstable mode matches $\lambda_0(1-\varepsilon)$. The first such instability to occur is the well known helical instability for $m = 1$, $n = 1.2\,R/a$ and $\lambda_0(1-\varepsilon)a = 3.1$. The overall conclusion about magnetic fluctuations is that for $\lambda_0(1-\varepsilon)a$ smaller than 3.1 the spectrum of fluctuations as a function of m and n is flat.

Finally the main results and qualifications may be summarized as follows.

1) A statistical mechanical theory of turbulence has shown that, in thermodynamic equilibrium, the mean magnetic field is force free.

2) It was necessary to neglect all dissipation. We are watching a closed system over a short enough time period so that dissipation would seem unimportant, but the question of how to properly include dissipation remains unresolved.

3) There are, in certain cases, δ-function currents at the wall.

4) The magnetic field fluctuations are independent of m and n except near the threshold of the helical instability, where they may be enhanced.

References

1. D. Montgomery, L. Turner, and G. Vahala, Phys. Fluids 21, 757 (1978).

2. T. D. Lee, Q. Appl. Math. 10, 69 (1952).

3. A. I. Khinchin, Mathematical Foundations of Statistical Mechanics, (Dover, 1949).

SOME NECESSARY CONDITIONS FOR
A STEADY STATE REVERSED FIELD PINCH

C.G. Gimblett

Culham Laboratory, Abingdon, Oxon., OX14 3DB, UK
(Euratom/UKAEA Fusion Association)

Abstract

Several necessary conditions for steady state reversed field configurations sustained by an externally applied toroidal electric field are obtained. It is confirmed that in a straight cylinder the magnetic field at the reversal point must depart from cylindrical symmetry for sustainment. Conditions obtained place restrictions on the applied electric field and on certain quantities associated with the toroidal plasma flow, perhaps indicating the presence of toroidal convective rolls in the steady state. Various other special cases are considered.

INTRODUCTION

This paper explores some details of the suggestion (Sykes and Wesson 1977, Bunting et.al. 1977) that a reversed field pinch configuration once set up can autonomously counterbalance its ohmic diffusive tendencies provided it continues to be driven by an externally applied toroidal electric field, E_{zo}.

Ostensibly, a sustained pinch does not provide a 'classical' dynamo problem - the global loss of the former is met by E_{zo} (§1,) while the latter relies on a non-conservative fluid body force. However, we can isolate dynamo processes in the pinch by considering those ingredients of the ohmic loss which are not explicitly influenced by E_{zo} but require balancing by internal inductive effects (§2). Section 3 establishes a result complimentary to that of Robinson 1974 concerning cylindrically symmetric pinches.

In all sections the pinch wall is a straight cylinder and toroidicity is simulated by assuming periodicity over a length L along the cylinder.

§1. Global energy balance and the applied electric field.

The equations governing the steady state of the plasma are taken to be

$$E_{zo} \hat{z} + \nabla\phi + \underline{v} \wedge \underline{B} = \underline{\underline{\eta}} . \nabla \wedge \underline{B} \qquad , \qquad (1)$$

$$(\nabla \wedge \underline{B}) \wedge \underline{B} = \mu o \, \nabla p \qquad , \qquad (2)$$

$$\nabla . (\rho \underline{v}) = \nabla . \underline{B} = 0 \qquad , \qquad (3a,b)$$

together with an appropriate thermodynamic equation.

A global energy balance is obtained by taking $\int dV \, \nabla \wedge \underline{B}$. of (1) over the pinch volume V. For illustrative purposes consider an incompressible plasma with no current flowing to the wall; if $v_n = 0$ at the wall we find

$$E_{zo} \, L \, Ip = \mu_o \int_V (\eta_{\shortparallel} j_{\shortparallel}^2 + \eta_\perp j_\perp^2) dV \qquad , \qquad (4)$$

where Ip is the toroidal plasma current. Of course, E_{zo} and Ip must have the same sign. Taking $\int dV \, \underline{B}$. of (1) with $B_n = 0$ at the wall gives

$$E_{zo} \, L \, \Gamma_z = \mu_o \int_V \eta_{\shortparallel} j_{\shortparallel} B \, dV \qquad , \qquad (5)$$

where Γ_z is the toroidal magnetic flux.

Between (4) and (5) we can fashion the inequality

$$V_z = \text{applied volts} = E_{zo} L \le 2 \, \mu_o^2 \, \frac{M}{\Gamma_z^2} \, \bar{\eta}_{\shortparallel} \, Ip \qquad , \qquad (6)$$

where $\bar{\eta}_{\shortparallel}$ is a weighted average of $\eta_{\shortparallel}$, and M is the total magnetic energy within the pinch. Eq. (6) can be rewritten to express a relationship between the 'observed' value of the plasma resistance and it's classical value. As a supplement note that using (1) and (2), the Poynting flux is $\int_{wall} \eta_\perp \nabla p . d\underline{S}$,

which in particular rules out force-free fields as steady state contenders.

§2. Some necessary conditions for the sustainment of reversed toroidal field.

A R.F.P. configuration requires in particular an internally generated **poloidal** electromotive force for sustainment. To show this consider an incompressible plasma with scalar resistivity, and disengage the appropriate component of Ohm's law from eq.(1):

$$\underline{B}\cdot\nabla v_z - \underline{v}\cdot\nabla B_z - \hat{\underline{z}}\cdot\left\{\nabla\eta\wedge(\nabla\wedge\underline{B})\right\} + \eta\nabla^2 B_z = 0 \qquad , \qquad (7)$$

Now form a 'partial' energy balance by multiplying eq.(7) by B_z, and integrating over the volume V_+ enclosed by the surface S_+ on which $B_z = 0$. Assuming S_+ is single-valued and does not intersect the pinch wall we find

$$\int_{V_+} B_z\,\underline{B}\cdot\nabla v_z^*\,dV = \int_{V_+} \eta(\nabla B_z)^2 dV \qquad , \qquad (8)$$

where $\underline{v}^* = \underline{v} + \nabla\eta$. Physically, the diffusive tendencies of the toroidal field can be countered by suitable 'stretching' of the field lines by the toroidal velocity and by toroidal variation of the resistivity (which promotes a preferential current flow). In fact, it follows that

$$\max_{V_+}\left|\frac{v_z^*}{\sqrt{\eta}}\right| \geq \left\{\frac{\displaystyle\int_{V_+} \eta(\nabla B_z)^2\,dV}{\displaystyle\int_{V_+} B^2\,dV}\right\}^{1/2} \qquad (9)$$

provides a necessary condition for sustainment.[†]

Independent information concerning the generation term of eq. (8) results by invoking eq. (2). After some manipulation we find

$$0 = -\int_{S_+} v_z^*(\mu_0 p + \tfrac{1}{2}B^2)\,\frac{\partial\,rs}{\partial z}\,dS - \int_{V_+}(\mu_0 p + \tfrac{1}{2}B^2)\frac{\partial v_z^*}{\partial z}dV + \int_{V_+}\eta\,(\nabla B_z)^2 dV \quad , \tag{10}$$

[†] One might expect the inclusion of compressibility and paramagnetism to decrease the non-symmetric activity required.

where $r_s(\Theta,z)$ is the defining radius of S_+. We see that contributions to the 'poloidal' ohmic loss can come from toroidal variations of v_z^* and S_+. Certainly, sustainment fails if $\partial/\partial z \equiv 0$.

§3. The surface averaged Ohm's law and reversed toroidal field.

The result we shall derive in this section is allied with that of Robinson 1974. The starting point is to subject the poloidal component of (1) to an average, $< >$, over embedded concentric cylinders.

If $\underline{B}$ were cylindrically symmetric, $\underline{B} = \underline{B}(r)$ and

$$- <v_r> B_z = \mu_o J_\theta \left\{ <\eta_\perp> + <\eta_\| - \eta_\perp > \frac{B_\theta^2}{B^2} \right\} + \mu_o J_z \left\{ <\eta_\| - \eta_\perp> \frac{B_\theta B_z}{B^2} \right\} \quad . \quad (11)$$

Now consider (11) as $B_z \to 0$. The L.H.S. $\to 0$ while the R.H.S. $\to \mu_o <\eta_\|> J_\theta$. However, the latter is $- <\eta_\|> dB_z/dr$ and must tend to zero to a lower order than B_z does. These statements are incompatible – the inductive effect of flow across field lines is ineffective at this point. (The same phenomenon that was exploited in Cowling's 1933 theorem).

DISCUSSION.

We have seen that there is a subset of pinch configurations that cannot possibly be time independent. In particular non-symmetric inductive processes, perhaps in the form of toroidal convective rolls, appear to be necessary for sustained reversal. A précis of the main results is given in the table below.

TABLE 1

ASSUMPTIONS	STEADY DISCHARGE[†] CANNOT EXIST IF:
(T1), $\nabla \wedge \underline{B} . d\underline{S} = 0$	sign $(E_{zo}) \neq$ sign (Ip)
(T1), (T2), adiabatic source-free flow, $\underline{B} . d\underline{S} = \underline{v} . d\underline{S} = \nabla \wedge \underline{B} . d\underline{S} = 0$	$E_{zo} L > 2\mu_o^2 M \, \bar{\eta}_{\parallel} Ip \, \Gamma_z^{-2}$ (see §1 for details)
(T1), (T2), $\underline{v} . d\underline{S} = \underline{B} . d\underline{S} = 0$	$\int_{wall} \eta_{\perp} \nabla p . d\underline{S} = 0$ (see §1)
	STEADY R.F.P.[††] CANNOT EXIST IF:
(T1)	$\underline{B} = \underline{B}$ (r) (see §3)
(T1) with scalar η, $\nabla . \underline{v} = 0$	Insufficient $\left\| v_z * \right\|$ in V+ (see §2)
(T1) with scalar η, $\nabla . \underline{v} = 0$, (T2)	No toroidal variation (see §2)

with: $E_{zo}\hat{\underline{z}} + \nabla\phi + \underline{v} \wedge \underline{B} = \underline{\underline{\eta}} . \nabla \wedge \underline{B}$, $\nabla . \underline{B} = 0$ (T1)

        $(\nabla \wedge \underline{B}) \wedge \underline{B} = \mu_o \nabla p$ (T2)

† Other than $\nabla \wedge \underline{B} \equiv \underline{0}$.

†† The toroidal magnetic field at the wall is everywhere reversed.

REFERENCES

[1]   SYKES A and WESSON J A, VIII European Conference on Controlled Fusion and Plasma Physics, Prague, 1, 80,1977.

[2]   BUNTING C A, GOWERS C W, OGAWA K, ROBINSON D C, and WATTS M R C, ibid, 1, 79,1977.

[3]   ROBINSON D C, HBTX II(74)3a, 1974 (Culham Lab.internal note).

[4]   COWLING T G, Mon.Not. R.Astro. Soc., 94, 39,1933.

WHY SHOULD ENERGY DECAY WHILE MAGNETIC HELICITY IS CONSERVED?: THE ESSENTIALS OF TURBULENT SPECTRAL TRANSFER
by W. H. Matthaeus & D. C. Montgomery

This meeting contains numerous contributions which extend, modify, or test the consequences of the Taylor[1,2] hypothesis that the energy of a toroidal Z pinch might decay while the magnetic helicity, $\int \underset{\sim}{A} \cdot \underset{\sim}{B} \, d^3 x$, might be approximately conserved. There has been relatively little discussion, however, of the dynamical foundations of such a decay process: as to why it might occur, and under what circumstances; as to exactly what is meant by "energy"; and so on. Here, it is our hope to open some of these questions at an elementary level, with an eye to assessing the accuracy of such conjectures, and their possible utility. The discussion is given a more extended presentation elsewhere[3,4,5].

We have been unable to see a compelling argument for the existence of the process in any other terms than those of the theory of spectral transfer in incompressible magnetohydrodynamic (MHD) turbulence. The incompressibility is important because the energy integrals for compressible and incompressible MHD differ by an important term: the compressible case contains a thermal pressure term in the energy integral which is absent in the incompressible case. To our knowledge, no one has given any argument as to why this thermal pressure term ought to decay to a minimum. If it did, such a minimum would be an ice-cold plasma with no pressure at all: interesting neither from a theoretical nor experimental standpoint, and fundamentally different from a finite-pressure wall-supported plasma with zero pressure gradient.

Arguments for the use of incompressible MHD equations as a satisfactory description of the dynamics seem to be justified by about the same arguments used to justify the incompressible approximation for ordinary fluid mechanics[6]: flow speeds small compared to the sound speed and slowly varying boundary conditions. In addition, one new assumption seems to be required: that the change in the Alfvén speed shall be small, for a given fluid element, compared to the sound speed.

Fortunately, incompressible MHD turbulence theory in three dimensions[7,8] does provide the basis for a selective decay hypothesis in which

energy (magnetic plus kinetic energy of fluid motion) decays much more rapidly than magnetic helicity in a dissipative initial-value situation. The selective decay hypothesis can be formulated in ways that have common features for those diverse situations for which dual cascades and inverse cascades are relevant processes. In a forced, dissipative situation, 3D MHD, 2D MHD, and 2D Navier-Stokes flow share the common property that some supplied global quantity may be carried to short wavelengths and dissipated at the same time that some "inversely cascaded" quantity is being transferred to long wavelengths and accumulated there. If the system is not forced, the decay process is less clear cut, but it is still undoubtedly true that the quantity transported to short wavelengths in the forced situations (the "directly cascaded" quantity) is transported selectively to the small spatial scales and more readily dissipated. The directly cascaded quantity may be expected to decay selectively, for the various situations, as summarized in the following table.

Situation	Directly Cascaded Quantity	Inversely Cascaded Quantity
3D Navier-Stokes	None	None
[9,10,11,12]2D Navier-Stokes	Enstrophy	Energy
[13,14,15]2D MHD	Energy and Cross Helicity(?)	Mean-Square Magnetic Vector Potential
[7,8,3]3D MHD	Energy and Cross Helicity(?)	Magnetic Helicity

Each decay process in its extreme form implies a variational principle, with the directly-cascaded quantity being minimized, while the inversely cascaded one is approximately conserved.

The arguments for the selective decay of the directly cascaded quantity are the same qualitatively, as those given for the forced dissipative case. The first step in establishing them is the establishment of the existence of non-dissipative global invariants such as the energy

$$E \equiv \int_V (\tfrac{1}{2} \rho_0 \, \underset{\sim}{v}^2 + \underset{\sim}{B}^2 / 8\pi) \, d^3 x \qquad (1)$$

(ρ_0 = density = const.) or the magnetic helicity

$$H_m \equiv \int_V \underset{\sim}{A} \cdot \underset{\sim}{B} \, d^3 x \qquad (2)$$

(where $\underset{\sim}{B} = \nabla \times \underset{\sim}{A}$). The existence of such zero-dissipation invariants as H_m or E is proved from the dynamical equations for MHD <u>under certain boundary conditions</u>. Two sets of boundary conditions which guarantee (1) and (2) are: periodic boundary conditions, and $\underset{\sim}{v} \cdot \hat{n} = 0 = \underset{\sim}{B} \cdot \hat{n}$, where $\hat{n}$ is the unit normal to the surface bounding the volume V. If other boundary conditions are desired (such as boundary conditions on the current, for example), the first step is to see what global non-dissipative invariants they imply; E and H_m cannot automatically be assumed.

Decisive analytic evidence for the validity of the "selective decay" conjectures is lacking. Direct simulations of the two dimensional Navier-Stokes and MHD equations at moderate Reynolds numbers allows several tests to be done. (Here the vocabulary of 2D – MHD is used; E = energy and A = mean square vector potential, J = mean square current, Ω = mean square vorticity.) Some of these tests are:

1) The basic conjecture is E/A $\rightarrow$ minimum via a nonlinear decay process which critically depends on the conservation of <u>both</u> E and A when there is exactly zero dissipation. 2) The enhanced decay of E at large Reynolds numbers requires that Ω and J be nonlinearly amplified by spectral transfer to large wavenembers. Thus (for unit magnetic Prandtl number) $(\Omega + J)/E$ increases in time or, at least it must decrease slower than E/A. 3) The instantaneous ratio of decay rates $(\frac{d}{dt} \ln A)/(\frac{d}{dt} \ln E) = E^2/A (\Omega + J) \equiv f$ should decrease and remain small for a substantial period of time. 4) The extremal state for 2D MHD flows in periodic geometry is that for which all the magnetic energy is locked into the longest wavelength. For finite Reynolds numners, we expect the fluid to move toward this state via the selective decay process, but to reach it strictly only in the infinite time linear decay regime. Appropriate diagnostics for this purpose are contour plots of vector potential (which are magnetic field lines in 2D).

Here we briefly present some results of these numerical tests. The simulation reported is 2D MHD; computational details are reported in Ref 4 and 5. The fields, represented by their Fourier coefficients, are initially non zero only for $9 \leq k^2 \leq 25$. The magnetic energy is initially twice the kinetic energy, and each are equipartitioned in their respective Fourier modes. Both the magnetic and kinetic Reynolds numbers are 200. Figures 1

261

and 2 show initial and t = 9.8 (units of Alfvén transit time) magnetic field lines. The mean island size has grown but is not yet maximal. Figure 3 shows the ratios $(J + \Omega)/E$ and magnetic energy to A as functions of time. The behavior of these ratios indicates that spectral transfer is occuring in both directions in wavenumber space. As discussed above in 2), this observation is consistent with the conjectures. Finally, Figure 4 shows the time history of f (see 3) above). Since f decreases and remains small for at least 9 Alfvén transit times, the energy decays much more than the vector potential does.

Other runs we have done display similar behavior. More complete results of this type as well as related non-linear stability properties will be reported elsewhere[5].

References

1. J. B. Taylor 1974 in _Plasma Physics and Controlled Fusion_ I, I.A.E.A., Vienna, 1975.
2. J. B. Taylor 1976 in _Pulsed High Beta Plasmas_,ed. by D. E. Evans, Pergamon Press, Oxford, U.K.
3. D. Montgomery, L. Turner and G. Vahala 1978 Phys. Fluids 21, 757.
4. W. Matthaeus and D. Montgoemry, Proceedings of the International Conference on Nonlinear Dynamics, sponsored by the New York Academy of Sciences, New York. Dec.19, 1979.
5. W. Matthaeus and D. Montgomery submitted to Phys. Fluids.
6. L. Landau and E. Lifshitz, _Fluid Mechanics_, Pergamon, 1959, p. 24.
7. U. Frisch, A. Pouquet, J. Leorat and A. Mazure 1975 J.Fluid Mech. 68,769
8. A. Pouquet, U. Frisch and J. Leorat 1976 J.Fluid Mech. 77, 321.
9. R. Kraichnan 1967 Phys. Fluids 10, 1417.
10. G. K. Batchelor 1969 Phys. Fluids Suppl. 12, II, 233.
11. C. E. Leith 1968 Phys. Fluids 11, 671.
12. R. Kraichnan and D. Montgomery 1979 "Two Dimensional Turbulence", to appear in Rep. Prog. Phys.
13. D. Fyfe and D. Montgomery 1976 J. Plasma Phys. 16, 181.
14. D. Fyfe, G. Joyce and D. Montgomery 1977 J. Plasma Phys. 17, 317.
15. D. Fyfe, D. Montogomery and G. Joyce 1977 J. Plasma Phys. 17, 369.

Fig.1: Magnetic field lines
at t=0.0
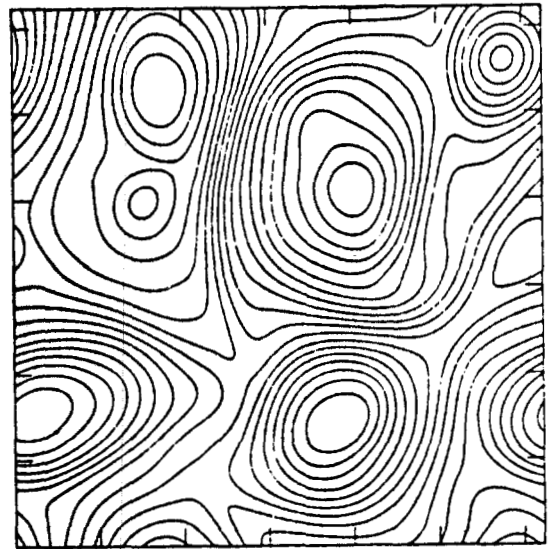
Fig.2: Magnetic field lines
at t=9.8

Fig.3: Time history of $(J+\Omega)/E$
and E_{mag}/A. Both quantities have
dimension of wavenumber squared.
The former is the ratio of the
dissipation rate of E to that
of A. The latter is the average
wavenumber (squared) of the
magnetic excitation.
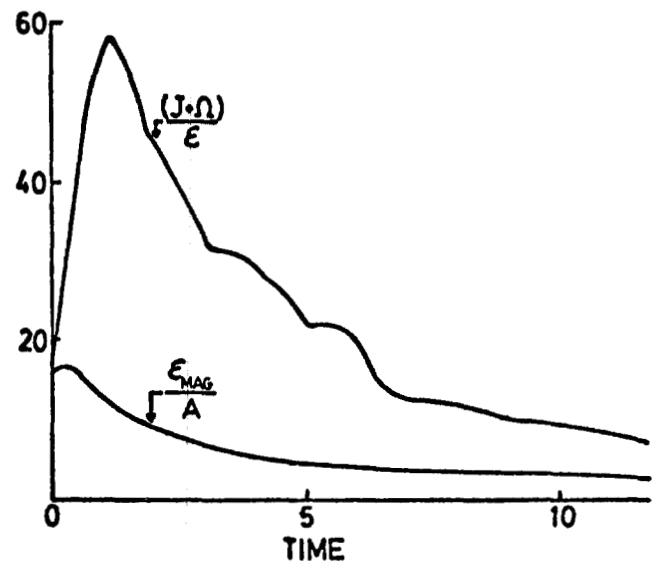
Fig.4: Time history of f. This
is the ratio of instantaneous
decay rates of E and A.
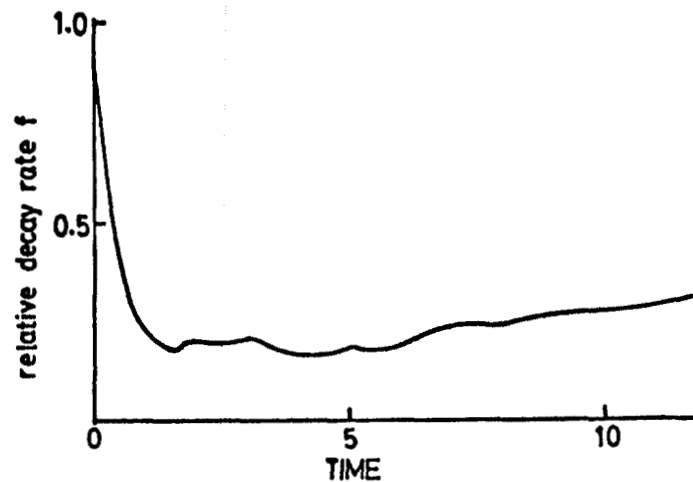
Models of the Field Reversal in Zeta

M.G. Rusbridge

Physics Dept., U.M.I.S.T., Sackville St.,

Manchester M60 1QD, U.K.

I wish to discuss the possible origin of the reversed field (RF) in Zeta in the light of experimental knowledge, particularly of the character of the turbulence and larger scale fluctuations. The relevant observations in Zeta are:

(1) reversed axial field for $\theta \gtrsim 1.35$

(2) the compression of the current channel is relatively small,

(3) the field configuration is not very close to the Bessel Function model (BFM): in particular, $j_{\parallel}$ /B tends towards zero at the wall while in the BFM $j_{\parallel}$ /B is constant;

(4) large-scale m = 1 kinks occur but with low amplitude: current channel displacement δ satisfies $\delta/a \lesssim 0.1$ where a is the tube radius, and δ/a increases roughly linearly with θ with no critical value for onset;

(5) fine-scale turbulence occurs, of quasi-two-dimensional character, aligned along the local field and with scale lengths $\Lambda_{\perp} \sim$ 5cm, $\Lambda_{\parallel} \gtrsim$ 100cm (Robinson & Rusbridge 1971).

Of these, (4) rules out the possibility that RF is generated by large scale helical kinks as in HBTX-1 (Verhage et al 1978), and (3) does not permit a simple reliance on the Taylor relaxation theory (Taylor 1974). There are two other theories I shall consider: the 'tangled discharge' (Rusbridge 1977) and the 'dynamo model' (Gimblett & Watkins 1975).

In the tangled discharge model it is assumed that the magnetic surfaces are broken by random resistive reconnection of lines of force which become stochastic and eventually fill the entire discharge ergodically. The current at a point is then determined not by the local electric field but by the average electric field seen over the whole path of a line of force, and the average current is found by averaging over all such paths. In this extreme form the model is an exact realisation of Taylor's theory and leads to the BFM; it is modified by allowing random transverse current exchanges between neighborouring field lines, as a result of which the influence of distant parts of the field lines is attenuated and the configurations are incompletely relaxed. It is proposed that the $\underline{J} \wedge \underline{B}$ forces associated with the random current exchanges constitute 'stirring' forces which represent the direct energy input into turbulence found necessary on energetic grounds by Rusbridge (1969). Explicit configurations can be calculated by an iterative technique.

The following comments may be made on this theory:

(1) in its present form it is set up in terms of tubes of force rather than lines, and appears to require that a given tube retain its identity through a large number (10-100) of transitions from one magnetic surface to another, which seems implausible.

(2) the configurations produced are significantly more compressed than those observed;

(3) nevertheless, it has been shown (Rusbridge, 1980) that the model can account, almost quantitatively, for all the features of the density fluctuations observed in Zeta which have so far resisted explanation, and this is strong evidence that the basic premise of the theory, that the magnetic surfaces are broken, is correct.

The 'dynamo theory' (Gimblett & Watkins 1975) assumes that the turbulence has properties such that there is a component of the covarience $< \tilde{v} \wedge \tilde{b} >$ of velocity and magnetic field fluctuations parallel to the mean field B which can therefore drive a parallel current. We therefore write:

$$j_{\shortparallel} = \sigma(E_{\shortparallel} + \alpha B)$$

where

$$\alpha = \int \left\langle v_x(t) \frac{dv_y}{dz}(t - T) - v_y(t) \frac{dv_x}{dz}(t - T) \right\rangle dT$$

vanishes by symmetry unless the turbulence possesses a net helicity (here the z- direction is parallel to the local field). Assuming this, we can write the order of magnitude of α as

$$\alpha \sim \gamma \frac{\tilde{v}_{\perp}^2 \tau}{\Lambda_{\shortparallel}}$$

where γ measures the correlation and satisfies $|\gamma| \underset{\sim}{<} 1$ and τ is the auto-correlation time. In Zeta, it is approximately true that $\tilde{v}_{\perp} \tau \sim \Lambda_{\perp}$, so

$$\alpha B \sim \frac{\tilde{v}_{\perp} B \Lambda_{\perp}}{\Lambda_{\shortparallel}} = \frac{\tilde{E}_{\perp} \Lambda_{\perp}}{\Lambda_{\shortparallel}}$$

where $\tilde{E}_{\perp}$ is the observed fluctuating electric field. Thus

$$j_{\shortparallel} = \sigma(E_{\shortparallel} + \gamma \frac{\tilde{E}_{\perp} \Lambda_{\perp}}{\Lambda_{\shortparallel}}) \qquad (1)$$

If this equation is to produce significant reversal, the second term must be at least comparable to the first. In Zeta, $E_{\shortparallel} \sim 0.1$ v/cm, $\tilde{E}_{\perp} \sim 10$v/cm so this condition can be satisfied for γ as small as ~ 0.1. However we also observe that $\tilde{E}_{\perp}$ scales as I^2/ρ where I is gas current and ρ the mass

density, so at high filling pressures we would expect the reversed field generation to be less effective. There is some evidence that configurations at high pressure are more compressed than those at low pressure (Lees & Rusbridge 1960); and since one role of the FR process is to enhance the toroidal flux in the discharge core and thus lower the compression, the observations do suggest a less effective FR process at high filling pressures.

Finally, to determine actual configurations we need a plausible value of γ. In a uniform field, $\gamma = o$ by symmetry since there is no reason for the turbulence to have a net helicity. In an actual configuration, the sense of the helicity can be defined by the magnetic shear. Further, the shear length L_s is of the same order as the correlation length $\Lambda_{,,}$. We therefore propose that γ should be related to the configuration by

$$\gamma = \gamma_o \, \Lambda_{,,}/L_s \tag{2}$$

Substituting (2) in (1), assuming a uniform toroidal applied electric field and assuming the discharge to be force-free, we arrive at the equation for toroidal field:

$$\frac{dB_z}{dx} = - \frac{B_z B_\theta}{B^2} \frac{\left(1 - \frac{2WB_\theta}{B^2} \right)}{\left(\frac{1}{B_{zo}} - \frac{W}{B} \right)}$$

where: $\qquad B^2 = B_\theta^2 + B_z^2$

$\qquad x = r/r_o$ is normalised radius

$\qquad r_o = B_{zo}/4 \; \sigma E_o$

$\qquad B_{zo} = $ field at $r = o$

$\qquad W = \frac{\gamma_o \tilde{E}_{\perp}}{E_o} \frac{\Lambda_{\perp}}{r_o}$

$\qquad E_o = $ applied electric field

If $dB_z/dx \, \alpha B_z$ everywhere there will be no reversal, B_z only tending asymptotically to zero in the limit $x \rightarrow \infty$ (as in the force-free paramagnetic model). Thus the only possibility for a reversal is that B_z may vanish at a radius x_o such that $W = B(x_o)/B_{zo}$. If W is taken to be uniform thus

266

thus requires $W < 1$ (and to agree with observation W must in fact be confined to a narrow range around 0.5); more probably $W \to 0$ at the wall and then the requirement is that $W(0) > 1$ (see figure).
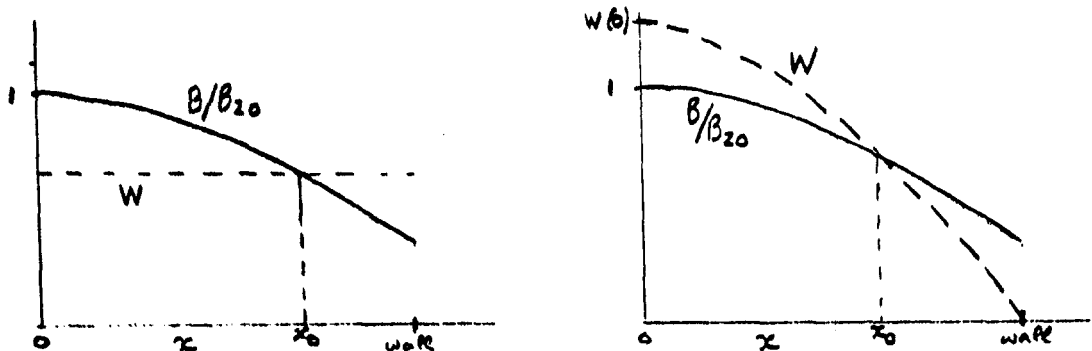
In either case, however, a further condition on W must be met, arising as follows. The solution for B_z near $x = x_0$ is of the form $B_z \ \alpha (x - x_0)^k$, where k is a function of x_0, W and dW/dx. Unless $k = 1$, the current density will be either zero or infinity at the reversal point, both contrary to observation. The condition for $k = 1$ is

$$W' = 3W/x_0 - 1$$

so that, for example, for constant W we would require $W = x_0/3$. There is likely to be at most one value of W satisfying both this condition and $W = B(x_0)/B_{z0}$, whereas in fact W varies strongly with the discharge conditions.

A closer examination shows that this pathological behaviour arises because at the reversal point $1/L_s \ \alpha \ j_\theta$: thus, in effect, eg. (1) requires j_θ to drive itself. It would, probably, be more plausible to take note of the radial extent of the motions driving the α-term and average this term over a radial correlation length (C.G. Gimblett, private communication); however, preliminary attempts along these lines do not seem to yield any significant change.

I conclude that we do not yet have a satisfactory description of the FR process in Zeta, and in particular none which explain the low values of the observed compression.

References

C.G. Gimblett and M.A. Watkins (1975) 7th Euro. Conf. on Cont. Fusion and Plasma Phys., Lausanne.

D.J. Lees and M.G. Rusbridge (1960) 4th I.C.I.P.G., vol 2 p.954 (Uppsala).

D.C. Robinson and M.G. Rusbridge (1971) Phy. Fluids 14, 2499.

M.G. Rusbridge (1969) Plasma Phys. 11, 35.

M.G. Rusbridge (1977) Plasma Phys. 19, 499.

M.G. Rusbridge (1980) Plasma Phys. 22, 331.

J.B. Taylor (1974) Phys. Rev. Lett. 33, 1139.

A.J.L. Verhage, A.S. Furzer, D.C. Robinson (1978) Nuc. Fusion 18, 457.

Energy Principle with Global Invariants

A. Bhattacharjee, R. L. Dewar, and D. A. Monticello

Princeton Plasma Physics Laboratory,
Princeton, New Jersey 08544

The formulation of a variational principle for a complete class of static equilibria of toroidal plasmas is due to Kruskal and Kulsrud.[1] They characterized equilibria for ideal plasmas by a nondenumerable set of topological invariants derivable from the ideal hydromagnetic equations of motion. A laboratory plasma, however, is inevitably subject to nonideal effects such as those associated with resistivity or microturbulence. Taylor[2] has conjectured that the global invariant $K = \int_{V_o} d\vec{r}\, \vec{A} \cdot \vec{B}/2$, first introduced in the astrophysical literature by Woltjer[3] for a perfectly conducting plasma, remains an invariant even in the presence of a small but finite amount of dissipation. By minimizing the energy $W = \int_{V_o} dr\, B^2/2$ subject to the invariant K, Taylor has argued that a toroidal discharge, initially violently unstable, may relax into a force-free equilibrium state given by $\vec{j} = \lambda\vec{B}$, where λ is a constant. Taylor has provided no detailed justification for K-conservation, but his theory has attracted much attention because it agrees satisfactorily with experimental observations on field-reversal from Zeta. Unfortunately, for tokamak discharges, where the toroidal field is approximately constant across the plasma, Taylor's theory predicts flat current profiles, which are usually not observed experimentally. Even in reversed field pinches, the toroidal current is observed to be small near the wall[4] which in general violates $\vec{j} = \lambda\vec{B}$. We interpret these observations to imply that the replacement of Kruskal and Kulsrud's infinity of constraints by a single one was too drastic a step; that a reasonably well-confined plasma preserves at least a few more approximate invariants over the time scale on which the growth and nonlinear development of tearing instabilities takes place. This time scale is of course short compared with the time scale of plasma transport, which is what determines the gross features of the current and pressure profiles. Thus we seek a variational principle which selects a special subset of the complete class of equilibria of Kruskal and Kulsrud, including those which can be sustained even on the transport time scale.

The shorter the time scale considered, the better preserved are any approximate invariants of motion. We are thus led naturally to consider the growth and decay of the fastest growing tearing modes to be the mechanism responsible for

the breaking of the ideal constraints. From linear and nonlinear theory of tokamak stability, we know this mode to be the $m = 1$, $n = 1$ tearing mode.[5] Indeed, there is experimental evidence[6] that particularly favorable for confinement in tokamaks are discharges in the "internal sawtooth" regime in which the plasma exhibits soft $m = 1$, $n = 1$ activity uncoupled to weak higher harmonics (as opposed to conditions under which strong coupling to $m \geq 2$, $n = 1$ modes leads to a major disruption with global flattening of the current profile, in accordance with Taylor's theory). Even during fast experiments in pinches,[4] $m = 1$ helices are observed prior to field reversal. For pinches the n-number of the dominant mode should be such that the resonant surface $q_s = m/n$ falls within the plasma during relaxation. However, predictions for $F - \theta$ and other qualitative features in this theory are not very sensitive to the choice of dominant mode. We shall, therefore, confine ourselves to the $m = 1$, $n = 1$ mode, given its importance for tokamaks.

In the following, we first assume the existence of a tearing mode of single helicity which grows from an axisymmetric state, saturates, and decays back to a new axisymmetric state. Although we are mainly considering the $m = 1$, $n = 1$ mode, it is instructive to allow a mode of arbitrary helicity. Within the quasi-ideal model,[7] we then show that there is an infinite set of constants of the motion for each assumed helicity.[8] The special role of the invariant K is confirmed by the observation that it is the sole occupant of the intersection of these sets. The infinite set may be represented by the functional

$$G(w) = \int_{V_0} d\vec{r} \; w(\chi) \; \frac{\vec{A} \cdot \vec{B}}{2}$$

where $w(\chi)$ is an arbitrary function of χ, the helical flux preserved by the mode of pitch q_s.

We suggest now the following variant of the thought experiment of Kruskal and Kulsrud.[1] We imagine a slightly nonideal plasma contained in a toroidal vessel with perfectly conducting walls. The plasma is turbulent with tearing modes of different m and n. The existence of fine-scale tearing destroys all invariants to some extent, except $K = \int_{V_0} d\vec{r} \; \vec{A} \cdot \vec{B}/2$. On a short time scale, however, the $m = 1$, $n = 1$ mode may be assumed to be least affected by other modes, and the "first moment" with respect to $\chi (\equiv \psi - \phi)$, $K_1 = \int_{V_0} d\vec{r} \; \chi \vec{A} \cdot \vec{B}/2$ the best conserved of all invariants other than ϕ_p and K. Since the two

269

latter invariants are respectively linear and quadratic in the fluxes, the choice of the functional K_1, cubic in the fluxes, as the next best invariant seems eminently reasonable.

We seek, therefore, minima of $W = \int_{V_0} d\vec{r} \; B^2/2$ subject to the global invariants $K = \int_{V_0} d\vec{r} \; \vec{A} \cdot \vec{B}/2$ and $K_1 = \int_{V_0} d\vec{r} \; \chi \vec{A} \cdot \vec{B}/2$. We must have $\delta W - \lambda \delta K - \lambda_1 \delta K_1 = 0$ where λ and λ_1 are Lagrange multipliers. We obtain the Euler-Lagrange equation $\vec{j} = \lambda[1 + (\psi-\phi)/\phi_p]\vec{B}$, where we have chosen $3\lambda_1/2 = \lambda/\phi_p$ in order that the toroidal (and poloidal) current density vanish at the wall. This is an experimental boundary condition violated by Taylor's theory.[4]

For a straight cylinder we use cylindrical polar coordinates (r,θ,z) and assume that equilibrium quantities depend only on $r(B_r = 0)$. We have defined $\bar{B} \equiv \vec{B}/2\phi_p$, $\bar{\psi} \equiv \psi/2\phi_p$, and $\bar{\phi} \equiv \phi/2\phi_p$. The boundary conditions are $(a \equiv 1)\bar{B}_\theta(0) = 0$, $\bar{\psi}(1) = 0$, $\bar{\phi}(0) = 0$, and $\bar{\phi}(1) = 1/2$. This two-point boundary-value problem has been solved numerically by a shooting procedure. The numerical results are qualitatively similar for aspect ratios from 10 to 1, and we have reported the results for $R/a = 5$. For any given $\lambda \epsilon(-\infty,+\infty)$ there are two distinct branches, which we have broadly classified as "pinchlike" (P) and "tokamaklike" (T). The predictions of our theory agree remarkably well with recent experimental measurements of the $F - \theta$ trajectory $[F = \bar{B}_z(1), \; \theta = \bar{B}_\theta(1)]$ during self-reversal in ZT-40[9] and ETA-BETA II.

Figure 1 shows a plot of $V \equiv 1/R \; W/(2\pi\phi_p)^2$ versus $1/R \; K/(2\pi\phi_p)^2$ for the solutions. The point zero, which corresponds to $|\lambda| = \infty$, is a branch-point from which four solutions emerge. For a given value of $K/(2\pi\phi_p)^2$ (volt-seconds/toroidal flux), the plasma should prefer the lower energy states indicated by the solid lines. In fact, if experimental conditions should drive the plasma to the higher energy states indicated by the dashed lines, instabilities would immediately set in, forcing the plasma to lower energy states. A preliminary examination of the stability of these states indicates stable windows of operation for $\theta \lesssim 0.2$ and $1.6 \lesssim \theta$ for $R/a = 5$. The first window is "tokamaklike" and the latter, "pinchlike." Figures 1b and 1c show typical stable q-profiles. The equilibrium equations admit an expansion in powers of inverse aspect ratio. The leading order solutions are

270

$$\overline{B}_z(r) \simeq 1, \ \overline{B}_\theta(r) \simeq \sum_{n=1}^{\infty} \frac{8\lambda}{\lambda_n^2(\lambda_n^2 + 2R\lambda)} \frac{j_1(\lambda_n r)}{j_1(\lambda_n)},$$

where λ_n corresponds to the solutions of $j_0(\lambda_n) = 0$. The above equation agrees very well with the numerical solutions for the "tokamaklike" branch.

An important aspect of this theory is that it allows a natural extension to equilibria with nonzero pressure gradients, unlike the equilibria in Taylor's theory which are force-free even in the presence of finite pressure. Details will be reported elsewhere.

ACKNOWLEDGMENTS

REFERENCES

[1] Kruskal, M. D., and Kulsrud, R. M., Physics of Fluids 1 (1958) 265.

[2] Taylor, J. B., Physical Review Letters 33 (1974) 1139.

[3] Woltjer, L., Proceedings National Academy of Sciences 44 (1958) 489.

[4] Butt, E. P., Newton, A. A., and Verhage, A. J. L., Proceedings Third Topical Conference, UKAEA Culham Laboratory, UK (September 1975).

[5] Waddell, B. V., Rosenbluth, M. N., Monticello, D. A., White, R. B., Nuclear Fusion 16 (1976) 5.

[6] Hosea, J. C., Course and Workshop on Physics of Plasmas Close to Thermonuclear Conditions, Varenna, Italy (August 1979).

[7] Kadomtsev, B., Soviet Journal of Plasma Physics 1 (1973) 389; Plasma Physics and Controlled Nuclear Fusion Research (Proceedings 6th International Conference, Berchtesgaden, 1976) Vol. 1, IAEA, Vienna, 1977, 555.

[8] Bhattacharjee, A., Dewar, R. L., and Monticello, D. A., Physical Review Letters, to be published.

[9] Baker, D., private communication.
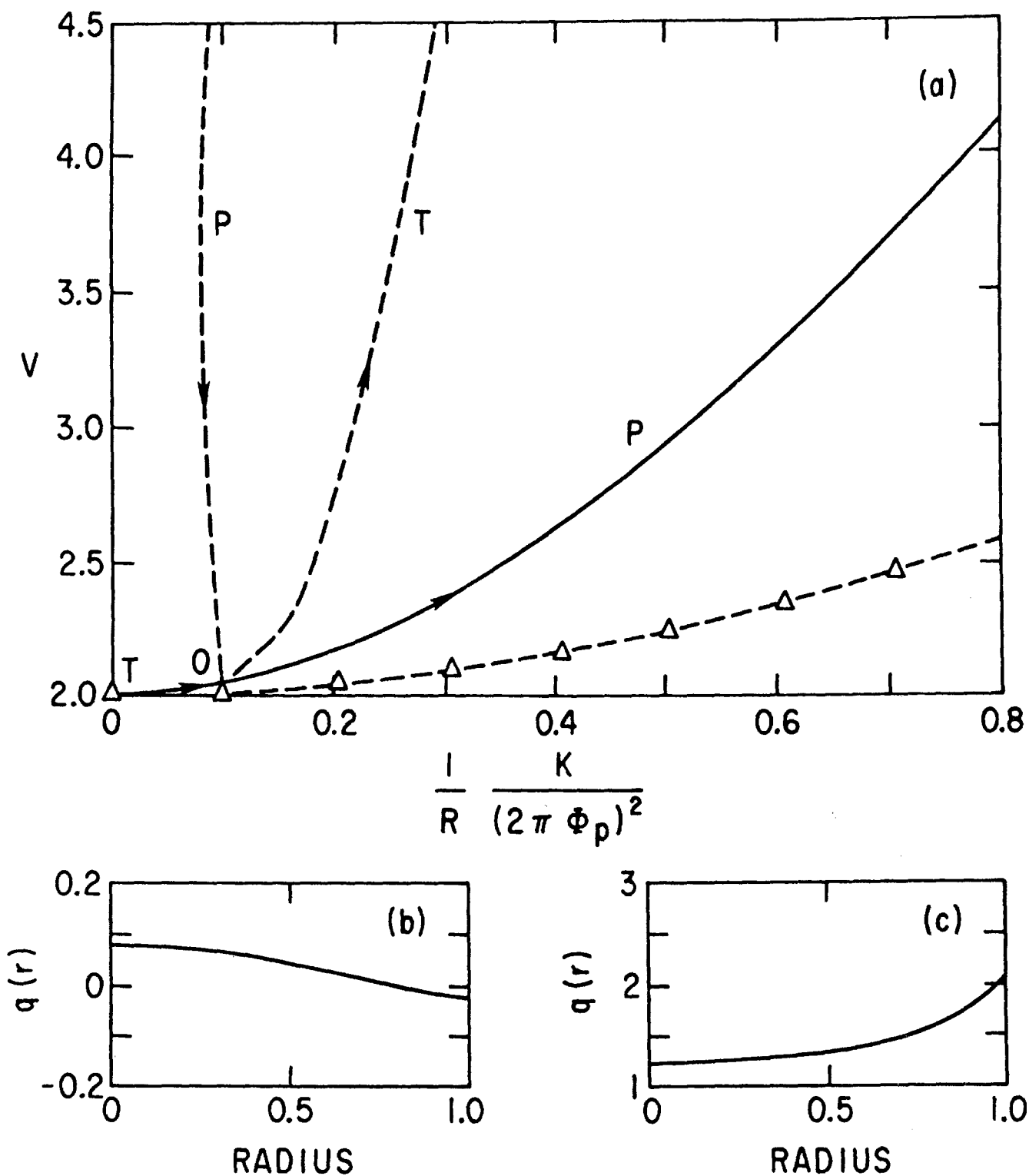
Fig. 1(a) Energy of equilibria in present theory compared with energy of Taylor states (marked by Δ). Arrows indicate direction of increasing λ. Labels P and T distinguish pinchlike and tokamaklike equilibria. Dashed lines indicate unstable equilibrium (energy stationary, but not minimum). (b) Typical q-profile on the stable P-branch. (c) Typical q-profile on the stable T-branch.

272

EQUILIBRIUM DENSITY FLUCTUATIONS FOR AN IDEAL MHD MODEL NEAR THE TAYLOR MINIMUM ENERGY STATE

Harvey A. Rose
Los Alamos Scientific Laboratory
Los Alamos, NM 87544

Density fluctuations in a reverse field z pinch, even during the quiescent phase, can be large but the level varies from one experimental situation to another[1]. There have been simple arguments proposed[2], based on the high compressibility of a low β plasma, which show that small relative fluctuations in magnetic field strength can produce large relative fluctuations in density.

In this paper we examine the specific predictions of an adiabatic, isentropic MHD model. The principle conclusion is that the mass density fluctuations in a quiscient state are likely to have a bimodal distribution with peaks in the neighborhood of zero and in the neighborhood of some value greater than the mean. The sharpness of the latter peak varies directly with the product of β and a parameter which characterizes the proximity to the Taylor[3] minimum energy state. There is one free parameter, ρ_p, which can be interpreted as a density pedestal. As this pedestal is lowered, the probability peak near the pedestal assumes a greater weight, while the mass density characteristic of the second peak increases.

To guaranty both the conservation and <u>positivity</u> of the total mass and mass density, ρ, respectively, we shall dynamically evolve ρ with a lattice centered finite difference scheme in which $\rho(x,y,z) \to n^2(i,y,k) + \rho_p$ and it is $\partial n/\partial t$ which is calculated. For simplicity, choose the equation of state $p = 1/2 \, \rho_0 \, C_s^2 \, \rho^2$ where ρ is the mass density normalized to ρ_0. The total energy density is $E(\underset{\sim}{U}, \rho, \underset{\sim}{B}) = 1/2 \, \rho_0 \, \rho \, U^2 + 1/2 \, \rho_0 \, C_s^2 \, \rho^2 + 1/2 \, \underset{\sim}{B}^2$ The velocity field $\underset{\sim}{U}$ is represented on the lattice, while $\underset{\sim}{B}$ is in terms of a truncated fourier expansion.

Since the mass, M; energy, E; and magnetic helicity, H, are time independent, the probability distribution, P, must contain the delta functions: $\delta(M - M_0) \, \delta(E - E_0) \, \delta(H - H_0)$. The canonical (à la Gibbs) approximation to these constraints is $P = P'(\underset{\sim}{U}, n, \underset{\sim}{B}) \, \exp{-[\alpha E + \gamma M + \delta H]}$, where $\rho = n^2 + \rho_p$. If a Liouville theorem were satisfied by the dynamics, then P' could be replaced by a constant. Since the conservation constraints are strong for a small level (i.e. quiescient) of fluctuations, the model $P' = $ constant is worth examining in any case.

Integrate this model distribution over U and B, and make the replacement $dn/n^3 \to d\rho/\rho^2$ to obtain the <u>single lattice site distribution</u>

$$P(\rho) \sim \frac{1}{\rho^{3/2}(\rho - \rho_p)^{1/2}} \exp\left[\frac{\alpha}{2} \rho_o\, C_s^2\, \rho^2 + \gamma\rho\right]$$

with $\rho \geqslant \rho_p > 0$ in order that P be normalizable.

Let the energy in excess of that in the Taylor state be a small fraction, ε, of the total energy. It can be shown that $\alpha\,\rho_o\,C_s^2 \sim \beta/\varepsilon$ where $\beta = C_s^2/\langle V_a^2\rangle$. If $\beta/\varepsilon \gg 1$, then $\gamma < 0$, in order that $\int P(\rho)d\rho = 1$ and $\int \rho P(\rho)d\rho = 1 = \langle \rho \rangle$. $P(\rho)$ has spikes at ρ_p and at $\rho*$, $\rho* = |\gamma|/\alpha\,\rho_o\,C_s^2$.

In the figure, $P(\rho)$ is plotted for $P_\rho = .1$, and several values of β/ε:

$(\beta/\varepsilon)^{1/2}$	γ	$\langle\rho^2\rangle$
2.00	-10.6	1.20
1.50	-7.08	1.36
1.00	-4.20	1.71
$1/(2)^{1/2}$	-2.76	2.13

The assumptions used in this model include those in the usual absolute equilibrium ensemble models.[4,5,6,7,8,9] Spatially non local density-density correlations have been ignored in favor of the conservation constraints which should be of primary importance near the Taylor state. Our predictions should be considered only in that limit.

REFERENCES

1. A. R. Jacobson, "Experiments on the ZT-S Reversed-Field Pinch" L.A.S.L. Report LA-7862-MS, (1979).

2. A. R. Jacobson, "A Simple Model for an Upper Bound on Density Fluctuations in a Turbulent Pinch," L.A.S.L. Report LA-8198-MS, (1980).

3. J. B. Taylor, Phys. Rev. Lett. 33, 1139 (1974).

4. J. M. Burgers, Verh. K. Akad. Wet. Amst. 32, 643 (1929).

5. E. Hopf, J. Ration. Mech. Anal. 1, 87 (1952).

6. T. D. Lee, Q. Appl. Math. 10, 69 (1952).

7. R. H. Kraichnan, J. Acoust. Soc. 27, 438 (1955).

8. U. Frisch et al; J. Fluid Mech. 68, 769 (1975).

9. D. Montgomery, L. Turner, and G. Vahala, Phys. Fluids 21, 757 (1978).
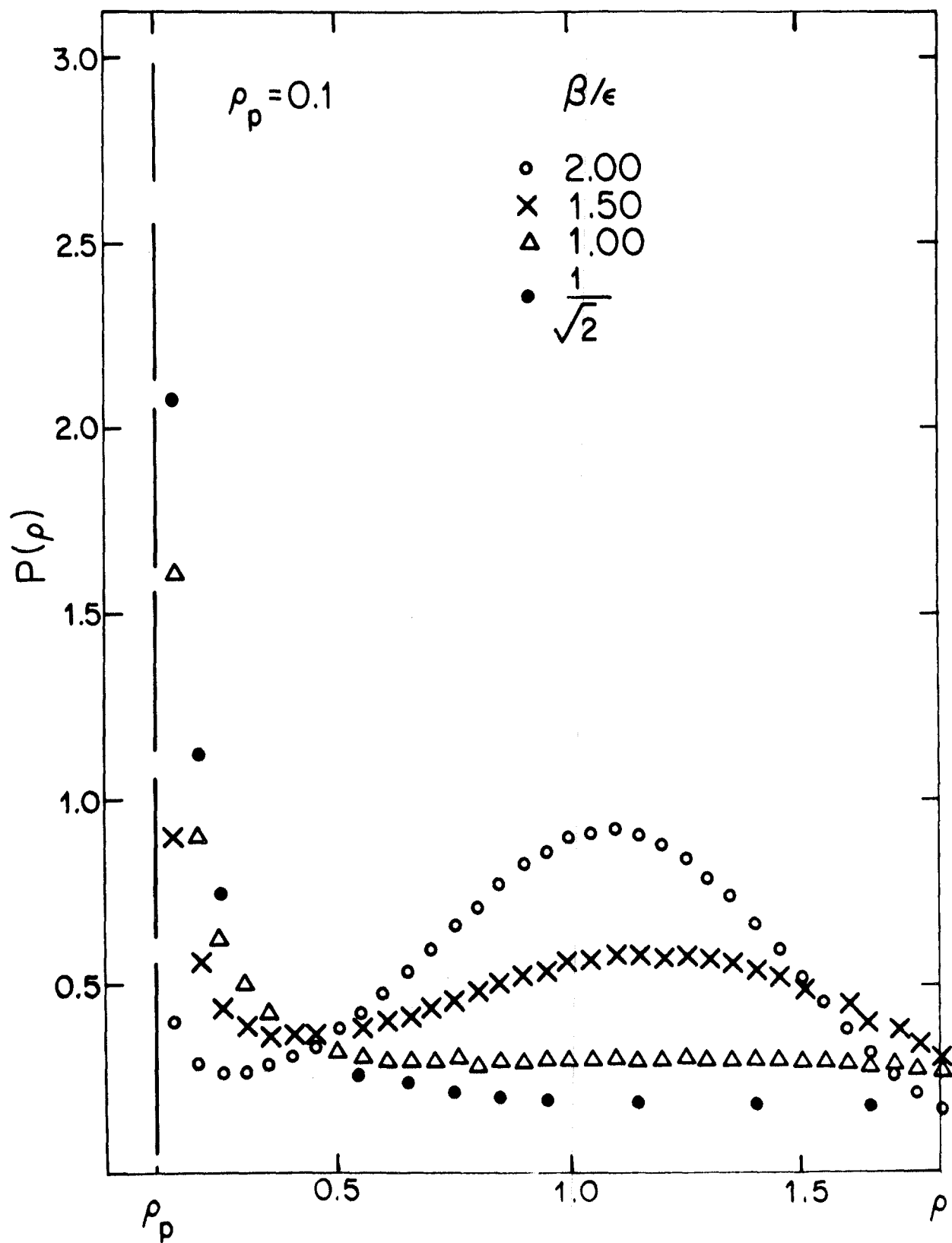
EFFECT OF INDUCED WALL CURRENTS ON TAYLOR RELAXATION*

Allan Reiman

Laboratory of Plasma Studies
Cornell University
Ithaca, New York 14853

In a self-reversed z-pinch the induced wall current must be greater than the current carried by the external field coils. The contribution of these wall currents to the energy was neglected by Taylor in his work on the relaxation of a z-pinch plasma. We redo Taylor's analysis including the neglected term. We also generalize the analysis to arbitrary cross-section and aspect ratio. Although the energy due to wall currents can be large, and must be included in the analysis, we show that this contribution never alters the minimum energy state.

For the spheromak configuration the equilibria of interest have no surface current. Nevertheless, to determine the stability of these equilibria we must compare their energy to that of other force-free equilibria which do have surface currents.

Taylor's theory of plasma relaxation in a z-pinch[1] is phenomenological, in the sense that its assumptions must be justified by the successful predictions of the theory. Although the assumptions are intuitively plausible, they have not been derived from first principles. Nevertheless, the successes of Taylor's theory are impressive. The theory describes remarkably well the experimentally observed evolution of z-pinch plasmas. In this paper we begin with the assumptions proposed by Taylor, and correct and generalize Taylor's analysis.

Taylor assumes that the plasma evolves to a state of minimum energy, subject to the constraints of constant toroidal flux, Ψ, and constant magnetic helicity,

$$K = \frac{1}{8\pi} \int_V A \cdot B,$$

(1)

where the integration in eq. (1) is over the plasma volume. Because the constraints do not involve the pressure, only the magnetic energy,

$$W = \frac{1}{8\pi} \int_V B^2,$$

need be considered. From the method of Lagrange multipliers it follows

---

that the state of minimum energy must satisfy

$$\nabla x \underset{\sim}{B} = \lambda \underset{\sim}{B}, \tag{2}$$

where λ is a constant independent of position. This is a necessary condition, but not a sufficient condition, for minimum energy.

To make further progress, integrate by parts the expression for the magnetic energy, using eq. (2) to find

$$W = \lambda K + \frac{1}{8\pi} \int_S \hat{n} \cdot \underset{\sim}{A} \times \underset{\sim}{B}, \tag{3}$$

where S denotes the plasma surface, and $\hat{n}$ is a unit vector normal to the plasma surface. Taylor neglects the surface integral, and concludes that the lowest energy state is that having lowest eigenvalue. But the surface integral is in general a nonvanishing function of λ, and cannot be neglected.

From eq. (2) we see that

$$\lambda K = \frac{1}{2c} \int_V \underset{\sim}{j} \cdot \underset{\sim}{A}. \tag{4}$$

This is the energy of the plasma currents.[2] We will show later that the surface integral gives the contribution to the energy due to induced wall currents. To see that this contribution can be large, note that

$$\int_C \underset{\sim}{B} \cdot \underset{\sim}{d\ell} = \frac{4\pi}{c} I_h \tag{5}$$

where C is any toroidal path around the wall of the torus, and I_h is the current through the hole of the torus. The current through the hole is a sum of two components,

$$I_h = I_{ext} + I_\theta, \tag{6}$$

where I_θ is the induced poloidal wall current and I_{ext} is the current through the external field coil windings that link the torus. At field reversal the integral in eq. (5) vanishes, so the induced poloidal wall current must be equal to the current through the external field coils. In a self-reversed z-pinch the induced wall current must be greater than the current through the external field coils. The induced wall currents play an essential role in the process of self reversal. In properly determining whether the field reversed state has lower energy than the nonreversed state, we must include the energy of these induced wall currents.

In ref. (3), Taylor's analysis for a large aspect ratio torus of circular cross-section is redone using the corrected expression for the energy of a force-free state. It is shown that for this geometry the energy of the induced wall currents does not affect the minimum energy state. In practice other geometries are also of interest. For the z-pinch we would like to know whether finite aspect ratio effects are important. For the spheromak the geometry is considerably different.

For the pure spheromak, the sphere without a hole, the surface term vanishes and Taylor's original analysis goes through. The spheromak with a hole is of greater interest because of its improved shear.[4] Here again the equilibria of interest have no surface current. However, to determine the stability of these equilibria we must compare their energy to that of other

force-free equilibria which do have surface currents. The required analysis is the same as that for a z-pinch of the same geometry.

In the remainder of this paper we show how to generalize the corrected Taylor analysis to arbitrary cross-section and aspect ratio. We will show that the contribution to the energy due to induced wall currents never alters the minimum energy state. This will follow from a relation we derive between surface and volume energy for equilibria satisfying eq. (2).

We begin by obtaining general expressions for A and B at the wall of the torus. Set up a coordinate system (θ, ϕ) on the wall such that θ increases by one in going once around in the poloidal direction while ϕ increases by one for each toroidal circuit. The Jacobian is $1/|\nabla\theta \times \nabla\phi|$. From eq. (2) and the perfectly conducting boundary condition it follows that $\hat{n} \cdot \nabla \times B = 0$ at the wall, so that B can be written as the gradient of some function, $B = \nabla\chi$. From the requirement that B be single-valued it follows that χ must be of the form $\chi = \alpha\theta + \beta\phi + \Gamma(\theta,\phi)$, where α and β are constants, while Γ is a periodic function of θ and ϕ.

From eq. (2) it follows that A must be of the form $A = B/\lambda + \nabla\eta$, for some function η. We must in addition satisfy the condition

$$\int_C A \cdot d\ell = \Psi_h, \tag{7}$$

where Ψ_h, the flux through the hole of the torus, is a constant independent of time. This condition follows from

$$E = - \nabla\phi - \frac{1}{c}\frac{\partial A}{\partial t},$$

and from the perfectly conducting boundary condition. To satisfy eq. (7) we take $\eta = (\Psi_h - \beta/\lambda)\phi$.

We can now evaluate α and β. Expressing the poloidal line integral of $\nabla\chi$ in terms of A we find that $\alpha = \lambda\Psi$. Similarly, expressing the toroidal line integral of $\nabla\chi$ in terms of B, we find that $\beta = 4\pi I_h/c$. Our final expressions for A and B at the wall are

$$B = \lambda\Psi\nabla\theta + \frac{4\pi}{c}I_h\nabla\phi + \nabla\Gamma, \tag{8a}$$

$$A = \Psi\nabla\theta + \Psi_h\nabla\phi + \frac{1}{\lambda}\nabla\Gamma. \tag{8b}$$

Using eqs. (8) we can evaluate the surface integral in eq. (3). Because Γ is periodic, its contribution to the integral vanishes. We find

$$\int_S \hat{n} \cdot A \times B = \Psi[\frac{4\pi}{c}I_h - \lambda\Psi_h]. \tag{9}$$

In this expression only I_h is not a conserved quantity. In determining the difference in energy between two force-free states, the term proportional to Ψ_h cancels out. The value of Ψ_h will therefore not affect the results of our analysis, as we would expect.

We are now in a position to verify our physical interpretation of the surface term. Using eq. (8b) and $\nabla \cdot J = 0$, we find

$$\int_S J \cdot A = \Psi I_\theta,$$

where $\underset{\sim}{J}$ is the surface current density at the wall. It follows from eqs. (9) and (6) that

$$\frac{1}{8\pi} \int_S \hat{n} \cdot \underset{\sim}{A} \times \underset{\sim}{B} = \frac{1}{2c} \int_S \underset{\sim}{J} \cdot \underset{\sim}{A} + \frac{\Psi}{2c} I_{ext} - \frac{\lambda}{8\pi} \Psi \Psi_h. \tag{10}$$

In determining energy differences the constant terms cancel out, to leave the difference in energy of the induced wall currents.

As a first step towards obtaining a relation between surface and volume energies, we derive a Green's theorem for eq. (2). Let $\underset{\sim}{B}_1$ and $\underset{\sim}{B}_2$ be two solutions of eq. (2), with eigenvalues λ_1 and λ_2. We use the vector identity

$$\underset{\sim}{B}_1 \cdot \nabla \times \underset{\sim}{B}_2 - \underset{\sim}{B}_2 \cdot \nabla \times \underset{\sim}{B}_1 = \nabla \cdot (\underset{\sim}{B}_1 \times \underset{\sim}{B}_2),$$

integrating over the volume and using eq. (2) to find

$$(\lambda_2 - \lambda_1) \int_V \underset{\sim}{B}_1 \cdot \underset{\sim}{B}_2 = \int_{wall} (B_{2\theta} B_{1\phi} - B_{1\theta} B_{2\phi}) d\theta d\phi.$$

This is our Green's theorem. We can evaluate the right hand side further using eq. (8a) to find

$$(\lambda_2 - \lambda_1) \int_V \underset{\sim}{B}_1 \cdot \underset{\sim}{B}_2 = \frac{4\pi}{c} (\lambda_2 I_{h1} - \lambda_1 I_{h2}). \tag{11}$$

Now use the positivity of $(\underset{\sim}{B}_1 - \underset{\sim}{B}_2)^2$, integrating over the volume to show

$$W_1 + W_2 \geq \frac{1}{4\pi} \int_V \underset{\sim}{B}_1 \cdot \underset{\sim}{B}_2.$$

If $\lambda_2 > \lambda_1$, we conclude that

$$(\lambda_2 - \lambda_1)(W_1 + W_2) \geq \frac{\Psi}{c} (\lambda_2 I_{h1} - \lambda_1 I_{h2}). \tag{12}$$

This is a relation between the surface energy and the total energy for the solutions of eq. (2). We finally use eqs. (3) and (9) to eliminate the surface energy from eq. (12). Setting $K_1 = K_2$, we find that the K's cancel. After some algebra, we establish

$$W_2 \geq W_1. \tag{13}$$

Eq. (13) is not quite what we would have liked. We would like to show that in fact $W_2 > W_1$. In eq. (13) we have not ruled out the possibility that the surface energy leads to a degeneracy of the lowest energy mode.

Let λ_2 approach λ_1 in eq. (12), writing $\lambda_2 = \lambda_1 + \Delta\lambda$. Taylor expand all quantities in eq. (12) to first order in $\Delta\lambda$. Using also eqs. (3) and (9) we now find that

$$\frac{\partial W}{\partial \lambda} = \lambda \frac{\partial K}{\partial \lambda}. \tag{14}$$

It follows that the plot of W vs. K cannot have degenerate branches.

To complete our generalization of Taylor's analysis, we should say something about the character of the solutions of eq. (2) in a torus of arbitrary cross-section and aspect ratio. To do so we specialize to a torus whose walls have azimuthal symmetry. We can then Fourier transform in ϕ.

Write $\underset{\sim}{B} = \sum_\ell \underset{\sim}{B}^{(\ell)} e^{i\ell\phi}$, where the $\underset{\sim}{B}^{(\ell)}$ do not depend on ϕ. For the $\ell \neq 0$

modes, $I_h = 0$. It follows from the boundary condition that for these modes $\Psi = 0$ also.

Now focus on the $\ell = 0$ modes. For these modes the boundary condition implies that B_ϕ is a constant on the wall. When $B_\phi = 0$ on the wall, $W = \lambda K$. It follows from standard variational arguments that the $\ell = 0$, $B_\phi = 0$ modes are discrete and form a complete set in the poloidal plane defined by ϕ = constant.

For $\ell = 0$, $B_\phi \neq 0$ at the wall, we use the Green's theorem derived earlier. Construct a dyadic Green's function for eq. (2) using the $\ell = 0$, $B_\phi = 0$ eigenmodes. We then find for the $B_\phi \neq 0$ solution

$$\underset{\sim}{B}(\underset{\sim}{r}) = \frac{4\pi}{c} I_h \sum_n \frac{\Psi_n \underset{\sim}{B}_n(\underset{\sim}{r})}{\lambda_n - \lambda} \, ,$$

where the sum is over all $\ell = 0$, $B_\phi = 0$ eigenmodes, normalized to $K_n = 1$. It is easily shown that for a given λ this continuum eigenfunction is unique.

References

1. J. B. Taylor in Plasma Physics and Controlled Fusion, Tokyo 1974 (IAEA, Vienna, 1975).

2. See, e.g., Stratton, Electromagnetic Theory, pp. 122-124, McGraw Hill, N.Y. 1941.

3. A. Reiman, Phys. Fluids 23, 230 (1980).

4. M. N. Bussac, H. P. Furth, M. Okabayashi, M. N. Rosenbluth, and A. M. Todd in Plasma Physics and Controlled Fusion, Innsbruck 1978 (IAEA, Vienna, 1979).

5. Courant and Hilbert, Methods of Mathematical Physics, Ch. VI, Interscience Publishers, Inc., New York (1953).

STEADY STATE MAGNETIC DIFFUSION FROM RESISTIVE INTERCHANGE MODES

Wallace M. Manheimer
Plasma Theory Branch
Naval Research Laboratory
Washington, D.C. 20375

Abstract

It is shown that a likely nonlinear state for resistive interchange modes
is one in which velocity vortex structure is balanced by Ohmic dissipation.
Macroscopically this is manifested as magnetic diffusion and anomalous energy
transport. The results are discussed and compared with recent experiments.

It is now generally assumed that reverse field pinches (RFPs) can exist
neither in states which are MHD unstable nor in states which are tearing mode
unstable. Indeed, diffuse pinch profiles which are stable to all of these have
been calculated.[1,2,3] It seems reasonable that this conclusion also applies
to spheromaks. The remaining problem is the effect of resistive interchange
modes. The simplest theory, which mocks up pressure gradient with an effective
gravity, indicates that any pressure gradient drives these modes unstable.[4,5,6]
Apparently the plasma must either exist in such an unstable state, or else be
driven to the Taylor configuration with zero pressure gradient.[7] This seems to
be a crucial issue and one can examine it in two ways. First one can do the
linear theory more accurately, modeling geometry and/or kinetic effects more
realistically, and hope that stable regimes emerge. Second, one can examine
whether the plasma can exist in the presence of these modes. This report
follows the second approach. It finds that the plasma can indeed exist (but
has anomalous transport), with a spectrum of nonlinearly saturated resistive
interchange modes. The anomalous magnetic diffusion is calculated in terms of

281

the fluid velocity fluctuation and an estimate is then given of an upperbound for this. Also, it is worth pointing out that since mode rational surfaces for resistive g modes occur everywhere in an RFP, a theory which predicts stabilization by flattening the pressure profile over for instance a few widths of the interaction region is not a viable theory, because these interaction regions will almost certainly overlap.

This work is motivated to a large extent by recent studies in Eta-Beta II.[8] There it was found that a reverse field pinch plasma with $n \approx 2 \times 10^{14}$, $T \approx 100$ ev and $I = 200$ kA could exist in a quiescent state for as long as 500 μ sec before disrupting. The growth time for the resistive g mode is less than 10 μ sec, while the resistive diffusion time is about 10-20 milisec. Thus something allows this plasma to exist for many growth times, but to be lost rapidly compared to a classical diffusion time. Also, while magnetic probes show that low frequency fluctuations virtually disappear during the quiescent phase, the high frequency fluctuations are reduced, but are still present.

For a resistive interchange mode, Ohm's law is

$$\eta \, \tilde{\underline{J}} = \frac{\tilde{\underline{V}}}{c} \times B \tag{1}$$

where a top squiggle indicates a fluctuating quantity, and η is assumed to be a constant. In slab geometry, with $\underline{B} = B_o(\underline{i}_z + \frac{x}{L_s} \underline{i}_y)$, incompressible perturbed motion and with the fluctuating quantities varying as $f(x) \exp (iky + \gamma t) + c.c.$, Ref. 6 calculates the mode structure and growth rate. The result is

$$\tilde{V}_x = \frac{ik\ell^2}{x} \tilde{V}_y = - \frac{\eta c^2}{4\pi \frac{\partial B_y}{\partial x} \ell^2} \tilde{B}_y = \tilde{V}_o \exp - 1/2 \, (\frac{x}{\ell})^2 \tag{a}$$

$$\tilde{B}_x = ik \, \frac{4\pi \tilde{V}_o}{\eta c^2} \, \frac{\partial B_y}{\partial x} \, \ell^3 \, \sqrt{\pi/2} \, \text{erf} \left(\frac{x}{\sqrt{2} \ell} \right) \tag{b} \tag{2}$$

282

$$\ell = (\eta c^2)^{1/3} \, k^{-1/3} \, \left(\frac{\partial B_y}{\partial x}\right)^{-2/3} \left(-g \, \frac{\partial \rho}{\partial x} \, \rho\right)^{1/6} \qquad (c)$$

$$\tag{2}$$

$$\gamma = \left\{- \, g \, \frac{\partial \rho}{\partial x} \, k \, \frac{\partial B_y}{\partial x}\right\}^{2/3} \left(\frac{\eta c^2}{4\pi}\right)^{1/3} \qquad (d)$$

where g is the equivalent gravity $g \sim \frac{T}{MR}$, and R is the radius of curvature of the field line. The plasma is unstable only if $\partial \rho / \partial x$ and R have opposite sign. For a reversed field pinch, R. is roughly the minor radius r. Also, it is important to note that for a resistive interchange mode, $\widetilde{E} = 0$ according to Eq. (1).

Now imagine that some nonlinear effect stops the growth of the fluctuation (i.e., so $\gamma = 0$) at some saturated value which we will denote $\widetilde{V}_o$. (In addition to specifying a $\widetilde{V}_o$, there are other subtle requirements on such a nonlinear effect which will be discussed more fully else where). This paper does not speculate on what this nonlinear effect is; it only assumes a saturated value for $\widetilde{V}_o$ and proceeds.

The idea then is that the plasma is not quiescent, but has a fluctuating velocity. This fluctuating velocity is balanced by Ohmic dissipation in steady state according to Eq. (1). However, this fluctuating velocity gives rise to a steady state electric field in the z direction according to Ohms law:

$$E_z = - \, \frac{1}{c} \left(\widetilde{V}_x \widetilde{B}_y{}^* - \widetilde{V}_y \widetilde{B}_x{}^*\right)^{+c.c.} + \eta J. \qquad (3)$$

This field gives rise to a diffusion in the magnetic field

283

$$\frac{\partial B_y}{\partial t} - \frac{\partial}{\partial x} \frac{\eta c^2}{4\pi} \frac{\partial B_y}{\partial x} = -\frac{\partial}{\partial x} \left(V_x B_y^* - V_y B_x^* \right) + \text{c.c.}$$

$$= 2 \frac{\partial}{\partial x} \sum_i \frac{4\pi}{\eta c^2} |V_{oi}|^2 \left(\ell_i^2 \exp-\left(\frac{x-x_i}{\ell_i}\right)^2 \right) \tag{4}$$

$$+ \sqrt{\frac{\pi}{2}} \ell_i (x - x_i) \operatorname{erf} \frac{x-x_i}{\sqrt{2}\ell} \exp - \frac{1}{2} \left(\frac{x-x_i}{\ell_i}\right)^2 \right) \frac{\partial B_y}{\partial x}$$

where the term on the right hand side is obtained from Eq. (2) and the factor of 2 in front comes from adding the complex conjugate. Also, we have changed the notation slightly and now the index i denotes the ith rational surface. Thus the stabilized resistive interchange mode gives rise to magnetic diffusion on each rational surface. If the different mode widths overlap, there will be magnetic diffusion over the entire plasma.

To get a rough estimate for the anomalous magnetic diffusion, let us assume that nonlinear effects limit the y fluctuating velocity to some fraction α of the sound speed so that $V_o = 0.5\, \alpha k \ell \frac{T}{M}$. In this case, the value of the magnetic diffusion coefficient at $x = x_i$ is given roughly by

$$D \approx \frac{1}{2} \left(\frac{4\pi}{\eta c^2}\right) \alpha^2 k^2 \ell^4 \left(\frac{T}{M}\right). \tag{6}$$

It is interesting to note that in this case $D \sim \eta^{1/3}$ as one might expect for resistive interchange modes. Also $\tilde{B}_x$ is given by $1/2\, \beta \frac{\tilde{V}_o}{\sqrt{T_M}} B_y \approx 1/2\, \beta k \ell$ αB_o so that the basic phenomena is fluid convection and vortex motion; the radial fluctuating magnetic field being, by contrast, small. For Eta-Beta II, we find that if $kr \sim 10$, Eq. (6) with $a \lesssim 1$ gives roughly the correct confinement time. However, we emphasize that since $\ell \sim \rho_i$ (the ion larmor radius), the theory developed here does not directly apply. Nevertheless, it would undoubtedly be interesting to try to measure small scale velocity fluctuations during the quiescent phase of a reverse field pinch.

References

1. D. C. Robinson, Plasma Phys. $\underline{13}$, 439 (1971).

2. D. A. Baker et al, Plasma Physics and Controlled Fusion Research 1971, Vol. I, p.203 (IAEA Vienna, 1971).

3. D. C. Robinson, Nucl. Fusion $\underline{18}$, 7 (1978).

4. H. P. Furth, J. Kileen and M. N. Rosenbluth, Phys. Fluids $\underline{6}$, 459 (1963).

5. G. Bateman, <u>MHD Instabilities</u>, MIT Press 1978.

6. W. M. Manheimer, <u>An MHD Instability Primer</u>, NRL Memo Report 4000, June 1979.

7. J. B. Taylor, Phys. Rev. Lett. $\underline{33}$, 1139 (1974).

8. J. N. DiMarco et al, to be published, also Bull. Am. Phys. Soc. 940 (1979).

RFP THEORY WORKSHOP SUMMARY

D. A. Baker

Los Alamos Scientific Laboratory

I. INTRODUCTION

The summarizing of the results of a workshop as extensive as this one is indeed a challenging task. I have attempted to point out the major issues and new important developments. In particular, an attempt has been made to indicate where more theoretical work on outstanding RFP problems is needed. It is hoped that this will materially accelerate RFP theory in the areas of greatest need and will aid any theorist attempting to make new and pertinent contributions in the field. It was not possible to discuss specifically every piece of work; this would have significantly lengthened an already lengthy summary. The topics are discussed in subject headings essentially as they appeared in the workshop but their order was changed in an attempt to aid in the logical presentation.

II. RESULTS OF RFP EXPERIMENTS

The results of RFP experiments were reviewed to set the stage for subsequent theoretical papers and to provide input for the discussion groups. Newton reviewed the poloidal flux consumption and energy losses observed in the setting up of the quiescent operation of Zeta. He reported that the energy loss, up to the time of peak current, was $\sim 1/3$ of the toroidal circuit energy input for a self-reversal start-up with a current rise time of 1.4 ms. The Zeta shell had no slots running in the toroidal direction and precluded aided reversal operation. The flux and energy inputs increased nearly linearly with the pinch parameter Θ ($\Theta = B_{\theta wall}/B_{\phi ave}$) over the range $1.2 < \Theta < 1.8$. The $\dot{I}$ fluctuation level and the effective resistance were observed to decrease as the current rise time increased from 0.8 to 2.6 ms. The current penetrated the plasma column rapidly and the plasma energy at peak current was a small fraction of both the total magnetic energy and the energy dissipated. These results point to a need to find a more efficient means of setting up the RFP.

286

Ortolani summarized the results obtained by the Padua group on the ETA Beta II experiment (R/a = 12.5cm/0.65cm) with aided reversal. Quiescent operation following self-reversal had not yet been obtained. The I/N value of ~ 10^{-14} A·m was optimum for making long current decay and low $\dot{I}$ fluctuation level discharges. This value is close to that observed in the quiescent Zeta discharges. Evidence was presented that the quiet discharges were bracketed by high fluctuation levels at low fill pressure and by high impurity radiation losses at higher pressures. Electron temperatures were reported to be 40-80 eV. Short current decay times were obtained when the toroidal field at the wall was reduced to zero. This result is of importance to spheromaks.

The recent ZT-40 experimental results were summarized in a paper by Haberstich, et al. Electron temperatures of ~ 80 eV were reached, well above the OVI radiation barrier. Self-reversal operation was readily obtained and quiet periods in the density fluctuations were observed with reversed toroidal magnetic and electric fields. The quiet period had the noticeable difference that the $\dot{I}$ fluctuations were not greatly reduced as observed in ETA Beta II. The ZT-40 circuit had a 1/4 to 1 primary to (plasma) secondary turns ratio as compared to the 12 to 1 used in ETA Beta II. This means the circuit losses in ZT-40 had a much more dominating effect on the current decay time (<0.4ms) as compared to the ~ 1ms decay time of ETA Beta II. Measurements of external field fluctuations and electron density fluctuations were reported in a paper by Jacobson and Buchenauer. The field fluctuations are consistent with the interpretation that the effects are associated with $\vec{k} \cdot \vec{B}$ singular surfaces. The chord-averaged density fluctuations were observed to peak at the outermost region of the discharge.

Both experiments indicate that many important features of Zeta behavior can be obtained on smaller bore experiments both with a metallic vacuum liner (ETA Beta II) and an insulating ceramic liner (ZT-40) using ~ 100 µs current rise times. A theoretical understanding of the nature of the physics controlling the occurrence and duration of the quiet periods in the RFP is needed.

III. RELATED CONCEPTS

Experiments and theory for the concepts very closely related to the RFP were reviewed. These include the spheromak, gun generated compact tori, and the OHTE concepts. The spheromak and gun generated compact tori differ primarily from the RFP in that the hole in the torus is shrunk to zero (i.e., unit aspect ratio and no external conductors link the plasma) and the resulting toroidal field at the plasma edge is of necessity zero. Theoretically, the stability properties are expected to be similar to that of RFP, relying on high shear and wall stabilization. An additional unstable tilting mode is possible in the spheromak and compact torus configurations. The successful production of gun produced compact tori lasting ~ 150 μs were reported by the LASL group. The tipping mode was observed and then eliminated by using an oblate flux conserving wall as predicted by theory. The production of a spheromak-like configuration was also reported by the Maryland group. The Princeton spheromak was just beginning operation at the time of the workshop.

The OHTE concept was discussed (Schaffer, et al.) and has relevance to the RFP program. OHTE combines the high ohmic heating properties of the RFP with the rotational transform produced by stellarator-like helical windings. Like the RFP, the high shear is expected to give stability. The pitch reversal is produced by the external helical windings and the pitch profile is expected to be less sensitive to the decay of the plasma currents than the RFP. The stability theory for the OHTE is in the beginning stages. At present it depends heavily on the analogy with RFP stability results. There may be important differences associated with the external helical fields; Taylor pointed out the stability criterion associated with the field line pitch is altered for a non-circular cross section.

The related concepts are of interest to RFP investigators and a close exchange of ideas and experimental results can materially help each program.

IV. START-UP

The start-up problem is critical in the operation of an RFP. The Zeta self-reversing type of start-up of the RFP configuration tends to be favored by the fusion engineers since it is simplest. It involves simply turning on the toroidal current in the presence of an appropriate toroidal field. There are concerns that the energy loss with this type of start-up may be excessive. The high wall loading may release too many impurities into the discharge. Large

losses can result in excessive wall damage. In the extreme case, an unfavorable reduction in the power balance of a reactor could result. Relevant to this is the existence of a global energy balance theorem (Baker, Mann, Oliphant, Phillips) which indicates that a minimum loss is necessary for the slow Taylor state-like set-up of the plasma. There is yet an open question to what extent departures from symmetry during a turbulent start-up may alter the predictions of the theorem. The pitch convection method of start-up using gas injection was originally proposed by Newton as a possible means of reducing the set-up energy loss.

Six papers on simulation codes (Newton and Johnston; Oliphant; Caramana; Byrne and Chu; Nebel and Moses; Matsuda, et al.;) giving RFP start-up calculations were discussed. Of particular interest is the demonstration of a slow set-up of an RFP equilibrium by pitch convection, that is at all times ideal MHD stable (Nebel, Moses). The calculation demonstrated a RFP set-up having an energy loss of a few percent. The energy losses associated with the plasma production were not treated. The question of possible instability due to a vacuum edge region in a real system with a vacuum liner inside the stabilizing shell was raised and the effects of resistive modes are yet to be determined. The pitch convection method in which the fields and plasma are convected inward to build up the desired configuration appears to have promise for reducing start-up losses if self-reversal and aided reversal start-up procedures prove unacceptable. Perkins and Caramana reported necessary conditions for a pitch convection start-up.

V. EQUILIBRIUM AND STABILITY
MHD

Since RFP configurations exist which are stable against ideal MHD and resistive tearing modes, the resistive g mode continues to be of interest since it is driven by the pressure gradients and unfavorable field line curvatures present in an RFP.

Previous work (Robinson, Ortolani) on the g mode using a cylindrical nonideal MHD code indicates growth rates are above the resistive diffusion times only for beta values above $\sim 10\%$. The g mode becomes very localized around the $\vec{k} \cdot \vec{B} = 0$ surface when the Lundquist number becomes high. A fully kinetic description is needed for hot plasmas since the fluid description, even

with approximate finite gyro radius corrections, become invalid for the very localized phenonemon.

Recent work at Livermore (Schnack) using a fluid code and LASL (Hewitt) with a Vlasov-fluid code predict a nonlinear resistive m = 0 unstable g mode in an RFP configuration which does not saturate at small amplitude. The nonlinear states of these calculations look similar for both calculations. The early start-up position of the growing modes is different for the two calculations, however (at the toroidal field zero in the first case and at the pinch axis in the second). The electron heat conduction has been neglected in both calculations and should have a stabilizing effect. Only g modes saturating at low levels were found in the corresponding Culham work (Robinson). Further work is needed to clarify several issues raised in the first calculations, but if such a mode exists it may indicate the need for a start-up which remains low beta (where the mode is not dangerous) until a high enough Lundquist number is reached to obtain possible stabilization by kinetic effects. Studies are underway to clarify the above results and to examine the effects of large gyro radii and beta. An approach using the Vlasov-fluid model was described by Lewis.

Parallel viscosity is stabilizing to the resistive g mode for m = 0 (Robinson). Calculations (Dagazian) indicate that parallel viscosity is destabilizing at high m numbers where the mode is less dangerous. The work of Chang, et al., shows that the growth rate of the resistive g mode decreases considerably as the electron temperature gradient increases.

Plasma rotation or electron fluid motion at the diamagnetic drift frequency can make a resistive liner appear as a conducting shell to tearing and ideal MHD modes, and it was stated that there are indications that a full conducting shell may not be necessary for the RFP (Robinson). Effects of finite wall conductivity were discussed in a paper by Nalesso.

Microinstabilities

Microinstabilities can cause an increase in the resistivity, heat conductivity, and cross-field transport of particles and energy.

A considerable amount of work has been done in the past on possible microinstabilities in the RFP. The work has concentrated on modes driven by diamagnetic cross-field currents. The work to date (which includes the important lower hybrid drift, drift cyclotron, and universal modes) yields the

result that the high shear and finite beta of the RFP configuration stabilizes all such modes for devices on the order of ZT-40 size and larger. Further work is needed in the area of possible microinstabilities driven by currents flowing parallel to the field lines. Such modes are of interest since they can affect the heating and transport of the RFP when large current densities are used for ohmic heating. Linsker described a method for studying low frequency modes in the high shear, arbitrary beta RFP configurations. Two instabilities which may not be stabilized by shear were reported at the meeting by Gladd. These modes have been studied for tokamaks and need further studies to determine their effect in RFP configurations. The first is the electron temperature gradient microtearing mode. It is an electromagnetic mode which can form island chains about $\vec{k} \cdot \vec{B} = 0$ surfaces. These islands can overlap for $\delta B/B \sim 10^{-4}$ and thus break up the magnetic surfaces leading to enhanced thermal transport. The mode saturates by transferring energy to other wavelengths. The second mode of interest is a parallel-current-driven drift mode which becomes unstable for $v_{\parallel}/v_{1thermal} \gtrsim 2$. Further work in this area is needed. Whether a parallel current driven mode which enhances resistivity is unfavorable or not depends on the resulting ratio of ohmic heating to transport energy loss.

Helical Ohmic Equilibria

The possibility of a steady-state helical ohmic reversed-field equilibrium having plasma flows was first suggested by Wesson as a result of 3-D RFP self-reversal simulations. Such states may be the end result of driving an RFP to large Θ values. Such a stable steady state may possess good heating and confinement properties without requiring plasma activity to maintain the configuration against resistive field diffusion.

Necessary conditions for the existence of ohmic steady states were reported by Gimblett. This paper constitutes a proof of principle of the existence of helical ohmic states. The states can be considered as produced by resistive tearing modes at marginal stability. The analysis used constant resistivity. Analytic and computer calculations of such states were reported by Schnack and Dagazian.

Questions for further study:

1. Is constant resistivity a requirement for the existence of a helical ohmic state?

2. Can one expect a plasma to adjust its transport coefficients to the values required to give a stationary ohmic state?

VI. HEATING AND TRANSPORT

There is need for establishing scaling laws for the energy confinement time τ_E of an RFP. Many scaling formulas from tokamaks and elsewhere exist and have been used for predictions. None are known to be valid for RFP. The important problems of τ_E scaling and establishing a proper relationship between the current decay time and stable configuration time was discussed by Christiansen and Roberts. Impurity effects in RFP's were discussed by Piotrowicz and Christiansen.

The heating and transport of the RFP are being studied with one- and two-dimensional codes. These codes have been used to study the effects of impurities, thermal instabilities, and ohmic heating on the evolution of the equilibrium. Oliphant described a new 1-D nonideal MHD transport code which can run a plasma problem from a dynamic start where inertial effects are important to a quasi-equilibrium diffusing state. He presented results of calculations on running Z pinches to the Pease limit and RFP calculations for different current risetimes.

One-dimensional transport calculations (Christian) have shown that an initially low beta RFP can be ohmically heated to ignition temperatures without the associated resistive diffusion destroying the RFP configuration provided the initial state has a low parallel current in the outer region.

A powerful one-dimensional quasi-equilibrium code was described by Caramana. The code uses the poloidal flux function as the independent variable and treats the full set of rate equations for the ionization states of various impurity ions. An enhancement of thermal instabilities by impurity radiation losses was found. These instabilities are suppressed by a nonclassical enhanced cross-field heat conduction.

A theory which balances ohmic dissipation against the vortex motion due to resistive g modes was given by Manheimer. A diffusion coefficient scaling as $\eta^{1/3}$ results. The basic phenomenon is fluid convection and vortex motion; the radial fluctuating B field is small. The diffusion coefficient gives an

approximate agreement with the ETA Beta II confinement time. It was further pointed out that the many $\vec{k} \cdot \vec{B} = 0$ surfaces of the RFP don't exist in tokamaks so that tokamak scaling laws should not be expected to apply to the RFP.

Questions that need answering for transport codes:

1. How should the plasma-wall boundary be treated? Should gas be emitted from the wall? If so, how is the gas emission time dependence determined?

2. What transport coefficients should be used?

3. How can self-reversal realistically be simulated in one- and two-dimensional codes?

4. Do three-dimensional codes have enough resolution to give meaningful results?

VII. RELAXATION AND TURBULENCE

The Taylor state continues to be a model which guides the thinking of many RFP physicists. Two papers in the session had the basic goal of finding modified lowest energy states. The motivation is twofold: (1) The Taylor state implies large currents extending to the walls. This is undesirable and is not expected because of a high resistivity in the outer colder plasma region. (2) The Taylor state is force-free and cannot support a plasma pressure gradient. It is the departures from a Taylor state that are vitally important for producing a magnetically confined plasma. Turner and Christiansen described an incomplete relaxation using a resistive truncation procedure while Bhattacharjee changed the basic constraint by introducing a factor which is a function of the helical flux into the integrand $\vec{A} \cdot \vec{B}$ of the magnetic helicity integral. Both systems give lowest energy states which can have finite beta and zero currents at the walls. There is a considerable degree of freedom in the choice of the resistive cut-offs used in the first approach and of the function introduced in the second.

Reiman has redone the Taylor minimization of the magnetic field energy including a neglected term. The correction left the lowest energy states unaltered from Taylor's original result. It is worth noting that questions about the procedure for minimizing the energy including the plasma pressure were raised during the workshop but were left unclear.

The double cascade theory (Montgomery, Turner, Vahala) where dissipation operates preferentially on the field energy, whose spectrum is peaked at shorter wavelengths than the spectrum of the magnetic helicity, continues to be the best answer to the question of why the field energy should be dissipated faster than the $\vec{A} \cdot \vec{B}$ integral. Two-dimensional simulations of the cascade process were described (Matthaeus and Montgomery) showing a more rapid decay of magnetic energy than the mean square vector potential. Three-dimensional calculations are needed in order to be directly relevant to the RFP. The main problem may be getting enough resolution from a numerical three-dimensional calculation to properly describe the short wavelength activity during the decay. Present day three-dimensional codes should be used to examine the cascade process.

The tangled discharge model (Rusbridge) and the dynamo theory reported previously still remain viable candidates for explaining a turbulent self-reversal effect. The dynamo model has not yet satisfactorily explained the data of experiments. The tangled discharge model can give a large enough effect to give the reversal. It was pointed out that the F-Θ diagram is an insensitive measure of an RFP configuration.

Mean field theory using anisotropic turbulent resistivity was shown (Rasband) to reduce the amount of nonmirror symmetry required in the fluctuating velocity field and can extend the parameter range of field reversal in a dynamo theory. This theory is kinematical with motions prescribed. A fully dynamic description following Newton's laws and Maxwell's equations does not yet exist and is needed. We still have a long way to go in getting a self-consistant method of calculating field reversal. Three-dimensional codes show the effect but the work to date (Wesson and Sykes) was done in a straight cylinder with a rectangular cross section on a coarse mesh. A fully toroidal nonideal MHD three-dimensional code is being developed at LASL (Barnes, et al.) which can be used to study self-reversal.

Two statistical mechanics papers were given, one using a nondissipative system (Miller) and the other a non-Liouville system (Rose). The first approach predicts force-free mean fields and surface currents at walls. Doubts were expressed (Montgomery) about leaving out dissipation in such a statistical theory. The second theory used a conjecture that the Gibbs ensemble is a good approximation when fluctuations are small. A probability distribution curve

was obtained. The model predicts reduced turbulence at low plasma densities. The relevance of these approaches to RFP's is yet to be determined.

A paper by Bevir and Gray described a novel method of programming magnetic helicity $K = \int \vec{A} \cdot \vec{B} \, d\tau$ into the pinch assuming that a continuous mechanism is available for the Taylor relaxation. They suggest the intriguing idea that a dc component of the toroidal current might be produced by applying ac toroidal and poloidal voltages to the pinch. This possibility stems from the potential of the relaxation process to exchange toroidal and poloidal fluxes. There are many theoretical questions to be answered, for example: why should the Taylor argument apply to the case of applied E_Θ fields when it assumes a perfectly conducting flux conserving shell? This work is part of the interesting sequel to the original Taylor conjecture which has stimulated much theoretical interest.

VIII. THE RFP REACTOR

RFP Tokamak Comparison

The parameters for present pulsed RFP and pulsed tokamak reactor designs are comparable as can be seen from Table I of Spears' paper. The cost analyses indicated the RFP reactor to be somewhat cheaper than the tokamak.

The advantages of high ohmic heating, freedom of choice of toroidal aspect ratio, low magnetic fields at the coils and lower capital cost for the pulsed RFPR are to be compared with the lack of the need for a metal stabilizing shell and lower expected start-up losses for the pulsed tokamak reactor.

There is a need for steady-state RFP reactor designs allowing comparisons with the steady-state tokamak reactor designs such as STARFIRE. These designs will have to deal with the issues of limiters, diverters, refueling, ash removal and methods for steady-state current drive. The mounting pressure for steady-state reactors stems chiefly from the severe materials fatigue problems associated with pulsed-field designs.

General Points of Interest

It should be noted that the paper by Gerwin, Moses, Nebel and Spears gives formulas for ohmic heating, ignition, and burning which have been shown to produce satisfactory agreement with computer code results and can be very useful for future reactor optimization studies.

A compact RFP reactor has been discussed by Miley and a ZT-40 size "wetwood burner" was discussed in the paper by Gerwin, et al. The need for small, low capital cost pilot reactors has been pointed out by the electrical industry to be important in the early stages of the development of commercial fusion power.

The need for further studies of alpha-particle heating and physics should be stressed. For example beam-type instabilities can transfer energy from alpha-particles directly to the ions. Alpha-particle effects were discussed at the workshop by Miller.

The question of a limiter in the RFP was raised. It should be noted that for an RFP the field near the wall is largely poloidal and the limiter should extend the long way around the torus. This can affect the poloidal symmetry properties.

Another important point discussed in the session was whether quiescent operation of the RFP requires a reversed E field at the wall. In Zeta, ETA Beta II, and ZT-40, quiet periods were obtained only during the current decay and with reversed E_ϕ and B_ϕ. The problems that arise are associated with the accompanying expansion of the plasma wall when the Poynting vector is negative. Newton pointed out the possibility of controlling the expansion with the poloidal electric field even if the toroidal field must be negative. Further theoretical work leading to an understanding of the RFP quiet period operating conditions is needed to shed light on the experimental results.

Critical Issues and Theory Problems for RFP Reactors

Listed below are critical physics issues and high priority theory problems which are relevant for further progress on RFP reactor designs:

1. Energy Containment Time and Transport

The values of energy containment time used in the reactor designs are critical. The RFP designers lack a credible scaling law upon which to base reactor study. There is a lengthy list of possible scaling laws (i.e., Alcator, Sheffield, Calibrated Bohm, Neoclassical, I/N, etc.) to choose from. Since the design depends crucially on the τ_E used, the reactor designers ask "Can the theorists examine the scaling laws and recommend a preferred scaling law for use with future deliberations?" Spears emphasized the importance of

achieving the reactor condition $\tau_E < \tau_{burn} < \tau_{particle}$ during the burn to allow temperature control and avoid thermal runaway.

2. Current and Plasma Densities and Ohmic Heating to Ignition

The achievability of the possible ohmic heating to ignition may depend on the limits placed on I/N by possible current driven instabilities. The lower the value of the current density for a given plasma density, the larger is the required τ_E in order to achieve ignition. This fact was demonstrated at the workshop when the work of Christiansen and Roberts, which concluded that τ_E values of 10-30 μs or more are needed to reach ignition, is compared with the corresponding work of Hagenson and Krakowski which predicts $\tau_E \sim 1sec$ $(\sim 200\tau_{Bohm})$.

3. Energy Losses During Start-up and Rundown

The amount of energy loss during the start-up of the RFP is critical since it will ultimately determine the viable start-up procedure that can be used. Large losses during the formation phase could lead to unacceptable wall loading. Pure self-reversal operation may have to be replaced by suitable slow programming to overcome this problem. The allowable rate of rundown of the current and the fraction of field energy recovered are unknowns for which more physics knowledge is needed.

4. Role and Configuration of the Conducting Shell, Equilibrium and Stability Control

Considerable theoretical work is needed to answer questions arising from the fact that the reactor plasma will be surrounded by a segmented metal shell whose resistive diffusion time is shorter than the plasma sustainment time. How short can the shell segments be? This question bears critically on the modular construction of the reactor. How and on what time scales must the corrective fields be applied to compensate for the diffusion of the magnetic field into the conducting shell? More theoretical work is needed to answer this question both from the view of correcting the equilibrium shift and stabilizing modes that may grow slowly as a result of the finite resistivity of the stabilizing metal shell. What are the allowable field errors for a realistic surrounding shell? The effects of field errors in producing islands and ergodic field line behavior were discussed by Spencer. It was pointed out by Boozer

that a ripple field of 1/2% can lead to a factor of five enhancement of neoclassical transport in the collisionless regime. Detailed theoretical work in the above areas is needed.

5. Methods of Attaining Steady-State Operation

Little work has been done in the area of producing a steady-state RFP. Methods of dc current drive which have been suggested include beam injection, RF drive, and time modulation of the external fields (Bevir and Gray). Some self-reversing actions of the discharge or nonaxisymmetric ohmic steady states are needed to sustain the RFP profile against diffusion. Exhaust, refueling, and impurity control of a steady-state RFP reactor are problems needing attention.

Conclusions

The final conclusions of the workshop reactor discussion group on needed future RFP reactor studies were as follows:

1. Current density, τ_E, and burn studies are critical and should be varied in the calculations before attempting definitive conclusions.

2. High current density operation should be studied more thoroughly.

3. A benchmark calculation using the LASL (RFP BURN) and the Culham (ATHENE) burn simulation codes is needed to give a basecheck and to better define the effects of τ_E and current density variations. This should result in a better unanimity for the RFPR design point.

298

Page Range	Domestic Price	NTIS Price Code	Page Range	Domestic Price	NTIS Price Code	Page Range	Domestic Price	NTIS Price Code	Page Range	Domestic Price	NTIS Price Code	Page Range	Domestic Price	NTIS Price Code
001-025	$ 5.00	A02	151-175	$11.00	A08	301-325	$17.00	A14	451-475	$23.00	A20			
026-050	6.00	A03	176-200	12.00	A09	326-350	18.00	A15	476-500	24.00	A21			
051-075	7.00	A04	201-225	13.00	A10	351-375	19.00	A16	501-525	25.00	A22			
076-100	8.00	A05	226-250	14.00	A11	376-400	20.00	A17	526-550	26.00	A23			
101-125	9.00	A06	251-275	15.00	A12	401-425	21.00	A18	551-575	27.00	A24			
126-150	10.00	A07	276-300	16.00	A13	426-450	22.00	A19	576-600	28.00	A25			
									601-up	†	A99			

†Add $1.00 for each additional 25-page increment or portion thereof from 601 pages up.

Los Alamos